

Information-theoretic Analysis of Neuronal Communication

Thesis by
Amit Manwani

In Partial Fulfillment of the Requirements
for the Degree of
Doctor of Philosophy



California Institute of Technology
Pasadena, California

2000
(Submitted April 28, 2000)

© 2000

Amit Manwani

All Rights Reserved

Dedicated with love and extreme gratitude to my parents.

Acknowledgements

As I set to reflect on the past nearly six years of my graduate life and recount all the associations and influences that have played their part in my odyssey as it nears its destination, I am immediately struck by the monumental impossibility of the task. A long graduate career such as mine is a microcosm of my life itself and the task of expressing gratitude to those who nudged me ahead during my journey is similarly daunting, and I approach it with justified trepidation. I hope those individuals whom I inadvertently overlook to acknowledge here will be kinder in their forgiveness than I am infirm in my memory.

I would like to express my deep gratitude to my research advisor (or “Doctor Father” as he would probably fondly like to be called) Professor Christof Koch, who has been a source of great wisdom, knowledge, guidance and encouragement. Knowing and working with him all these years has been a truly inspirational and enlightening experience, serving me as one of the most important lessons of my graduate education. His contributions, either by way of infusion of novel ideas, or objective critique, or provision of the requisite context and perspective, has touched nearly every aspect of this work. I deeply honor his deep devotion to the cause of science, his personal integrity and his unparalleled preceptorship.

During the course of my graduate career, I have also had the privileged opportunity to work and collaborate with a set of very special and distinguished individuals, some of whom I have the added pleasure of calling my friends. Notable among these are Dr. (Dr.) Peter Steinmetz, Professor Idan Segev and Professor Yossef Yarom, Michael London, Elad Schneidman and Dr. Fabrizio Gabbiani. My special thanks go to my senior colleague and office-mate, Dr. Peter Steinmetz, who not only contributed intimately and organically to this work through excellent ideas, fecund discussions and even the nuts and bolts of software implementations, but also helped create a very pleasant, congenial, and stimulating atmosphere at work. I am greatly indebted to him for it. My collaborators, Professors Idan Segev and Yossef Yarom, and Michael London and Elad Schneidman were extremely patient

with my umpteen requests for data and figures, very willing with their helpful advice and suggestions, and a true joy to work with.

On the personal front, I am extremely grateful for the unconditional love and unstinting encouragement I have received from my parents and my younger brother. Their warm thoughts, best wishes and heartfelt blessings have served as guiding beacons to an occasionally clouded mind. I would also like to sincerely thank my aunts who affectionately provided me with welcoming hearths, my homes away from home. I owe a special vote of thanks to Dr. Laurent Itti and Grace Chang who were delightful company, helpful colleagues and warming friends all rolled into one. I will fondly remember Laurent for his “French” insouciance and his invaluable advice to “relax,” and Grace for making me pleasantly aware of the fact that people hailing from seemingly different worlds can still be alike in their thinking and outlook to life. I am filled with gratitude and appreciation for Umesh Bhide and Vineet Aggarwal for their decade-long close friendships which have endured the tests of time and distance and have been at once comforting and inspirational. I would like to thank my roommates, both present and erstwhile, for jolly conversations and stimulating discussions to break the monotony of research. I am grateful to all my friends who parted so generously with their time and joined me in countless hours of refreshing and engaging merriment, either playing cricket in the field, watching movies or simply socializing. Their bonhomous company added the much needed spice and relish to my life at Caltech.

A number of other people, too innumerable to mention here, have touched my life during my memorable and enjoyable years at Caltech. The motley members, both past and present, of the interestingly diverse Koch Lab, the venerable professors who taught me all I know, the inquisitive and eager students I had the privilege of assisting in the classes for which I served as a TA, countless members of the patient and accommodating Caltech staff: I deeply thank them all.

Abstract

One of the most fundamental functions of brains is to process information. Whether we are engaged in tasks like reading a book, listening to our favorite music station on radio, smelling a flower in bloom or relishing our favorite gourmet cuisine, we invariably employ our brains to process the information received through our senses and create a perception of the world around us. The physical signals incident on our sensory organs, either in the form of photon fluxes, acoustic vibrations, or plumes of chemical concentrations, are transduced, represented and processed as electrical signals within our brains. One of the essential inquiries in neuroscience is the nature of this representation of information in the brain. This is often referred to as the “**neural coding**” problem which has been and continues to be the object of a lot of theoretical and experimental scientific effort.

In most theoretical approaches that address the problem, nerve cells are characterized empirically by collection of their input-output responses. The knowledge of constraints imposed on information processing due to biophysics of the underlying biological hardware is generally ignored. This thesis reports the outcome of our efforts to combine techniques from stochastic processes, information theory and single neuron biophysics to unravel the neural coding problem. We believe that a systematic reductionist analysis which takes into account the extant noise due to biological processes specific to neuronal processing will provide fundamental insights overlooked in earlier approaches. We analytically characterize the sources of biological noise associated with different stages in the neuronal information pathway, namely the synapse, the dendritic tree and the spike-initiation zone and employ information-theoretical measures to compute the ability of these components to transmit information in specific signal processing tasks. For analytical tractability, we demonstrate our results using abstract and simplified mathematical models. However, our approach can be readily applied to realistic and complicated descriptions of single neurons to provide a greater understanding of the role of noise in neuronal communication.

Contents

Acknowledgements	iv
Abstract	vi
1 Introduction	1
1.1 The neural coding conundrum	1
1.2 Membrane noise sources and neural codes	3
1.3 Organization of the thesis	8
2 Information-theoretic Analysis of Synaptic Transmission	10
2.1 Introduction	10
2.2 The stochastic nature of synaptic transmission in cortical neurons	11
2.3 Channel model of synaptic transmission	13
2.4 The signal estimation paradigm	17
2.5 The signal detection paradigm	26
2.6 Discussion	34
3 Subthreshold Noise Sources in Biological Membranes	37
3.1 Introduction	37
3.2 Sources of subthreshold membrane noise	38
3.2.1 Thermal noise	39
3.2.2 Channel noise	46
3.2.3 Noise due to background synaptic activity	51
3.2.4 Other sources of membrane noise	54
3.3 Subthreshold noise in a membrane patch	56
3.3.1 Summary of parameter values used	61
3.4 Results	62

3.4.1	Dependence on patch area	65
3.4.2	Dependence on channel densities	66
3.5	Discussion	67
4	Information-theoretic Analysis of Electrotonic Propagation in Weakly-Active Dendrites	69
4.1	Introduction	69
4.2	The one-dimensional cable equation	70
4.3	Subthreshold noise in linear cables	75
4.4	Electrotonic signal propagation in linear cables	79
4.5	The signal estimation paradigm	82
4.6	The signal detection paradigm	88
4.7	Results	92
4.7.1	Subthreshold noise in a weakly-active dendrite	92
4.7.2	Signal propagation in a weakly-active dendrite	93
4.7.3	Efficacy of signal estimation	96
4.7.4	Efficacy of signal detection	99
4.7.5	Comparing cable theory and information theory	99
4.7.6	Dependence on biophysical parameters	105
4.8	Discussion	106
5	Analysis of Preliminary Experimental Data	114
5.1	Introduction	114
5.2	Proposed plan of experiments	115
5.3	Summary of performed experiments	120
5.3.1	Preparation and recordings	120
5.3.2	Measurement of instrumental noise	121
5.3.3	Measurement of biological noise	122
6	Subthreshold Membrane Noise due to Channel Fluctuations	128
6.1	Introduction	128

6.2	Methods	130
6.2.1	Monte-Carlo simulations	133
6.2.2	Linearized approximations	135
6.3	Results	138
6.3.1	Magnitude of subthreshold noise	138
6.3.2	Power spectral density of subthreshold noise	142
6.3.3	Amplitude distribution of subthreshold noise	142
6.3.4	Dependence of noise magnitude on patch area	142
6.3.5	Dependence of noise magnitude on temperature	146
6.3.6	Dependence of noise magnitude on channel densities	149
6.3.7	Application to dendritic cables	150
6.4	Discussion	150
7	Variability and Coding Efficiency of Noisy Neural Spike Encoders	156
7.1	Introduction	156
7.2	Models of spike encoding	156
7.2.1	Integrate-and-fire models	157
7.2.2	Stochastic ion channel models	163
7.3	Optimal linear estimation	164
7.4	Results	165
7.5	Discussion	171
8	Conclusions	175
9	Appendix	178
A	The signal estimation problem	178
B	Estimation with multiple synapses	182
C	The signal detection problem	184
D	Detection with multiple synapses	188
E	Stochastic analysis of two-state channels	189
F	Derivation of current noise spectra	197

G	Linearization of active membranes	198
H	Theoretical analysis of fast multiplicative conductance fluctuations	206
I	Analysis of nonlinear Poisson encoding schemes	221

References**231**

List of Figures

1.1	Biophysical noise sources in a single neuron	5
2.1	Schematic block diagram of a synapse under the signal estimation and signal detection paradigms	16
2.2	Channel models of synaptic transmission under signal estimation and signal detection	18
2.3	Performance in the signal estimation paradigm	25
2.4	Effect of redundancy on estimation performance	27
2.5	Performance in the signal detection paradigm	32
2.6	Effect of redundancy on detection performance	33
3.1	Equivalent thermal noise models for a resistor	41
3.2	Electrical ladder network model of an infinite 1-D linear cable	44
3.3	Thermal noise models for an infinite 1-D cable	45
3.4	Electric circuit of a membrane patch	57
3.5	Equivalent linearized electric circuit of a membrane patch	58
3.6	Subthreshold noise in a patch of neuronal membrane	63
3.7	Dependence of noise magnitude on biophysical parameters	64
4.1	Channel model of a weakly-active dendrite	71
4.2	Equivalent circuit diagram of a 1-D dendritic cable	72
4.3	Channel models for the signal estimation and signal detection paradigms . .	89
4.4	Subthreshold membrane noise in a dendritic cable	94
4.5	Electrotonic signal propagation in an infinite dendritic cable	97
4.6	Performance in the signal estimation task	100
4.7	Channel capacity in signal estimation using the water-filling algorithm . . .	101
4.8	Performance in the signal detection task	102

4.9	Comparison of classical cable theory and information theory	104
4.10	Dependence of subthreshold noise on biophysical parameters	107
5.1	Outline of a research program to study the influence of neuronal noise on information transfer	116
5.2	3-D reconstruction of a cortical pyramidal neuron	119
5.3	Experimental procedure to measure membrane noise	124
5.4	Analysis of measured biological noise	125
6.1	Finite state Markov kinetic schemes for voltage-gated ion channels	134
6.2	Example of a Monte-Carlo simulation	136
6.3	Steady-state i-v curves for a membrane patch	137
6.4	Models of a membrane patch containing stochastic voltage-gated ion channels	139
6.5	Magnitude of subthreshold voltage noise	140
6.6	Power spectral densities of subthreshold voltage noise	143
6.7	Amplitude distribution of subthreshold voltage noise	144
6.8	Dependence on subthreshold voltage noise on patch area	145
6.9	Dependence of subthreshold voltage noise on temperature	147
6.10	Dependence of subthreshold voltage noise on channel densities	148
7.1	f-I curve of the adapting I&F model	160
7.2	Noisy encoding models of spike timing variability	162
7.3	Variability and coding performance of spike encoding models	167
7.4	Information rates in signal estimation for spiking models	169
7.5	Is it signal or is it noise?	170
7.6	Coding efficiency as a function of $\bar{\lambda}/B_m$	172
9.1	Stochastic fluctuations of a two state binary channel	193
9.2	Statistical properties of current noise for a binary channel	195
9.3	Phenomenological impedance of active voltage-gated conductances	201
9.4	Linearized equivalent electrical circuit for the membrane patch	204
9.5	Classification of membrane conductances	210

9.6	Voltage distribution for passive multiplicative noise	218
9.7	Potential surface for regenerative conductances	219
9.8	Optimal linear estimation performance for nonlinear encoding schemes . . .	224

List of Tables

2.1	List of symbols for Chapter 2	36
3.1	Analytical expressions of membrane current noise sources	55
3.2	Magnitude of subthreshold noise in a membrane patch	65
4.1	Subthreshold noise magnitude in an infinite cable	95
4.2	List of symbols for Chapter 3 and Chapter 4	111
5.1	Electrode resistance and instrumental noise magnitudes	122
6.1	Comparison of parameters for the Mainen <i>et al.</i> (MJHS) and Hodgkin-Huxley (HH) kinetic schemes	155

Chapter 1 Introduction

1.1 The Neural Coding Conundrum

Understanding the nature and limits of the strategies employed by neural systems to represent, process and transmit sensory information to higher-level areas which make behavioral decisions crucial to the survival of the organism, is fundamental to learning how brains work. This is often referred to as the problem of *neural coding* and is a central issue in neuroscience (Rieke *et al.*, 1997; Theunissen & Miller, 1995).

A vast majority of neurons respond to sensory or synaptic inputs by generating a train of stereotypical responses called *action potentials* or spikes. Deciphering the encoding process which transforms continuous, analog signals (photon fluxes, acoustic vibrations, chemical concentrations and so on) or outputs from other neurons into discrete, fixed-amplitude spike trains is essential to understand neural information processing and computation, since often the nature of representation determines the nature of computation possible (Hopfield, 1995; Hopfield, 1999). Researchers, however, remain divided on the issue of the neural code used by neurons to represent and transmit information.

On the one hand, it is commonly assumed that the mean firing rate of a neuron, defined as its averaged response to stimulus presentations, is the primary variable relating neuronal response to sensory experience (Adrian, 1932; Lettvin *et al.*, 1959; Barlow, 1972). The average might represent a neuron's output summed over a given temporal interval or a mean response computed by multiple repeated presentations of the same signal. This belief is supported by the existence of a quantitative causal relationship between the average firing rate of single cortical neurons and psychophysical judgments made by animals trained to perform specific tasks. It has been demonstrated that an animal's behavior in a visual discrimination task can be statistically predicted by counting spikes over a long time interval (typically one second or more) in a single neuron in visual cortex (Werner & Mountcastle, 1963; Barlow *et al.*, 1987; Newsome *et al.*, 1989; Vogels & Orban, 1990; Zohary *et al.*,

1990; Britten *et al.*, 1992). The highly variable temporal structure of neural spike trains observed *in vivo* (Softky & Koch, 1993; Holt *et al.*, 1996; Shadlen & Newsome, 1998) further strengthens the view that any statistic other than the averaged response is too random to convey information.

On the other hand, recent findings have indicated that spike timing can be precise and have demonstrated that the fine structure of spike intervals can potentially convey more information than a firing rate code, providing evidence for *temporal coding*. The precise relative temporal relationships between the outputs of different neurons also appears to be relevant for coding in certain cases. The literature on such codes is too vast to cite comprehensively and thus, the reader is referred to the lucid exposition in (Rieke *et al.*, 1997) as well as to (Perkel & Bullock, 1968; Lestienne & Strehler, 1987; Abeles, 1990; Bialek *et al.*, 1991; Bialek & Rieke, 1992; Eskandar *et al.*, 1992; Richmond & Optican, 1992; Softky & Koch, 1993; König *et al.*, 1996; Bair & Koch, 1996; Stopfer *et al.*, 1997).

Presently, it is unclear which, if any, is the universal coding strategy used in the brain. In fact, it is quite plausible that different neural systems use different neural codes, or perhaps, even a combination of several coding strategies, depending on the nature of the behavioral task at hand, the level of training of the animal and so on. It is quite clear, nonetheless, that the level of temporal precision of spike trains critically determines the range of neural codes possible. Neuronal hardware (synapses and a variety of ion channels) is inherently unreliable and behaves probabilistically. Thus, the process of encoding is potentially noisy and may result in irregular timing of individual action potentials in response to identical inputs (Lecar & Nossal, 1971a; Lecar & Nossal, 1971b; Schneidman *et al.*, 1998). The representation used by the nervous system depends on precision with which neurons respond to their synaptic inputs (Theunissen & Miller, 1995). The variability of neural spike trains is, in turn, influenced by the sources of biological noise intrinsic to the biophysics of neuronal hardware (Koch, 1997; Koch, 1999). Thus, a quantitative understanding of neuronal noise sources and their effect on firing reliability and precision allows a determination of the constraints under which neuronal codes must operate (Mainen & Sejnowski, 1995; Nowak *et al.*, 1997; van Steveninck *et al.*, 1997; Reich *et al.*, 1997; Bair & Koch, 1996).

Moreover, if we assume that biological systems have evolved to perform the tasks of information and signal processing optimally (Bialek, 1987), it can be argued that noise considerations must fundamentally limit the precision, speed and accuracy of computation in neural systems (Koch, 1999). On the other hand, variability in spike timing may represent faithful encoding of non-linear or chaotic network dynamics rather than noise in the encoding neurons, especially in large networks of neurons (van Vreeswijk & Sompolinsky, 1996; van Vreeswijk & Sompolinsky, 1998). The idea of high spike timing reliability is intuitively appealing and can provide a substrate for fine temporal coding (Abeles, 1990; Bialek *et al.*, 1991; Bialek & Rieke, 1992; Theunissen & Miller, 1995).

Similarly, the widely debated question of whether cortical neurons behave as integrators—summing over hundreds of synaptic inputs on the time scale of 10-30 milliseconds, or whether they act as temporal coincidence detectors—responding to the simultaneous arrival (on a sub-millisecond time scale) of a handful of strategic synaptic inputs, can potentially be answered by assessing the nature and magnitude of noise present at the level of a single neuron (Abeles, 1982; Shadlen & Newsome, 1994; Shadlen & Newsome, 1995; Softky, 1995; König *et al.*, 1996; Koch, 1997; Shadlen & Newsome, 1998).

1.2 Membrane Noise Sources and Neural Codes

A great deal of effort in cellular biophysics and neurophysiology has concentrated on characterizing nerve cells as input-output devices. A host of experimental techniques like voltage clamp, current clamp, whole-cell recordings, and so on, have been used to study how neurons transform their synaptic inputs (which are in the form of conductance changes) to their outputs (usually in the form of a train of action potentials). It has been firmly established by now that neurons are highly sophisticated entities, potentially capable of implementing a rich panoply of powerful non-linear computational primitives (Koch, 1999).

A systematic investigation of the efficacy of neurons as communication devices dates back to well over 40 years ago (MacKay & McCulloch, 1952). More recently, tools from statistical estimation and information theory have been used by researchers (Rieke *et al.*, 1997) to quantify the ability of neurons to transmit information about random inputs through their

spike outputs. Based on Wiener's earlier work (Wiener, 1949), Bialek (Bialek *et al.*, 1991; Bialek & Rieke, 1992) pioneered the use of the "reconstruction technique" towards this end. These techniques have successfully been applied to understand the nature of the neural codes in peripheral sensory neurons in various biological neural systems (Rieke *et al.*, 1997). Subsequent theoretical investigations into this problem have given rise to better methods of assessing the capacity of neural codes (Theunissen & Miller, 1991; Gabbiani, 1996; Strong *et al.*, 1998).

Most of the earlier approaches for assessing the capacity of single neurons have treated the neuron as a black-box and characterized it empirically by its input-output function. However, it is well-known that neurons receive inputs at their synapses; synaptic inputs are integrated in the dendrites and delivered to the spike-initiation zone which generates the spike-train output and transmits it via the axon to the neuron's post-synaptic targets. The specific nature of information processing in the nervous system is determined by the details of this neural hardware. Systematic experimental and theoretical effort over the past thirty years has provided new understanding about the manner in which neuronal signals are transformed and processed at various stages (modules) in individual neurons (Koch, 1999). However, the relationship between single neuron biophysics and neural information processing has still not been unraveled in a systematic and principled manner. Similar to its role in physical systems, noise potentially has a direct bearing on the information and computational capacity of biological systems and we believe that a detailed understanding of the different neuronal components can provide deeper insight into the role of neurons as communication devices. It is therefore important to quantitatively characterize and analyze neuronal noise sources to better understand how computation works in the brain. A reductionist approach of applying experimental and theoretical tools to individual neuronal components will reveal aspects of the neural code which cannot be uncovered using conventional black-box approaches.

An essential step towards this goal is a characterization of noise associated with each of the above biophysically distinct stages (synapses, dendritic tree, axon and so on; see **Fig. 1.1**). Each stage in neuronal processing introduces a potential source of noise. Noise

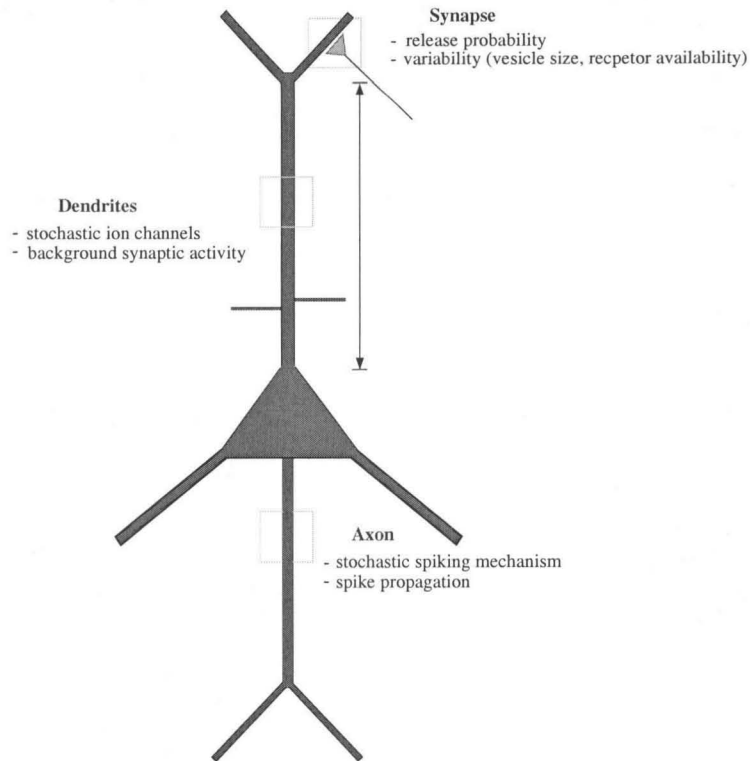


Figure 1.1: Biophysical Noise Sources in a Single Neuron.

Illustration of the sources of noise associated with different components of a single neuron. The synapse, the site of input to a neuron, itself introduces noise due to the probabilistic nature of vesicular release as well as the variability in the quantal amplitude (due to non-uniform vesicle size, receptor availability and other factors). The existence of stochastic, voltage-gated, ion channels and the incidence of a large number of constantly active synaptic inputs, distributed over the extent of the dendritic tree further corrupt the input as it propagates along the dendrite. The spike-generating mechanism which converts the integrated synaptic input into a train of action potentials which travel down the axon is also inherently noisy. All these sources of noise introduce jitter in the temporal structure of the inputs and limit the reliability and the information transmitting capability of a neuronal link.

at the input stage arises from the probabilistic nature of synaptic release mechanism as well as the variability of the amplitude of the postsynaptic response. Studies indicate that synaptic transmission in cortical neurons can be highly unreliable and variable (Dobrunz & Stevens, 1997; Mainen *et al.*, 1999) and might contribute to the variability of spike timing as well (Zador, 1998). There are several sources of noise at the level of the dendritic tree, thermal noise, spontaneous stochastic opening and closing of the ligand- and voltage-gated membrane channels along the dendritic membrane and “background” *pre-synaptic* network activity, assuming that this “spontaneous” activity is noise (*e.g.*, in anesthetized primary visual cortex with no visual input). Ion channels are protein macromolecules subject to random changes of conformational state due to thermal agitation. Random transitions between conducting and non-conducting states give rise to membrane voltage fluctuations (Hille, 1992; DeFelice, 1981). Previous investigations have demonstrated that spontaneous channel fluctuations can influence the reliability and precision of spike timing (Clay & DeFelice, 1983; DeFelice & Isaac, 1992; Horikawa, 1991; Horikawa, 1993b; Horikawa, 1993a; Strassberg & DeFelice, 1993; Fox & Lu, 1994; Chow & White, 1996; Schneidman *et al.*, 1998; White *et al.*, 1998), thus limiting the efficacy of neuronal communication. Recent experimental and computational studies suggest that background synaptic activity may be the dominant noise source *in vivo* (Azouz & Gray, 1999; Destexhe & Pare, 1999). It is still unclear which noise source is most critical in determining how information is encoded and processed in the central nervous system.

Our overall research strategy then is to quantify noise sources at the level of individual neurons, using both *in vitro* and *in vivo* preparations, as well as detailed computer simulations of these at the membrane and cellular level, and to combine this knowledge with studies of small neuronal circuit models (on the order of 1000 neurons) to understand how noise sources affect both measurable variables, such as spike times, and the transmission of information through such networks. This should, ultimately, lead to a better understanding of information coding in the nervous system.

This thesis pursues a reductionist approach by theoretical tools to assess the efficacy of individual neuronal components in the information-transfer capability of neurons. Towards

this end, we plan to experimentally measure and theoretically characterize and quantify the sources of membrane noise associated with these components. The whole-cell patch technique in an *in vitro* preparation of rat neocortex will be used for the experiments. Signal detection and signal estimation techniques will be used to analyze the loss of information of a signal originating at the synapse and propagating to the soma. The noise sources that affect this signal are the probabilistic nature of the synaptic mechanism, the stochastic ion channels in the dendrites and the bombardment of random synaptic activity over the dendritic surface. Compartmental modeling based on detailed morphology and physiology will enable us to combine the theoretical and experimental results for the different noise sources and develop a stochastic model for neocortical neurons. This model will be used to highlight how the different sources of noise interact with each other to determine the information transmission capability of the cell from its inputs to its outputs.

The strength of our approach lies in the combination of techniques from different scientific fields—single-neuron biophysics (Hille, 1992; Koch, 1999), membrane noise analysis (DeFelice, 1981), cable theory, estimation theory (Poor, 1994) and information theory (Cover & Thomas, 1991)—and in their application to the question of neural coding from a novel perspective. Ultimately, our goal is to answer questions like, “is the length of the apical dendrite of a neocortical pyramidal cell limited by considerations of signal-to-noise,” “what influences the noise level in the dendritic tree of a real neuron endowed with voltage-dependent channels,” “how accurately can the time course of an synaptic signal be reconstructed from the voltage at the spike initiation zone,” “what is the channel capacity of an unreliable synapse onto a spine” and so on.

Using this approach, we can address critical questions such as, which stage represents a bottle-neck in information transfer, are the different stages matched to each other in order to maximize the amount of information transmitted, how does neuronal information processing depend on the different biophysical parameters which characterize neuronal hardware and so on. Thus, the rewards from such a biophysical approach to studying neural coding are multifarious.

1.3 Organization of the Thesis

In Chapter 2, we consider the question of how reliably cortical synapses can convey information between neurons. Synapses are indispensable components of neuronal communication, yet little work has been done so far to study their role as communication devices. Incorporating the intrinsic unreliability and variability observed in central synapses into a simple mathematical model of synaptic transmission, we apply tools from information theory to estimate the performance in two distinct signal processing tasks. Results of this analysis have been published in (Manwani & Koch, 1998; Manwani & Koch, 2000).

In Chapter 3, we consider some sources of subthreshold membrane noise which can distort a synaptic signal as it propagates from the input location along the dendrite to the spike initiation zone. The noise sources we consider are: thermal noise, channel noise due to stochastic transitions of voltage-gated ion channels and noise due to background network activity. We derive analytical expressions for the variance and power spectra of the voltage noise due to these sources and compare their magnitudes for biophysically plausible parameter values. In Chapter 4, we use these results to study the ability of dendritic structures to electrotonically propagate information from the synaptic input location to the output. Using a combination of tools from linear cable theory and information theory, we derive analytical expressions for the performance under the signal estimation and signal detection paradigms. The results of these two chapters have appeared in (Manwani *et al.*, 1998; Manwani & Koch, 1999c; Manwani & Koch, 1999a; Manwani & Koch, 1999b).

Chapter 5 summarizes the results of preliminary experiments designed to measure subthreshold membrane noise in cortical neurons to verify our theoretical analysis. The experiments were performed in Professors Yossef Yarom's and Idan Segev's laboratory at the Hebrew University of Jerusalem, as a result of a two-year long collaborative effort between Professors Christof Koch, Idan Segev and Yossef Yarom to understand the role of noise in neural information processing. The data were collected by Yossef Yarom and his graduate students, and analyzed jointly by Michael London and Elad Schneidman at the Hebrew University and Dr. Peter Steinmetz and myself at Caltech.

In Chapter 6, the issue of noise due to stochastic transitions of voltage-gated ion channels is considered in greater detail. We carry out theoretical analysis of channel noise which improves on the accuracy of the expressions in Chapter 3. We also compare our analysis to numerical simulations of non-linear stochastic differential equations using Monte-Carlo methods. Software implementation of the simulations was carried out by Dr. Peter Steinmetz and the analysis was performed in close collaborations with him. The results of this investigation have been published in (Steinmetz *et al.*, 2000a; Manwani *et al.*, 2000a).

In Chapter 7 we investigate the role of the irregularity of neural firing observed *in vivo* on information processing. We employ the signal estimation paradigm to assess the influence of spike timing variability on neural coding. We consider two types of neural spiking models: integrate-and-fire models and stochastic ion channel models and estimate their ability to encode stimulus modulations as spike train sequences. This work was carried out in close collaboration with Dr. Peter Steinmetz. The results have been documented as (Manwani *et al.*, 2000b; Steinmetz *et al.*, 2000b).

Chapter 9 is an appendix containing pedagogical notes, mathematical derivations and some unpublished observations which supplement the analytical treatment in the previous chapters.

Chapter 2 Information-theoretic Analysis of Synaptic Transmission

2.1 Introduction

Here we study the effect of the unreliable, probabilistic nature of synaptic transmission on information transfer in cortical neurons. The synapse is the locus of input to a neuron and thus is a critical component of neural processing. Using the known biophysical details about cortical synapses (*e.g.*, unreliability of vesicle release and variability of response amplitude), we derive a simple mathematical model of a cortical synapse. Our model ignores the ubiquitous use-dependent plasticity of cortical synapses. It represents a simplified picture of synaptic transmission and can be viewed as a first step in quantifying the effect of non-ideality of synaptic transmission on information processing. We compute the information-theoretical capacity of this synaptic model under two coding paradigms, *signal estimation* and *signal detection*.

In the signal estimation paradigm, the information-bearing input is a random continuous signal encoded as the mean firing rate of a presynaptic neuron which transmits spikes across a noisy synapse to a postsynaptic neuron. Using tools from statistical estimation theory, we derive the optimal filter (in the sense of least mean-square-error) which reconstructs the continuous input from the postsynaptic voltage. In the signal detection paradigm, the input signal is in a binary all-or-none format (the presence or absence of a presynaptic spike). We derive the optimal detector (in the sense of minimum probability of error) of presynaptic action potentials from the postsynaptic voltage. The signal detection method is similar to the Yes/No decision paradigm used in psychophysics. We use the performance of the optimal estimator and optimal detector to characterize the synaptic efficacy for these two tasks and to derive bounds on the information capacity of cortical synapses.

2.2 The Stochastic Nature of Synaptic Transmission in Cortical Neurons

Our present understanding of synaptic transmission is based on the seminal work of Katz and his collaborators (Katz, 1969). Their central findings were that the release of neurotransmitter occurs in quanta through spherical, membranous, sacs called *vesicles* residing in the presynaptic terminal. Each vesicle is released independently of the others in a probabilistic manner and the postsynaptic responses to vesicular releases combine linearly. Their theory was developed using experiments at the frog neuromuscular junction but the stochastic and quantal nature of synaptic transmission has been found to be generally valid for central synapses as well. The probability of vesicle release at a single active zone of the frog neuromuscular junction was found to be quite low. However, the neuromuscular junction contains a large number of release sites (on the order of 1000) and as a result, the neuromuscular synapse is highly reliable. Thus, a presynaptic action potential invariably gives rise to a muscular response.

While central synapses share many principles in common with neuromuscular junctions, there are crucial differences between them as well (Redman, 1990; Stevens, 1993). Synaptic boutons in central synapses contain only one or a few active release zones as opposed to the thousands or more found at the neuromuscular junction. Thus, in response to an action potential in the presynaptic terminal, a maximum of one vesicle is released (Korn & Faber, 1991; Korn & Faber, 1993; Stevens & Wang, 1995). Moreover, *in vitro* studies in vertebrate and invertebrate systems have revealed that the probability of vesicle release (referred to as p) is generally low (Korn *et al.*, 1986; Laurent & Sivaramakrishnan, 1992; Bekkers & Stevens, 1994; Stevens & Wang, 1994; Bekkers & Stevens, 1995). The probabilistic release of vesicles is believed to be the dominant factor responsible for the unreliability of synaptic transmission in cortical and hippocampal neurons (Allen & Stevens, 1994). The origin of the random nature of release has not been fully understood yet, though it is known that the precise three-dimensional spatial relationship between calcium channels in the presynaptic membrane and the location of the vesicles determines release dynamics (Stevens *et al.*, 1994).

However, the probability of synaptic release is not constant; it depends on whether or not the last presynaptic action potential led to a vesicle release and the exact timing of the previous presynaptic spikes. Depending on the sequence of presynaptic action potentials, p can either decrease or increase over a variety of time-scales, from tens of milliseconds to seconds, minutes and longer. This history-dependent plasticity in the state of synaptic efficacy is believed to be one of the substrates of learning and memory in biological neural networks (Abbott *et al.*, 1997). p can also vary across synapses (Dobrunz & Stevens, 1997; Murthy *et al.*, 1997) and synaptic (Stratford *et al.*, 1996) types impinging onto a single neuron.

The unreliability of synaptic transmission in cortical neurons is further compounded by the variability in the amplitude of the postsynaptic response to the successful release of a single vesicle (Bekkers *et al.*, 1990; Edwards *et al.*, 1990; Mason *et al.*, 1991). This response variability occurs due to factors like variation in vesicle size and therefore in the number of neurotransmitter molecules, the number of available postsynaptic receptors and so on. The trial-to-trial variability in postsynaptic amplitude can be quite large; in some cases, the variance in the size of the EPSP is as large as the mean (Bekkers *et al.*, 1990; Larkman *et al.*, 1991; Mason *et al.*, 1991). A note of caution is in order here: a majority of studies of central synapses have been carried out in culture or slice preparations that lack many of the neuromodulators present *in vivo*. This might significantly affect synaptic release properties. Only after a careful measurement of synaptic properties *in vivo* experiments will the true picture of synaptic transmission in real brains emerge.

In summary, central synapses appear to highly unreliable, binary connections. This unreliability is several orders of magnitude higher than that observed in engineering systems (Koch, 1999). Theoretically, the nervous system can combat the unreliability of its components by making use of anatomical redundancy using multiple synapses (Moore & Shannon, 1956; von Neumann, 1956). However, cortical axons typically make only a few synaptic contacts onto other cortical target neurons (Sorra & Harris, 1993). Thus, the reliability of synaptic transmission must have a profound influence on the manner in which signals are

encoded and transmitted (Abbott *et al.*, 1997; Lisman, 1997; Tsodyks & Markram, 1997; Zador, 1998) and the ways in which computation is performed in the brain (Stevens, 1994).

An important debate that rages on is whether synaptic unreliability is a “bug” or a “feature” (Koch, 1999). In other words, do biophysical constraints limit the potential reliability of cortical synapses (for instance, the need to pack on the order of one billion synapses into one cubic millimeter of cortex might dictate the small size of synapses) or are there any computational advantages to this unreliability? If reliable synapses that are as small and compact as hippocampal synapses are found experimentally, it would certainly give credence to the hypothesis that synaptic unreliability is probably a design feature used in the brain. One possible computational advantage to having unreliable synapses is for reasons of plasticity. It has been argued that the release probability can be modified more easily over a larger dynamic range than the number of release sites, or the size of the postsynaptic response (Smetters & Zador, 1996; Zador & Dobrunz, 1997). Thus, synaptic unreliability could lead to an increase in the bandwidth of modulation of the postsynaptic response.

It has also been suggested (Burnod & Korn, 1989) that the variability at central synapses plays the same role as the “temperature” parameter T in stochastic models of neuronal networks (Ackley *et al.*, 1985). Just as the presence of noise in large artificial neural networks prevents them from getting stuck in local minima, synaptic unreliability and variability might help brains to learn and generalize better.

2.3 Channel Model of Synaptic Transmission

Armed with the above knowledge about the physiology of central synapses, we can mathematically abstract a synapse by a model which accounts for probabilistic vesicle release and the variability in response amplitude. Using this model as a starting point, we will derive the information-theoretic channel equivalents of a cortical synapse under the signal estimation and signal detection tasks. These capacities will be used to quantify the efficacy of synaptic transmission under the two paradigms.

We will assume that the synaptic bouton contains only one release site. Thus, the vesicle release process can be modeled as a binary channel (inset of **Fig. 2.1**). The input to the channel is a binary variable which represents the presence or the absence of a presynaptic action potential, and its output is a binary variable representing the success or failure of release. The spontaneous release associated with cortical synapses is quite low and so we shall assume that it is zero here (Zador, 1998). Our analysis, however, does not depend on this assumption. Let p denote the probability of release due to a presynaptic spike. The unreliability of vesicle release is the dominant source of noise in the release process as p can be as low as 0.1 for some hippocampal synapses (Hessler *et al.*, 1993).

We model the postsynaptic response to the release of a single vesicle by a function $h(t)$ which corresponds to the EPSP waveform of a fast, voltage-independent AMPA-like synapse modeled as an alpha function (Rall, 1967),

$$h(t) = h_{\text{peak}} \frac{t}{t_{\text{peak}}} \exp\left(1 - \frac{t}{t_{\text{peak}}}\right),$$

where h_{peak} is the peak EPSP magnitude and t_{peak} is the corresponding time-to-peak. We assume that the postsynaptic responses to a sequence of vesicle releases add linearly. We incorporate synaptic variability by multiplying the response $h(t)$ by a random variable q drawn from a probability distribution $P(q)$ which can be measured empirically. Thus, q models the trial-to-trial variability in the amplitude of the postsynaptic responses observed for central neurons. Experimentally observed amplitude distributions are generally skewed towards higher amplitudes though the experimental difficulties of measuring very small synaptic events probably also contributes to these findings (Bekkers & Stevens, 1996). Here we model $P(q)$ by a Gamma distribution,

$$P(q) = a \frac{(aq)^{J-1}}{(J-1)!} \exp(-aq),$$

where J is the order of the distribution. However, it can be replaced by any one-sided probability density¹ for the purpose of subsequent analysis. a and J together determine

¹Here we assume that q is a non-negative random variable; inhibitory synapses can be analyzed identically by reversing the sign of $h(t)$.

the spread of the distribution. \bar{q} denotes the mean and σ_q denotes the standard deviation of the quantal amplitude q .

$$\bar{q} = \frac{J}{a}, \quad \sigma_q = \frac{\sqrt{J}}{a}.$$

The coefficient-of-variance (denoted by CV_q) is a measure of the amplitude variability and is given by

$$CV_q = \frac{\sigma_q}{\bar{q}} = \frac{1}{\sqrt{J}}.$$

Thus, J can be used to modify the variability of q . $J = 1$ corresponds to an exponential distribution which has the highest variability ($CV_q = 1$) and at the other extreme $J = \infty$ corresponds to a delta function for which there is no uncertainty in q ($CV_q = 0$).

In addition to these two sources of noise, we also assume that the postsynaptic membrane voltage is corrupted by additive, Gaussian noise $n(t)$ which models the effect of other membrane noise sources like thermal noise, channel noise, background synaptic noise from other synapses and so on (DeFelice, 1981). We denote the power spectral density of $n(t)$ by $S_{nn}(f)$. We assume that $n(t)$ is band-limited (over a bandwidth B_n),

$$\begin{aligned} S_{nn}(f) &= \frac{\sigma_n^2}{2B_n} & -B_n \leq f \leq B_n \\ &= 0 & \text{otherwise,} \end{aligned} \tag{2.1}$$

where σ_n^2 is the variance of $n(t)$. We define a signal-to-noise ratio SNR for the synapse as

$$SNR = \frac{1}{S_{nn}(f)} \int_0^\infty dt h^2(t) = \frac{2B_n}{\sigma_n^2} \int_0^\infty dt h^2(t). \tag{2.2}$$

We have mathematically modeled a cortical synapse as a binary channel in cascade with a random amplitude filter and an additive Gaussian noise source (see **Fig. 2.1**). We ignore history-dependent effects (paired-pulse facilitation, vesicle depletion, calcium buffering and so on) on synaptic transmission which endow central synapses with characteristics of sophisticated nonlinear filters (Markram & Tsodyks, 1996; Abbott *et al.*, 1997). This implies that the synaptic parameters in our model are constants.

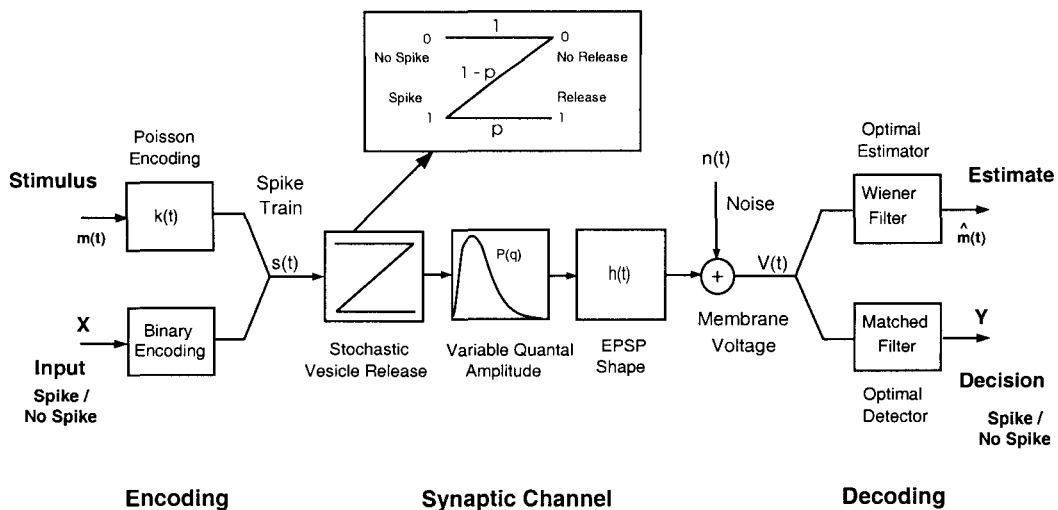


Figure 2.1: **Schematic Block Diagram of a Synapse under Signal Estimation and Signal Detection Paradigms.**

A cortical synapse is modeled as a binary channel followed by a filter $h(t)$. The amplitude of the filter is a random variable q which has probability density $P(q) = a(aq)^{J-1} \exp(-aq)/(J-1)!$. The binary channel (inset, $p = \text{Prob}[\text{vesicle release}]$, $1-p = \text{Prob}[\text{failure}]$) models probabilistic vesicle release and the random variable q models the variability in the size of the postsynaptic response of a single quantum observed in central synapses. The EPSP is approximated by an alpha function $h(t) = h_{\text{peak}} t/t_{\text{peak}} \exp(1-t/t_{\text{peak}})$. $n(t)$ denotes additive postsynaptic voltage noise which is assumed to be Gaussian and white (over bandwidth B_n). In signal estimation, the objective is to optimally estimate a continuous input $m(t)$ from the postsynaptic membrane voltage $V_m(t)$. This estimate is denoted by $\hat{m}(t)$. The presynaptic spike train $s(t)$ is assumed to be a Poisson process with firing rate modulated by the random input $m(t)$. Performance of the optimal linear estimator (Wiener filter) is used to quantify performance in the estimation task. In signal detection, the objective is to optimally detect the presence of a single presynaptic action potential on the basis of $V_m(t)$. Thus, the input X and the decision Y are binary variables. Performance of the optimal detector (Matched filter) quantifies performance in signal detection.

We derive closed-form expressions which provide lower-bounds on the capacity of this simple model of synaptic transmission under the two representational paradigms, *signal detection* and *signal estimation*. In signal estimation, the signal is assumed to be encoded in the mean firing rate of the presynaptic neuron and the objective is to estimate the continuous input signal from the postsynaptic voltage. In signal detection, the input is binary, and the presence or absence of a presynaptic action potential is to be detected from the postsynaptic voltage. The efficacy of information transfer in synaptic transmission is characterized by deriving optimal strategies under these two paradigms.

2.4 The Signal Estimation Paradigm

Let $m(t)$ be a zero-mean random stimulus presented to a presynaptic neuron and $s(t)$ the resulting spike train. $s(t)$ is modeled as point-process or as a sequence of delta functions

$$s(t) = \sum_i \delta(t - t_i),$$

where t_i denotes the time when the i^{th} spike occurs. We assume that $m(t)$ and $s(t)$ are (real-valued) jointly weak-sense stationary (WSS) processes with finite variances, $\langle m^2(t) \rangle = \sigma_m^2 < \infty$, $\langle |s(t) - \bar{\lambda}|^2 \rangle < \infty$, where $\bar{\lambda} = \langle s(t) \rangle$ is the mean firing rate of the presynaptic neuron. In these equations, $\langle \cdot \rangle$ denotes an ensemble average over the joint stimulus and spike train distribution. The membrane voltage $V_m(t)$ at the postsynaptic site due to the transmission of the spike train $s(t)$ across the synapse is

$$V_m(t) = \sum_i q_i W_i h(t - t_i) + n(t), \quad (2.3)$$

where q_i is the EPSP amplitude in response to the i^{th} spike and W_i is a binary variable which represents vesicle release. Thus, $W_i = 0$ implies that the i^{th} presynaptic action potential did not lead to a vesicle release, whereas, $W_i = 1$ denotes a successful release. The mean voltage $\langle V_m(t) \rangle$ does not contain any information about the input $m(t)$ and can be ignored.

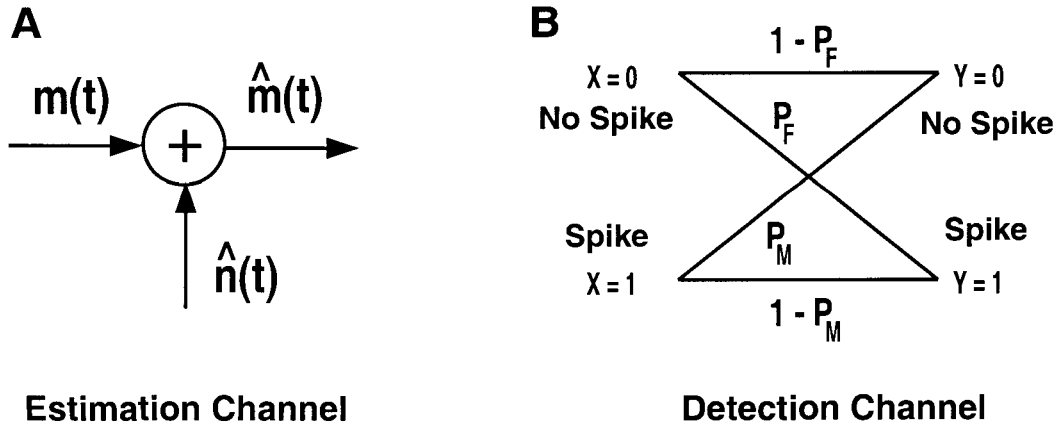


Figure 2.2: Channel Models of Synaptic Transmission under Signal Estimation and Signal Detection.

A: Effective channel model of the synapse for the signal estimation paradigm. The random stimulus $m(t)$ is the continuous input to the channel, and $\hat{m}(t)$ is the best linear estimate of the input based on the postsynaptic voltage (**Fig. 2.1**). The effective reconstruction noise $\hat{n}(t)$ is the difference between the input and the estimate, $\hat{n}(t) = m(t) - \hat{m}(t)$. **B:** Effective channel model of the synapse for the signal detection paradigm. X and Y are binary random variables corresponding to the input and the decision respectively. The false alarm and the miss probabilities (P_F and P_M respectively) which minimize the detection error P_e are the cross-over error rates of the binary detection channel.

Let $v(t)$ refers to a zero-mean process obtained by subtracting the mean voltage from $V_m(t)$,

$$v(t) = V_m(t) - \langle V_m(t) \rangle . \quad (2.4)$$

We further assume that the spike train $s(t)$ of the presynaptic neuron is a Poisson process with a mean firing rate $\lambda(t)$ which is a function of the stimulus $m(t)$

$$\lambda(t) = \langle s(t) \rangle_{s|m} = f(k(t) \star m(t)) , \quad (2.5)$$

where $\langle \cdot \rangle_{s|m}$ denotes an ensemble average over the spike train distribution for a fixed value of the stimulus $m(t)$. Since the stimulus itself is a stochastic (Gaussian) process, the spike train $s(t)$ is called a *doubly stochastic* Poisson process. Although, in general, the Poisson assumption is not strictly valid for neural spike trains, it is fairly common in theoretical neuroscience as it allows for derivation of closed-form analytical expressions (Gabbiani, 1996; Gabbiani & Koch, 1996).

$k(t)$ is a phenomenological filter which models the transformation of the stimulus modulations $m(t)$ into the neuron's firing rate and $f(\cdot)$ is a static, memoryless non-linearity which incorporates the non-linear aspects of the neuron's input-output transformation, like half-wave rectification, saturation and so on. The exact form of $k(t)$ is not important, although, in order to derive closed-form expression later, we will assume that $k(t)$ has the form of a simple low-pass filter.

For simplicity, here we assume that the input-output transformation is linear, $f(x) = \bar{\lambda} + x^2$. The power spectrum of the spike train $s(t)$ can be expressed as

$$S_{ss}(f) = \bar{\lambda} + |K(f)|^2 S_{mm}(f) , \quad (2.6)$$

where $\bar{\lambda}$ is the mean firing rate and $K(f)$ is the Fourier transform of the filter $k(t)$. The variance of the firing rate σ_λ^2 is given by

$$\sigma_\lambda^2 = \int_{-\infty}^{\infty} df |K(f)|^2 S_{mm}(f) . \quad (2.7)$$

²We assume that $\bar{\lambda}$ is high enough so that the probability of $\lambda(t) < 0$ is negligible.

We define the “contrast” of the firing rate as $c_\lambda = \sigma_\lambda/\bar{\lambda}$. The positivity of $\lambda(t)$ imposes a restriction on how large the contrast can be. For linear encoding we will require that the mean firing rate be at least three times as large as the standard deviation of the firing rate fluctuations, ensuring that the probability that $\lambda(t)$ is negative is less than 0.01. This implies that $c_\lambda \leq 1/3$. Refer to Appendix I for the extension of the analysis to other non-linear encoding schemes. The presynaptic spike train is gated by a binary process corresponding to the stochastic vesicle release mechanism. Thus, the vesicle release is a Poisson process with rate $p\lambda(t)$ and $v(t)$ is a filtered shot noise process (equation 2.3). The power spectrum of the post-synaptic voltage is denoted by $S_{vv}(f)$ and is given by

$$S_{vv}(f) = |H(f)|^2 \left[(\bar{q}^2 + \sigma_q^2) p \bar{\lambda} + \bar{q}^2 p^2 |K(f)|^2 S_{mm}(f) \right] + S_{nn}(f). \quad (2.8)$$

The cross-spectral density between the post-synaptic membrane voltage and the input is denoted by $S_{vm}(f)$ and is given by

$$S_{vm}(f) = \bar{q} p S_{mm}(f) H(f) K(f). \quad (2.9)$$

The objective in signal estimation paradigm is to find the optimal estimator of $m(t)$ from the postsynaptic voltage $v(t)$, where optimality is in the sense of least mean-square-error (MSE). In general, the optimal MSE estimator is non-linear and complicated to treat analytically. Instead, we restrict ourselves to the optimal linear estimation. The solution of the optimal linear estimation problem is presented in Appendix A. We use the results derived therein to obtain the corresponding expressions here with the modification that the output process here is the postsynaptic membrane voltage and is denoted by $v(t)$. Using equations A9, 2.8 and 2.9, the coding fraction can be expressed as

$$\xi = \frac{1}{\sigma_m^2} \int_S df \frac{[S_{mm}(f)]^2}{S_{mm}(f) + S_{neff}(f)}, \quad (2.10)$$

where

$$S_{\text{neff}}(f) = \frac{\bar{\lambda}(1 + CV_q^2)}{p|K(f)|^2} + \frac{S_{\text{nn}}(f)}{p^2 \bar{q}^2 |H(f)|^2 |K(f)|^2}. \quad (2.11)$$

Using equation A7, the power spectrum of the reconstruction noise $\hat{n}(t)$ can be written as

$$S_{\hat{n}\hat{n}}(f) = \frac{S_{\text{mm}}(f) S_{\text{neff}}(f)}{S_{\text{mm}}(f) + S_{\text{neff}}(f)}. \quad (2.12)$$

Synaptic transmission is ideal when the vesicle release is perfectly reliable, there is no variability in the EPSP amplitude and membrane noise at the postsynaptic site is negligible ($p = 1$, $CV_q = 0$, $\sigma_n = 0$); the coding fraction corresponding to this ideal case is denoted by ξ^* , where

$$\xi^* = \frac{1}{\sigma_m^2} \int_S df \frac{|K(f)|^2 S_{\text{mm}}^2(f)}{|K(f)|^2 S_{\text{mm}}(f) + \bar{\lambda}}. \quad (2.13)$$

In general, even for perfect synaptic transmission, $\xi^* < 1$ due to the stochastic Poisson nature of the spike train. For the parameter values we consider here (summarized in the caption of **Fig. 2.3**), the second term in equation 2.11 can be neglected. The dominant first term in equation 2.11 indicates that signal estimation is limited by shot noise, *i.e.*, the inability to estimate the stimulus reliably is primarily due to the error in accurately estimating the firing rate of the neuron. It can be shown that for a fixed firing rate contrast, as $\bar{\lambda} \rightarrow \infty$, $\xi \rightarrow 1$. In other words, perfect reconstruction takes place in the limit of infinite firing rates. This agrees well with intuition, since the stimulus modulations are linearly encoded in the firing rate $\lambda(t)$, an accurate estimate of $\lambda(t)$ can be deconvolved to recover the input. Thus, for the signal estimation task, synaptic unreliability and variability make it harder to estimate the firing rate from the postsynaptic voltage. As compared to the ideal case, the shot noise for a single synapse increases by a factor

$$\kappa = \frac{1 + CV_q^2}{p}.$$

To illustrate these results, we now apply them to a specific example modified from Gabbiani, (1996). Let $m(t)$ be a white, band-limited signal over a bandwidth B_m ,

$$\begin{aligned} S_{mm}(f) &= \frac{\sigma_m^2}{2B_m}, & -B_m \leq f \leq B_m, \\ &= 0 & \text{otherwise.} \end{aligned} \quad (2.14)$$

If $k(t)$ is modeled as a simple low-pass filter, $k(t) = A \exp(-t/\tau)$,

$$|K(f)|^2 = \frac{A^2 \tau^2}{1 + (2\pi f \tau)^2}.$$

Using the above quantities, a closed-form expression for the coding fraction (denoted by ξ_{lp}) can be obtained (Gabbiani, 1996),

$$\xi_{lp} = \frac{\gamma}{\theta \sqrt{1+\gamma}} \tan^{-1} \left(\frac{\theta}{\sqrt{1+\gamma}} \right), \quad (2.15)$$

where

$$\begin{aligned} \theta &= 2\pi B_m \tau, \\ \gamma &= \frac{c_\lambda^2 \bar{\lambda} \pi \tau}{\kappa \tan^{-1} \theta}. \end{aligned}$$

θ is the ratio of the signal bandwidth to the filter's bandwidth and γ is the effective number of spikes available per unit signal bandwidth. As in Gabbiani (1996), one can also derive the optimal encoding filter which maximizes the coding fraction for a given stimulus power spectrum $S_{mm}(f)$ under the constraint that the variance of the mean firing rate σ_λ^2 is fixed,

$$|K(f)|^2 = \frac{\sigma_\lambda^2}{\sigma_m^2}, \quad -B_m \leq f \leq B_m.$$

The coding fraction corresponding to the optimal filter above (denoted by ξ_{opt}) is given by

$$\xi_{opt} = \left(1 + \frac{2\kappa B_m}{c_\lambda^2 \bar{\lambda}} \right)^{-1}. \quad (2.16)$$

Similarly, the lower bound for the low-pass filter I_{LB} can be obtained as

$$I_{\text{LB}} = \frac{1}{2\pi\tau \ln(2)} \left[\theta \ln \left(1 + \frac{\gamma}{1 + \theta^2} \right) + 2\sqrt{1 + \gamma} \tan^{-1} \left(\frac{\theta}{\sqrt{1 + \gamma}} \right) - 2 \tan^{-1} \theta \right]. \quad (2.17)$$

In the equation above \ln refers to the natural logarithm. The lower bound corresponding to the optimal encoding filter is given by

$$I_{\text{LB}} = B_m \log_2 \left(1 + \frac{c_\lambda^2 \bar{\lambda}}{2\kappa B_m} \right), \quad (2.18)$$

$$= -B_m \log_2(1 - \xi_{\text{opt}}). \quad (2.19)$$

Notice that when $\theta \ll 1$, $\xi_{\text{lp}} \rightarrow \xi_{\text{opt}}$ and the lower bound on the information rate I_{LB} for the low-pass filter and the optimal filter converge. Plots of ξ and I_{LB} as functions of the mean firing rate $\bar{\lambda}$ and the input bandwidth B_m are shown in **Fig. 2.3**. It can be observed that ξ increases with $\bar{\lambda}$ and decreases with B_m . This can be understood as follows: $\bar{\lambda}/B_m$ denotes the average number of spikes available in the ideal case to estimate the mean firing rate of the spike train (thus the input) over a time period ($1/B_m$) during which the input is relatively stationary. The fewer the number of spikes available, the poorer the estimate and lower the coding fraction. On the other hand, I_{LB} increases with $\bar{\lambda}$ and increases with B_m for low B_m but saturates at high B_m . This is because the decrease in the quality of estimation (ξ decreases with B_m) is compensated by an increase in the number of independent samples ($2B_m$) transmitted per second. This can be observed by taking the limit $\bar{\lambda} \rightarrow 0$ (equivalently, $B_m \rightarrow \infty$) in equation 2.18,

$$\lim_{\bar{\lambda} \rightarrow 0} I_{\text{LB}} = \frac{B_m}{\ln 2} \frac{c_\lambda^2 \bar{\lambda}}{2\kappa B_m} = \frac{1}{\ln 2} \frac{c_\lambda^2 \bar{\lambda}}{2\kappa},$$

which is independent of B_m . We refer to this condition as the low signal-to-noise regime.

The information transmitted per spike is given by

$$\lim_{\bar{\lambda} \rightarrow 0} \frac{I_{\text{LB}}}{\bar{\lambda}} = \frac{c_\lambda^2}{2\kappa \ln 2}.$$

Notice that the maximum information per spike depends only on the contrast c_λ of the firing rate modulations and the factor κ . In the case of an ideal synapse, the maximum information per spike is around 0.08 bits/spike for $c_\lambda = 1/3$. For a noisy synapse, the maximum information per spike decreases by a factor of κ . However, if we assume that the signal is encoded by a pair of half-wave rectifying neurons each representing one-half (positive/negative) of the input $m(t)$ as in (Gabbiani, 1996; Gabbiani & Koch, 1996), the maximum amount of information that can be transmitted by an ideal synapse is approximately equal to 1.13 bits/spike. This corresponds to $c_\lambda = \sqrt{\pi/2}$ (roughly 1.25). Thus, the low information rates we obtain here are a consequence of our assumption of linear encoding, which limits the magnitude of the firing rate contrast. Nevertheless, the analysis can be readily extended (see Appendix I) to include other encoding schemes (integrate and fire models, non-linear Poisson encoding models with sigmoidal, half-wave rectification and other nonlinearities, and so on) which yield qualitatively similar results to those obtained here.

The analysis can be generalized to the case of multiple independent synaptic connections between two neurons. Let N_{syn} denote the number of parallel synaptic connections between two neurons which can occur in the form of N_{syn} independent release sites driven by the same presynaptic process at the same postsynaptic location or as multiple synapses made at different locations. In either case it is assumed that the vesicle release at a given synapse is statistically independent of the release at other synapses. However, this does not imply that the EPSP waveforms corresponding to the different synapses are independent. In fact, EPSPs are correlated since they are driven by the same presynaptic spike train $s(t)$. The postsynaptic membrane voltage can be written as

$$V_m(t) = \sum_{l=1}^{N_{\text{syn}}} \sum_i q_i^l W_i^l h^l(t - t_i) + n(t), \quad (2.20)$$

where the superscript l refers to the l^{th} synaptic connection. As before we define $v(t) = V_m(t) - \langle V_m(t) \rangle$. If the synapses are distributed at different electrotonic locations on the postsynaptic neuron, the corresponding EPSP waveforms $h^l(t)$ are different. Similarly, if

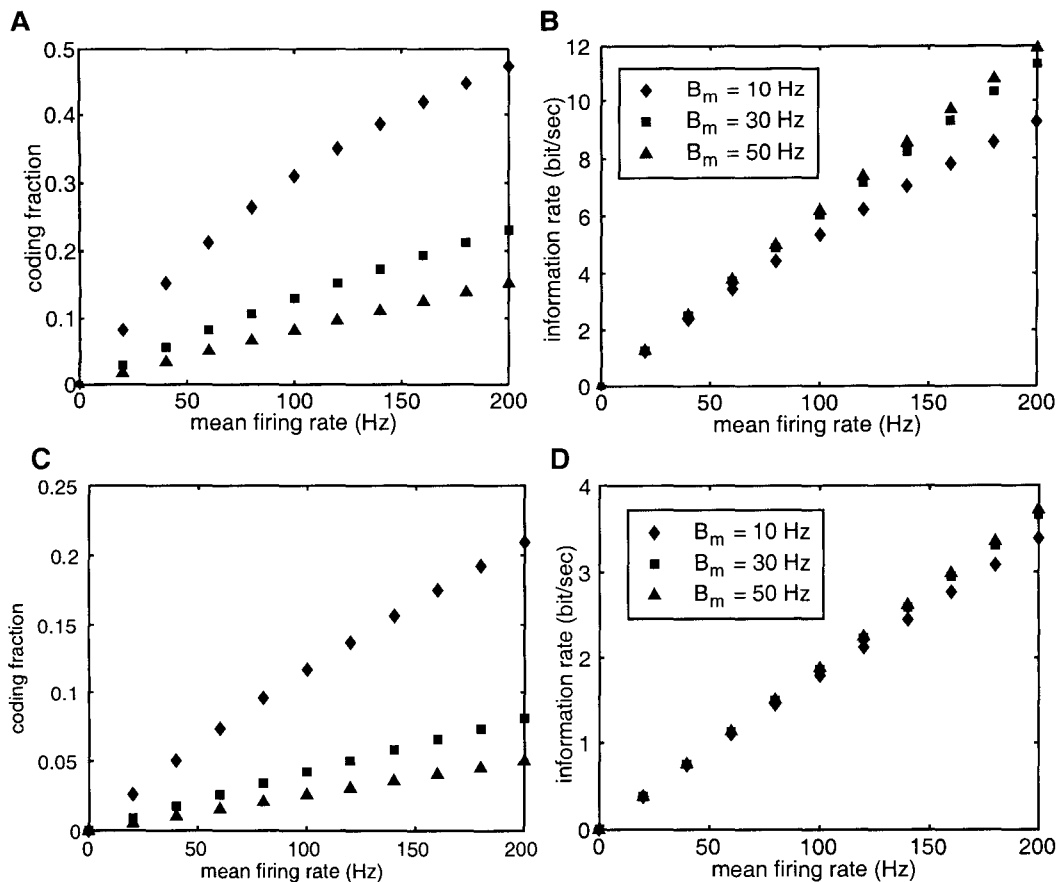


Figure 2.3: Performance in the Signal Estimation Paradigm.

A: The coding fraction ξ and **B:** the lower bound on information rate I_{LB} as a function of the mean firing rate $\bar{\lambda}$ for different stimulus bandwidths B_m for an ideal synapse ($p = 1$, $CV_q = 0$). **C** and **D** show the corresponding ξ and I_{LB} for a single unreliable and noisy synapse. We report the estimation performance for the optimal filter given by equation 2.16 and equation 2.18. Parameters are loosely based on those reported for cortical synapses: $\tau = 20$ msec, $c_\lambda = 0.3$, $p = 0.4$, $CV_q = 0.6$, $h_{peak} = 1$ mV, $t_{peak} = 0.5$ msec, $\sigma_n = 0.1$ mV, $B_n = 100$ Hz.

the release properties across the synaptic population are non-uniform (Rosenmund *et al.*, 1993; Dobrunz & Stevens, 1997), the random variables (q_i^l, W_i^l) are governed by different distributions. However, for the sake of analytical tractability, we assume that the synapses are identical and are at the same electrotonic location. For the parameter values we consider here, the effect of the post-synaptic voltage noise $n(t)$ is negligible and it can be shown that the shot noise increases from the ideal case by a factor,

$$\kappa_N = \frac{1}{N_{\text{syn}}} \frac{1 + CV_q^2}{p} + \frac{N_{\text{syn}} - 1}{N_{\text{syn}}}. \quad (2.21)$$

The details of this derivation are provided in Appendix B. In the limit of a large number of synapses ($N_{\text{syn}} \rightarrow \infty$), $\kappa_N \rightarrow 1$. Thus, the effect of synaptic unreliability and variability can be offset by redundancy in the number of synaptic connections between neurons. Plots of the coding fraction and the information rate for the signal estimation task as a function of the number of parallel synapses are shown in **Fig. 2.4**. Thus, though a single synapse has very low capacity, a small amount of redundancy causes a considerable increase in performance.

2.5 The Signal Detection Paradigm

We now consider the problem of detecting the presence of a presynaptic action potential from measurements of membrane voltage at the postsynaptic site. The problem we consider here has two possibilities, the absence or presence of a presynaptic spike within a fixed temporal window. In our problem, the corresponding postsynaptic voltage waveform $V_m(t)$, measured over a period $0 \leq t \leq T$, corresponds to either the noise process $n(t)$ (denoted by hypothesis H_0) or to a noisy version of the EPSP $h(t)$ gated by stochastic vesicle release W (denoted by hypothesis H_1). Let X and Y be binary variables denoting occurrence of a presynaptic spike and the decision respectively. Thus, $X = 1$ if a spike occurred, else $X = 0$. Similarly, $Y = 1$ expresses the decision that a spike occurred. The binary signal detection problem

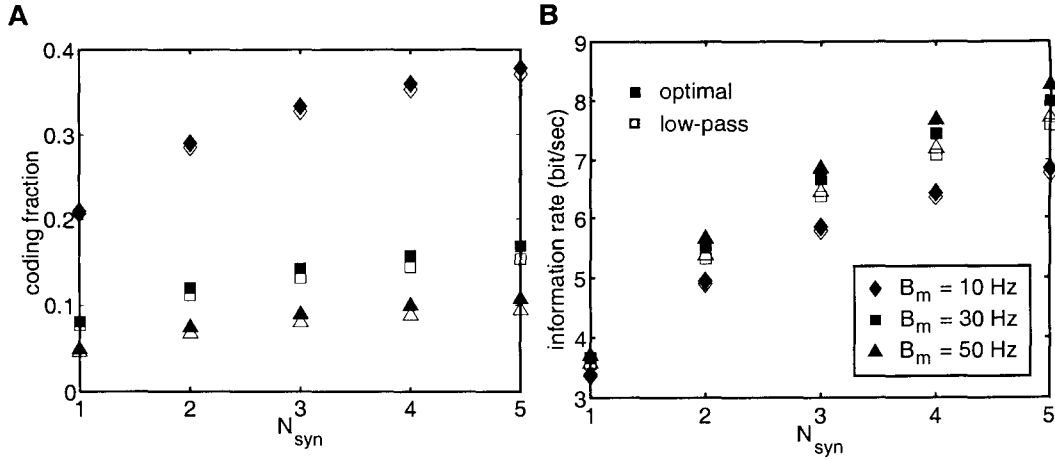


Figure 2.4: **Effect of Redundancy on Estimation Performance.**

A: The coding fraction ξ and **B:** the information rate I_{LB} in signal estimation as a function of the number of parallel, identical synaptic connections N_{syn} between a presynaptic and a postsynaptic neuron. The empty symbols correspond to performance in the presence of the low-pass filter, whereas, the solid symbols correspond to the optimal encoding filter. There is little difference in estimation performance when $k(t)$ (**Fig. 2.1**) is chosen to be a low-pass filter and an optimal encoding filter matched to the stimulus. The performance saturates at high N_{syn} as it approaches the performance of an ideal synapse ($p = 1$, $CV_q = 0$). The mean firing rate $\bar{\lambda}$ is 200 Hz. Other parameter values used are summarized in the caption of **Fig. 2.3**.

can be formally expressed as

$$\begin{aligned} \mathbf{H}_0 : V_m(t) &= n(t), && \text{Noise} \\ \mathbf{H}_1 : V_m(t) &= qW h(t) + n(t), && \text{Signal + Noise} \end{aligned}$$

where q is the random EPSP amplitude and W is a binary variable representing the spike-conditioned vesicle release process. Thus, the goal is to design an optimal decision rule that minimizes the probability of error of detecting the presynaptic spike from the postsynaptic membrane voltage. The false alarm (F) and miss probabilities (M) are defined as

$$P_F = \text{Prob}[Y = 1 | X = 0], \quad P_M = \text{Prob}[Y = 0 | X = 1].$$

The probability of detection error P_e is given by

$$P_e = p_0 P_F + (1 - p_0) P_M, \quad (2.22)$$

where p_0 and $1 - p_0$ are prior probabilities of occurrence of H_0 and H_1 respectively. The solution of the signal detection problem has been presented in Appendix C. By analogy, the membrane voltage $V_m(t)$ here corresponds to the signal $s(t)$. Thus, the decision rule which minimizes P_e is given by

$$\begin{aligned} \mathcal{L}(V) \geq 1 &\Rightarrow Y = 1 \\ \mathcal{L}(V) < 1 &\Rightarrow Y = 0, \end{aligned}$$

which can be written as

$$\begin{aligned} \Lambda_X(V) \geq \mathcal{L}_0^{-1} &\Rightarrow Y = 1 \\ \Lambda_X(V) < \mathcal{L}_0^{-1} &\Rightarrow Y = 0. \end{aligned} \quad (2.23)$$

Using Bayes' rule, the spike conditional probabilities of the membrane voltage can be expressed in terms of release conditional probabilities as

$$\begin{aligned}\text{Prob}[V | X = 1] &= p \text{Prob}[V | W = 1] + (1 - p) \text{Prob}[V | W = 0] \\ \text{Prob}[V | X = 0] &= \text{Prob}[V | W = 0].\end{aligned}$$

As before, it is assumed that the spontaneous release probability is zero. The likelihood ratio $\Lambda_X(V)$ can be expressed as

$$\Lambda_X(V) = p \Lambda_W(V) + (1 - p),$$

where

$$\Lambda_W(V) = \frac{\text{Prob}[V | W = 1]}{\text{Prob}[V | W = 0]}.$$

In terms of Λ_W , the optimal decision rule in equation 2.23 is given by

$$\begin{aligned}\Lambda_W(V) \geq \frac{(\mathcal{L}_0^{-1} - 1 + p)}{p} &\Rightarrow Y = 1 \\ \Lambda_W(V) < \frac{(\mathcal{L}_0^{-1} - 1 + p)}{p} &\Rightarrow Y = 0.\end{aligned}\tag{2.24}$$

In the event of a vesicle release, the amplitude of the EPSP is a random variable drawn from a probability distribution $P(q)$, which allows us to write $\Lambda_W(V)$ as

$$\Lambda_W(V) = \int dq P(q) \frac{\text{Prob}[V | q; W = 1]}{\text{Prob}[V | W = 0]},\tag{2.25}$$

where $\text{Prob}[V | q; W = 1]$ is the probability distribution of the postsynaptic voltage conditioned on the quantal amplitude of a spike-triggered vesicle release. If $n(t)$ is a white Gaussian noise process with a sufficiently large bandwidth B_n which satisfies $B_n t_{\text{peak}} \gg 1$, equation 2.25 can be simplified as (Helstrom, 1968),

$$\Lambda_W(V) = \int dq P(q) \exp\left(2 q r_T \sqrt{SNR_T} - q^2 SNR_T\right),$$

where

$$SNR_T = \frac{1}{S_{nn}(f)} \int_0^T dt h^2(t), \quad r_T = \frac{\int_0^T dt h(t) V_m(t)}{\sqrt{S_{nn}(f) \int_0^T dt h^2(t)}}.$$

The temporal support of $h(t)$ is very small (on the order of a few milliseconds) and so SNR_T quickly saturates with T . Thus, when the interval length T is greater than a few milliseconds (which we shall assume here), the upper limit T in the integrals above can be replaced with ∞ . Thus,

$$\begin{aligned} \lim_{T \rightarrow \infty} SNR_T &= SNR = \frac{1}{S_{nn}(f)} \int_0^\infty dt h^2(t), \\ \lim_{T \rightarrow \infty} r_T &= r = \frac{\int_0^\infty dt h(t) V_m(t)}{\sqrt{S_{nn}(f) \int_0^\infty dt h^2(t)}}. \end{aligned}$$

When q is a one-sided random variable (here q is positive), it can be shown that Λ_W is a monotonic function of r . Thus, the decision rule in equation 2.24 reduces to

$$\begin{aligned} r \geq \Theta &\Rightarrow Y = 1, \\ r < \Theta &\Rightarrow Y = 0, \end{aligned} \tag{2.26}$$

where the threshold Θ depends on \mathcal{L}_o , p , $P(q)$ and so on. Thus, the optimal decision rule involves comparing the correlation, r between $V_m(t)$ and $h(t)$, to a threshold Θ and deciding $Y = 1$ if r exceeds the threshold and $Y = 0$ otherwise. The error probabilities (P_F and P_M) can be written as

$$\begin{aligned} P_F &= \text{Prob}[r \geq \Theta | X = 0] = \text{Prob}[r \geq \Theta | W = 0], \\ P_M &= \text{Prob}[r < \Theta | X = 1], \\ &= p \text{Prob}[r < \Theta | W = 1] + (1 - p) \text{Prob}[r < \Theta | W = 0]. \end{aligned}$$

Let P_F^0 ($\text{Prob}[r \geq \Theta | W = 0]$) and P_M^0 ($\text{Prob}[r < \Theta | W = 1]$) denote the corresponding errors when the vesicle release is deterministic and no spontaneous release occurs. P_F and

P_M can be expressed in terms of P_F^0 and P_M^0 as

$$P_F = P_F^0, \quad P_M = P_M^0 + (1 - p)(1 - P_M^0 - P_F^0). \quad (2.27)$$

When the postsynaptic noise $n(t)$ is negligible ($SNR \rightarrow \infty$), both the conditional errors P_F^0 and $P_M^0 \rightarrow 0$. However, in the limit of no postsynaptic voltage noise, $P_M \rightarrow (1 - p)$ due to the unreliability of vesicle release. Let $P_e^* = (1 - p_0)(1 - p)$ denotes the minimum possible detection error when $SNR \rightarrow \infty$. The probability of error P_e can be written as

$$P_e = P_e^* + P_F^0 [p_0 - (1 - p_0)(1 - p)] + P_M^0 (1 - p_0)p. \quad (2.28)$$

Since r is a conditional Gaussian random whose distribution depends on the value of the release variable W , the conditional means and variances of r can be derived as

$$\begin{aligned} \langle r \rangle_0 &= 0, & \langle r \rangle_{1,q} &= q\sqrt{SNR}, \\ \langle r^2 \rangle_0 &= \left\langle (r - q\sqrt{SNR})^2 \right\rangle_{1,q} = 1, \end{aligned}$$

where $\langle \cdot \rangle_0$ denotes an ensemble average conditioned on $W = 0$ and $\langle \cdot \rangle_{1,q}$ denotes an ensemble average conditioned on $W = 1$ and amplitude q . Thus, P_F^0 and P_M^0 can be parametrically expressed in terms of the threshold Θ ,

$$P_F^0 = \frac{1}{2} [1 - \text{Erf}(\Theta)], \quad P_M^0 = \frac{1}{2} \left[1 + \int_0^\infty dq P(q) \text{Erf} \left(\Theta - q\sqrt{SNR} \right) \right], \quad (2.29)$$

where $\text{Erf}(x)$ is the error function defined as $\text{Erf}(x) = 2/\sqrt{\pi} \int_0^x dt \exp(-t^2)$.

In general, it is not possible to derive closed-form expressions for P_M^0 . Both P_F^0 and P_M^0 depend on the choice of the threshold Θ ; if Θ is large, P_F^0 is low but P_M^0 is high, whereas if Θ is small, P_M^0 is low but P_F^0 is high. Thus as Θ is varied, the probability of error P_e goes through a minimum. By plotting P_e as a function of the threshold, we can graphically obtain the optimal value of Θ which minimizes P_e (**Fig. 2.5**). We can model the detection task as a binary information channel with the binary variable X as its input and the decision

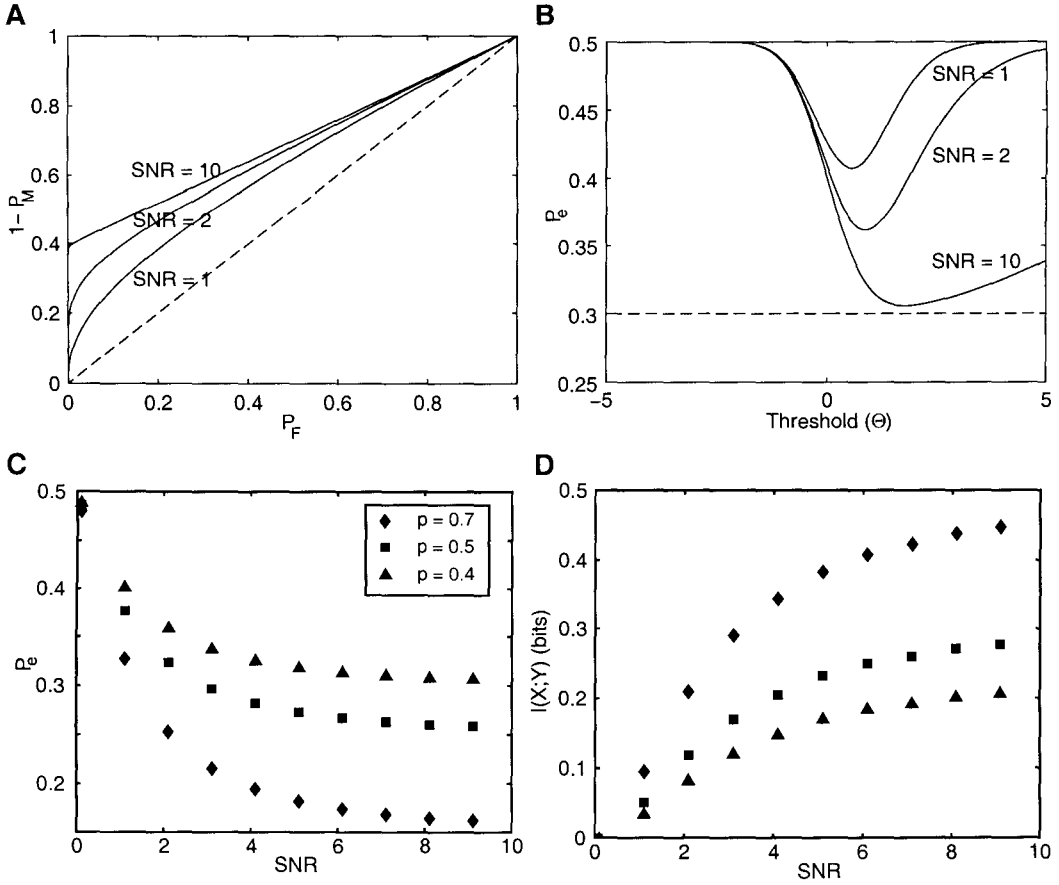


Figure 2.5: **Performance in the Signal Detection Paradigm.**

A: Plot of detection error ($1 - P_M$) vs. false alarm error P_F for a single synapse as the threshold Θ , used to detect a presynaptic action potential, is varied from $-\infty$ to ∞ . The curves correspond to different values of the signal-to-noise ratio SNR, a measure of the size of the EPSP peak relative to the post-synaptic noise magnitude. The dashed diagonal line corresponds to chance performance (SNR = 0). Parameters: $p = 0.4$. See below for a summary of the other parameters. **B:** Probability of error $P_e = 0.5P_F + 0.5P_M$ (prior probability of a spike $p_0 = 0.5$) plotted against Θ to determine the optimal value of the threshold which minimizes P_e . The dashed horizontal line corresponds to the minimum possible detection error for the synaptic parameters in the limit $\text{SNR} \rightarrow \infty$. **C:** Plot of the optimal P_e vs. SNR for different values of the synaptic release probability p . The optimal P_e for a given SNR is given by the minimum of the corresponding curve in (B). The curves saturate at high SNR to their minimum values $P_e^* = (1 - p_0)(1 - p)$. **D:** Plot of the mutual information $I(X;Y)$ in the detection task as a function of SNR. Parameter values used: $\bar{q} = 1$, $CV_q = 0.6$, $h_{\text{peak}} = 2$ mV, $t_{\text{peak}} = 1$ msec, $B_n = 100$ Hz.

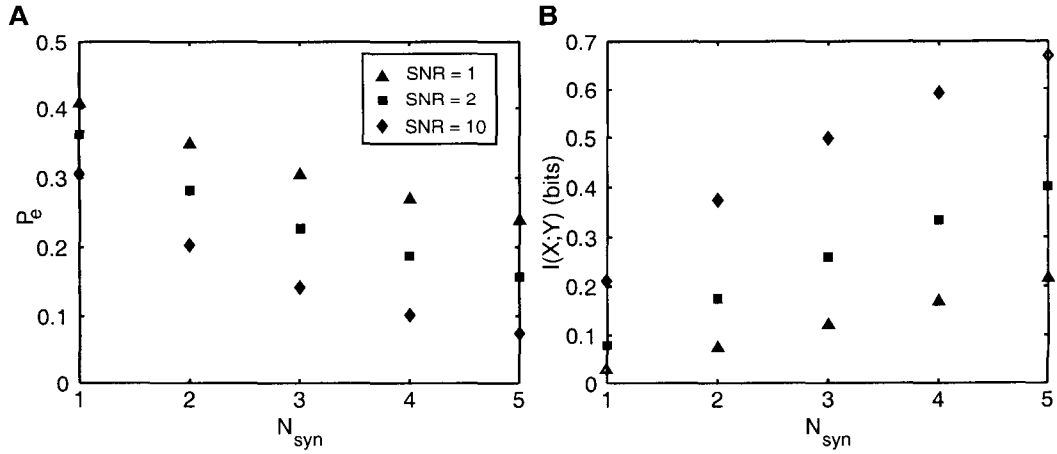


Figure 2.6: **Effect of Redundancy on Detection Performance.**

A: Probability of error P_e and **B:** the mutual information between X and Y $I(X;Y)$ as a function of the number of synapses N_{syn} for the signal detection task for different values of SNR. Synaptic parameters: $p = 0.4$, other parameters are summarized in the caption of **Fig. 2.5**.

Y as the output. The error probabilities P_F and P_M denote the cross-over probabilities of the binary channel shown in **Fig. 2.2B**. Performance in the detection task can be quantified either by P_e or the mutual information between the binary random variables, X and Y , denoted by $I(X; Y)$. The synapse is ideal when $P_e = 0$ and $I(X; Y) = 1$ bit, and at chance, when $P_e = 0.5$ and $I(X; Y) = 0$ bits. $I(X; Y)$ can be computed using the formula for the mutual information for a binary channel (Cover & Thomas, 1991),

$$I(X; Y) = \mathcal{H}(P_Y) - p_0 \mathcal{H}(P_F) - (1 - p_0) \mathcal{H}(P_M), \quad (2.30)$$

where $P_Y = p_0(1 - P_F) + (1 - p_0)P_M$ and $\mathcal{H}(x) = -x \log_2(x) - (1 - x) \log_2(1 - x)$ is the binary entropy function (Cover & Thomas, 1991).

The analysis can be generalized to the case of N_{syn} independent parallel synapses (Appendix C). Plots of P_e and $I(X; Y)$ versus N_{syn} for different values of SNR for the case of identical synapses are shown in **Fig. 2.6A** and **Fig. 2.6B** respectively. Once again, we observe the poor performance of a single synapse and the substantial improvement due to anatomical redundancy. The linear increase of I with N_{syn} is similar to the result obtained for signal estimation.

2.6 Discussion

We formulated a simple mathematical model of a cortical synapse which incorporates the known unreliable and variable nature of central synapses. By assessing the performance of this model in the signal estimation and signal detection tasks, we showed that a single synapse (meant to mimic a central synapse in cortex) was relatively ineffective in transmitting information between neurons. However, a small amount of redundancy in the number of synaptic connections between neurons was sufficient to make the synaptic transmission robust and reliable. These results were valid for both the signal estimation and signal detection tasks.

In order to obtain analytical expressions for measures of synaptic efficacy, we made some simplifying assumptions. In our model, the vesicle release probability for the synapse was

assumed to be constant. This is a gross oversimplification since it has been shown that the release probability can be strongly modulated by the temporal pattern of presynaptic spike trains and can vary over a large range (Dobrunz & Stevens, 1999). In fact, cortical synapses exhibit history-dependent plasticity over a variety of time scales (Markram & Tsodyks, 1996; Abbott *et al.*, 1997; Dobrunz & Stevens, 1997; Dobrunz *et al.*, 1997). Moreover, though we assumed synaptic parameters to be the same at all synapses, there is substantial non-uniformity in the values of the release probability among synapses impinging on the same neuron (Hessler *et al.*, 1993; Rosenmund *et al.*, 1993; Dobrunz & Stevens, 1999). These assumptions allowed us to derive closed-form expressions for the amount of information that can be transmitted across noisy synapses. It is noteworthy that our conclusions depend on the values of signal and synaptic parameters that we have chosen here to demonstrate the applicability of our analysis and need not hold for synapses whose properties depart strongly from our choice of parameters. However, the generality of the closed-form expressions allows an assessment of synaptic efficacy in cases when the parameters can be obtained from empirical data as well.

Our results agree qualitatively with a recent study that investigated the influence of synaptic unreliability on information transfer (Zador, 1998), though the information rates we obtain here are much smaller in magnitude. This is a consequence of our assumption that the encoding relationship between the mean firing rate of the presynaptic neuron and the input is linear. This assumption constrains the contrast of the firing rate c_λ (less than 1/3) and limits the amount of information that can be transmitted by the spike train over the ideal synapse (**Fig. 2.3A** and **Fig. 2.3B**). Moreover, our spike encoding model is a doubly stochastic Poisson process with a stimulus-dependent mean firing rate as compared to the leaky integrate-and-fire model used in (Zador, 1998) to transform the continuous input to a spike train. It can be shown that for the same mean firing rate the leaky integrate-and-fire model can transmit much more information than a Poisson process since the latter is more random than the former. If we normalize the synaptic information rates with respect to the corresponding rates for the ideal synapse (using the spike train directly), we obtain the same behavior for a host of different encoding models.

Table 2.1: List of Symbols for Chapter 2.

Symbol	Description
σ_λ	standard deviation of the presynaptic neuron's firing rate
σ_m	standard deviation of input signal in signal estimation
σ_n	standard deviation of postsynaptic membrane noise
σ_n	standard deviation of quantal amplitude
τ	time constant of encoding filter in signal estimation
ξ	normalized coding fraction in signal estimation
B_m	bandwidth of input signal in signal estimation
B_n	bandwidth of postsynaptic membrane noise
c_λ	contrast of the presynaptic neuron's firing rate
CV_q	coefficient of variation of quantal amplitude
$h(t)$	shape of the EPSP waveform
h_{peak}	peak of the EPSP waveform
$k(t)$	linear encoding filter in signal estimation
$K(f)$	Fourier transform of $k(t)$
$I(X; Y)$	mutual information for signal detection
I_{LB}	information rate for signal estimation
$m(t)$	input signal in signal estimation
N_{syn}	number of parallel synapses
$n(t)$	postsynaptic membrane noise
$P(a)$	probability distribution of the quantal amplitude
P_e	probability of error in signal detection
p_0	prior probability of presynaptic spike in signal detection
p	probability of vesicle release due to a presynaptic spike
q	random variable quantal amplitude
\bar{q}	mean quantal amplitude
$s(t)$	presynaptic spike train
t_{peak}	time at which EPSP reaches its peak
$V_m(t)$	postsynaptic voltage

Chapter 3 Subthreshold Noise Sources in Biological Membranes

3.1 Introduction

In the following two chapters, we consider the influence of subthreshold membrane noise sources on the electrotonic propagation of a synaptic signal. Our analysis is divided into two parts. In the first part, described in the present chapter, we characterize three sources of subthreshold noise which arise in nerve membranes: thermal noise due to membrane resistance (also called *Johnson Noise*), noise due to stochastic channel openings and closings of two voltage-gated membrane channels (*viz.*, K^+ and Na^+), and noise due to spontaneous random background synaptic activity. We derive analytical expressions for the magnitude and power spectral densities of these noise sources and estimate the subthreshold voltage noise for an isopotential patch of membrane containing synapses and ion channels.

In a second step, reported in Chapter 4, we carry out a theoretical analysis of the information loss of a synaptic signal as it propagates to the soma, due to the presence of these noise sources distributed along the dendritic membrane. We model the dendrite as a weakly-active linear cable with noise sources distributed all along its length and derive expressions for the capacity of this dendritic information channel under the signal detection and estimation paradigms. Our calculus can be regarded as a model for electrotonic propagation of synaptic signals to the soma along a linear, yet weakly-active dendrite.

For real neurons, propagation is never entirely linear; the presence of voltage-dependent membrane conductances in the dendritic tree can dramatically influence dendritic integration and propagation of information. Depending on their relative densities, the presence of different dendritic ion channel species can lead to either non-linear amplification of synaptic signals which can combat the loss due to electrotonic attenuation (Bernander *et al.*, 1994; Stuart & Sakmann, 1994; Stuart & Sakmann, 1995; Cook & Johnston, 1997; Schwandt &

Crill, 1995; Magee *et al.*, 1998) or a decrease in dendritic excitability and attenuation of synaptic signals (Hoffman *et al.*, 1997; Magee *et al.*, 1998; Stuart & Spruston, 1998).

The work discussed here is restricted to linear cables (passive or quasi-active (Koch, 1984); that is, the membrane can contain inductive-like components arising from time-dependent conductances) and can be regarded as a first order approximation to dendritic integration, which is amenable to closed-form analysis. Biophysically accurate scenarios which consider the effect of strong active non-linear membrane conductances can only be analyzed using numerical simulations which are reported in Chapter 6.

3.2 Sources of Subthreshold Membrane Noise

In general, currents flowing through ion-specific membrane proteins (channels) depend non-linearly on the voltage difference across the membrane (Johnston & Wu, 1995),

$$i = f(V_m), \quad (3.1)$$

where i represents the ionic current through the channel and V_m is the membrane voltage. Often the current satisfies Ohm's law (Hille, 1992); i can be expressed as the product of the driving potential across the channel $V_m - E_{ch}$ and the voltage- (or ligand concentration) dependent channel conductance g_{ch} as

$$i = g_{ch}(V_m)(V_m - E_{ch}), \quad (3.2)$$

where E_{ch} (the membrane voltage for which $i = 0$) is the reversal potential of the channel.

If i is small enough so that the flow of ions across the membrane does not significantly change V_m , the change in ionic concentrations is negligible (E_{ch} does not change) and so the driving potential is almost constant and $i \propto g_{ch}$. Thus, for a small conductance change, the channel current is approximately independent of V_m and is roughly proportional to the conductance change. Thus, even though neuronal inputs are usually in terms of conductance changes, for small inputs, currents can equivalently be regarded as the inputs. This argument holds for both ligand-gated and voltage-gated channels. We shall use this

assumption throughout this chapter and regard currents, and not conductances, as the input variables.

The neuron receives synaptic signals at numerous locations along its dendritic tree. These current inputs are integrated by the tree and they propagate as voltages towards the soma and the axon hillock, close to the site where the action potentials are generated. Thus, if we restrict ourselves to the study of the information loss due to the dendritic processing that precedes spike generation, currents are the input variables and the membrane voltage at the spike initiating zone can be considered to be the output variable.

We first consider some of the current noise sources present in nerve membranes which distort the synaptic signal as it propagates along the cable. As excellent background source text on noise in neurobiological systems, we recommend the monograph by DeFelice (1981)

3.2.1 Thermal Noise

Electrical conductors are sources of thermal noise resulting from random thermal agitation of the electrical charges in the conductor. Thermal noise, also known as *Johnson noise*, represents a fundamental lower limit of noise in a system and can be reduced only by decreasing the temperature or the bandwidth of the system (Johnson, 1928). Thermal noise is also called *white noise* because its power spectral density is flat for all frequencies (except at very high frequencies where quantum effects come into play). Since thermal noise results from a large ensemble of independent sources, its amplitude distribution is Gaussian as dictated by the Central Limit Theorem (Papoulis, 1991). The power spectral density of the voltage fluctuations due to thermal noise (denoted by $S_{V_{th}}$) in a conductor of resistance R in equilibrium, (no current flowing through the conductor) is given by,

$$S_{V_{th}}(f) = 2kTR \quad (\text{units of } V^2/\text{Hz}), \quad (3.3)$$

where k denotes the Boltzmann constant and T is the absolute temperature of the conductor. Consequently, the variance of the voltage fluctuations due to thermal noise, $\sigma_{V_{\text{th}}}^2$, is

$$\sigma_{V_{\text{th}}}^2 = \int_{-B}^B S_{V_{\text{th}}}(f) df = 4kTRB \quad (\text{units of V}^2), \quad (3.4)$$

where B denotes the bandwidth of the measurement system.¹

Thus, a conductor of resistance R can be replaced by an ideal noiseless resistor R in series with a voltage noise source $V_{\text{th}}(t)$, which has a power spectral density given by $S_{V_{\text{th}}}(f)$ (**Fig. 3.1A**). Equivalently, one can replace the conductor with a noiseless resistor R in parallel with a current noise source, $I_{\text{th}}(t)$ with power spectral density denoted by $S_{I_{\text{th}}}(f)$ (**Fig. 3.1B**) given by the expression,

$$S_{I_{\text{th}}}(f) = \frac{2kT}{R} \quad (\text{units of A}^2/\text{Hz}). \quad (3.5)$$

Since we assume the inputs to be currents, we shall use the latter representation. A passive one-dimensional cable can be modeled as a distributed network of resistances and capacitances as shown in **Fig. 3.2**. r_m and c_m denote the resistance and the capacitance across the membrane (transversely) respectively. r_i represents the resistance (longitudinal) of the intra-cellular cytoplasm. c_m arises due to the capacitance of the thin, insulating, phospholipid bilayer membrane which separates the intra-cellular cytoplasm and external solution. In general, excitable membrane structures containing active voltage- and time-dependent conductances cannot be modeled as ladder networks consisting of resistances and capacitances alone, even if they behave linearly in a given voltage range. The time-dependent nature of voltage-gated channel conductances gives rise to *phenomenological* inductances (Sabah & Leibovic, 1969; Mauro *et al.*, 1970; Sabah & Leibovic, 1972; Mauro *et al.*, 1972; Koch, 1984). Thus, in general, the small-signal circuit equivalent of an active, linearized membrane is an RLC (resistor-inductor-capacitor) circuit consisting of resistances, capacitances and inductances. For an illustration of this linearization procedure, refer to Appendix G.

¹All power spectral densities are assumed to be double-sided, since the power spectra of real signals are even functions of frequency.

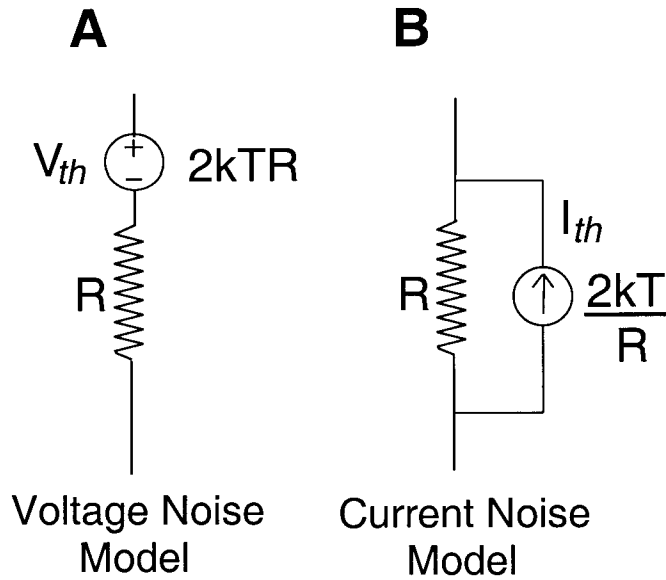


Figure 3.1: **Equivalent Thermal Noise Models For a Resistor.**

Thermal noise due to a resistor R in thermal equilibrium at temperature T can be considered equivalently as **A**: a voltage noise source V_{th} with power spectral density $2kTR$ in series with a noiseless resistance R or as **B**: a current noise source I_{th} with power spectral density $2kT/R$ in parallel with a noiseless R .

However, when the time constants corresponding to the ionic currents are much smaller than the passive membrane time constant, the phenomenological inductances are negligible and the equivalent circuit reduces to the passive ladder model for cable. This is true for the case we consider, the passive membrane time constant is about an order of magnitude greater than the slowest time-scale of the noise sources and so the approximation above is a reasonable one. r_m reflects the effective resistance of the lipid bilayer (very high resistance) and the various voltage-gated, ligand-gated and leak channels embedded in the lipid matrix. Here we ignore the external resistance, r_e , of the external medium surrounding the membrane. All quantities (r_i , r_m , c_m) are expressed in per unit length of the membrane and have the dimensions of $\Omega/\mu\text{m}$, $\Omega \mu\text{m}$ and $\text{F}/\mu\text{m}$ respectively. For a linear cable, modeled as a cylinder of diameter d , $r_m = R_m/\pi d$, $c_m = \pi d C_m$, $r_i = 4R_i/\pi d^2$ where R_m , C_m and R_i (*specific membrane resistance*, *specific membrane capacitance* and *axial resistivity* respectively) are the usual biophysical parameters of choice.

The current noise due to r_m , has power spectral density,

$$S_{\text{Ith}}(f) = \frac{2kT}{r_m} \quad (\text{units of } \text{A}^2/\text{Hz } \mu\text{m}). \quad (3.6)$$

However, r_m is not the only source of thermal noise. The resistance r_i , representing the axial cytoplasmic resistance, also contributes thermal noise. In general, the power spectral density of the voltage noise due to thermal fluctuations in an impedance Z is given by

$$S_{\text{Vth}}(f) = 2kT \text{Re}\{Z(f)\}, \quad (3.7)$$

where $\text{Re}\{Z(f)\}$ is the real part of the impedance as a function of frequency. Thus, the voltage variance is given by

$$\sigma_{\text{Vth}}^2 = \int_{-\infty}^{\infty} S_{\text{Vth}}(f) df \quad (\text{units of } \text{V}^2). \quad (3.8)$$

For an infinite passive cable (**Fig. 3.2**), the input impedance is given as

$$Z(f) = \frac{\sqrt{r_i r_m}}{\sqrt{1 + j2\pi f \tau_m}}, \quad (3.9)$$

$$\Rightarrow \text{Re}\{Z(f)\} = \frac{\sqrt{r_i r_m}}{[1 + (2\pi f \tau_m)^2]^{1/4}} \cos\left(\frac{\tan^{-1} 2\pi f \tau_m}{2}\right) \quad (3.10)$$

which yields

$$S_{V_{\text{th}}}(f) = \frac{2kT\sqrt{r_i r_m}}{[1 + (2\pi f \tau_m)^2]^{1/4}} \cos\left(\frac{\tan^{-1} 2\pi f \tau_m}{2}\right). \quad (3.11)$$

The integral of $S_{V_{\text{th}}}(f)$ in the equation above is divergent, and so $\sigma_{V_{\text{th}}}^2$ is infinite. This can be seen easily by rewriting the expression for $S_{V_{\text{th}}}$ as

$$S_{V_{\text{th}}}(f) = \sqrt{2r_i r_m} kT \left[\frac{1}{1 + (2\pi f \tau_m)^2} + \frac{1}{\sqrt{1 + (2\pi f \tau_m)^2}} \right]^{1/2}. \quad (3.12)$$

In the limit of large f , $S_{V_{\text{th}}}(f) \sim f^{-1/2}$, the indefinite integral of which diverges. This divergence is not due to r_m , but due to r_i . The noise due to r_m alone is of finite variance since the cable introduces a finite bandwidth. The resolution of this non-physical phenomenon lies in realizing that a pure resistance is a non-physical idealization. The cytoplasm is associated with a longitudinal capacitance in addition to its axial resistance, since current flow through the cytoplasm does not occur instantaneously. Ionic mobility is much smaller than that of electrons and charge accumulation takes place along the cytoplasm as a consequence. This can be modeled by the addition of an effective capacitance, c_i (in dotted lines in **Fig. 3.2**) in parallel with r_i . Now, $S_{V_{\text{th}}}(f)$ is given by

$$S_{V_{\text{th}}}(f) = \frac{2kT\sqrt{r_i r_m}}{[(1 + \theta_1^2)(1 + \theta_2^2)]^{1/4}} \cos\left(\frac{\tan^{-1} \theta_1 + \tan^{-1} \theta_2}{2}\right), \quad (3.13)$$

where

$$\theta_1 = 2\pi f \tau_m \quad \text{and} \quad \theta_2 = 2\pi f \tau_i.$$

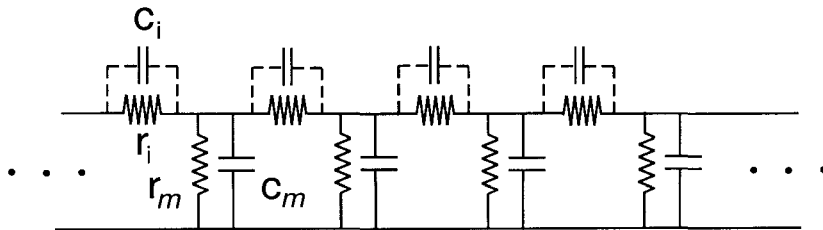


Figure 3.2: **Electrical Ladder Network Model of an Infinite 1-D Linear Cable.** r_i represents the longitudinal (axial) resistance due to the cytoplasm, whereas r_m and c_m denote the transverse membrane resistance and capacitance respectively. c_i denotes the (usually negligible) axial capacitance (shown using dotted lines) which ensures that the thermal noise has a bounded variance.

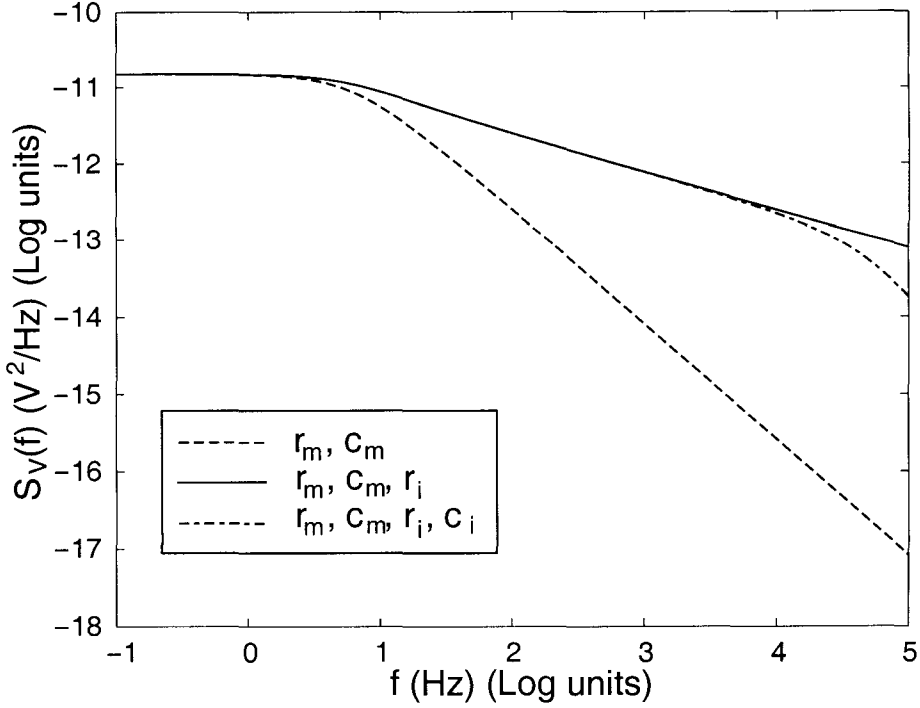


Figure 3.3: **Thermal Noise Models for an Infinite 1-D Cable.**

Comparison of power spectral densities of thermal voltage noise in an infinite cable corresponding to different assumptions. When the contribution due to the cytoplasmic resistance r_i is neglected (labeled as r_m, c_m), $S_{V_{th}}(f)$ represents the current noise due to the trans-membrane resistance r_m filtered by the Green's function of the infinite cable. $S_{V_{th}}(f) \sim f^{-3/2}$ for large f . When noise due to r_i is included (labeled as r_m, c_m, r_i) and equation 3.12 is used, $S_{V_{th}}(f) \sim f^{-1/2}$ and the resulting variance is infinite. When filtering due to cytoplasmic capacitance c_i is taken into account (labeled as r_m, c_m, r_i, c_i) and equation 3.13 is used, $S_{V_{th}}(f) \sim f^{-2}$. Since the integral of this power spectrum is bounded, the variance remains finite. Parameter values: $R_m = 40,000 \Omega/\text{cm}^2$, $R_i = 200 \Omega\text{cm}$, $\tau_m = 30 \text{ msec}$, $\tau_i = 3 \mu\text{sec}$.

τ_i is the time constant of the axial RC segment. τ_i is usually very low, on the order of 3 μsec (Rosenfalck, 1969). In this case, for large f , $S_{\text{Vth}}(f) \sim f^{-2}$, thus its integral converges and σ_{Vth}^2 remains finite. The additional filtering due to the cytoplasmic capacitances imposes a finite bandwidth on the system, rendering the variance finite. Since $\tau_i \ll \tau_m$, its effect is significant only at very large frequencies, as is shown in **Fig. 3.3**. Thus, neglecting the noise due to the cytoplasmic resistance is a very reasonable approximation for our frequency range of interest (1-1000 Hz).

3.2.2 Channel Noise

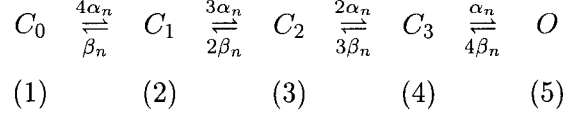
The membrane conductances we consider here are a consequence of microscopic, stochastic ionic channels (Hille, 1992). Since these channels open and close randomly, fluctuations in the number of channels constitutes a significant source of noise. In this section, we restrict the discussion to voltage-gated channels. However, ligand-gated channels can also be analyzed using the techniques discussed here. In Appendix E, we present an analysis of the noise due to channel fluctuations for a simple two-state channel model for completeness. We apply well-known results from the theory of Markov processes, reviewed in DeFelice (1981) and Johnston & Wu (1995), to Hodgkin-Huxley-like models of voltage-gated K^+ and Na^+ channels. It is straight forward to extend these results to any other channel type with discrete states.

K^+ channel noise

The seminal work by Hodgkin and Huxley (Hodgkin & Huxley, 1952) represents the first and very successful attempt at explaining the nature of membrane excitability in terms of voltage-gated particles. Most of our present understanding of membrane channels has been directly or indirectly influenced by their ideas (Hille, 1992).

In the Hodgkin-Huxley formulation, a K^+ channel comprises of four identical two-state sub-units. The K^+ channel conducts only when all are in their open states. Each sub-unit can be regarded as a two-state binary switch (like the model above) where the rate constants (α and β) depend on V_m . Hodgkin and Huxley used data from voltage-clamp experiments

on the giant squid axon to obtain empirical expressions for this voltage dependence. Since they are identical, the channel can be in one of five states; from the state corresponding to all sub-units closed to the open state in which all are open. In general, a channel composed of n sub-units has $n + 1$ distinct states if they are all identical and 2^n states if they are individually distinct. The simplest kinetic scheme corresponding to a K^+ channel can be written as



where C_i denotes the state in which i sub-units are open, O is the open state with all sub-units open. Thus, the evolution of a single K^+ channel can be regarded as a five state Markov process with the following state transition matrix:

$$\mathbf{Q}_K = \begin{bmatrix} -4\alpha_n & 4\alpha_n & 0 & 0 & 0 \\ \beta_n & -(3\alpha_n + \beta_n) & 3\alpha_n & 0 & 0 \\ 0 & 2\beta_n & -(2\alpha_n + 2\beta_n) & 2\alpha_n & 0 \\ 0 & 0 & 3\beta_n & -(\alpha_n + 3\beta_n) & \alpha_n \\ 0 & 0 & 0 & 4\beta_n & -4\beta_n \end{bmatrix}.$$

\mathbf{Q}_K is a singular matrix with 4 non-zero eigenvalues which correspond to the cut-off frequencies in the K^+ current noise spectrum. If the probability of a sub-unit being open is denoted by $n(t)$, the open probability of a single K^+ channel, p_K , is equal to $n(t)^4$. At steady state, the probability of a sub-unit being open at time t given that it was open at $t = 0$ ($\Pi_{55}(t)$ according to our convention) is given by

$$\Pi_{55}(t) = n_\infty + (1 - n_\infty)e^{-|\tau|/\theta_n}, \text{ where} \quad (3.14)$$

$$n_\infty = \frac{\alpha_n}{\alpha_n + \beta_n} \text{ and } \theta_n = \frac{1}{\alpha_n + \beta_n} \quad (3.15)$$

denote the steady-state open probability and relaxation time constant of the n sub-unit respectively. Thus, the auto-covariance of the current fluctuations due to the random opening

and closing of K^+ channels in the nerve membrane can be written by analogy,

$$C_{IK}(\tau) = \eta_K \gamma_K^2 (V_m - E_K)^2 [\Pi_{55}(\tau)^4 n_\infty^4 - n_\infty^8], \quad (3.16)$$

$$= \eta_K \gamma_K^2 (V_m - E_K)^2 \left[n_\infty^4 \{ n_\infty + (1 - n_\infty) e^{-|\tau|/\theta_n} \}^4 - n_\infty^8 \right], \quad (3.17)$$

where η_K , γ_K and E_K denote the K^+ channel density in the membrane, the open conductance of a single K^+ channel and the potassium reversal potential respectively. On expansion we obtain

$$C_{IK}(\tau) = \eta_K \gamma_K^2 (V_m - E_K)^2 n_\infty^4 \sum_{i=1}^4 \binom{4}{i} (1 - n_\infty)^i n_\infty^{4-i} e^{-i|\tau|/\theta_n}, \quad (3.18)$$

$$\text{where } \binom{n}{i} = \frac{n!}{(n-i)! i!}.$$

The variance of the K^+ current, $\sigma_K^2 = C_{IK}(0)$, is

$$\sigma_{IK}^2 = \eta_K \gamma_K^2 (V_m - E_K)^2 n_\infty^4 (1 - n_\infty^4), \quad (3.19)$$

$$= \eta_K \gamma_K^2 (V_m - E_K)^2 p_K (1 - p_K). \quad (3.20)$$

Taking the Fourier transform of $C_{IK}(\tau)$ gives us the power spectrum of the K^+ current noise

$$S_{IK}(f) = \eta_K \gamma_K^2 (V_m - E_K)^2 n_\infty^4 \sum_{i=1}^4 \binom{4}{i} (1 - n_\infty)^i n_\infty^{4-i} \frac{2 \theta_n / i}{1 + 4\pi^2 f^2 (\theta_n / i)^2}. \quad (3.21)$$

Notice that $S_{IK}(f)$ is given by a sum of 4 Lorentzian functions with different amplitude and cut-off frequencies. For $n_\infty \ll 1$, one can obtain a useful approximation for $S_{IK}(f)$

$$S_{IK}(f) \approx \eta_K \gamma_K^2 (V_m - E_K)^2 n_\infty^4 (1 - n_\infty)^4 \frac{2 \theta_n / 4}{1 + 4\pi^2 f^2 (\theta_n / 4)^2}, \quad (3.22)$$

$$\approx \frac{S_{IK}(0)}{1 + (f/f_K)^2} \quad (\text{units of } A^2/\text{Hz}), \quad (3.23)$$

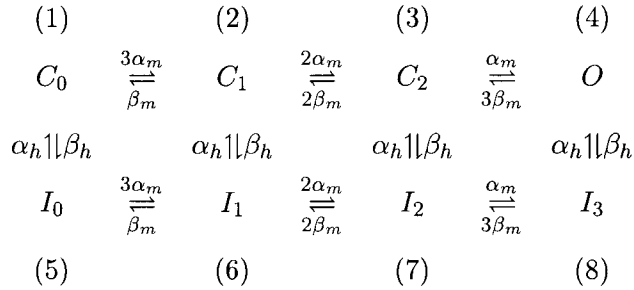
where

$$S_{\text{IK}}(0) = \frac{\eta_{\text{K}}}{2} \gamma_{\text{K}}^2 (V_{\text{m}} - E_{\text{K}})^2 n_{\infty}^4 (1 - n_{\infty})^4 \theta_n \quad \text{and} \quad f_{\text{K}} = \frac{4}{2\pi\theta_n}. \quad (3.24)$$

For small values of n_{∞} , the transitions $O \rightarrow C_3$ and $C_0 \rightarrow C_1$ dominate and the power spectrum can be approximated by a single Lorentzian with amplitude $S_{\text{IK}}(0)$ and cut-off frequency f_{K} . In this case the bandwidth² of K^+ current noise is given by $B_{\text{K}} \approx 1/\theta_n$. This approximation holds when the membrane voltage V_{m} is close to its resting potential V_{rest} .

Na^+ channel noise

The Hodgkin-Huxley Na^+ current is characterized by three identical activation subunits denoted by m and an inactivation sub-unit denoted by h . The Na^+ channel conducts only when all the m sub-units are open and the h sub-unit is not inactivated. Each of the sub-units may flip between their open (respectively, not inactivated) and closed (respectively, inactivated) states with the voltage-dependent rate constants α_m and β_m (respectively, α_h and β_h) for the m (respectively, h) sub-unit. Thus, the Na^+ channel can be in one of eight states from the state corresponding to all m sub-units closed and the h sub-unit inactivated to the open state with all m sub-units open and the h sub-unit not inactivated:



where C_i (respectively, I_i) denotes the state corresponding to i open sub-units of the m type and the h sub-unit not inactivated (respectively inactivated). The state transition matrix is given by $\mathbf{Q}_{\text{Na}} =$

²Defined as $B_{\text{K}} = \sigma_{\text{IK}}^2 / 2 S_{\text{IK}}(0)$, the variance divided by twice the magnitude of the power spectrum.

$$\begin{bmatrix} -(3\alpha_m + \beta_h) & 3\alpha_m & 0 & 0 & \beta_h & 0 & 0 & 0 \\ \beta_m & -(2\alpha_m + \beta_m + \beta_h) & 2\alpha_m & 0 & 0 & \beta_h & 0 & 0 \\ 0 & 2\beta_m & -(2\beta_m + \alpha_m + \beta_h) & \alpha_m & 0 & 0 & \beta_h & 0 \\ 0 & 0 & 3\beta_m & -(3\beta_m + \beta_h) & 0 & 0 & 0 & \beta_h \\ \alpha_h & 0 & 0 & 0 & -(3\alpha_m + \alpha_h) & 3\alpha_m & 0 & 0 \\ 0 & \alpha_h & 0 & 0 & \beta_m & -(2\alpha_m + \beta_m + \alpha_h) & 2\alpha_m & 0 \\ 0 & 0 & \alpha_h & 0 & 0 & 2\beta_m & -(\alpha_m + 2\beta_m + \alpha_h) & \alpha_m \\ 0 & 0 & 0 & \alpha_h & 0 & 0 & 3\beta_m & -(3\beta_m + \alpha_h) \end{bmatrix}$$

Q_{Na} has 7 non-zero eigenvalues and so the Na^+ channel has 7 time constants. Thus, the Na^+ current noise spectrum can be expressed as a sum of 7 Lorentzians with cut-off frequencies corresponding to these time constants. The auto-covariance of the current fluctuations due to the sodium channels is given as

$$C_{\text{INa}}(\tau) = \eta_{\text{Na}} \gamma_{\text{Na}}^2 (V_m - E_{\text{Na}})^2 \left[m_\infty^3 h_\infty \{ m_\infty + (1 - m_\infty) e^{-|\tau|/\theta_m} \}^3 \right. \\ \left. \{ h_\infty + (1 - h_\infty) e^{-|\tau|/\theta_h} \} - m_\infty^6 h_\infty^2 \right], \quad (3.25)$$

where η_{Na} , γ_{Na} and E_{Na} denote the Na^+ channel density, the Na^+ single channel conductance and the sodium reversal potential respectively. The steady-state values and time constants of the m and h sub-units are given by

$$m_\infty = \frac{\alpha_m}{\alpha_m + \beta_m} \quad \theta_m = \frac{1}{\alpha_m + \beta_m} \quad (3.26)$$

$$h_\infty = \frac{\alpha_h}{\alpha_h + \beta_h} \quad \theta_h = \frac{1}{\alpha_h + \beta_h}. \quad (3.27)$$

The variance of the current noise can be written as

$$\sigma_{\text{INa}}^2 = \eta_{\text{Na}} \gamma_{\text{Na}}^2 (V_m - E_{\text{Na}})^2 m_\infty^3 h_\infty (1 - m_\infty^3 h_\infty) \quad (3.28)$$

$$= \eta_{\text{Na}} \gamma_{\text{Na}}^2 (V_m - E_{\text{Na}})^2 p_{\text{Na}} (1 - p_{\text{Na}}), \quad (3.29)$$

where $p_{\text{Na}} = m_\infty^3 h_\infty$ is the steady-state open probability of a Na^+ channel. The power spectrum, obtained by taking the Fourier transform of $C_{\text{INa}}(\tau)$, is given by a combination

of 7 Lorentzian components. The general expression is tedious and lengthy to express and so we shall restrict ourselves to a reasonable approximation. For $m_\infty \ll 1$ and $h_\infty \approx 1$, around the resting potential.

$$S_{\text{INa}}(f) \approx \eta_{\text{Na}} \gamma_{\text{Na}}^2 (V_m - E_{\text{Na}})^2 m_\infty^3 (1 - m_\infty)^3 h_\infty^2 \frac{2 \theta_m / 3}{1 + 4\pi^2 f^2 (\theta_m / 3)^2} \quad (3.30)$$

$$\approx \frac{S_{\text{INa}}(0)}{1 + (f/f_{\text{Na}})^2} \quad (\text{units of A}^2/\text{Hz}), \quad (3.31)$$

where

$$S_{\text{INa}}(0) = \frac{2\eta_{\text{Na}}}{3} \gamma_{\text{Na}}^2 (V_m - E_{\text{Na}})^2 m_\infty^3 h_\infty (1 - m_\infty)^3 h_\infty \theta_m \quad \text{and} \quad f_{\text{Na}} = \frac{3}{2\pi\theta_m}. \quad (3.32)$$

Thus, for voltages close to the resting potential, $S_{\text{INa}}(f)$ can be approximated by a single Lorentzian. The bandwidth of Na^+ current noise under this approximation is given by $B_{\text{Na}} \approx 3/(4\theta_m)$.

In general, the magnitude and shape of the power spectrum is determined by the kinetics of corresponding single channels. For any given state transition matrix describing the channel kinetics, we can derive expressions for the noise power spectral densities using the procedure outlined above. For most kinetic models, when $V_m \approx V_{\text{rest}}$, the single Lorentzian approximation suffices. A variety of kinetic schemes modeling different types of voltage-gated ion channels exist in the literature. We shall choose a particular scheme to work with, but the formalism is very general and can be used to study arbitrary finite-state channels.

3.2.3 Noise Due to Background Synaptic Activity

In addition to voltage-gated channels which open and close in response to membrane potential changes, dendrites (and the associated spines, if any) are also awash in ligand-gated synaptic receptors. We shall restrict our attention to the family of channels specialized for mediating fast chemical synaptic transmission in a voltage-independent manner, excluding NMDA-type of currents for now

Chemical synaptic transmission is usually understood as a conductance change in the post-synaptic membrane caused by the release of neurotransmitter molecules from the presynaptic neuron in response to presynaptic membrane depolarization. A commonly used function to represent the time course of the postsynaptic change in response to a presynaptic spike is the *alpha* function (Rall, 1967; Koch, 1999)

$$g_\alpha(t) = \frac{g_{\text{peak}}}{t_{\text{peak}}} t e^{-t/t_{\text{peak}}} u(t), \quad (3.33)$$

where g_{peak} denotes the peak conductance change and t_{peak} is the time-to-peak of the conductance change. $u(t)$ is the unit step function which ensures that $g_\alpha(t) = 0$ for $t < 0$. More general kinetic descriptions have been proposed (Destexhe *et al.*, 1994), but are not considered here.

We shall assume that for a spike train $s(t) = \sum_j \delta(t - t_j)$, modeled as a sum of impulses occurring at times t_j , the postsynaptic change is given by a sum of time-shifted conductance functions,

$$g_{\text{Syn}}(t) = \sum_j g_\alpha(t - t_j). \quad (3.34)$$

This means that each spike causes the same conductance change and that the conductance change due to a sequence of spikes is the sum of the changes due to individual spikes in the train. For now, we ignore the effect of paired-pulse facilitation or depression (Abbott *et al.*, 1997; Tsodyks & Markram, 1997). The synaptic current $i_{\text{Syn}}(t)$ is given by

$$i_{\text{Syn}}(t) = g_{\text{Syn}}(t) (V_m - E_{\text{Syn}}), \quad (3.35)$$

where E_{Syn} is the synaptic reversal potential. As before, we assume that the synaptic current is small enough so that V_m is nearly constant. If the spike train of the presynaptic neuron can be modeled as a homogeneous Poisson process with mean firing rate λ_n , one can compute the mean and variance of the synaptic current arriving at the membrane using

Campbell's theorem (Papoulis, 1991):

$$\langle i_{\text{Syn}}(t) \rangle = \lambda_n (V_m - E_{\text{Syn}}) \int_0^\infty g_\alpha(t) dt, \quad (3.36)$$

$$\sigma_{\text{ISyn}}^2 = \lambda_n (V_m - E_{\text{Syn}})^2 \int_0^\infty (g_\alpha(t))^2 dt. \quad (3.37)$$

It is straight forward to compute the auto-covariance $C_{\text{ISyn}}(\tau)$ of the synaptic current,

$$C_{\text{ISyn}}(\tau) = \lambda_n (V_m - E_{\text{Syn}})^2 g_\alpha(\tau) \star g_\alpha(-\tau), \quad (3.38)$$

$$= \lambda_n (V_m - E_{\text{Syn}})^2 \int_0^\infty g_\alpha(t) g_\alpha(t + \tau) dt. \quad (3.39)$$

Similarly, the power spectral density of the synaptic current is given by

$$S_{\text{ISyn}}(f) = \mathcal{F}\{C_{\text{ISyn}}(\tau)\} = \lambda_n (V_m - E_{\text{Syn}})^2 |G_\alpha(f)|^2, \quad (3.40)$$

where

$$G_\alpha(f) = \mathcal{F}\{g_\alpha(t)\} = \int_0^\infty g_\alpha(t) e^{-j2\pi ft} dt \quad (3.41)$$

denotes the Fourier transform of $g_\alpha(t)$. For the alpha function,

$$G_\alpha(f) = \frac{e g_{\text{peak}} t_{\text{peak}}}{(1 + j 2\pi f t_{\text{peak}})^2}. \quad (3.42)$$

It has been shown that if the density of synaptic innervation is high or alternatively if the firing rates of the presynaptic neurons are high and the conductance change due to a single impulse is small, the synaptic current tends to a Gaussian process (Tuckwell & Wan, 1980). This is called the *diffusion approximation*. Since a Gaussian process is completely specified by its power spectral density, one only needs to compute the power spectrum of current noise due to random synaptic activity. If η_{Syn} denotes the synaptic density, the variance, auto-covariance and the power spectral density of the synaptic current noise are

given by

$$\sigma_{\text{ISyn}}^2 = \eta_{\text{Syn}} \lambda_n \left(\frac{g_{\text{peak}} e}{2} \right)^2 (V_m - E_{\text{Syn}})^2 t_{\text{peak}}, \quad (3.43)$$

$$C_{\text{ISyn}}(\tau) = \sigma_{\text{ISyn}}^2 [1 + |\tau| \tau_{\text{peak}}] e^{-|\tau|/t_{\text{peak}}}, \quad (3.44)$$

$$S_{\text{ISyn}}(f) = \eta_{\text{Syn}} \lambda_n \frac{[e g_{\text{peak}} t_{\text{peak}} (V_m - E_{\text{Syn}})]^2}{[1 + (2\pi f t_s)^2]}, \quad (3.45)$$

$$= \frac{S_{\text{ISyn}}(0)}{[1 + (f/f_{\text{Syn}})^2]^2} \quad (\text{units of A}^2/\text{Hz}), \quad (3.46)$$

where

$$S_{\text{ISyn}}(0) = 4 \sigma_{\text{ISyn}}^2 t_{\text{peak}} \quad \text{and} \quad f_{\text{Syn}} = \frac{1}{2\pi t_{\text{peak}}}. \quad (3.47)$$

A power spectrum of the above form is called a *double Lorentzian* spectrum. As before, the power spectrum can be represented in terms of its DC amplitude $S_{\text{Syn}}(0)$, and its cut-off frequency f_{Syn} . The double Lorentzian spectrum falls twice as fast with the logarithm of frequency as compared to a single Lorentzian because of the double pole at f_{Syn} . Thus, f_{Syn} is the frequency for which the magnitude of the power spectrum is one-fourth of its amplitude. Using our definition of bandwidth, the bandwidth of the synaptic current noise, $B_{\text{Syn}} = \frac{\pi}{4} f_{\text{Syn}} = 1/8 t_{\text{peak}}$.

3.2.4 Other Sources of Membrane Noise

In addition to these sources, there are several other sources of noise in biological membranes (Verveen & DeFelice, 1974; Neher & Stevens, 1977; DeFelice, 1981). The neuronal membrane contains ionic channels (Hille, 1992) with different kinetics, in different proportions. Random fluctuations in the number of these channels also contributes to membrane noise. Additionally, myriad types of ligand-gated channels also contribute to the noise level. Using the analysis above, it is clear that if accurate estimates of their relevant parameters (densities, kinetics and so on) are made available, one can potentially compute their contributions to membrane noise as well.

Noise type	K ⁺	Na ⁺	Synaptic
σ_I^2	$\eta_K I_{K,\max}^2 p_K(1 - p_K)$	$\eta_{Na} I_{Na,\max}^2 p_{Na}(1 - p_{Na})$	$(e/2)^2 \eta_{Syn} \lambda_n I_{Syn,\max}^2 t_{peak}$
$C_I(\tau)/\sigma_I^2$	$\exp(- \tau /4 \theta_n)$	$\exp(- \tau /3 \theta_m)$	$(1 + \tau /t_{peak}) \exp(- \tau /t_{peak})$
f_c	$4/(2\pi\theta_n)$	$3/(2\pi\theta_m)$	$1/(2\pi t_{peak})$
$S_I(0)$	$\sigma_{IK}^2 \theta_n/2$	$2 \sigma_{INa}^2 \theta_m/3$	$4 \sigma_{ISyn}^2 t_{peak}$
$S_I(f)/S_I(0)$	$1/[1 + (f/f_K)^2]$	$1/[1 + (f/f_{Na})^2]$	$1/[1 + (f/f_{Syn})^2]^2$
B	$1/\theta_n$	$3/(4 \theta_m)$	$1/(8 t_{peak})$

Table 3.1: **Analytical Expressions of Membrane Current Noise Sources.**

For Na⁺ and K⁺ channel noise we have made the assumption that the membrane voltage is around the resting value. $I_{K,\max} = \gamma_K(V_m - E_K)$, $I_{Na,\max} = \gamma_{Na}(V_m - E_{Na})$ and $I_{Syn,\max} = g_{peak}(V_m - E_{Syn})$ denote the maximum possible values of current through a single K⁺ channel, Na⁺ channel and synapse respectively. Since densities are expressed in terms of per unit area, σ_I^2 , and S_I have units of A²/μm² and A²/Hz μm² respectively.

Other types of membrane noise are 1/ f noise (Neumcke, 1978; Clay & Shlesinger, 1977), (also called *excess* or *flicker noise*), shot noise due to ions in transit through leak channels or pores (Frehland & Faulhaber, 1980; Frehland, 1982), carrier-mediated transport noise in ionic pumps and burst noise. We did not include these in our analysis, either due to a lack of a sound theoretical understanding of their origin or the relative insignificance of their magnitudes.

A summary of the expressions we have used to characterize the noise sources is provided in **Table 3.1**. We have modeled the sources as current fluctuations by assuming that the membrane voltage was clamped at V_m . The magnitude and nature of the current fluctuations depend on the kinetics and the driving potential, and thus on V_m . In the next section, we investigate the effect of embedding a membrane patch with these noise sources. There we assume that the current fluctuations are small enough so that V_m does not deviate significantly from its resting value, V_{rest} . In general, this approximation must be verified for the different noise sources considered. We use the expressions in **Table 3.1** to identify the contribution of each noise source to the total membrane voltage noise for different biophysically relevant parameter values. In Chapter 4, deriving similar expressions for membrane noise sources in a linear cable, we quantify the information lost by synaptic signal as it propagates down a dendrite due to these noise sources.

3.3 Subthreshold Noise in a Membrane Patch

Consider a patch of neuronal membrane of area A , containing Hodgkin-Huxley type rapid sodium I_{Na} and delayed rectifier I_{K} currents as well as fast (AMPA) voltage-independent synapses. If the patch is small enough, it can be considered as a single point, making the membrane voltage solely a function of time. We shall make this “point-like” assumption here and defer analysis of the general case of spatial dependence of the potential to Chapter 4.

Let C denote the capacitance of the patch, given by the product $C = C_m A$. The passive membrane conductance due to voltage-independent leak channels is given by g_L . Current injected into the membrane from all other sources is denoted by $I_{\text{inj}}(t)$. Since the area of the patch is known, the absolute values of the conductances can be obtained by multiplying their corresponding specific values by the patch area A . On the other hand, if we wish to continue working with specific conductances and capacitances, the injected current needs to be divided by A to obtain the current density. Here we use the former convention. The electric circuit corresponding to the membrane patch is shown in **Fig. 3.4**. Using Kirchoff’s law we have

$$C \frac{dV_m}{dt} + g_K(V_m - E_K) + g_{\text{Na}}(V_m - E_{\text{Na}}) + g_{\text{Syn}}(V_m - E_{\text{Syn}}) + g_L(V_m - E_L) = I_{\text{inj}}. \quad (3.48)$$

Since the ion channels and synapses are stochastic, g_K , g_{Na} and g_{Syn} in the above equation are stochastic processes. Consequently, equation 3.48 is, in effect, a *stochastic differential equation*. Moreover, since the active conductances (g_K and g_{Na}) depend on V_m , equation 3.48 is non-linear in V_m and in all likelihood intractable to theoretical analysis. However, as a consequence of the assumption that the system is in quasi-equilibrium, one can effectively linearize the active conductances and express them as deviations around their

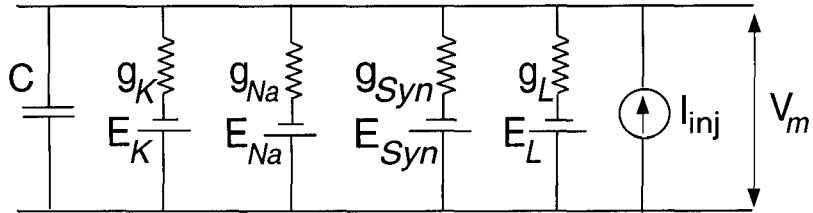


Figure 3.4: **Electric Circuit of a Membrane Patch.**

C denotes the patch capacitance and, g_L , the passive membrane resistance due to leak channels. The membrane also contains active channels (K^+ , Na^+) and fast voltage-independent synapses, and their conductances are represented by g_K , g_{Na} and g_{Syn} respectively. Current injected from other sources is denoted by I_{inj} .

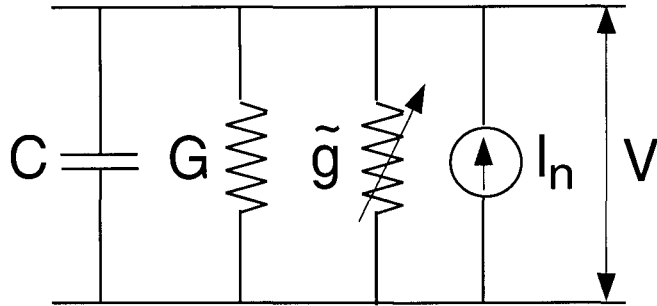


Figure 3.5: **Equivalent Linearized Electric Circuit of a Membrane Patch.**

Circuit diagram of the membrane patch containing different noise sources, close to equilibrium. The membrane voltage V is measured as a deviation from the resting value V_{rest} . G is the deterministic resting conductance of the patch and \tilde{g} is the random component due to the fluctuating conductances. The conductance fluctuations also give rise to an additive current noise source I_n .

respective steady-state equilibrium values,

$$g_K = g_K^o + \tilde{g}_K, \quad (3.49)$$

$$g_{Na} = g_{Na}^o + \tilde{g}_{Na}, \quad (3.50)$$

$$g_{Syn} = g_{Syn}^o + \tilde{g}_{Syn}, \quad (3.51)$$

$$V_m = V_m^o + V. \quad (3.52)$$

This perturbative approximation can easily be verified by self-consistency. If the approximation is valid, the deviations (V) of the membrane voltage from the resting voltage should be small. For the cases we consider, the membrane fluctuations are indeed small and so the approximation holds. However, in general, the validity of this approximation needs to be verified on a case by case basis.

V_m^o is chosen such that it satisfies the equation

$$V_m^o = \frac{g_K^o E_K + g_{Na}^o E_{Na} + g_{Syn}^o E_{Syn} + g_L E_L}{G} \quad (3.53)$$

where $G = g_K^o + g_{Na}^o + g_{Syn}^o + g_L$ is the total baseline input conductance of the patch, equal to the sum of all the baseline conductances. Similarly, $\tilde{g} = \tilde{g}_K + \tilde{g}_{Na} + \tilde{g}_{Syn}$ denotes the total random component of the patch conductance. Substituting for equation 3.49-equation 3.52 in equation 3.48 gives us the following equation:

$$C \frac{dV_m}{dt} + G(V_m - V_m^o) + \tilde{g}_K(V_m - E_K) + \tilde{g}_{Na}(V_m - E_{Na}) + \tilde{g}_{Syn}(V_m - E_{Syn}) = I_{inj}. \quad (3.54)$$

Since the steady-state (resting) solution of equation 3.48 is $V_m = V_{rest}$, we can choose to linearize about the resting potential, $V_m^o = V_{rest}$. The effective time constant of the patch depends on G and is given by $\tau = C/G$. When $V_m(t) \approx V_{rest}$, g_L is usually the dominant conductance and so $G \approx g_L$. However, during periods of intense synaptic activity, or for strongly excitable systems, G can be significantly larger than g_L (Bernander *et al.*, 1991;

Rapp *et al.*, 1992). If no external current is injected, the only other source of current is the thermal current noise and I_{inj} is equal to I_{th} .

Expressing $V_m(t)$ as deviations around V_{rest} in the form of the variable $V(t) = V_m(t) - V_{rest}$ allows us to simplify equation 3.54 to

$$\tau \frac{dV}{dt} + (1 + \delta)V = \frac{I_n}{G}, \quad (3.55)$$

where

$$\delta = \frac{\tilde{g}_K + \tilde{g}_{Na} + \tilde{g}_{Syn}}{G} = \frac{\tilde{g}}{G}, \quad (3.56)$$

$$I_n = \tilde{g}_K(E_K - V_{rest}) + \tilde{g}_{Na}(E_{Na} - V_{rest}) + \tilde{g}_{Syn}(E_{Syn} - V_{rest}) + I_{th}. \quad (3.57)$$

The circuit diagram corresponding to the above is shown in **Fig. 3.5**. The random variable δ corresponds to fluctuations in the membrane conductance due to synaptic and channel contributions and has a multiplicative effect on V . On the other hand, I_n corresponds to an additive current noise source arising due to conductance fluctuations at V_{rest} ($V = 0$). We assume that the conductance fluctuations about the V_{rest} are zero-mean wide-sense-stationary (WSS) processes. Since the noise sources have different origins, it is also plausible to assume that they are statistically independent. Thus, I_n is also a zero-mean WSS random process, $\langle I_n \rangle = 0$.

Our perturbative approximation implies that the statistical properties of the processes δ and I_n are evaluated at $V = 0$. We are unable to solve equation 3.55 analytically because of the nonlinear (multiplicative) relationship between δ and V . However, since the membrane voltage does not change significantly, in most cases, the deviations of the conductances are small compared to the resting conductance of the cell³, implying $\delta \ll 1$, which allows us to further simplify equation 3.55 to

$$\tau \frac{dV}{dt} + V = \frac{I_n}{G}. \quad (3.58)$$

³The validity of this assumption can easily, and must, be verified on a case by case basis.

This equation corresponds to a linear system driven by an additive noise source. It is straight forward to derive the statistical properties of V in terms of the statistical properties of I_n . For instance, the power spectral density of $V(t)$, $S_V(f)$ can be written in terms of power spectral density of I_n , $S_{I_n}(f)$ as

$$S_V(f) = \frac{S_{I_n}(f)}{G^2 [1 + (2\pi f\tau)^2]}. \quad (3.59)$$

Since the noise sources are independent,

$$S_{I_n}(f) = A [S_{IK}(f) + S_{INa}(f) + S_{ISyn}(f) + S_{Ith}(f)]. \quad (3.60)$$

Using the single Lorentzian approximations for the K^+ and Na^+ spectra, one can write an expression for the variance of the voltage noise as

$$\sigma_V^2 \approx \frac{\pi A}{G^2} \left[S_{IK}(0) \frac{f_m f_K}{f_m + f_K} + S_{INa}(0) \frac{f_m f_{Na}}{f_m + f_{Na}} + S_{ISyn}(0) \frac{f_m f_{Syn}}{f_m + f_{Syn}} \frac{f_m^2 + f_{Syn} f_m - 2f_{Syn}^2}{f_m^2 - f_{Syn}^2} + S_{Ith}(0) f_m \right], \quad (3.61)$$

where $f_m = 1/2\pi\tau$ is the cut-off frequency corresponding to the membrane's passive time constant.

3.3.1 Summary of Parameter Values Used

We consider a space-clamped cell body of a typical neocortical pyramidal cell as the substrate for our noisy membrane-patch model. Estimates of the somatic/dendritic Na^+ conductance densities in neocortical pyramidal cells range from 4 to 12 mS/cm² (Huguenard *et al.*, 1989; Stuart & Sakmann, 1994). We assume $\eta_{Na} = 2$ channels/ μm^2 with $\gamma_{Na} = 20$ pS. K^+ channel densities are not known as reliably mainly because there are a multitude of different K^+ channel types. However, some recent experimental and computational studies (Hoffman *et al.*, 1997; Mainen & Sejnowski, 1998; Magee *et al.*, 1998; Hoffman & Johnston, 1998) provide estimates for the K^+ densities in the soma and dendrites of cortical neurons. We choose $\eta_K = 1.5$ channels/ μm^2 , adopted from Mainen & Sejnowski, (1998). The channel

kinetics and the voltage dependence of the rate constants also correspond to Mainen *et al.*, (1995). We use $R_m = 40,000 \Omega\text{cm}^2$ and $C_m = 1 \mu\text{F}/\text{cm}^2$ obtained from recent studies based on tight-seal whole cell recordings (Spruston *et al.*, 1994; Major *et al.*, 1994), giving a passive time constant of $\tau_m = 40$ msec. The entire soma is reduced to a single membrane patch of area $A = 1000 \mu\text{m}^2$.

The number of synapses at the soma is usually small, which leads us to $\eta_{\text{Syn}} = 0.01$ synapses/ μm^2 , that is, 10 synapses. Other synaptic parameters are: $g_{\text{peak}} = 100$ pS, $t_{\text{peak}} = 1.5$ msec, $\lambda_n = 0.5$ Hz. No account is made of synaptic transmission failure, but see Chapter 2 for an analysis of synaptic unreliability and variability.

3.4 Results

We compute the current and voltage power spectra (shown in **Fig. 3.6**) over the frequency range relevant for fast computations for the biophysical scenario discussed above. Experimentally, the current noise spectrum can be obtained by performing a voltage-clamp experiment, while the voltage noise spectra can be measured under current-clamp conditions. The voltage noise spectrum includes the effect of filtering (which has a Lorentzian power spectrum) due to the passive RC circuit corresponding to the patch. In a following chapter, we show that in a real neuron the cable properties of the system recorded from give rise to more complex behavior. Since we have modeled the membrane patch as a passive RC filter and regarded the active voltage-gated ion channels as pure conductances, we obtained monotonic low-pass voltage spectra. In general, as we have mentioned before, the small-signal membrane impedance due to voltage and time dependent conductances can exhibit resonance giving rise to band-pass characteristics in the voltage noise spectra (Koch, 1999). The relative magnitudes of the current noise power spectral densities ($S_I(0)$) and the amplitudes of voltage noise due to each noise source (S_{V_i} and σ_{V_i}) are compared in **Table 3.2**.

The contribution of each noise source to the overall spectrum depends on the exact values of the parameters—including the channel kinetics—which can vary considerably across neuronal types and even from one neuronal location to another. For the parameter values

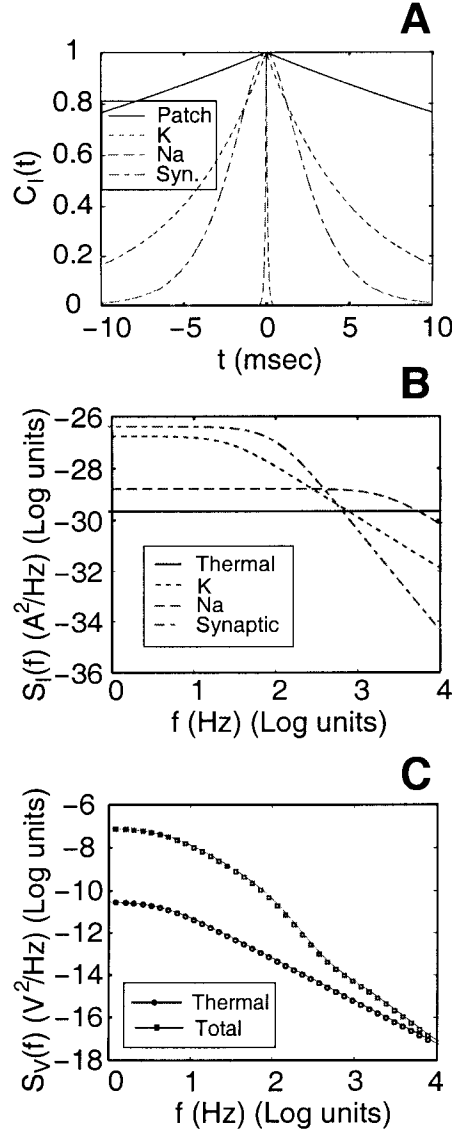


Figure 3.6: **Subthreshold Noise in a Patch of Neuronal Membrane.**

A: Comparison of the normalized correlation functions $C_I(t)/C_I(0)$ of the different noise sources with the autocorrelation of the Green's function of an RC circuit ($e^{-t/\tau}$), for parameter values summarized below. **B:** Comparison of current power spectra $S_I(f)$ of the different membrane noise sources, *viz.*, thermal noise, K⁺ channel noise, Na⁺ channel noise and synaptic background noise as a function of frequency (up to 10 kHz). **C:** Voltage spectrum $S_V(f)$ of the noise in a somatic patch due the influence of the above sources. Power spectrum of the voltage fluctuations due to thermal noise alone $S_{V_{th}}(f)$ is also shown for comparison. Summary of the parameters adopted from Mainen & Sejnowski, (1998): $R_m = 40 \text{ k}\Omega \text{ cm}^2$, $C_m = 1 \text{ }\mu\text{F}/\text{cm}^2$, $\eta_K = 1.5 \text{ channels per } \mu\text{m}^2$, $\eta_{Na} = 2 \text{ channels per } \mu\text{m}^2$, $\eta_{Syn} = 0.01 \text{ synapses per } \mu\text{m}^2$ with spontaneous firing rate $\lambda_n = 0.5 \text{ Hz}$. $E_K = -95 \text{ mV}$, $E_{Na} = 50 \text{ mV}$, $E_{Syn} = 0 \text{ mV}$, $E_L = -70 \text{ mV}$, $\gamma_K = \gamma_{Na} = 20 \text{ pS}$. Synaptic parameters: $g_{peak} = 100 \text{ pS}$, $t_{peak} = 1.5 \text{ msec}$.

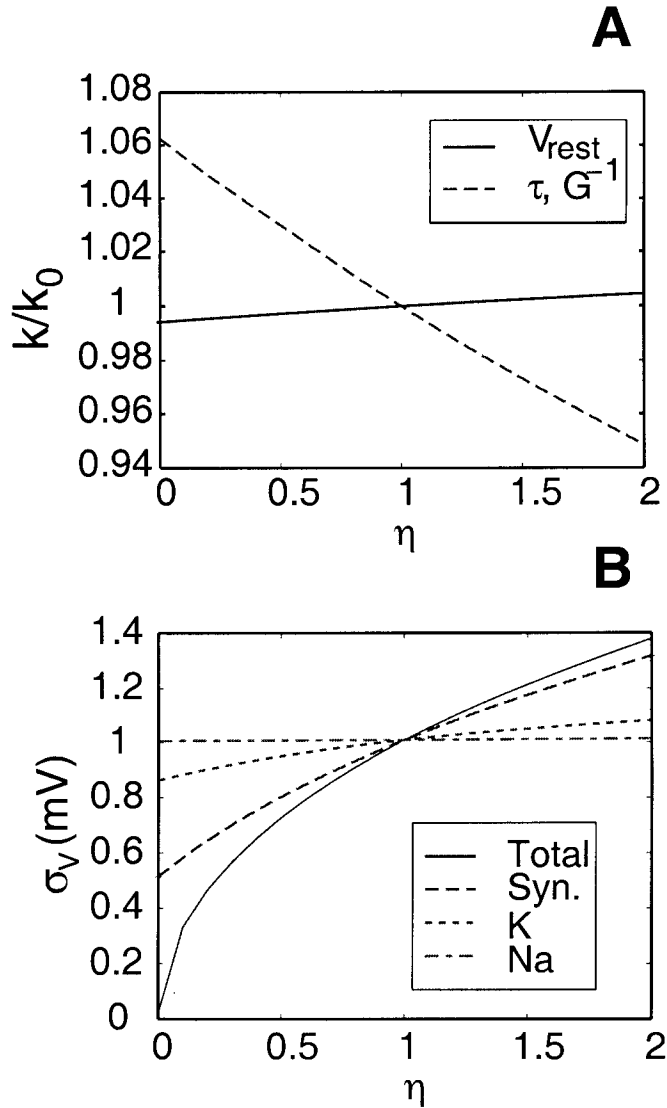


Figure 3.7: **Dependence of Noise Magnitude on Biophysical Parameters.**

A: Dependence of the passive membrane parameters (V_{rest}, τ) on the channel and synaptic densities. The K^+ and Na^+ channel densities and the synaptic density are scaled by the same factor η which varies from $\eta = 0$ (corresponding to a completely passive system) to $\eta = 2$. $\eta = 1$ corresponds to the nominal parameter values used to generate **Fig. 3.6**. The membrane parameters (denoted generically by κ) are expressed as a ratio of their nominal values at $\eta = 1$ (denoted by κ_0). **B:** Effect of varying individual densities (the remaining densities are maintained at their nominal values) on the magnitude of the voltage noise σ_V .

Noise type	$A * S_I(0)$ (A^2/Hz)	$S_V(0)$ (V^2/Hz)	σ_V (mV)
Thermal	2.21×10^{-30}	3.14×10^{-11}	2.05×10^{-2}
K^+	1.74×10^{-27}	2.46×10^{-8}	5.33×10^{-1}
Na^+	1.67×10^{-28}	2.36×10^{-10}	5.59×10^{-2}
Synaptic	4.12×10^{-27}	5.84×10^{-8}	8.54×10^{-1}
Total	5.88×10^{-27}	8.33×10^{-8}	1.01

Table 3.2: Magnitude of Subthreshold Noise in a Membrane Patch.

Current power spectral densities ($A * S_I(0)$, units of A^2/Hz), voltage power spectral densities ($S_V(0)$, units of V^2/Hz) and voltage standard deviations (σ_V , units of mV) of the different noise sources (thermal, K^+ , Na^+ conductance fluctuations and synaptic background) in a space-clamped somatic membrane patch.

we considered, thermal noise made the smallest contribution, and is at the limit of what is experimentally resolvable using modern amplifiers. Background synaptic noise due to spontaneous activity was the dominant component of neuronal noise. The magnitude of noise for the scenario we consider here is small enough to justify the perturbative approximation, but it can be expected that for small structures, especially thin dendrites or spines, the perturbative approximation might be violated. However, treating a dendritic segment as a membrane patch is not an accurate model for real dendrites where currents can flow longitudinally. We shall address this problem again in the context of noise in linear cables in Chapter 4.

There are numerous parameters in our analysis and it would be extremely tedious to consider the combinatorial effect of varying them all. We restrict ourselves to studying the effect of varying a few biological relevant parameters.

3.4.1 Dependence on Patch Area

Notice that varying the patch area A does not affect the resting membrane potential V_{rest} or the passive membrane time constant τ . From equation 3.59 one can deduce the scaling behavior of S_V with respect to A in a straight forward manner. The numerator increases linearly with A since the noise sources are independent and in parallel and so their con-

tributions add. However, all the individual membrane conductances scale linearly with A , thus, the total conductance G also scales linearly with A . As a consequence, $S_V(f)$ and σ_V^2 scale inversely with A : the larger the area, the smaller the variance. Equivalently, σ_V scales inversely as the square root of A .

This might appear counterintuitive since the number of channels increases linearly with A , but can be understood as follows. The current fluctuations are integrated by the RC filter corresponding to the membrane patch and manifest as voltage fluctuations. As the area of the patch increases, the variance of the current fluctuations increases linearly but the input impedance decreases as well. Since the variance of the voltage fluctuations is proportional to the square of the impedance, the decrease in impedance more than offsets the linear increase due to the current and so the resulting voltage fluctuations are smaller. If all the channel and synaptic densities are increased by the same factor (a global increase in the number of channels), an identical scaling behavior is obtained.

This suggests that the voltage noise from small patches might be large. Indeed, it is plausible to assume that for small neurons, the voltage fluctuations can be large enough to cause “spontaneous” action potentials. This phenomenon of noise-induced oscillations has indeed been borne out by simulations (Skaugen & Walløe, 1979; Skaugen, 1980b; Strassberg & DeFelice, 1993; Schneidman *et al.*, 1998).

3.4.2 Dependence on Channel Densities

We first consider the effect of varying the different individual channel densities on the resting properties of the patch, that is on V_{rest} , G and τ . The K^+ and Na^+ channel densities and the synaptic densities (except g_L) are first scaled individually and then together by the same factor. We denote the scale parameter by η . When all densities are scaled together, $\eta = 0$ corresponds to a purely passive patch containing leak channels alone and $\eta = 1$ corresponds to the membrane patch scenario considered above (referred to as the nominal case). Similarly, when only the K^+ density is varied, $\eta = 0$ corresponds to a membrane patch without K^+ channels and $\eta = 1$ denotes the nominal value. The results of this exercise are summarized in **Fig. 3.7A**. Instead of using absolute values for the quantities of interest, we

normalize them with respect to their nominal values corresponding to $\eta = 1$. Notice that when all the densities, except leak, are varied from $\eta = 0$ to $\eta = 2$, V_{rest} varies (becomes more hyper-polarized) by less than 1% and τ and G^{-1} vary from about a 6% increase ($\eta = 0$) to a 5% decrease ($\eta = 2$). Despite the non-linearities due to the active K^+ and Na^+ conductances, it is noteworthy that the quantities vary almost linearly with η , further justifying our perturbative approximation.

The effect of varying individual densities on σ_V is explored in **Fig. 3.7B**. In order to consider the contribution of a given process to the noise magnitude, we vary the associated density in a similar manner as above (η goes from 0 to 2), while maintaining the others at their nominal values. We also compare the individual profiles to the case when all densities are scaled by the same factor. It is clear from the figure that the synaptic noise is the dominant noise source. The noise magnitude drops approximately from 1 mV to 0.5 mV in the absence of synaptic input (as η varies goes from 1 to 0), but only to about 0.85 mV in the absence of K^+ channels. Varying the Na^+ density has a negligible effect on the noise magnitude. Similarly, the noise increases to 1.35 mV when the synaptic density is doubled ($\eta = 2$) with respect to its nominal values, but the increase to about 1.07 mV due to the doubling of K^+ density is much smaller.

3.5 Discussion

The key result of this chapter is that we were able to derive closed-form expressions for the membrane voltage fluctuations due to the three dominant noise types in neuronal preparations: thermal noise, channel noise and background synaptic noise. However, these results were derived under some simplifying conditions. We assumed that the deviations of the membrane potential about its resting value, as a result of “spontaneous” synaptic input and channels switching, are small. This allowed us to make a perturbative approximation and express conductance changes as small deviations around their resting values, treating them as sources of current noise. The validity of this assumption needs to be carefully evaluated empirically. This can be considered analogous to the linearization of non-linear

differential equations about a quiescent point, except here the underlying quantities are stochastic as well. For a related approach, see Larsson *et al.* (1997).

This approximation made it possible for us to write down the stochastic differential equation 3.55 for the dynamics of voltage fluctuations. We use techniques derived from the theory of stochastic processes to solve equation 3.55 analytically for simplified kinds of conductance fluctuations in Appendix H and show that when the conductance fluctuations are small, the membrane voltage reduces to a Gaussian stochastic process. This analytical approach cannot be used to analyze the effect of multiple conductance fluctuations. However, under the simplifying assumption that the conductance fluctuations are small compared to the total resting conductance, equation 3.55 reduces to a linear stochastic differential equation which is straight forward to analyze. The validity of this assumption can also be easily verified.

Using this assumption, all the three noise sources could be regarded as additive. Solving the associated linear stochastic membrane equation, we obtained analytical expressions for the spectra and variance of the voltage fluctuations. We shall show in Chapter 4 that a similar calculus can be applied when the noise sources are distributed in complex one-dimensional neuronal cable structures. Estimating the properties of the subthreshold noise in a linear cable can allow us to determine the influence of noise on the capacity of dendritic information processing.

Chapter 4 Information-theoretic Analysis of Electrotonic Propagation in Weakly-Active Dendrites

4.1 Introduction

In this chapter our goal is to quantify the information loss in linear cables under the signal estimation and signal detection representational paradigms due to sources of subthreshold membrane noise. The noise sources which have been modeled and characterized in Chapter 3 include thermal noise due to the passive membrane resistance, noise due to the stochastic channel openings and closings of membrane voltage-gated ion channels (K^+ and Na^+) and noise due to random background synaptic activity. Using results from Chapter 3, we derive closed-form expressions for the magnitude and power spectral densities of the noise sources in linear cables and compare the noise magnitudes for the simplified case of an infinite linear cable. Our analysis, however, is quite general and can be used to estimate the properties of noise in other more complicated cable geometries.

Quantifying the magnitude of the membrane noise sources allows us to assess the efficacy of information transfer in dendritic cable structures under two different paradigms. As before, the goal in the signal estimation paradigm is to estimate a random current waveform injected at a particular location from the membrane voltage at another location on the cable. We define a quantity called the normalized coding fraction, ξ , and use it to assess signal fidelity in the signal estimation task. In the signal detection paradigm, the objective is to detect the presence or absence of a presynaptic signal (a single spike) on observing the post-synaptic membrane voltage. The probability of detection error, P_e , is used to quantify performance in the signal detection task. Much of modern psychophysical research (Green & Swets, 1966) uses a signal-detection paradigm to assess performance. The framework

is illustrated schematically in **Fig. 4.1**. We derive expressions for the corresponding information theoretical measures of signal efficacy (mean square error and information rate for signal estimation and probability of error and mutual information for signal detection) and examine their dependence on different biophysical parameters. A list of mathematical symbols used in Chapter 3 and Chapter 4 is summarized in **Table 4.2** at the end of this chapter.

4.2 The One-Dimensional Cable Equation

We model the dendrite as the usual one-dimensional ladder network shown in **Fig. 4.2**. For assumptions underlying one-dimensional cable theory, see Koch (1999). r_a represents the axial resistance of the intra-cellular cytoplasm. r_a (expressed in units of $\Omega/\mu\text{m}$) can be obtained in terms of the more commonly used intra-cellular resistivity R_i as

$$r_a = \frac{4 R_i}{\pi d^2}, \quad (4.1)$$

where d is the dendritic diameter (expressed in μm). g_K , g_{Na} and g_L denote the transverse membrane conductances due to K^+ , Na^+ and leak channels distributed throughout the dendritic membrane. Recent research has established the existence of several types of active voltage-gated ion channels in dendrites (Johnston *et al.*, 1996; Colbert & Johnston, 1996; Yuste & Tank, 1996; Magee *et al.*, 1998). The dendritic membrane also has an incidence of a large number of synapses, from a vast multitude of other neurons. However, as in Chapter 3, we restrict ourselves to fast voltage-independent synapses (AMPA-type) here. Let g_{Syn} denote the transverse membrane conductance due to these fast AMPA-like synapses. All the conductances above are expressed in units of $S/\mu\text{m}$. The membrane capacitance due to the phospholipid bi-layer is denoted by c_m . The units of c_m are $F/\mu\text{m}$ and it can be expressed in terms of the more commonly used specific capacitance C_m as

$$c_m = \pi d C_m. \quad (4.2)$$

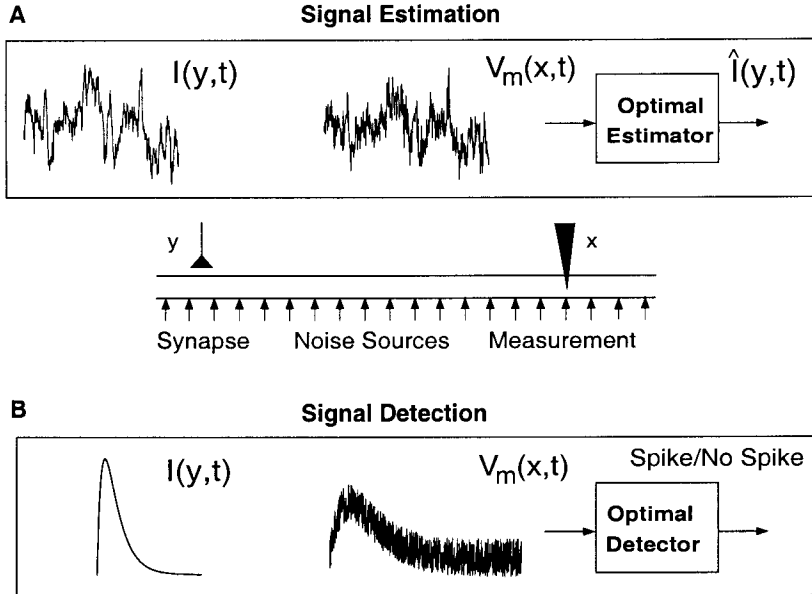


Figure 4.1: **Channel Model of a Weakly-Active Dendrite.**

The dendrite is modeled as a weakly-active 1-D cable with noise sources distributed along its length. By “weakly-active,” we mean that the magnitude of the conductance fluctuations due to these sources is small compared to the baseline conductance of the membrane. Formally, this can be stated as $\delta \ll 1$ (equation 4.10). These noise sources distort the synaptic signal as it propagates from its postsynaptic site y to a measurement (output) location x . Loss of fidelity is studied under two representational paradigms. **A:** In signal estimation, the objective is to optimally estimate the input current $I(y, t)$ from the membrane voltage $V_m(x, t)$. The normalized coding fraction ξ and the mutual information are used to quantify signal fidelity in the estimation task. **B:** In signal detection, the objective is to optimally detect the presence of the synaptic input $I(y, t)$ (in the form of a unitary synaptic event) on the basis of $V_m(x, t)$. The probability of error, P_e , and mutual information are used to quantify signal fidelity in the detection task.

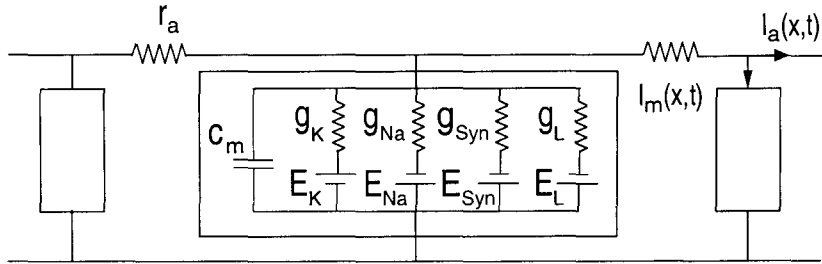


Figure 4.2: **Equivalent Circuit Diagram of a One-Dimensional Dendritic Cable.** The cable is modeled as an infinite ladder network. r_a ($\Omega/\mu\text{m}$) denotes the longitudinal cytoplasmic resistance; c_m ($\text{F}/\mu\text{m}$) and g_L ($\text{S}/\mu\text{m}$) denote the transverse membrane capacitance and conductance (due to leak channels with reversal potential E_L) respectively. $I_a(x, t)$ denotes the longitudinal current, whereas $I_m(x, t)$ is the transverse membrane current. The membrane also contains active channels (K^+ , Na^+) with conductances and reversal potentials denoted by (g_K, g_{Na}) and (E_K, E_{Na}) respectively, and fast, voltage-independent (AMPA-like) synapses with conductance g_{Syn} and reversal potential E_{Syn} . All conductances are in units of $\text{S}/\mu\text{m}$.

The membrane voltage V_m satisfies the following partial differential equation,

$$\frac{\partial^2 V_m}{\partial x^2} = r_a \left[c_m \frac{\partial V_m}{\partial t} + g_K(V_m - E_K) + g_{Na}(V_m - E_{Na}) + g_{Syn}(V_m - E_{Syn}) + g_L(V_m - E_L) + I_{inj} \right], \quad (4.3)$$

where $I_{inj}(x, t)$ represents the current injected into the membrane from other sources which we have not explicitly considered here (thermal noise, synaptic input, stimulating electrode, *etc.*).

Since the conductances g_K , g_{Na} , g_{Syn} (and possibly even I_{inj}) are stochastic processes, equation 4.3 denotes a highly non-linear stochastic reaction-diffusion equation (Tuckwell, 1988b) since the ionic conductances are functions of V_m in themselves. However, it is more illustrative to express the random variables as deviations around some baseline values, as in Chapter 3,

$$g_K = g_K^o + \tilde{g}_K, \quad (4.4)$$

$$g_{Na} = g_{Na}^o + \tilde{g}_{Na}, \quad (4.5)$$

$$g_{Syn} = g_{Syn}^o + \tilde{g}_{Syn}, \quad (4.6)$$

$$V_m = V_m^o + V. \quad (4.7)$$

V_m^o is chosen such that it satisfies the equation

$$V_m^o = \frac{g_K^o E_K + g_{Na}^o E_{Na} + g_{Syn}^o E_{Syn} + g_L E_L}{G}, \quad (4.8)$$

where $G = g_K^o + g_{Na}^o + g_{Syn}^o + g_L$ is the total input conductance, given by the sum of all the baseline conductances. Substituting for equations 4.4-4.7 in equation 4.3 gives us the equation,

$$-\lambda^2 \frac{\partial^2 V}{\partial x^2} + \tau \frac{\partial V}{\partial t} + (1 + \delta)V = \frac{I_n}{G}, \quad (4.9)$$

where $\lambda = 1/\sqrt{r_a G}$ is the characteristic length constant (in μm) and $\tau = c_m/G$ is the characteristic passive time constant (in msec) of the cable. δ and I_n are random processes defined as

$$\delta = \frac{\tilde{g}_K + \tilde{g}_{\text{Na}} + \tilde{g}_{\text{Syn}}}{G}, \quad (4.10)$$

$$I_n = \tilde{g}_K(E_K - V_m^o) + \tilde{g}_{\text{Na}}(E_{\text{Na}} - V_m^o) + \tilde{g}_{\text{Syn}}(E_{\text{Syn}} - V_m^o) + \tilde{I}_{\text{inj}}. \quad (4.11)$$

δ corresponds to membrane conductance fluctuations due to synaptic and channel contributions and has a multiplicative effect on V . I_n , on the other hand, is a sum of the additive noise current due to these conductance fluctuations and the random component of the injected current \tilde{I}_{inj} (the expected value of I_{inj} is assumed to be zero). We assume that the conductance fluctuations are spatially white, zero-mean, wide-sense stationary (WSS) random processes, *i.e.*, the fluctuations at a location x are independent of those at another location y . It is plausible to assume that the individual conductance fluctuations are statistically independent since they have different origins. Thus, I_n is also a zero-mean WSS random process, $\langle I_n(x, t) \rangle = 0$.

We now make a simplifying assumption that $\delta \ll 1$ and can be neglected in equation 4.9. We refer to this as the “weakly-active” assumption. This allows us to reduce equation 4.9 to a linear, stochastic, partial differential equation. We shall also assume that the dynamics of components of the noise current I_n are given by their values at $V_m = V_m^o$. The steady-state (resting) solution of equation 4.9 (obtained by setting δ and I_n to zero) is $V = 0$, which implies that we choose $V_m^o = V_{\text{rest}}$. Consequently, G is the resting membrane conductance. Similarly, the baseline conductances g_i^o satisfy $g_i^o = g_i^\infty(V_{\text{rest}})$ where $g_i^\infty(V_m)$ denotes the steady-state value of the conductance as a function of the membrane voltage. Thus, our assumptions are equivalent to saying that conductances fluctuations around V_{rest} are negligible compared to the resting conductance G . Additionally, the dynamics of the resulting current noise can be obtained from the dynamics of conductance fluctuations evaluated around V_{rest} . These assumptions need to be verified on a case-by-case basis. The simplest way to ensure their validity is to check for self-consistency of the solutions. Notice

that equation 4.9 is an extension of the membrane patch analysis in Chapter 3 to a 1-D cable.

Thus, our simplified version of the equation 4.9 reads,

$$-\lambda^2 \frac{\partial^2 V}{\partial x^2} + \tau \frac{\partial V}{\partial t} + V = \frac{I_n}{G} \quad (4.12)$$

and is, in effect, a stochastic version of the one-dimensional cable equation (Rall, 1969a; Tuckwell, 1988a; Tuckwell, 1988b). Details of the derivation of the cable equation can be found in literature (Rall, 1969a; Tuckwell, 1988a). For the most part our notation is similar to the one used in Tuckwell & Walsh (1983).

4.3 Subthreshold Noise in Linear Cables

The cable equation has a unique solution once the initial conditions and the boundary conditions are specified. For resting initial conditions ($V = 0$ for $t \leq 0$), the membrane fluctuations V are linearly related to the current input I_n and can be mathematically expressed as convolution of I_n with the Green's function of the cable equation for the given boundary conditions. The Green's function of the cable, denoted by $g(x, x', t, t')$, specifies the voltage response of the cable at the location x at time t to a current impulse $\delta(x - x') \delta(t - t')$ injected at the location x' at time t' . $g(x, x', t, t')$ has units of $\mu\text{m}^{-1}\text{msec}^{-1}$. By superposition, $V(x, t)$ can be written as

$$V(x, t) = \frac{1}{G} \int_{-\infty}^{\infty} dx' \int_0^t dt' g(x, x', t, t') I_n(x', t'). \quad (4.13)$$

Since the system is time-invariant, $g(x, x', t, t') = g(x, x', t - t')$. The exact form of $g(x, x', t - t')$ depends on the nature of the boundary conditions of the partial differential equation. The expected value of $V(x, t)$ is given by

$$\langle V(x, t) \rangle = \frac{1}{G} \int_{-\infty}^{\infty} dx' \int_0^t dt' g(x, x', t - t') \langle I_n(x', t') \rangle. \quad (4.14)$$

Since the current noise I_n is a zero-mean process, $\langle V(x, t) \rangle = 0$. Thus the variance of the membrane voltage fluctuations $\sigma_V^2(x, t) = \langle V^2(x, t) \rangle$ is given by

$$\sigma_V^2(x, t) = \frac{1}{G^2} \int_{-\infty}^{\infty} dx' \int_{-\infty}^{\infty} dx'' \int_0^t dt' \int_0^t dt'' g(x, x', t - t') g(x, x'', t - t'') \langle I_n(x', t') I_n(x'', t'') \rangle. \quad (4.15)$$

The quantity $\langle I_n(x', t') I_n(x'', t'') \rangle$ represents the auto-covariance of the current input which we denote by $C_n(x', x'', t', t'')$. Since $I_n(x, t)$ is a spatially-white WSS process, C_n is of the form $C_n(x', x'', t', t'') = C_n(t' - t'') \delta(x' - x'')$ which simplifies equation 4.15 to

$$\sigma_V^2(x, t) = \frac{1}{G^2} \int_{-\infty}^{\infty} dx' \int_0^t dt' \int_0^t dt'' g(x, x', t - t') g(x, x', t - t'') C_n(t' - t''). \quad (4.16)$$

Since we assume that the cable starts receiving inputs at time $t = 0$, the membrane voltage fluctuations V cannot be a WSS process. This can be easily seen as σ_V^2 depends on t . However, if we wait long enough for the transients associated with the initial condition to die out, at long time-scales the statistical properties of $V(x, t)$ do not depend on t . In fact, it can be shown that $V(x, t)$ is asymptotically ($t \rightarrow \infty$) WSS (Tuckwell, 1988a). Another way to observe the same is by assuming that the system starts receiving its input at $t = -\infty$, in which case, the dynamics stabilize by t . This can be observed by changing the limits of the time variable to $(-\infty, t)$ in equation 4.15. The steady-state variance of $V(x, t)$ is given by

$$\sigma_V^2(x, \infty) = \frac{1}{G^2} \int_{-\infty}^{\infty} dx' \int_0^{\infty} dt' \int_{-t'}^{\infty} dz g(x, x', t') g(x, x', t' + z) C_n(z). \quad (4.17)$$

When the auto-covariance of the current noise $C_n(z)$ decays much faster (has a much smaller support) than $g(x, x', t')$, one can approximate it by $C_n(z) \approx C_0 \delta(z)$, which allows equation 4.17 to be written as¹

$$\sigma_V^2(x, \infty) \approx \frac{C_0}{G^2} \int_{-\infty}^{\infty} dx' \int_0^{\infty} dt' g^2(x, x', t'). \quad (4.18)$$

¹By definition, $C_0 = S_n(0)$ where $S_n(f)$ is the Fourier transform of C_n , or equivalently, the power spectrum of the current noise.

This approximation holds when the membrane time constant τ , which determines the temporal support of $g(x, x', t')$, is much larger than the time constants governing the dynamics of the noise sources. We call this approximation the *white noise approximation* (WNA), since we approximate the current noise covariance C_n by an impulse, the correlation function of a spectrally-white stochastic process. The validity of this approximation can be verified easily by comparing the temporal width of C_n with the membrane time constant.

In general, the steady-state covariance $C_V(x, s)$ of $V(x, t)$ is given by

$$\begin{aligned} C_V(x, s) &= \lim_{t \rightarrow \infty} \langle V(x, t) V(x, t + s) \rangle, \\ &= \frac{1}{G^2} \int_{-\infty}^{\infty} dx' \int_0^{\infty} dt' \int_{-t'}^{\infty} dz g(x, x', t') g(x, x', t' + z) C_n(z - s). \end{aligned} \quad (4.19)$$

Notice that $C_V(x, s)$ is of the form $C_V(x, s) = \int_{-\infty}^{\infty} dx' g(x, x', s) \star g(x, x', -s) \star C_n(s)$ where \star denotes a convolution operation. Consequently, the voltage noise power spectrum is given by

$$S_V(x, f) = \mathcal{F}\{C_V(x, t)\} = \underbrace{\frac{S_n(f)}{G^2}}_{SF_n} \underbrace{\int_{-\infty}^{\infty} dx' |\mathcal{G}(x, x', f)|^2}_{GF_n}, \quad (4.20)$$

where $S_n(f) = \mathcal{F}\{C_n(s)\}$ is the power spectral density of the current noise and $\mathcal{G}(x, x', f) = \mathcal{F}\{g(x, x', t)\}$ is the transfer function of the Green's function of the system. $\mathcal{F}\{g(x)\}$ denotes the Fourier transform operation defined as $\int_{-\infty}^{\infty} dx g(x) \exp(-i2\pi f x)$.

Notice that we have expressed the voltage spectrum $S_V(x, f)$ (in units of V^2/Hz) in equation 4.20 as a product of two factors. The first factor SF_n (Source Factor) represents the power spectral density of the current noise source scaled appropriately (by $1/G^2$) to have the units of $V^2\mu\text{m}/\text{Hz}$. SF_n depends on the properties of the noise sources and the resting membrane conductance. The second factor GF_n (Geometry Factor) characterizes the transformation of the current noise input by the cable into membrane voltage fluctuations and has the units of μm^{-1} . GF_n depends on factors (geometry, boundary conditions, and so on) which determine the Green's function of the cable. This decomposition allows us to

decouple the effects of cable geometry from those of the current noise sources. When the WNA holds, SF_n is a constant ($SF_n \approx S_n(0)/G^2$) and in effect GF_n describes the spectral properties of $V(x, t)$.

Special Case: The Infinite Cable

Here we consider the simplistic case of an infinite cable. Though this theoretical idealization approximates reality only very loosely, it offers significant insight in understanding more complicated scenarios. The analytical tractability of the infinite case allows us to derive closed-form expressions for the quantities of interest and use them to develop an intuitive understanding of some of the fundamental issues of the problem. Unfortunately, closed-form expressions for other cable geometries (semi-infinite cable with a sealed end, finite cable with sealed/killed ends) cannot be derived and one has to take recourse to numerical techniques. Nevertheless, the Green's functions for these cable geometries have been derived in semi-closed form (Jack *et al.*, 1975; Tuckwell, 1988a). Moreover, compartmental modeling of realistic dendritic trees (Segev & Burke, 1998) has become routine. Thus, using numerical approaches, it is relatively straight forward to extend the analysis to more complicated scenarios.

The Green's function for the infinite cable is given as (Jack *et al.*, 1975)

$$g(x, x', t) = \frac{1}{\lambda\tau} \frac{e^{-T}}{\sqrt{4\pi T}} e^{-\frac{(x-x')^2}{4T}} \quad -\infty < x, x' < \infty, \quad 0 \leq t < \infty, \quad (4.21)$$

where $X = x/\lambda$, $X' = x'/\lambda$ and $T = t/\tau$ are the corresponding dimensionless variables. It can be shown that the geometry factor corresponding to the voltage variance is given by (Tuckwell & Walsh, 1983)

$$\sigma_V^2(x, t) = \frac{1}{4\lambda\tau} \left[1 - \text{Erfc} \left(\sqrt{2t/\tau} \right) \right], \quad (4.22)$$

where $\text{Erfc}(\cdot)$ is the complementary error function,

$$\text{Erfc}(x) = \frac{2}{\sqrt{\pi}} \int_x^{\infty} dy e^{-y^2}. \quad (4.23)$$

Thus, in steady-state, the voltage variance geometry factor is given by

$$\sigma_V^2(x) = \lim_{t \rightarrow \infty} \sigma_V^2(x, t) = \frac{1}{4 \lambda \tau}. \quad (4.24)$$

Note that the voltage noise variance σ_V^2 is independent of the measurement location x . This is also intuitively consistent with the inherent symmetry of the infinite cable. The expressions for the geometry factors for $C_V(x, s)$ and $S_V(x, f)$ are given as

$$C_V(x, s) = \frac{1}{4 \lambda \tau} \text{Erfc}(\sqrt{s/\tau}), \quad (4.25)$$

$$S_V(x, f) = \frac{1}{2 \lambda} \frac{\sin[\tan^{-1}(2\pi f \tau)/2]}{2\pi f \tau [1 + (2\pi f \tau)^2]^{1/4}}. \quad (4.26)$$

Notice that in the limit of high frequencies

$$S_V(x, f) \sim \frac{1}{8 \lambda (\pi f \tau)^{3/2}}. \quad (4.27)$$

Thus, for the infinite cable, the voltage noise spectrum decays asymptotically as $f^{-3/2}$ with frequency. This holds for frequencies larger than $f_m = 1/\tau$ but smaller than those for which $S_n(f)$ can no longer be regarded as a constant (equal to its value at $f = 0$, $S_n(0)$). For very high frequencies, $S_V(f)$ decays faster than $f^{-3/2}$ due to the spectral profile of the current noise $S_n(f)$. The exact expression (after multiplying by SF_n) for $S_V(x, f)$ is given as

$$S_V(x, f) = \frac{S_n(f)}{2 \lambda G^2} \frac{\sin[\tan^{-1}(2\pi f \tau)/2]}{2\pi f \tau [1 + (2\pi f \tau)^2]^{1/4}}. \quad (4.28)$$

4.4 Electrotonic Signal Propagation in Linear Cables

Up to this point, we have addressed the problem of noise accumulation in a linear cable as a result of fluctuations due to different membrane conductances distributed along the

dendritic length. We now analyze the attenuation of a synaptic signal, delivered at a particular dendritic location, as it propagates passively along the dendrite. Our approach is to exploit the linearity of the cable equation and decompose the voltage at a given location into “signal” and “noise” components. The input signal depends on the paradigm we use. In the signal estimation paradigm, the input is in the form of a random current waveform $I_s(t)$, injected at a given dendritic location, while in the signal detection paradigm, the input is a unitary, excitatory, postsynaptic current pulse (EPSC) delivered across a dendritic synapse at the given location.

In principle, a synaptic input should be treated as a conductance change triggered by a presynaptic action potential in parallel with a synaptic battery. However, in the signal estimation paradigm, where our goal is to assess how well continuous signals can be reconstructed from the membrane potential, we would need to invoke a mechanism that transforms a continuous signal into a spike train driving the synapse. For now, we bypass this problem and assume that the synaptic input corresponds to a continuous current that is directly injected into the cable. We will return to the problem of linking a presynaptic spike train to the postsynaptic synaptic current in a future publication.

We now use the appropriate Green’s function $g(x, y, t)$ for a given cable geometry to derive expressions for the voltage response $V(x, y, t)$ due to a current $I_s(t)$ injected at location y . By superposition,

$$V(x, y, t) = \frac{1}{G} \int_0^t dt' g(x, y, t - t') I_s(t'). \quad (4.29)$$

In the signal detection task, $I_s(t)$ is a deterministic signal, which we model by the α function, first introduced by Rall, (1967), $I_s(t) = I_{\text{peak}} t/t_{\text{peak}} \exp(-t/t_{\text{peak}})$. Whereas, in the signal estimation task, $I_s(t)$ is a continuous random process. Consequently, $V(x, y, t)$ is a (non-stationary) random process, which is asymptotically wide-sense stationary as $t \rightarrow \infty$ (steady-state). It is straight forward to derive expressions for the signal component (due to

$I_s(t)$), of the voltage power spectra $S_V(x, y, f)$ and variance $\sigma_V^2(x, y)$ as

$$S_V(x, y, f) = \frac{S_s(f)}{G^2} |\mathcal{G}(x, y, f)|^2, \quad (4.30)$$

$$\sigma_V^2(x, y) = \int_{-\infty}^{\infty} df S_V(f), \quad (4.31)$$

where $S_s(f)$ is the power spectral density of the input $I_s(t)$. Thus, using equation 4.30 and equation 4.31, we can analyze how the signal component of the membrane voltage decreases as a function of the distance from the input location, for different cable geometries.

Special Case: The Infinite Cable

As before, we restrict ourselves to the case of an infinite cable. The expression for the signal component $S_V(x, y, f)$ for the infinite cable is given by

$$S_V(x, y, f) = \frac{S_s(f)}{4\lambda^2 G^2} \frac{\exp(-\rho|x-y|/\lambda)}{[1 + (2\pi f\tau)^2]^{1/2}}, \quad (4.32)$$

where

$$\rho = 2 [1 + (2\pi f\tau)^2]^{1/4} \cos [\tan^{-1}(2\pi f\tau)/2]. \quad (4.33)$$

Notice that $S_V(x, y, f)$ is symmetric with respect to x and y , and depends only on the electrotonic distance $X = |x - y|/\lambda$ between the input and the measurement location. For $f \rightarrow \infty$, $S_V(x, y, f)$ varies as

$$S_V(x, y, f) \sim \frac{S_s(f)}{4\lambda^2 G^2} \frac{\exp(-\sqrt{4\pi f\tau} X)}{2\pi f\tau}. \quad (4.34)$$

If $S_s(f)$ is almost flat over the bandwidth of the cable, we can derive a simplified expression for the variance $\sigma_V^2(X)$ as

$$\sigma_V^2(X) = \frac{S_s(0)}{\lambda^2 G^2 \tau} \frac{K_0(2X)}{2\pi}, \quad (4.35)$$

where $K_0(\cdot)$ denotes the zeroth-order modified Bessel function of the second kind. $K_0(u)$ has a singularity at the origin and so the variance at the input location ($x = y$) is unbounded. The asymptotic behavior of $K_0(u)$ can be expressed as (Wan & Tuckwell, 1979)

$$K_0(u) \sim -\log(u) \quad (u \rightarrow 0), \quad (4.36)$$

$$K_0(u) \sim \sqrt{\frac{\pi}{2u}} e^{-u} \quad (u \rightarrow \infty). \quad (4.37)$$

Thus, the variance $\sigma_V^2(X)$ has a logarithmic singularity at the origin and decays approximately exponentially with X for large X . The singularity is a result of the approximation of the auto-correlation of $I_s(t)$ by a δ function, in comparison to the Green's function of the cable. This approximation breaks down for $X \approx 0$ for which $g(x, y, t)$ has a very small temporal support, comparable to or smaller than the correlation time of $I_s(t)$. This eliminates the singularity in σ_V^2 .

More realistic models like the ‘‘cylinder with a lumped soma model’’ (Rall, 1960; Rall, 1969b), which includes the effect of the low somatic impedance, or compartmental models of neurons with extensive dendritic trees (Segev & Burke, 1998), are not amenable to closed-form analysis and can only be studied numerically. However, a knowledge of the Green's function of the cable enables us to determine the spectral properties of both the signal and noise contributions to the membrane voltage fluctuations. As we will see subsequently, knowledge of the signal and noise spectra are sufficient to quantify the information loss.

4.5 The Signal Estimation Paradigm

We can use optimal linear estimation theory to analyze the problem of signal estimation in linear cables. We assume that information is encoded in the time variations of the input current $I_s(t)$ which is injected at a certain location along the cable. We are interested in quantifying how much information is lost due to electrotonic attenuation and the membrane noise sources as the signal corresponding to this input propagates passively down the cable. We estimate this by assessing how well we can recover $I_s(t)$ from the voltage fluctuations $V(x, t)$ as a function of distance from the input location. By analogy with the problem in

Appendix A, $m(t)$ corresponds to $I_s(t)$ and $s(t)$ to $V(x, t)$. We can decompose $V(x, t)$ into two components, a signal component, $V_s(x, t)$, due to the input current $I_s(t)$ ($V(x, y, t)$ in equation 4.29), and a noise component, $V_n(x, t)$ ($V(x, t)$ in equation 4.13), reflecting the combined influence of all the noise sources that have been discussed in detail in Chapter 3. Due to linearity, $V(x, t) = V_s(x, t) + V_n(x, t)$.

The power spectrum of the signal component $V_s(x, t)$ defined as $S_V^s(x, y, f)$ can be written as

$$S_V^s(x, y, f) = \frac{S_s(f)}{G^2} |\mathcal{G}(x, y, f)|^2, \quad (4.38)$$

where $S_s(f)$ denotes the power spectral density of $I_s(t)$, $\mathcal{G}(x, y, f)$ denotes the Fourier transform of the Green's function of the cable and G is the input conductance. Similarly, the power spectrum of the noise component, $V_n(x, t)$, defined as $S_V^n(x, y, f)$, is given by

$$S_V^n(x, f) = \frac{S_n(f)}{G^2} \int_{-\infty}^{\infty} dy |\mathcal{G}(x, y, f)|^2. \quad (4.39)$$

We assume that the noise component $V_n(x, t)$ and the signal component $V_s(x, t)$ are uncorrelated with each other. Thus, the power spectrum of $V(x, t)$, denoted by $S_{VV}(x, f)$, can be expressed as

$$S_{VV}(x, f) = S_V^s(x, y, f) + S_V^n(x, f), \quad (4.40)$$

$$= \frac{S_s(f)}{G^2} |\mathcal{G}(x, y, f)|^2 + \frac{S_n(f)}{G^2} \int_{-\infty}^{\infty} dy |\mathcal{G}(x, y, f)|^2. \quad (4.41)$$

Similarly, the cross-spectrum between $I_s(t)$ and $V(x, t)$, denoted by $S_{iV}(x, f)$, is

$$S_{iV}(x, f) = S_V^s(x, y, f), \quad (4.42)$$

$$= \frac{S_s(f)}{G^2} |\mathcal{G}(x, y, f)|^2. \quad (4.43)$$

Thus, using equation A5, the expression for the optimal filter can be derived in the frequency domain as

$$\frac{S_V^s(x, y, f)}{S_V^s(x, y, f) + S_V^n(x, f)} \quad (4.44)$$

and the mean-square error \mathcal{E} for the signal estimation task is

$$\mathcal{E} = \int_{-\infty}^{\infty} df \frac{S_s(f) S_V^n(x, f)}{S_V^s(x, y, f) + S_V^n(x, f)}. \quad (4.45)$$

Notice that the computation of \mathcal{E} requires the knowledge of only the signal and noise spectra ($S_s(f)$ and $S_n(f)$ respectively) and the Green's function $g(x, y, t)$ of the cable. We assume that the input $I_s(t)$ is a white, band-limited signal with bandwidth B_s and variance σ_s^2 . This implies that the signal spectra $S_s(f)$ is flat over the frequency range $[-B_s, B_s]$ and zero elsewhere,

$$S_s(f) = \begin{cases} \frac{\sigma_s^2}{2B_s}, & |f| \leq B_s, \\ 0, & \text{otherwise.} \end{cases} \quad (4.46)$$

Substituting for equation 4.46 in equation 4.45 gives

$$\mathcal{E} = \frac{\sigma_s^2}{B_s} \int_0^{B_s} df \frac{S_V^n(x, f)}{S_V^s(x, y, f) + S_V^n(x, f)}. \quad (4.47)$$

As in Appendix A, the coding fraction can be defined as

$$\xi = 1 - \frac{\mathcal{E}}{\sigma_s^2}. \quad (4.48)$$

The coding fraction ξ is an index of the efficacy in the signal estimation task; $\xi = 1$ implies perfect reconstruction, whereas $\xi = 0$ implies performance at chance. We can also define a frequency-dependent signal-to-noise ratio $SNR(x, y, f)$, which is a ratio of the signal and noise power at frequency f ,

$$SNR(x, y, f) = \frac{S_V^s(x, y, f)}{S_V^n(x, f)}. \quad (4.49)$$

This allows us to express ξ as

$$\xi = \frac{1}{B_s} \int_0^{B_s} df \frac{SNR(x, y, f)}{1 + SNR(x, y, f)}. \quad (4.50)$$

If $SNR(x, y, f)$ monotonically decreases with frequency, for a fixed amount of input power σ_s^2 , the coding fraction ξ decreases with the input bandwidth B_s , *i.e.*, the reconstructions become poorer as the signal bandwidth increases. For an infinite cable, the signal component of the voltage fluctuations $S_V^s(x, y, f)$ depends only on the relative electrotonic distance $L = |x - y|/\lambda$ between the input and measurement locations (y and x respectively) and not on their absolute values. Since the signal power attenuates with L , whereas the noise power is constant over the length of the cable, $SNR(x, y, f)$ (consequently ξ) decreases monotonically with L .

We can regard the signal estimation task as an effective continuous communication channel in the information theoretical sense (**Fig. 4.3A**). $I_s(t)$ denotes the input to the channel, whereas $\hat{I}_s(t)$, the optimal linear estimate obtained from $V(x, t)$, denotes its output. The effective additive noise added by the channel can be denoted by $\hat{I}_n(t)$. This channel model allows us to compute the mutual information between $I_s(t)$ and $V(x, t)$. If the input $I_s(t)$ is Gaussian and the voltage noise $V_n(x, t)$ can be assumed to be Gaussian (see Chapter 6 for conditions when this assumption holds), the membrane voltage $V(x, t)$ is also Gaussian and the mutual information between them is given by (Shannon, 1949)

$$\begin{aligned} I[I_s(t); V(x, t)] &= \frac{1}{2} \int_{-\infty}^{\infty} df \log_2 \left[\frac{S_{vv}(x, f)}{S_V^n(x, f)} \right], \\ &= \frac{1}{2} \int_{-\infty}^{\infty} df \log_2 \left[1 + \frac{S_V^s(x, y, f)}{S_V^n(f)} \right] \quad (\text{in bits/sec}). \end{aligned} \quad (4.51)$$

In terms of $SNR(x, y, f)$ and the bandwidth B_s , the mutual information can be expressed as

$$I[I_s(t); V(x, t)] = \frac{1}{2} \int_{-B_s}^{B_s} df \log_2 [1 + SNR(x, y, f)] \quad (\text{in bits/sec}). \quad (4.52)$$

The capacity of a communication channel is defined as the maximum amount of information that can be transmitted across it. If the noise properties of the system are given, we are left to vary only the properties of the input signal to achieve maximal information transfer. It is known that when the noise is additive and Gaussian, the mutual information is maximized when the signal itself is Gaussian (Cover & Thomas, 1991). Since a Gaussian process is completely specified by its power spectral density, we need to find the optimal input power spectrum which maximizes I . This optimization is well-defined only when we impose some constraints on the input spectra, since I can be made arbitrarily high by choosing an infinite power input signal. Thus, we assume that the input is both power and bandwidth limited which is equivalent to saying that the input spectra satisfies the following constraint.

$$\int_{-B_s}^{B_s} df S_s(f) = \sigma_s^2, \quad (4.53)$$

where σ_s^2 is the input variance (power) and B_s denotes the input bandwidth. The capacity of the estimation channel can be formally defined as

$$C = \operatorname{argmax}_{S_s(f)} I [I_s(t); V(x, t)] \text{ such that } \int_{-B_s}^{B_s} df S_s(f) = \sigma_s^2. \quad (4.54)$$

We express $SNR(x, y, f)$ as a ratio of the input spectrum $S_s(f)$ and an effective noise power spectral density denoted by $S_{en}(f)$,

$$SNR(x, y, f) = \frac{S_s(f)}{S_{en}(f)},$$

where

$$S_{en}(f) = \frac{S_n(f)}{|\mathcal{G}(x, y, f)|^2} \int_{-\infty}^{\infty} dy |\mathcal{G}(x, y, f)|^2. \quad (4.55)$$

This allows us to rewrite $I [I_s(t); V(x, t)]$ in equation 4.52 as

$$I [I_s(t); V(x, t)] = \frac{1}{2} \int_{-B_s}^{B_s} df \log_2 \left[1 + \frac{S_s(f)}{S_{en}(f)} \right]. \quad (4.56)$$

Setting up the optimization problem as a Lagrange multiplier problem, we need to maximize the following functional:

$$F(S_s, \nu) = \frac{1}{2} \int_{-B_s}^{B_s} df \log_2 \left[1 + \frac{S_s(f)}{S_{\text{en}}(f)} \right] - \nu \int_{-B_s}^{B_s} df S_s(f), \quad (4.57)$$

where ν is a Lagrange multiplier corresponding to the power constraint. A simple exercise in calculus of variations (Courant & Hilbert, 1989) reveals that at the extrema of $F(S_s, \nu)$, the following equation is satisfied:

$$S_s(f) = \left[\frac{1}{\nu} - S_{\text{en}}(f) \right]_+, \quad (4.58)$$

where

$$[x]_+ = \begin{cases} x, & \text{for } x \geq 0, \\ 0, & \text{for } x < 0. \end{cases} \quad (4.59)$$

The Lagrange multiplier ν can be determined by solving

$$\int_{-B_s}^{B_s} df \left[\frac{1}{\nu} - S_{\text{en}}(f) \right]_+ = \sigma_s^2. \quad (4.60)$$

The optimal way to distribute the available signal power is to transmit higher power at frequencies where the noise power is low and lesser or even zero power at frequencies for which the noise power is large. This procedure is graphically illustrated in **Fig. 4.3B**. Thus, when the effective noise spectrum is low-pass (high-pass respectively), the optimal input signal spectrum is high-pass (low-pass respectively). Those frequencies for which equation 4.58 can be satisfied without violating the power constraint (equation 4.53), the sum of the signal and noise power is constant. This is often referred to as the “water-filling” strategy (Cover & Thomas, 1991). By definition, the input power spectrum is non-negative ($S_s(f) \geq 0$) and so equation 4.58 cannot be satisfied for all frequencies in general, especially if the available input power σ_s^2 is small. Let Δ_s denote the set of frequencies, $\{f \mid -B_s \leq f \leq B_s, 1/\nu - S_{\text{en}}(f) \geq 0\}$, which is also referred to as the support of $S_s(f)$.

The capacity of the estimation channel can be formally expressed as

$$C = \frac{1}{2} \int_{\Delta_s} df \log_2 \left[\frac{\nu}{S_{\text{en}}(f)} \right] \quad (\text{in bits/sec}). \quad (4.61)$$

4.6 The Signal Detection Paradigm

We now consider the problem of detecting the presence of a synaptic input (in the form of a unitary synaptic event) from measurements of the membrane voltage $V_m(x, t)$ (over a period $0 \leq t \leq T$) at the location x along the length of the cable. The membrane voltage corresponds to either the noise process $V_n(x, t)$ (denoted by hypothesis H_0) or to a noisy filtered version of the EPSC (denoted by hypothesis H_1). As before, let X and Y be binary variables denoting occurrence of a presynaptic spike and the decision respectively. Thus, $X = 1$ if a spike occurred, else $X = 0$. Similarly, $Y = 1$ expresses the decision that a spike occurred. The binary signal detection problem can be formally expressed as

$$\begin{aligned} \mathbf{H}_0 : V_m(x, t) &= V_n(x, t), && \text{Noise} \\ \mathbf{H}_1 : V_m(x, t) &= V_s(x, t) + V_n(x, t), && \text{Signal + Noise} \end{aligned}$$

where

$$V_s(x, t) = \frac{1}{G} \int_0^t dt' g(x, y, t - t') I_s(t') \quad (4.62)$$

is the EPSP waveform given by the convolution of the EPSC $I_s(t) = I_{\text{peak}} t/t_{\text{peak}} \exp(1 - t/t_{\text{peak}})$ with the Green's function of the cable. The false alarm (F) and miss probabilities (M) are defined as

$$P_F = \text{Prob}[Y = 1 | X = 0], \quad P_M = \text{Prob}[Y = 0 | X = 1].$$

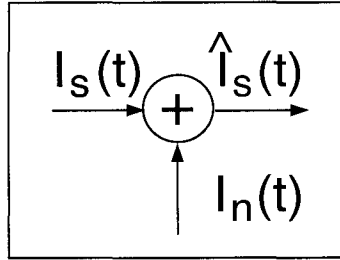
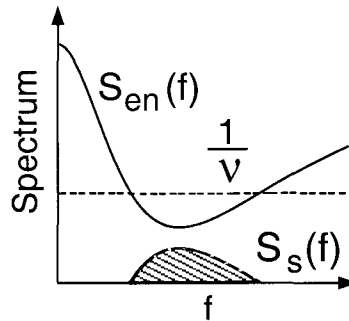
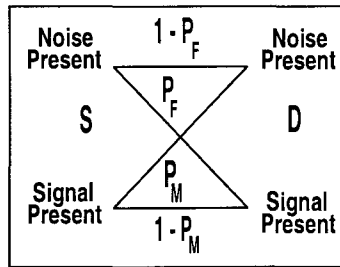
A Estimation Channel**B "Water Filling"****C Detection Channel**

Figure 4.3: Channel Models for the Signal Estimation and Signal Detection Paradigms. **A:** Effective communication channel model for the signal estimation task. The injected current $I_s(t)$ represents the input to the channel and the optimal linear estimate $\hat{I}_s(t)$ derived from the membrane voltage $V(x, t)$ represents the channel output. $\hat{I}_n(t) = \hat{I}_s(t) - I_s(t)$ is the equivalent additive noise introduced by the channel. **B:** Graphical demonstration of the “water-filling” algorithm used to compute the channel capacity for signal estimation. $S_{en}(f)$ represents the effective current noise spectral density due to the membrane noise sources (referred back to the input), ν represents the Lagrange multiplier (equation 4.58), and $S_s(f)$ represents the optimal signal power spectrum which maximizes channel capacity. For the given amount of signal power (σ_s^2), the optimal strategy is to transmit higher power at frequencies where the noise power is low and vice versa, such that, wherever possible, the sum of the signal power and noise power is a constant ($1/\nu$). **C:** Effective binary communication channel model for signal detection where the goal is to detect the presence of a synaptic input from the voltage $V(x, t)$ at a distance X from the input location. Binary random variables M and D denote the input and output of the channel respectively. False alarm P_F and miss error P_M rates of the optimal detector represent the cross-over probabilities of the binary detection channel.

The probability of detection error P_e is given by

$$P_e = p_0 P_F + (1 - p_0) P_M, \quad (4.63)$$

where p_0 and $1 - p_0$ are prior probabilities of occurrence of H_0 and H_1 respectively. The solution of the signal detection problem has been presented in Appendix C. By analogy, the membrane voltage $V_m(t)$ here corresponds to the signal $s(t)$. The decision rule which minimizes P_e is given by

$$r \underset{H_0}{\overset{H_1}{\gtrless}} \Theta, \quad (4.64)$$

where r is the output of the matched filter derived in Appendix C and Θ is the threshold chosen for optimal performance. Since r is a Gaussian random variable, it can be easily shown that its conditional means and variances (under H_0 and H_1) are given by

$$\mu_0 = 0; \mu_1 = \frac{1}{G^2} \int_{-\infty}^{\infty} df \frac{|N_{\text{syn}} \mathcal{G}(x, y, f) I_S(f)|^2}{S_V^n(f)}, \quad (4.65)$$

$$\sigma_0^2 = \sigma_1^2 = \sigma^2 = \frac{1}{G^2} \int_{-\infty}^{\infty} df \frac{|N_{\text{syn}} \mathcal{G}(x, y, f) I_S(f)|^2}{S_V^n(f)}, \quad (4.66)$$

where $I_S(f) = \mathcal{F}\{I_s(t)\}$ is the Fourier transform of the EPSC pulse and N_{syn} denotes the number of parallel synapses that are activated by a pre-synaptic action potential. Here we assume that the synaptic transmission is perfectly reliable and the synapses respond synchronously to the action potential. Thus, if there are N_{syn} synchronous synaptic connections between the dendrite and the pre-synaptic terminal, the current injected at the synaptic location due to a pre-synaptic action potential is scaled by a factor N_{syn} . For an investigation of the information loss due to synaptic unreliability, see Chapter 2.

The optimal value of the threshold Θ depends on the standard deviation σ and the prior probability p_0 . However, for equi-probable hypotheses ($p_0 = 1 - p_0 = 0.5$), the optimal threshold $\Theta = (\mu_0 + \mu_1)/2 = \sigma^2/2$ and the minimum probability of error is

$$P_e = P_F = P_M = \frac{1}{2} \text{Erfc} \left(\frac{\sigma}{2\sqrt{2}} \right). \quad (4.67)$$

The probability of error P_e ranges between $P_e = 0$, which implies perfect detection and $P_e = 0.5$ which implies chance performance (pure guessing). P_e decreases monotonically as σ varies from $\sigma = 0$ to $\sigma = \infty$. In the signal detection task, σ is equivalent to d' in psychophysics (Green & Swets, 1966) and plays the role that SNR does in the signal estimation task.

We can regard the overall decision system as an effective binary communication channel in the information theoretical sense. We denote the input and output of this channel by the binary random variables S and D , both of which assume values in the set $\{H_0, H_1\}$. The effective binary channel model corresponding to the detection task is shown in **Fig. 4.3C** with the errors P_F and P_M denoting the channel cross-over probabilities. In addition to P_e , the system performance can also be assessed by computing the mutual information $I(S; D)$ between S and D . For the binary detection channel, $I(S; D)$ can be computed as in Cover & Thomas (1991)

$$I(S; D) = \mathcal{H}[p_o(1 - P_M) + (1 - p_o)P_F] - p_o \mathcal{H}(P_M) - (1 - p_o) \mathcal{H}(P_F), \quad (4.68)$$

where $\mathcal{H}(x)$ denotes the binary entropy function,

$$\mathcal{H}(x) = -[x \log_2(x) + (1 - x) \log_2(1 - x)], \quad 0 \leq x \leq 1. \quad (4.69)$$

For equi-probable hypotheses

$$I(S; D) = 1 - \mathcal{H}(P_e) \quad (\text{in bits}). \quad (4.70)$$

Since S and D are binary random variables, $0 \leq I(S; D) \leq 1$. As before, $I(S; D) = 1$ bit implies perfect detection with no information loss whereas $I(S; D) = 0$ implies chance performance.

4.7 Results

We now use the formalism developed above to assess the efficacy of information transfer in an infinite, 1-D linear cable. As a first approximation, this can be regarded as a model of a weakly-active apical dendrite of a cortical pyramidal cell. Thus, the biophysical parameter values we shall use are obtained from the literature on pyramidal neuron models (Mainen & Sejnowski, 1998). In addition to estimating signal and noise magnitudes and studying the dependence of the different measures of signal fidelity (ξ , P_e , I) on the electrotonic distance X , we will also explore the effect of varying various biophysical parameters on these quantities.

4.7.1 Subthreshold Noise in a Weakly-Active Dendrite

The membrane noise sources we consider are thermal noise (due to thermal agitation of charge carriers), channel noise (due to stochastic channel openings/closings of K^+ and Na^+ voltage-gated ionic channels) and synaptic noise (due to the spontaneous background firing activity of presynaptic neurons). A discussion of the origins of these noise sources and their characterization was carried out in Chapter 3. Here we only make use of the expressions of the power spectral densities of the current noise sources, referring the reader to Chapter 3 for details. For $V_m \approx V_{rest}$, power spectral densities of these channel noise sources (K^+ , Na^+) are approximately Lorentzian ($[1 + (f/f_c)^2]^{-1}$). When the EPSC is modeled as an α function and the background activity assumed to be a homogeneous Poisson process, the power spectral density of the synaptic background noise is shaped like a double Lorentzian ($[1 + (f/f_c)^2]^{-2}$).

Using biophysical values for the K^+ and Na^+ channel densities and kinetics, synaptic innervation density, EPSC parameters and so on, obtained from the literature on the weakly-active properties of apical neocortical dendrites (Mainen & Sejnowski, 1998) (parameter values are summarized in the caption of **Fig. 4.4**), we computed the magnitudes of the different noise sources and quantified the corresponding voltage noise in a 1-D infinite cable (**Fig. 4.4**). The normalized auto-correlation functions of the noise sources and the Green's function of the cable are compared in **Fig. 4.4A**. Notice that the temporal spread of the

noise sources is much smaller (except for K^+ noise) than the Green' function of the cable. Thus, the noise spectra can be assumed to be approximately flat over the bandwidth of the cable thereby justifying the white noise approximation. The noise spectra are compared in **Fig. 4.4B** and the standard deviations of the voltage noise σ_V due to different sources are compared in **Table 4.1**. Notice that for the parameter values considered, the magnitude of voltage fluctuations σ_V is on the order of 1.4 mV, which is small enough to justify the perturbative approximation. Thus, in general, the magnitude of the voltage fluctuations can be used to test the validity of the approximation. It can also be seen that synaptic background activity is the dominant source of membrane noise. Thermal noise is almost negligible (at least up to 1000 Hz) in comparison to the other sources. Experimentally, these spectra can be computed by voltage-clamping the dendrite around V_{rest} and using different pharmacological manipulations to isolate individual contributions, *e.g.*, TTX to eliminate Na^+ noise, TEA to eliminate K^+ noise and so on (see Chapter 5). These spectra can then be compared with analytical expressions corresponding to different membrane noise sources derived in Chapter 3 and (DeFelice, 1981).

The power spectral density of the voltage noise in an infinite cable due to these distributed sources (using equation 4.28) is shown in **Fig. 4.4C**. The power spectral density of the contribution due to thermal noise alone is also shown alongside for comparison. Notice that the voltage noise spectrum is a monotonically decreasing function of frequency since the active membrane conductances are modeled as pure conductances. However, in general, the small-signal membrane impedance due to voltage and time dependent conductances can exhibit resonance and give rise to band-pass voltage noise spectra (Koch, 1999).

4.7.2 Signal Propagation in a Weakly-Active Dendrite

The filters responsible for shaping the synaptic input signal are scaled versions ($1/G$) of the Green's function of the infinite cable and are shown in **Fig. 4.5A**. Notice how the filter gain and bandwidth change with distance. At small distances from the input location (since $g(x, y, t)$ is symmetric, only the relative electrotonic distance X matters), the filter is sharply peaked and has a high gain. However, at larger distances, the filter becomes broader and

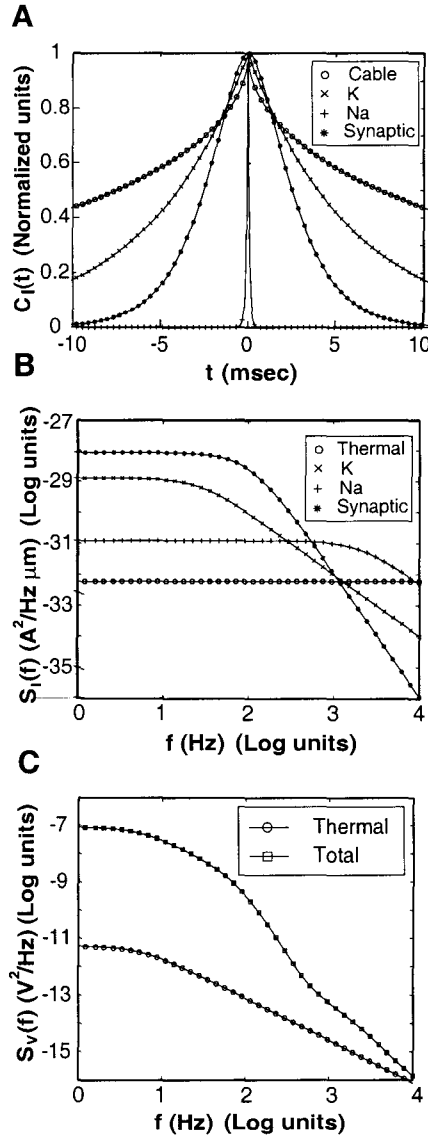


Figure 4.4: **Subthreshold Membrane Noise in a Dendritic Cable.**

A: Comparison of the normalized correlation functions $C_I(t)/C_I(0)$ of the different noise sources with the autocorrelation of the Green's function of an infinite cable, for parameter values summarized below. **B:** Comparison of current power spectra $S_I(f)$ of the different membrane noise sources, *viz.*, thermal noise, K^+ channel noise, Na^+ channel noise and synaptic background noise as a function of frequency (up to 10 kHz). **C:** Voltage spectrum $S_V(f)$ of the noise in a weakly-active dendrite due the influence of the above sources. Power spectrum of the voltage fluctuations due to thermal noise alone $S_{V_{th}}(f)$ is also shown for comparison. Summary of the parameters adopted from Mainen & Sejnowski (1998) to mimic the apical dendrite of a layer V pyramidal neuron: $R_m = 40 \text{ k}\Omega\text{cm}^2$, $C_m = 0.75 \text{ }\mu\text{F}/\text{cm}^2$, $r_i = 200 \text{ }\Omega\text{cm}$, d (dendritic diameter) = $0.75 \text{ }\mu\text{m}$, $\eta_K = 2.3$ channels per μm , $\eta_{Na} = 3$ channels per μm , $\eta_{Syn} = 0.1$ synapses per μm with backgrounds activity modeled as a Poisson process with mean firing rate $\lambda_n = 0.5 \text{ Hz}$, $E_K = -95 \text{ mV}$, $E_{Na} = 50 \text{ mV}$, $E_{Syn} = 0 \text{ mV}$, $E_L = -70 \text{ mV}$, $\gamma_K = \gamma_{Na} = 20 \text{ pS}$. Refer to Chapter 3 for details.

Noise Type	σ_V
Thermal	0.012 mV
K ⁺	0.459 mV
Na ⁺	0.056 mV
Synaptic	1.316 mV
Total	1.395 mV

Table 4.1: **Subthreshold Noise Magnitude in an Infinite Cable.**

Comparison of the magnitudes of voltage noise contributions due to different membrane noise sources in our weakly-active infinitely long dendrite. For parameter values, see the caption of **Fig. 4.4**.

has lower gain owing to the fact that some signal is lost due to leakage through the transmembrane resistance. The increase in temporal spread of the filter with distance is due to the increased capacitance that needs to be charged up as the measurement location moves further away from the input location (X increases), causing the effective time constant of the filter to increase.

The voltage change due to a synaptic input (in the form of an EPSC pulse) are obtained by convolving the EPSC waveform (shown in the inset) with $g(x, y, t)/G$. The membrane voltage depolarizations (from V_{rest}) due to the delivery of a unitary EPSC at different distances are shown in **Fig. 4.5B**. The peak of the depolarization occurs at the synaptic location and is about 2.2 mV. Notice that at $X = 0$, the EPSP is almost identical in shape to the excitatory post-synaptic current (EPSC) waveform, implying that the filtering due to the cable is minimal. However, at larger distances, the EPSP becomes smaller in magnitude and its temporal spread increases. For both these figures, distances are expressed in dimensionless electrotonic units, where λ is around 550 μm .

We also examine the dependence of variance of the voltage fluctuations σ_V^2 due to the injection of a random current input on the electrotonic distance X . The current $I_s(t)$ is in the form of a Gaussian random process of variance σ_s^2 . Its power spectrum is assumed to be spectrally flat over a bandwidth B_s (inset of **Fig. 4.5C**.) The standard deviations of the resulting voltage fluctuations σ_V as a function of X , for different values of B_s , are shown in **Fig. 4.5C**. Notice that except for signals with small bandwidths (*e.g.*, 10 Hz in

the mentioned figure), where the membrane voltage fluctuations might be strong enough to generate action potentials, our weakly-active assumption is not violated for the most part. Thus, by measuring the magnitude of the resulting fluctuations for a set of biophysical parameters, one can easily verify the validity of our perturbative approximation on a case-by-case basis. Like the peak of the EPSP above, σ_V also decreases monotonically with X , representative of the fact that the signal component of the voltage attenuates with distance from the input location. Since the cable acts like a low-pass filter, higher frequencies are transmitted less effectively and so σ_V decreases with B_s (for a fixed σ_s). This allows us to intuitively predict that the reconstructions of $I_s(t)$ from $V(t)$ should get poorer as B_s increases.

We are now equipped with all the information we need to estimate the information loss of the synaptic signal due to electrotonic attenuation and the membrane noise sources, under the two coding paradigms.

4.7.3 Efficacy of Signal Estimation

The effective communication channel corresponding to the estimation task is shown in **Fig. 4.3A**. The channel input is the random current $I_s(t)$ and the channel output is the estimate $\hat{I}_s(t)$, obtained from $V(x, t)$ after convolution with the optimal linear filter $h(t)$. The effective noise introduced by the channel is the difference, $I_n(t) = \hat{I}_s(t) - I_s(t)$. If we assume that $I_s(t)$ is a Gaussian process with variance σ_s^2 , the channel reduces to the classical additive white band-limited Gaussian noise channel (Cover & Thomas, 1991). It is straight forward to compute the mutual information and capacity for this channel model (equation 4.52).

The coding fraction ξ and the mutual information $I[I_s(t); V(t)]$ as functions of X are plotted in **Fig. 4.6A** and **Fig. 4.6B** respectively. ξ is close to one for short distances but falls rapidly as X increases because the signal attenuates with distance. Moreover, the rate of decay of ξ with respect to X depends on B_s . Additionally, if the signal-to-noise ratio is a monotonically decreasing function of frequency (equivalently, signal power spectrum decays faster than the noise spectrum), ξ also decreases with B_s . Similarly, the mutual information

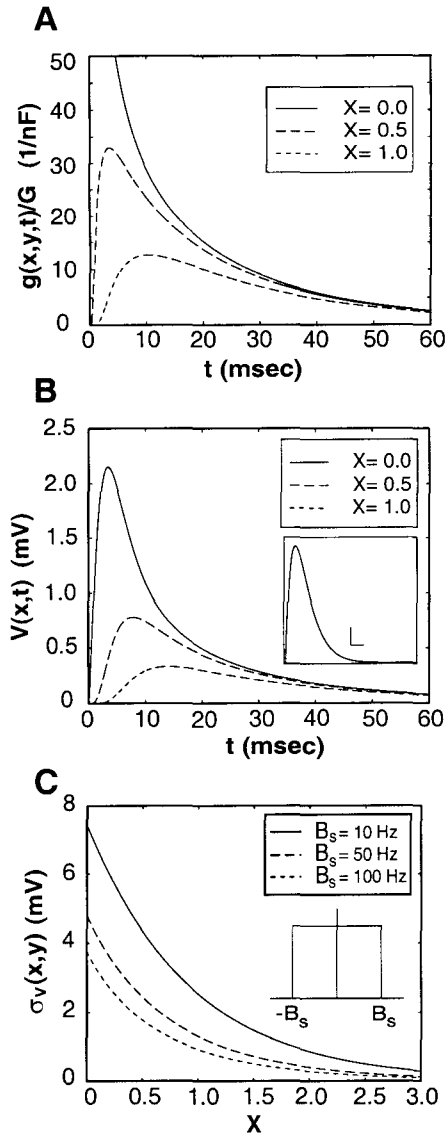


Figure 4.5: **Electrotonic Signal Propagation in an Infinite Dendritic Cable.**

A: Scaled version of the Green's function $g(x,y,t)/G$ for an infinite linear cable corresponding to different electrotonic distances expressed in dimensionless ($X = l/\lambda$) units. **B:** Excitatory post-synaptic potentials in response to an unitary EPSC input (**inset:** calibration 1 pA, 2 msec) at different electrotonic distances from the synapse, obtained by convolving the EPSC with the filters in A. **C:** The standard deviation of voltage fluctuations σ_V in response to a Gaussian white band-limited current waveform $I_s(t)$ of bandwidth B_s (**inset:** band-limited power spectrum of $I_s(t)$) and standard deviation $\sigma_s = 5$ pA plotted as a function of X for different values of B_s .

I decays monotonically with X . However, its dependence on B_s is slightly more complicated; at small distances I increases with B_s but this behavior reverses at larger distances.

An intuitive explanation for this phenomenon is as follows. The mutual information I broadly depends on two quantities, the signal-to-noise ratio (SNR) and the input bandwidth (B_s). In general, SNR is a function of frequency but for the moment let us assume that it is a frequency-independent constant. The expression for I in terms of SNR and B_s (a simplified version of equation 4.52) is given as $I = B_s \log(1 + SNR)$. SNR is inversely proportional to B_s ($SNR = \kappa/B_s$, where κ is the constant of proportionality) since for a fixed input power, if we increase B_s , the signal power per unit frequency (and thus SNR) decreases. For small values of X , the signal power is possibly much larger than the noise power and the SNR values for different B_s are large enough to lie in the saturating regime of the logarithm. Thus, for small X , the bandwidth component of the product ($I = B_s \log(1 + SNR)$) dominates and I increases with B_s . On the other hand, for large X , the magnitude of SNR is small, which implies $B_s \log(1 + SNR) \approx B_s SNR = \kappa$. Thus, one expects I to be independent of B_s for large X . The above analysis is valid exactly when the SNR does not depend on f (signal and noise spectra vary with f in a similar manner), which is not true in our case since the signal and noise spectra have different shapes. In our case, for large X , the product is marginally larger for a lower value of B_s as opposed to a higher value. This causes the slight reversal in I for large X .

We also numerically compute the information capacity for signal estimation using the “water-filling” algorithm, maximizing I by choosing the optimal $S_s(f)$ at each distance X (procedure illustrated in **Fig. 4.7**). In reality this is biophysically unrealistic since the optimal $S_s(f)$ depends on X , *i.e.*, the optimal signal power distribution is different for synaptic inputs received at different input locations. However, this allows us to compare performance for a particular choice of input spectra $S_s(f)$ (white band-limited spectrum, in our case) against the best achievable performance. We find that for the parameter values we consider, the capacity C is not significantly different in magnitude from I computed using a white band-limited input spectrum. I is indistinguishable from C for small X (high SNR) and is not significantly different in absolute terms for large X . As an example, the

maximum difference between C and I ($\sigma_s = 5$ pA, $B_s = 100$ Hz) is on the order of 8.5 bits/sec for $X \approx 1$. However, the magnitudes of C and I for $X \approx 1$ are about 22.4 bits/sec and 13.9 bits/sec respectively, and so as a percentage, the capacity is about 100% higher.

4.7.4 Efficacy of Signal Detection

The effective binary communication channel corresponding to the detection task is shown in **Fig. 4.3C**. The input to the channel is a random variable denoted by S which corresponds to the binary nature of the presence or the absence of an EPSC. Since the goal in the detection task is to detect whether or not such an event occurred, the output of the channel corresponds to this binary decision denoted by D . The cross-over probabilities of this detection channel are given by P_F and P_M .

The probability of error P_e and the mutual information $I(S; D)$ for the detection task are plotted in **Fig. 4.8A** and **Fig. 4.8B** respectively. P_e varies from $P_e = 0$ (perfect detection) for $X = 0$ to $P_e = 0.5$ (pure guessing) as $X \rightarrow \infty$. Correspondingly, $I(S; D)$ varies from 1 to 0 bits. We also vary the number of synchronous synapses N_{syn} , assumed to deliver EPSCs simultaneously in response to a pre-synaptic action potential. As can be seen from the figures, there is a critical distance before which an EPSC can be detected almost perfectly. However, once this threshold distance is exceeded, performance deteriorates considerably. This critical distance depends on the signal-to-noise ratio of the detection task, and increases with N_{syn} . This threshold behavior is due to the non-linear threshold decision rule of the signal detection task.

Thus, we find that considerations of signal-to-noise limit the distance over which synaptic signals can be reliably transmitted in noisy, weakly-active, dendritic cables. This is true for both the paradigms we consider here, though the threshold behavior is more pronounced for detection.

4.7.5 Comparing Cable Theory and Information Theory

In order to analyze and characterize the role of neurons as information-transmission and processing devices, we argue that the relevant metrics should not only be quantities like

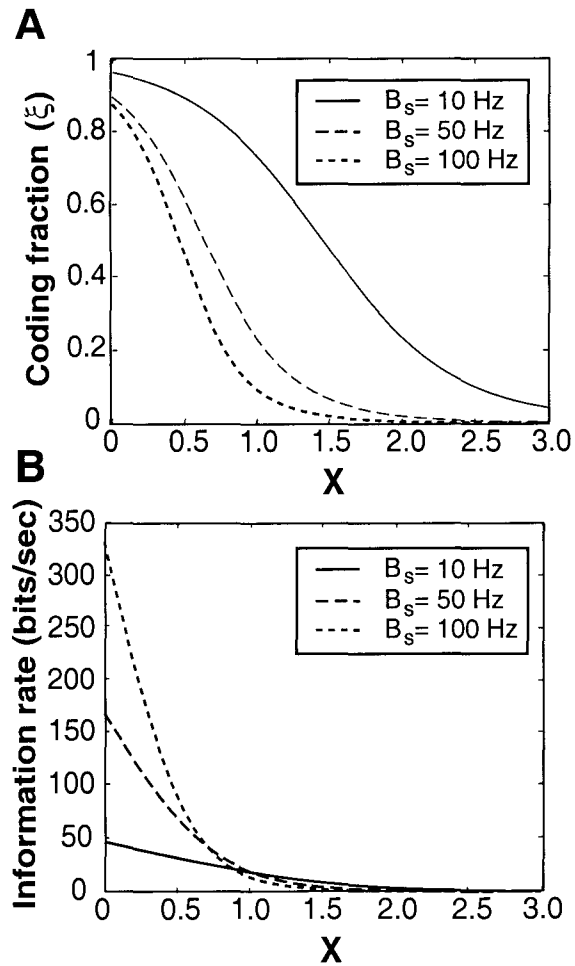


Figure 4.6: **Performance in the Signal Estimation Task.**

A: Coding fraction ξ and **B:** mutual information $I[I_s(t); V(t)]$ for an infinite 1-D cable as a function of electrotonic distance X from the input location for different values of the input bandwidth ($\sigma_s = 5$ pA). Parameter values are identical to those in Fig. 4.5.

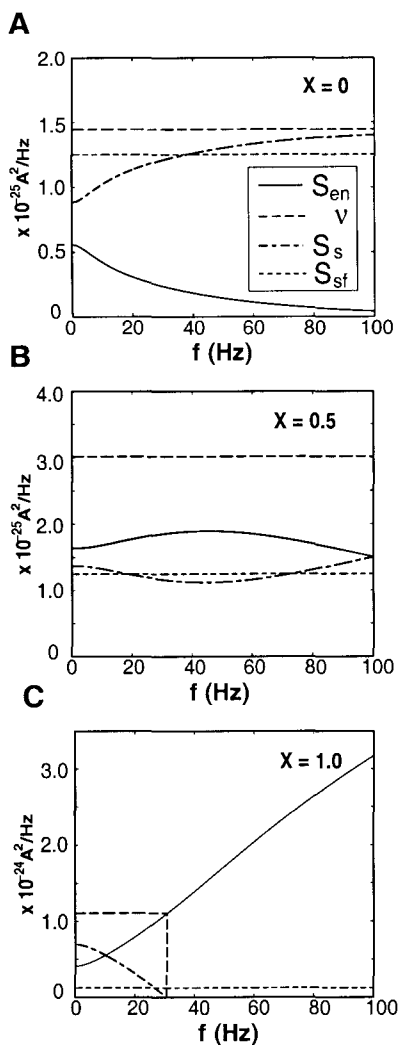


Figure 4.7: Channel Capacity in Signal Estimation Using the Water-Filling Algorithm. Graphical algorithm used to compute the channel capacity for the estimation task at three different electrotonic distances from the input location (see also **Fig. 4.3B**). The solid line denotes the effective noise $S_{\text{en}}(f)$, the broadly dashed line represents the Lagrange multiplier $1/\nu$ (equation 4.58), the dot-dashed curve represents the optimal signal power spectrum which maximizes channel capacity $S_s(f)$ and the narrowly dashed line represents the flat band-limited spectrum $S_{\text{sf}}(f)$ (equation 4.46). **A:** For $X = 0$, $S_{\text{en}}(f)$ is a low-pass spectrum, the optimal $S_s(f)$ is high-pass and is non-zero over the entire available bandwidth ($B_s = 100$ Hz) since there is sufficient input power available ($\sigma_s = 5$ pA). The channel capacity C and the mutual information I for a flat input spectrum S_{sf} are equal to 328 bits/sec. **B:** For $X = 0.5$ ($C, I \approx 88$ bits/sec), the band-pass nature of $S_{\text{en}}(f)$ reflects attenuation and filtering due to the cable. The optimal $S_s(f)$ has a complementary shape and is non-zero over the entire bandwidth. **C:** For $X = 1.0$ ($C = 22.4$ bits/sec, $I = 13.9$ bits/sec), the time constant of the cable filter is large and the signal power spectrum decays much faster than the noise spectrum. $S_{\text{en}}(f)$ is high-pass and due to signal attenuation, the magnitude of the noise is large compared to σ_s^2 . Equation 4.58 can only be satisfied over a limited portion of the available bandwidth. Parameter values are identical to those in **Fig. 4.5**.

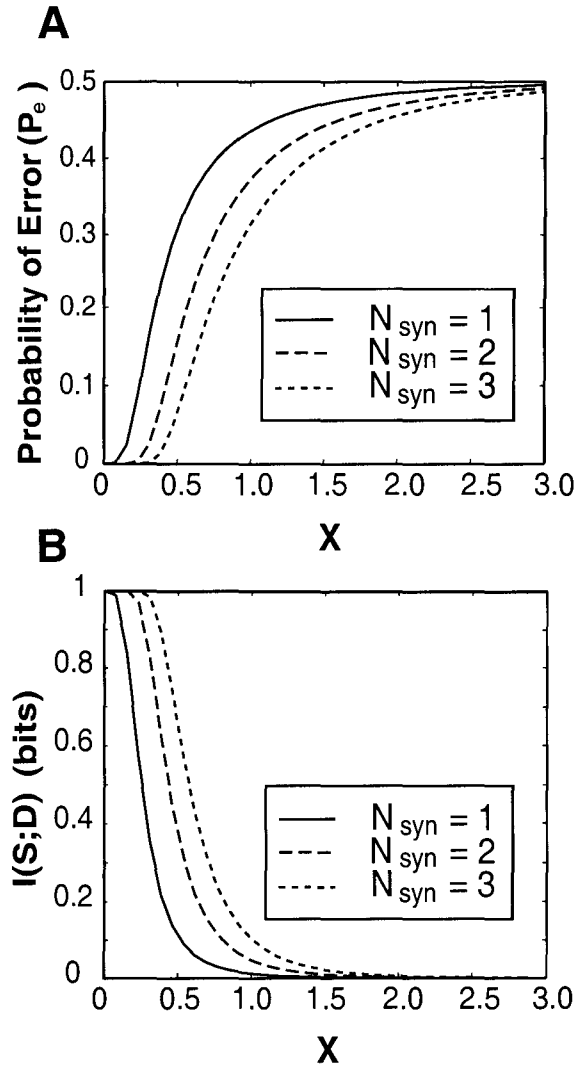


Figure 4.8: **Performance in the Signal Detection Task.**

A: Probability of Error P_e and **B:** mutual information $I(S;D)$ for an infinite cable as functions of the electrotonic distance X from the synaptic input. The number of synapses activated by a pre-synaptic action potential, N_{syn} , varies between one and three. The parameters associated with the EPSC are $g_{\text{peak}} = 100$ pS, $t_{\text{peak}} = 1.5$ msec, and $E_{\text{Syn}} = 0$ mV. Parameter values are identical to those in **Fig. 4.5**.

electrotonic length, attenuation of the EPSP peak or the charge delivered, and so on, which are motivated by physiology and an extensive application of cable theory over the last 40 years, but should also include information theoretical measures. As an application of our approach we have considered different information theoretical quantities like ξ , P_e , I and so on and examined how they vary with X .

In order to contrast our approach with that of classical cable theory, we compared some of our metrics against physiologically relevant quantities. In **Fig. 4.9A**, we plot the standard deviation of the voltage fluctuations σ_V in response to white band-limited noise injection as a function of X for different input bandwidths B_s . The standard deviations are normalized by their values at $X = 0$ ($\sigma_V(0)$) since their absolute values depend on B_s . The same procedure is carried out for the mutual information $I[I_s(t); V(x, t)]$, shown in **Fig. 4.9B**. It is clear that, for a given B_s , I decays relatively faster with X than σ_V . Moreover, the rate of decay with respect to X depends on B_s and is higher for I than σ_V . Thus for small X , even though I is higher for higher bandwidths (as seen in **Fig. 4.6C**), the rate of loss of information with distance is higher for signals with larger bandwidths. This can be intuitively expected since for large X the cable bandwidth is small and higher B_s signals have a greater portion of their power outside the bandwidth of the cable.

We also compared the mutual information $I(S; D)$ in the binary detection task with the peak of the synaptic potential and the steady-state voltage attenuation (e^{-X}) in response to DC current injection in **Fig. 4.9C**. It is clear that for small distances, $I(S; D)$ is almost constant even though the peak of the EPSP decays faster than e^{-X} . This is because the magnitude of the EPSP close to the postsynaptic location is large (around 2.2 mV at $X = 0$, **Fig. 4.5B**) compared to the level of the ambient noise ($\sigma_V = 1.395$ mV, **Table 4.1**) and can be detected almost perfectly. However, as soon as the EPSP becomes smaller than the noise, performance drops precipitously, much more steeply than the rate of decay of the peak post-synaptic potential. This threshold distance depends on the magnitude of the EPSP at $X = 0$ in comparison to the noise and is a measure of the signal-to-noise ratio of the detection task. This threshold behavior is quite characteristic of non-linear systems. The threshold nature of FM radio reception is a classic example of this phenomenon.

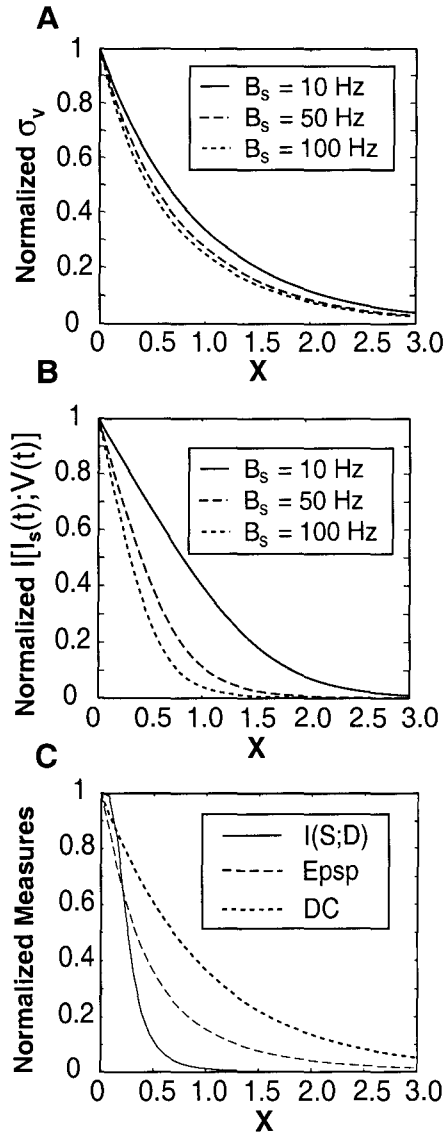


Figure 4.9: **Comparison of Classical Cable Theory vs. Information Theory.**

A: Standard deviation of voltage fluctuations σ_V and **B:** mutual information $I[I_s(t); V(t)]$ for the signal estimation paradigm as functions of the electrotonic distance X from the input location for different input bandwidths B_s ($\sigma_s = 5$ pA). For ease of comparison, all curves are normalized with respect to their values at $X = 0$. I is much more sensitive to B_s than σ_V . **C:** Comparison of the dependence of the normalized peak of the EPSP and the mutual information in the signal detection paradigm $I(S;D)$ ($N_{syn} = 1$) on X . The normalized steady-state electrotonic attenuation due to DC current injection is also shown. The detection performance is close to ideal for small X but after a certain threshold distance, performance drops significantly.

4.7.6 Dependence on Biophysical Parameters

There are several parameters in our analysis and it is neither prudent nor necessary to consider the effect of varying all of them, in multitude of different combinations possible, on the different variables of interest. Since the parameters belong to different equivalence classes (varying parameters within a class has the same effect on the variable of interest), it suffices to explore dependence with respect to the few abstract parameters characteristic of these classes instead of varying all the individual parameters. As a simple example to demonstrate this, consider the expression for the steady state synaptic conductance,

$$g_{\text{Syn}}^o = \eta_{\text{Syn}} \lambda_n g_{\text{peak}} e t_{\text{peak}}, \quad (4.71)$$

where η_{Syn} is the synaptic density, λ_n is the background mean firing rate of pre-synaptic Poisson neurons, g_{peak} is the peak synaptic conductance of a unitary synaptic event (modulated by an α function) and t_{peak} is the time when the peak is reached. Since g_{Syn}^o depends linearly on all the parameters in the product above, scaling the magnitude of any of the above parameters by a factor η causes g_{Syn}^o to be scaled by a corresponding factor η . Thus, these parameters belong to the same class (with respect to g_{Syn}^o) and can be represented by an abstract scale factor η .

First we consider the effect of simultaneously varying different parameters on the resting properties of the dendrite *viz.*, V_{rest} , G , τ and λ . We vary the abstract parameters corresponding to K^+ , Na^+ and synaptic conductances (except g_L) by the same factor. We denote this scale parameter η . Thus, $\eta = 0$ corresponds to a purely passive cable with only leak channels, whereas $\eta = 1$ corresponds to the nominal values of the parameters, obtained from the literature, that we have used so far. The results of this exercise are summarized in **Fig. 4.10A**. Instead of using absolute values for the quantities of interest, we normalize them with respect to their corresponding values at $\eta = 0$. Notice that V_{rest} changes (becomes more positive) by about 4%, λ changes (decreases) by about 9% and τ and G^{-1} change (decrease) by about 17%, as η is varied from 0 to 1. Despite the non-linearities due

to the active conductances K^+ and Na^+ , it is noteworthy that the quantities vary almost linearly with η . This further justifies our perturbative approximation.

The effects of parameter variation on the coding fraction ξ and the mutual information $I[I_s(t); V(t)]$ is explored in **Fig. 4.10B** and **Fig. 4.10C** respectively. Here, we allow parameters corresponding to the different noise sources to change individually (η goes from 0 to 1), while maintaining the others at their nominal values, in order to determine which noise source is dominant in determining performance. It is clear from the figures that the system performance is most sensitive to the synaptic noise parameters. The coding fraction ξ (for $X = 0.18$, corresponding to a distance of 100 μm from the input location) drops from around 0.96 in the absence of synaptic noise to around 0.78 when synaptic parameters are at their nominal values. This effect is even more dramatic for I which drops from around 480 bits/sec to around 225 bits/sec. The sensitivity to parameters associated with potassium channels is small and is almost negligible for Na^+ channel parameters.

4.8 Discussion

In this chapter, we investigated how neuronal membrane noise sources influence and ultimately limit the ability of one-dimensional dendritic cables to transmit information. In Chapter 3, we characterized some of the dominant sources of membrane noise (ion-channel fluctuations and background synaptic activity) that influence information processing of a signal as it propagates electrotonically over the neuronal membrane. By assuming that the conductance fluctuations due to these noise sources are small compared to the resting conductance of the membrane, we were able to derive a stochastic version of the cable equation satisfied by the membrane voltage fluctuations. We used this to derive analytical expressions for statistical properties of the voltage fluctuations (auto-covariance, power spectrum) in weakly-active dendrites in terms of the current noise spectra. Although we assumed arbitrary forms for the nature and properties of the synapses and the ion channel kinetics, our analysis can be readily generalized to include a variety of synapse types and ion channels governed by discrete-state Markov kinetic schemes.

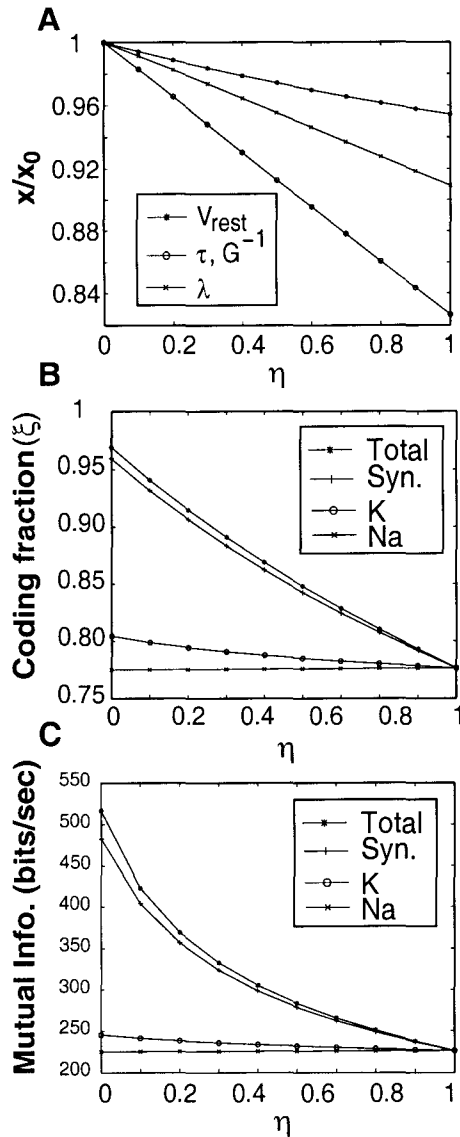


Figure 4.10: **Dependence of Subthreshold Noise on Biophysical Parameters.**

A: Dependence of the passive membrane parameters (V_{rest} , τ , λ) on the channel and synaptic densities. The K^+ and Na^+ channel densities and the synaptic density are scaled by the same factor η which varies from $\eta = 0$, corresponding to a completely passive system, to $\eta = 1$ which corresponds to the nominal weakly-active parameter values used to generate **Fig. 4.5**. The membrane parameters are expressed as a ratio of their values at $\eta = 0$. Effect of varying individual parameter values (the remaining parameters are maintained at their nominal values) on the **B:** coding fraction ξ and the **C:** mutual information I at a distance of $X = 100 \mu\text{m}$ ($X = 0.18$) from the input location. Thus, varying only the η associated with the synaptic background activity alone reduces both the coding fraction as well as the mutual information almost as much as changing the η associated with the synaptic and channel parameters.

We derived expressions for information theoretical measures, quantifying the information loss under the estimation and detection paradigms. In Chapter 2 we made use of these paradigms to estimate the information capacity of an unreliable cortical synapse. Thus, the present chapter should be seen as a next step in our efforts to understand the problem of neural coding in single neurons in terms of the properties of their distinct biophysical constituents (the synapse, the dendritic tree, the soma, axon and so on).

The present analysis can also be viewed within the context of a long-term research program to reformulate linear and non-linear cable theory in terms of an information theoretical framework. Instead of adopting the classical approach pioneered by Rall (Rall, 1959; Rall, 1969a; Rall, 1969b; Rall, 1989) which focuses on the voltage change in response to single or multiple synaptic inputs, its effect on the cell body, the initiation and propagation of action potentials and so on (Jack *et al.*, 1975; Johnston & Wu, 1995; Koch, 1999), here we evaluate the ability of biophysical model systems to estimate, detect and transmit information-bearing signals. We believe that like any information processing system, neural systems need to be analyzed with both the (bio)-physical and the information theoretical aspects in mind. For a related approach applied to electrical circuits, see Andreou & Furth (1998).

The novelty of our approach is that it combines classical cable theory with noise analysis and information theory in the context of neural coding allowing us to reinterpret results from cable theory using information theoretical measures. To be sure, membrane noise analysis has a long and successful history. Before the patch-clamp technique was developed, membrane noise analysis was traditionally used to provide indirect evidence for the existence of ionic channels and obtain estimates of their biophysical properties (DeFelice, 1977). The excellent monograph on membrane noise (DeFelice, 1981) contains a thorough treatment of different sources of noise in biological membranes, along with an exhaustive review of relevant early research in the field. Despite the universality of patch-clamp methods to study single channels today, noise analysis remains a useful tool for certain problems (Traynelis & Jaramillo, 1998; White *et al.*, 2000). Although most of the tools we use here are derived from DeFelice (1981) and the use of the signal estimation and signal detection paradigms

is also quite well documented in the literature, to the best of our knowledge, we believe that the marriage of these disciplines with a view to develop a reductionist bottom-up understanding of neural coding has not been attempted before.

Our theoretical analyses for a simplified cable geometry reveal that signal transmission is indeed limited by considerations of signal-to-noise and that information cannot be transmitted passively along dendrites over long distances due to the presence of distributed membrane noise sources. Our argument needs to be qualified, however, since the effect of realistic dendritic geometries and neuronal parameters needs to be more fully explored. Given the recent interest in determining the role of active channels in dendritic integration (Colbert & Johnston, 1996; Johnston *et al.*, 1996; Yuste & Tank, 1996; Mainen & Sejnowski, 1998), it seems timely to apply an information theoretical approach to study dendritic integration. The validity of our theoretical results need to be assessed by comparison with experimental data from a well-characterized neurobiological system. Refer to Chapter 5 for a summary of our preliminary experimental findings.

Our analysis makes a strong argument in favor of the presence of strongly active nonlinearities along apical dendrites for the sake of enhancing information transfer. As shown in **Fig. 4.8**, detecting the presence/absence of a synaptic signal over a distance greater than one space constant away is extremely difficult when the propagation takes place electrotonically. While the relevance of biophysical parameters used here to neocortical pyramidal cells needs to be examined, our results indicate that noise might limit the ability of extended apical dendrites to reliably signal distal events to the spike triggering zone and champions the need for “smart” amplifiers in the distal apical tuft that can amplify the signal but not the noise (Bernander *et al.*, 1994). Given the critical role of the apical dendrite in determining the thickness of the cortical sheet (Allman, 1990), it is plausible that signal-to-noise considerations also impose a fundamental constraint on the evolution of cortex.

Since our analysis only requires the Green’s function of the linear cable, it can easily be extended to complicated dendritic geometries. Morphological reconstructions of biological neurons, followed by compartmental modeling can be used to obtain realistic dendritic geometries (see Chapter 5). Using an information theoretical formalism to analyze different

dendritic morphologies can lead to the development of a graphical technique similar to the morpho-electrotonic transform (Zador *et al.*, 1995) to visualize the information transmission through the entire dendritic tree. Such a procedure will require the numerical computation of the Green's function between different locations along the dendritic tree and the soma. The expressions we have derived will allow a quantification of the information loss (in the detection/estimation paradigms) between the two locations. We believe that this procedure can be used to provide an important graphical abstraction of the dendritic tree from an information theoretical standpoint.

Table 4.2: List of Symbols for Chapter 3 and Chapter 4.

Symbol	Description	Dimension
γ_K	Single potassium channel conductance	pS
γ_{Na}	Single sodium channel conductance	pS
γ_L	Single leak channel conductance	pS
η_K	Potassium channel density	channels/ μm^2 (patch) channels/ μm (cable)
η_{Na}	Sodium channel density	channels/ μm^2 (patch) channels/ μm (cable)
η_{Syn}	Synaptic density	synapses/ μm^2 (patch) synapses/ μm (cable)
λ	Steady-state electrotonic space constant	μm
λ_n	Spontaneous background activity	Hz
σ_s	Standard deviation of injected current	pA
σ_V	Standard deviation of voltage noise	mV
θ_h	Time constant of sodium inactivation	msec
θ_m	Time constant of sodium activation	msec
θ_n	Time constant of potassium activation	msec
τ, τ_m	Membrane time constant	msec
ξ	Normalized coding fraction	1
A	Patch area	μm^2
B_s	Bandwidth of injected current	Hz
c_m	Specific membrane conductance per unit length	F/ μm
C	Total membrane capacitance	F
C_m	Specific membrane capacitance	$\mu\text{F}/\text{cm}^2$
C_{IK}	Autocorrelation of potassium current noise	$\text{A}^2/\mu\text{m}^2$ (patch) $\text{A}^2/\mu\text{m}$ (cable)
C_{INa}	Autocorrelation of sodium current noise	$\text{A}^2/\mu\text{m}^2$ (patch) $\text{A}^2/\mu\text{m}$ (cable)
C_{ISyn}	Autocorrelation of synaptic current noise	$\text{A}^2/\mu\text{m}^2$ (patch) $\text{A}^2/\mu\text{m}$ (cable)
d	Cable diameter	μm

Symbol	Description	Dimension
E_K	Potassium reversal potential	mV
E_{Na}	Sodium reversal potential	mV
E_L	Leak reversal potential	mV
E_{Syn}	Synaptic reversal potential	mV
g_K	Potassium conductance	S
g_L	Leak conductance	S
g_{peak}	Peak synaptic conductance change	pS
g_{Na}	Sodium conductance	S
g_{Syn}	Synaptic conductance	S
G	Total membrane conductance	S (patch) S/ μm (cable)
h_∞	Steady-state sodium inactivation	1
$I(S; D)$	Mutual information for signal detection	bits
$I(I_s, V)$	Information rate for signal estimation	bits/sec
m_∞	Steady-state sodium activation	1
n_∞	Steady-state potassium inactivation	1
N_{syn}	Number of synapses activated by a pre-synaptic spike	1
P_e	Probability of error in signal detection	1
r_a	Intracellular resistance per unit length	$\Omega/\mu\text{m}$
R_i	Intracellular resistivity	Ωcm
R_m	Specific leak or membrane resistance	Ωcm^2
S_{IK}	Power spectral density of potassium current noise	$\text{A}^2/\text{Hz } \mu\text{m}^2$ (patch) $\text{A}^2/\text{Hz } \mu\text{m}$ (cable)
S_{INa}	Power spectral density of sodium current noise	$\text{A}^2/\text{Hz } \mu\text{m}^2$ (patch) $\text{A}^2/\text{Hz } \mu\text{m}$ (cable)
S_{ISyn}	Power spectral density of synaptic current noise	$\text{A}^2/\text{Hz } \mu\text{m}^2$ (patch) $\text{A}^2/\text{Hz } \mu\text{m}$ (cable)
S_{ITh}	Power spectral density of thermal current noise	$\text{A}^2/\text{Hz } \mu\text{m}^2$ (patch) $\text{A}^2/\text{Hz } \mu\text{m}$ (cable)
S_V	Power spectral density of membrane voltage noise	V^2/Hz (patch) $\text{V}^2/\text{Hz } \mu\text{m}$ (cable)

Symbol	Description	Dimension
t	Time	msec
t_{peak}	Time-to-peak for synaptic conductance	msec
T	Normalized time (t/τ)	1
V	Membrane potential relative to V_{rest}	mV
V_{m}	Membrane potential	mV
V_{rest}	Resting potential	mV
x, y	Position	μm
X	Normalized distance (x/λ)	1

Chapter 5 Analysis of Preliminary Experimental Data

5.1 Introduction

In this chapter we propose experiments that can be performed to estimate subthreshold membrane noise in real neurons and validate the theoretical analysis in the previous chapters. We also summarize preliminary findings obtained upon analysis of data collected in the process of a two year long collaboration with Idan Segev's and Yossef Yarom's research groups at the Hebrew University of Jerusalem in Israel. The experiments were performed by Professor Yossef Yarom and his graduate students.

The analytical framework described in Chapter 3 was derived for simplistic models under a variety of assumptions, *e.g.*, the dendrite was modeled as an infinite 1-D cable, voltage fluctuations were assumed to be small enough to perform linearization, channel kinetics were assumed to be of Hodgkin-Huxley type and so on. Closed-form analytical expressions derived for these simplified models provide a general framework for characterization of biophysical noise sources in real biological neurons. We believe that a direct comparison between theoretical predictions derived for these simplified models and experimental measurements can help to refine the space of parameter values relevant to the design of more realistic compartmental models which have a large number of degrees of freedom.

We envision a broad interdisciplinary research program which combines theoretical, computational and experimental approaches to study the limits imposed by biophysical noise sources on neural information processing (see **Fig. 5.1**). The arrows indicate the interactions between theory, modeling and experiments and not a strict chronological progression. Existing statistical tools (*e.g.*, signal detection and estimation theory, information theory) can be combined with classical cable theory and experiments involving the measurement of subthreshold noise to gain insight into the ability of neurons to detect or estimate the

synaptic inputs that impinge at different locations on the dendritic tree in the presence of noise. Determination of the performance during these statistical tasks allows a direct assessment of influence of noise on limiting the information capacity of biological neurons.

5.2 Proposed Plan of Experiments

The proposed experiments we describe below have been designed to characterize three sources of neuronal noise, noise intrinsic to the stochastic nature of synaptic transmission, noise resulting from stochastic transitions of voltage-gated ion channels and noise due to spontaneous presynaptic bombardment. Neurons of different types and sizes, obtained from different cortical layers will be recorded from to study the effect of neuronal morphology and physiology on noise and information transfer.

Instrumental Noise

The first step is to quantify the measurement system as it represents the smallest source of noise that can be resolved. Thus, the magnitude and spectral characteristics of the instrumental noise due to the electrode, amplifier and the accompanying electronics need to be determined for comparison with biological noise measurements from neurons. The instrumental noise can be measured by placing an electrode in the physiological solution used to perfuse the preparation before creating a gigaohm seal on the cell. By using electrodes of different resistances, the contribution of thermal noise arising due to the additional serial resistance of the whole-cell configuration can be accounted for.

Estimation of Passive Membrane Properties

Before performing any pharmacological manipulations, it is important to determine the impedance and the time constant of the membrane. In a cell-attached configuration, the entire neuronal membrane cannot be successfully clamped. This implies that the area recorded from cannot be assumed to be isopotential and the impedance and time constant measurements are corrupted by geometric effects. However, if the soma is small enough and well-isolated from the dendritic tree, this effect is not very significant. Input impedance

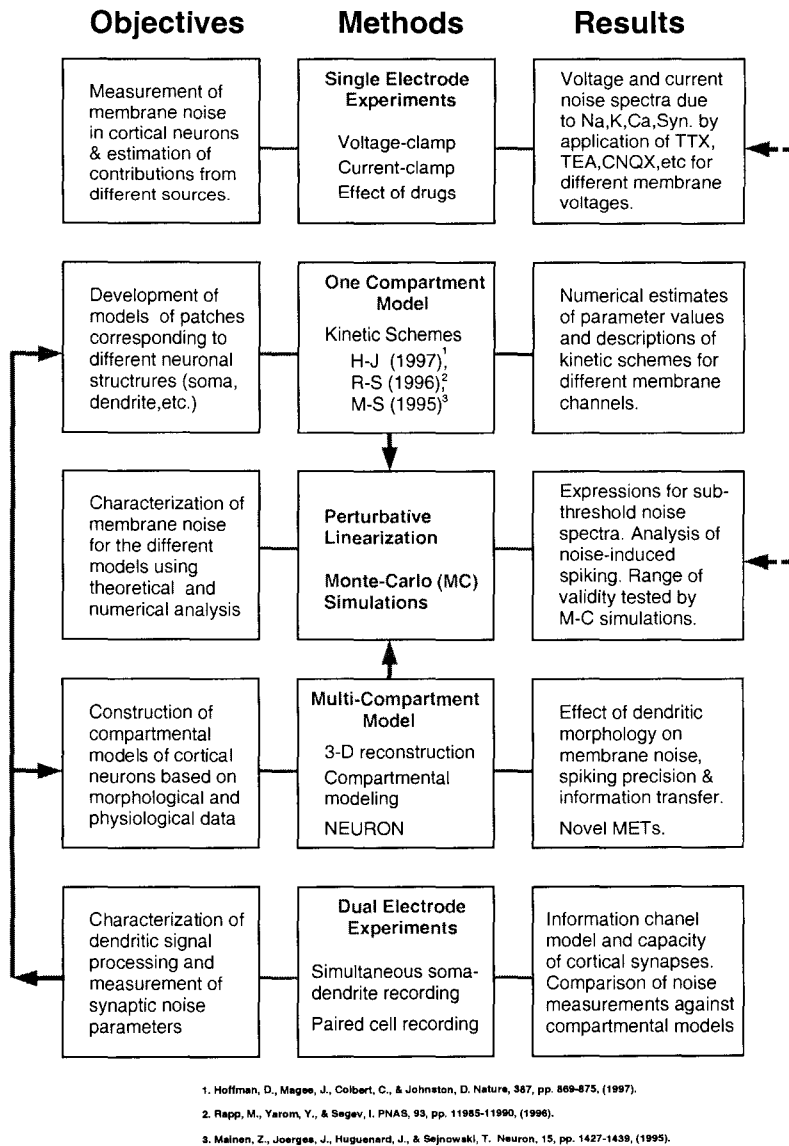


Figure 5.1: Outline of a Research Program to Study the Influence of Neuronal Noise on Information Transfer.

Schematic diagram describing the different methodologies as a part of a broad research initiative to understand the impact of neuronal noise sources on information processing. Solid arrows denote an application of techniques or results from one stage to refinement of a model of the other stage, whereas broken lines denote a comparison between results of two stages.

should be measured at different membrane voltages ranging from hyperpolarization to depolarization. It is important to ensure that within the voltage range chosen, the membrane behaves approximately linearly. Stimulating the soma by brief and small current pulses and measuring the resulting voltage changes allows us to estimate the membrane impedance and the passive time constant.

Single-Electrode Voltage- and Current-Clamp Recordings

The next step is to perform single-electrode voltage and current-clamp measurements (in the subthreshold regime) from the soma under different pharmacological conditions. The noise sources can be characterized by their magnitude (standard deviation), power spectra and amplitude distributions. In order to estimate the individual contributions of the different sources like stochastic conductance fluctuations due to ion channels (*e.g.*, K^+ , Na^+ , Ca^{2+}), synaptic background activity and so on, pharmacological agents which selectively block a specific source of noise can be applied.

For instance, addition of blockers of alpha-amino-3-hydroxy-5-methyl-4-isoxazolepropionic acid (AMPA) glutamate receptors such as 6-cyano-7-nitroquinoxaline-2,3-dione (CNQX) or 6,7-dinitroquinoxaline-2,3-dione (DNQX) can be used to eliminate noise due to fast excitatory synapses. Similarly, 2-amino-5-phosphonovaleric acid (APV) blocks N-methyl-D-aspartate (NMDA) glutamate receptors and bicuculline blocks gamma-amino-butyric acid (GABA) type synapses and can be used to eliminate noise due to slow excitatory synapses and inhibitory synapses respectively. With the synaptic noise eliminated, the residual noise is due to conductance fluctuations of voltage-dependent ionic channels, thermal noise and so on. Addition of tetrodotoxin (TTX) blocks voltage-dependent Na^+ channel activity, tetraethylammonium (TEA) and Cs^+ ions block K^+ channels and replacement of extracellular Ca^{2+} ions with Cd^{2+} or Co^{2+} ions eliminates Ca^{2+} channel noise.

Experiments in voltage-clamp mode measure the current noise due to stochastic conductance fluctuations, whereas, current-clamp experiments measure voltage fluctuations arising due to the global coupling of the voltage-dependent current noise sources through the membrane voltage and the filtering due to the impedance of the neuronal membrane. Thus, a

comparison of the noise measured in current-clamp versus voltage-clamp conditions reveals the synergistic effects between different noise sources.

Morphological Analysis

The three-dimensional morphology of the neurons recorded from can be reconstructed upon staining and be used to construct detailed compartmental models (see **Fig. 5.2**). Using Rall's 1-D cable theory, it is possible to estimate basic cable parameters, such as input resistance, membrane time constant and electrotonic length of the dendrites from voltage measurements in response to the injection of brief hyperpolarizing current pulses. By matching the experimental measurements to the model output in accordance with standard procedures documented in the literature (Segev *et al.*, 1998), detailed, physiologically accurate compartmental models for the stained cells can be constructed. Potential problems in obtaining faithful compartmental models, including problems with incomplete morphological reconstruction, non-uniqueness of biophysical parameters that match the experimental observations and so on, are elaborated in (Segev *et al.*, 1998).

Dual-Electrode Recordings

Using an infrared differential interface contrast (DIC) imaging system, it is possible to perform whole-cell patch recordings from different locations on the apical dendrites of pyramidal neurons. Recent experiments have shown that ionic channels expressed at distal dendritic locations differ from those present at the soma with respect to their densities and kinetics (Stuart & Spruston, 1998). Thus, characteristics of the noise in the apical tuft can be expected to be different from those of noise at the soma.

Dual-electrode recordings need to be performed in order to estimate the contributions of the dendritic and the synaptic components of the neuronal noise. Experiments involving dual recordings from the soma and the dendrite of the same cell, though difficult to perform, allow a direct comparison of the characteristics of the noise at different locations of the same neuron. Simultaneous measurements made at the soma and dendrites in response to the injection of subthreshold currents, either into the soma or the dendrite, can be used to reveal

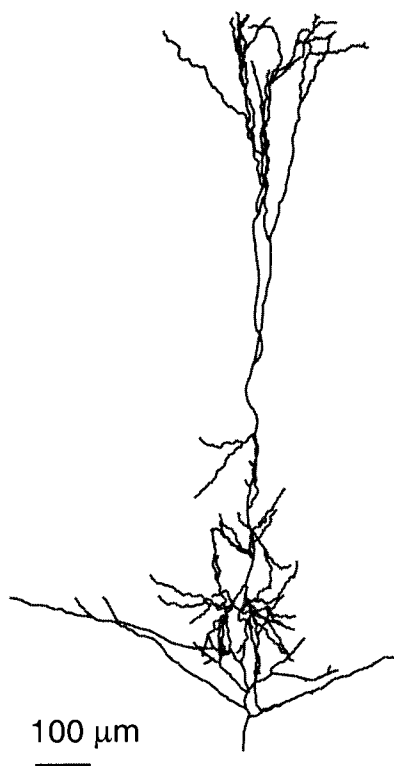


Figure 5.2: **3-D Reconstruction of a Cortical Pyramidal Neuron.**

The cell was stained intracellularly with 0.5% - 1% biocytin added to the pipette solution used to perform physiological recordings in the laboratory of Yossef Yarom. After establishing a whole-cell patch configuration, short (4 msec) hyperpolarizing pulses (50-100 pA) were applied for 2 minutes, after which the electrode was withdrawn. The slice was maintained at 32 °C for at least one hour, followed by overnight fixation in 4 °C in 0.1M cacodylate buffer containing 2% paraformaldehyde, 0.2% picric acid and 0.1% glutaraldehyde. After rinsing the slice several times with pento-barbitol sodium, it was treated with sodium borohydride (0.5%) to prevent non-specific staining and then rinsed and treated with MeOH (10%) and H₂O₂ (3%) to block endogenous peroxidases. Subsequently, it was incubated for at least 3 hours in biotinylated horseradish peroxidase conjugated to avidin with triton (0.5%) and rinsed and developed under visual control. Three-dimensional reconstructions were performed using the NeuroLucida system (microbrightfield), with the slice mounted on a glass slide in glycerol (50%), or dehydrated in ethanol. The cable properties and the different noise sources of a reconstructed cell are determined from the voltage response to brief current pulses. Subsequently, a detailed stochastic compartmental model of this cell is constructed.

the nature of the filtering due to the dendritic tree. Computation of the voltage attenuation function of the neuron can be performed by comparing the power spectral densities of the voltage responses at the two locations (Koch, 1999). Experiments studying the effect of excitable dendritic channels on dendritic signal transfer can be compared with theoretical results obtained in Chapter 4. Dual recordings from the soma and the dendrite are also very useful for constraining the passive cable properties of the measured neuron. Together with the morphological data obtained by reconstruction, cable properties can be used to construct a faithful compartmental representation of the neuron.

Similarly, dual recordings from pairs of synaptically connected layer V neurons can unravel the unreliability in the synaptic transmission. Presynaptic spikes with low temporal jitter can be induced in a presynaptic neuron and the statistics of the postsynaptic response can be used to estimate parameters like probability of vesicle release, coefficient of variation of the postsynaptic amplitude and so on of the synapse (see Chapter 2). The stimulation protocol needs to be performed at a frequency low enough to avoid synaptic depression or facilitation as well as adaptation effects in the spike generating mechanism.

5.3 Summary of Performed Experiments

The data summarized below were collected *in vitro* from pyramidal neurons in saggital slices of somatosensory cortex from two to three week-old rats. The neurons recorded from were usually of the simple-spiking type and belonged to layers IV or V. Recordings were made under visual inspection in whole-cell patch mode after creating a gigaohm seal between the patch electrode and the somatic membrane.

5.3.1 Preparation and Recordings

A brief description of the procedure used to obtain sagittal slices from the somatosensory cortex of 2-3 week old rats is as follows: rats were anesthetized with pentobarbitol sodium (Nembutal). Following decapitation, the brain was rapidly removed, mounted on a dissecting dish containing a cooled physiological solution (contents given below) and cut into 300 μm thick sections. Slices were then incubated in this solution at 37 °C for 30 minutes and

stored at room temperature. During the recordings, the slice was continuously perfused with the same solution at 32 °C. The physiological solution, aerated with 95% O₂ and 5% CO₂, was composed of (in mM): NaCl 123, KCl 2, MgSO₄ 1.3, KH₂PO₄ 1.2, NaHCO₃ 26, CaCl₂ 2.4, and Glucose 20.

The whole-cell patch technique was used for intra-cellular recordings with an Axoclamp 2A amplifier (Axon Instruments) for current-clamp experiments and Axopatch 1D for voltage-clamp experiments. The glass pipette was filled with intra-cellular solution composed of (in mM): potassium gluconate 120, NaCl 24, CaCl₂ 0.5, Mg-ATP 5, EGTA 5, and HEPES 10. The pH was set to 7.2 with KOH. With this solution, the microelectrodes have a DC resistance of 8-12 MΩ. For single channel recordings, Axopatch-1D or Axopatch-200B was used. For on-cell configuration, the glass pipette was filled with the extracellular medium and appropriate drugs (TTX, TEA, 4AP, Cs⁺, Cd²⁺) were used to block specific ion channels.

All experimental data was acquired and stored using a Pentium computer running Lab-View software. The sampling rate of data collection ranged between 3 and 10 kHz corresponding to a Nyquist frequency between 1.5 and 5 kHz. In hindsight, a sampling frequency of 5 kHz would have sufficed. A PCI MIO-16XE-10 A/D card (National Instrument) was used to generate the different current stimuli and digitize the data. The data was digitized and transferred directly to the computer hard disk. This procedure enabled the sampling of 3 minutes of data at 10 kHz for each measured condition. The data was subsequently written to a CD-ROM and successfully transferred using FTP over the Internet for further analysis.

5.3.2 Measurement of Instrumental Noise

In order to measure instrumental noise, the gain of the amplifier was adjusted so that the entire dynamic range of the A-D converter (± 32768 levels for a 16 bit card used for these experiments) was utilized. It can be assumed that in the presence of drifts and offsets the instrumental noise does not exceed 1 mV. Thus, the resolution of digitization available is on the order of 15 nV which is sufficient to estimate the magnitude and spectrum

Electrode	R (M Ω)	σ (μ V)
e3_s2	15.7	41.89
e5	12	37.65
e7	21.1	4.73
e7_s2	21.1	68.13
e8	14.8	37.03
e12	43	48.64
e13	46.8	92.27

Table 5.1: **Electrode Resistance and Instrumental Noise Magnitudes.**

Resistance and standard deviation of voltage noise for seven electrodes recorded after detachment from cell patch, placed in the extracellular space in the slice.

of instrumental noise accurately. Another issue to consider is the sampling rate. The sampling frequency should be high enough to prevent aliasing and low enough for reasons of data storage. In the absence of an anti-aliasing filter, a sampling frequency of 5 kHz was sufficient. The duration of the experimental recording determines the smallest frequency difference that can be resolved. In the following experiments, single recordings lasted 5-10 seconds each. In order to estimate the power spectrum of the noise accurately, 20 different sample records were collected. This permitted the collection of enough data to estimate the amplitude distribution of instrumentation noise and its power spectrum accurately.

Preliminary measurements of instrumental noise are summarized in **Table 5.1** and in **Fig. 5.4**. Approximately 10 samples each 10 seconds long were collected at $F_s = 3$ kHz giving us sufficient data to compute the relevant statistics.

5.3.3 Measurement of Biological Noise

Subsequent to the measurement of the instrumental noise, current clamp recordings were made from the soma of the pyramidal neurons under visual (IR) observation which measure the voltage noise due the conductance fluctuations from different sources. A three-minute-long recording session (at 10 kHz) was performed for a given experimental condition. A typical recording session in the control condition (in the absence of drugs) is shown in top and the second row of **Fig. 5.3**. Due to the high measurement gain, it is critical to ensure that the recordings are stable. Thus, the first and the last 20 seconds in each recording session include the injection of small hyperpolarizing test pulses, sufficient to perturb the

membrane by a few millivolts. The voltage response is used for assessing the stability of the recording session. Changes in the voltage response between the beginning and the end of each session imply instability (either in electrode or in membrane resistance) and the corresponding recording session is removed from the analysis. This significantly reduces the large variance expected in the experiments due to the high-resolution of recordings required for measuring neuronal noise. An example of the voltage response during these time epochs is shown in the third row of **Fig. 5.3**. The same experimental protocol is performed in all the experiments discussed below. Finally, voltage-clamp experiments allow us to measure the magnitude and characteristics of the fluctuations in the current entering the soma at different membrane potentials, ranging from hyperpolarization to depolarization (before spiking occurs). An important advantage of the voltage clamp technique is that it decouples the interaction between different noise sources (*e.g.*, between Na^+ and K^+ channels) that occurs as a result of global coupling due to membrane voltage changes in the current-clamp mode.

In a preliminary set of experiments, noise was measured from the soma of 25 layer V pyramidal neurons. Whole-cell patch recording in current clamp mode were used to measure voltage noise under different experimental conditions. These included different steady-state membrane voltages obtained by injection of appropriate holding currents, blockage of Na^+ channels by application of TTX at different levels of polarization, blockage of AMPA receptors with CNQX, DNQX and Co^+ ions, blockage of GABA receptors with bicuculline free-base, and blockage of K^+ channels with TEA.

Temperature is expected to have a significant effect on the magnitude and frequency composition of the different noise sources. Our experience shows that it is easier (more stable) to perform the experiments at a relatively low temperature (25 °C). However, in order to measure noise at near-physiological conditions, we will perform the experiments at a near-physiological range of 32 °C. If it does not prove possible to record at this temperature in a stable fashion for many hours, we will reduce the temperature until a stable regime will be found. Furthermore, we will assess the effect of temperature on noise by measuring noise

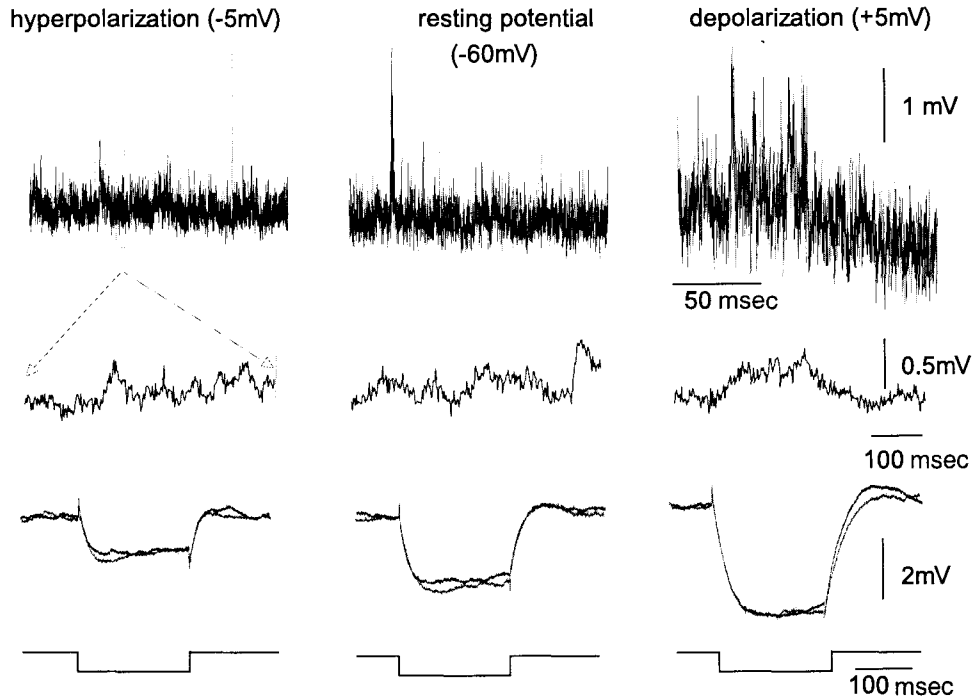


Figure 5.3: **Experimental Procedure to Measure Membrane Noise.**

Top row: Voltage recordings in current-clamp mode at resting potential (middle column); -5 mV hyperpolarization (left column) and +5 mV depolarization (right column), showing a clear increase in noise upon depolarization. **Second row:** Expanded time scale for the corresponding traces shown in upper traces. Slow fluctuations in the voltage noise, as well as the faster fluctuations, are clearly seen. **Third row:** At the beginning (red) and the end (blue) of each of the three-minute-long sessions, several hyperpolarizing current pulses (lower row) are applied. The voltage responses are compared to assess the stability of the recording during the session. Note the stability of recordings and the increase in apparent input resistance with depolarization.

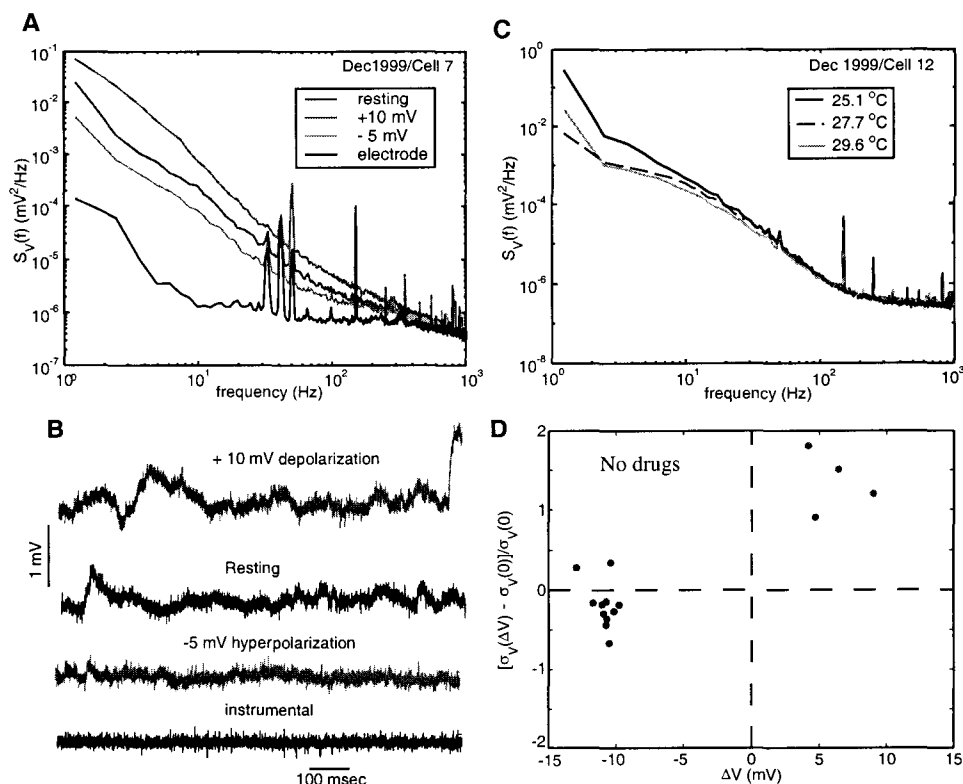


Figure 5.4: **Analysis of Measured Biological Noise.**

A: Power spectral densities of voltage noise recorded in current clamp mode from a layer V pyramidal neuron from the rat somatosensory cortex at different polarization levels. The membrane voltage was modified by injecting constant depolarizing or hyperpolarizing currents. The power spectral density of the instrumental noise, measured by placing the electrode in the physiological solution, is also displayed (black line). **B:** Sample traces of the voltage fluctuations recorded in the three corresponding membrane voltages and the instrumental noise as in **A**. Note the clear increase in voltage variability (noise) upon depolarization. **C:** Voltage noise spectrum from the soma of another layer V pyramidal neuron at the resting potential (-65 mV) for three different temperatures. There is surprisingly little effect of temperature on the noise measured. **D:** Dependence of the normalized variance of the noise on the membrane voltage for 15 neurons measured. The results clearly show the increase in variance with depolarization (red dots). We are currently performing voltage clamp measurements of current noise which will allow us to study the dependence of noise magnitudes on membrane voltage in the absence of the confounding effects of change in the membrane voltage due to spurious uncontrolled factors. The input impedance and time constant of the cells recorded from varied between 45-50 M Ω and 25-30 msec respectively.

(for a given pharmacological condition) at a range of different temperatures and different membrane voltages.

Instead of providing figures which indicate the effect of various drugs on noise here, below we summarize the salient observations that can be made from the data:

- The instrumental noise is an order of magnitude smaller in magnitude in comparison to the biological membrane noise. Its spectrum is flat over the range 10-1000 Hz and coincides with the biological noise spectra for frequencies above 1 kHz (see **Fig. 5.4A**). This implies that the biological noise has very little power at frequencies greater than 1 kHz.
- The magnitude of biological noise increases with depolarization of membrane voltage. On average, depolarization by 5 mV resulted in a 120% increase in the noise variance whereas hyperpolarization by 10 mV on average resulted in a 25% decrease in noise variance (see **Fig. 5.4D**). This is in rough agreement with the results of Chapter 3 and Chapter 6.
- It is possible, using different drugs, to consistently measure changes in noise magnitude and estimate the contribution due to different sources. The maximum absolute magnitude of noise was on the order of around 1 mV. In the neurons we recorded from, synaptic background activity was, in general, the most dominant source of subthreshold membrane noise. The magnitude of channel noise was small in comparison to background noise. The experiments were carried out in slices (*in vitro*) which are known to be “quieter” preparations. On the other hand, the magnitude of subthreshold membrane fluctuations *in vivo* can be quite large (on the order of 3-4 mV) (Destexhe & Pare, 1999) and the effect of voltage-gated ion channels can be greatly enhanced in those conditions. A collaborative effort to measure noise properties *in vivo* is currently underway.
- Around ten experiments were performed to study the variation of the magnitude and spectra of noise with temperature. **Fig. 5.4C** depicts the effect of temperature on the power-spectra of the noise. Although noise magnitude does seem to decrease with

an increase in temperature, the effect is very small in the case of noise measured at the resting state for temperature ranging between 25-32 °C. Our theoretical analysis (in Chapter 6) reveals that the noise magnitude should decrease with temperature. Thus, the experimental result possibly implies that decrease in noise is compensated by some yet unknown mechanism. This issue also needs further investigation.

Chapter 6 Subthreshold Membrane Noise due to Channel Fluctuations

6.1 Introduction

In this chapter we take a closer look at the noise generated due to random transitions of ion channels in neuronal membranes. Ion channels are macromolecules which are subject to random changes of conformational state due to thermal agitation. When these changes occur between a conducting and non-conducting state, the channel acts as a microscopic source of noise current injected into the membrane (Hille, 1992; DeFelice, 1981). Channel noise can change the spiking behavior of neurons, affect the distribution of response latencies (Lecar & Nossal, 1971a; Lecar & Nossal, 1971b; Clay & DeFelice, 1983; Rubinstein, 1995) and spike propagation in branched cable structures (Horikawa, 1991; Horikawa, 1993b), lead to the generation of spontaneous action potentials (Skaugen & Walløe, 1979; Skaugen, 1980b; Skaugen, 1980a; Strassberg & DeFelice, 1993; Chow & White, 1996) and influence the reliability and precision of spike timing (Schneidman *et al.*, 1998). For voltage-gated ion channels, such as the Na^+ and K^+ channels response for the generation of action potentials, the rates of transition between different conductance states are voltage dependent. This dependence on membrane voltage induces a coupling between otherwise independent stochastic channels. It has recently been shown that this coupling can affect spontaneous firing and bursting behaviors of neurons (DeFelice & Isaac, 1992; White *et al.*, 1995; Fox & Lu, 1994; Fox, 1997; White *et al.*, 1998).

In addition to the effects on action potential timing, channel noise can also cause subthreshold membrane voltage fluctuations. These fluctuations were studied extensively in the era prior to the development of patch-clamp techniques. For the analysis of membrane noise in the squid axon, see (Verveen & DeFelice, 1974; Wanke *et al.*, 1974; Fishman, 1975; Fishman *et al.*, 1975). (DeFelice, 1981) contains an extensive review of noise analysis in

other systems. See (Traynelis & Jaramillo, 1998; White *et al.*, 2000) for more recent applications. The main objective of these investigations was to argue for the existence of single ion-channels and to determine their properties.

Our interest in subthreshold voltage fluctuations stems from their potential impact on neural information processing. Although information is communicated in the neocortex and most of the peripheral nervous system using action potentials, it is important to understand subthreshold voltage fluctuations for several reasons: Firstly, these fluctuations may determine the reliability and accuracy of spike timing since voltage fluctuations near threshold affect precisely when an action potential is initiated. Secondly, computations within the dendritic tree, such as coincidence detection or multiplication of inputs, are performed in the subthreshold regime and the subthreshold channel noise might limit how well they can be performed. Thirdly, interaction between dendro-dendritic synapses in the olfactory bulb or the olivary nucleus and the operations of non-spiking neurons, such as in the retina or in the visual system of invertebrates, are all performed in the subthreshold regime.

At the biophysical level, the magnitude of subthreshold voltage noise is determined by ion channel kinetics. In Chapter 3, we derived expressions for the magnitude and power spectrum of the current noise by making simplifying assumptions for the stochastic state transitions of ion channels whose kinetics can be abstracted using finite state Markov models (Stevens, 1972; DeFelice, 1981; Colquhoun & Hawkes, 1982). In this chapter, we perform Monte-Carlo simulations to compute the subthreshold voltage fluctuations for two different kinetic schemes of neural excitability. The first kinetic scheme is the Hodgkin-Huxley (HH) model (Hodgkin & Huxley, 1952) of action potential generation in the squid giant axon. This model represents an excitable system which fires action potentials when depolarized by only a few millivolts from its resting state. The second kinetic scheme is one that has been proposed by (Mainen *et al.*, 1995) (MJHS) to model dendrites of a cortical pyramidal cell. This model is less excitable and does not fire action potentials for dendritic channel densities. These kinetic schemes represent two examples in the possible range of kinetic excitability.

The term goal of our research is to evaluate the effects of noise on information processing in model neurons with realistic cellular geometries. However, this type of modeling can be computationally very demanding and it is often useful to evaluate the ability of simpler approximations of channel kinetic schemes to reproduce membrane noise properties. Several approximations have been used to study subthreshold voltage fluctuations in the past. Koch (Koch, 1984) divided linear approximations of kinetic schemes into two categories: *passive linear* approximations, where active channels are replaced by pure conductances, and *quasi-active* linear approximations, where active channel kinetics are replaced by phenomenological impedances, which may have positive or negative resistive and reactive components. Mauro *et al.* (1970) used a quasi-active linearized approximation to the HH kinetic scheme to study subthreshold voltage responses to a current stimulus. In earlier chapters, we used a passive linear approximation to the MJHS kinetic scheme to study the predicted voltage noise fluctuations in both a patch of neuronal membrane (Chapter 3) and a semi-infinite cable model of a dendrite (Chapter 4). In Chapter 4 we also assessed the effect of the subthreshold noise fluctuations on information transfer.

In this chapter, we evaluate the subthreshold noise magnitudes predicted by the HH and MJHS kinetic schemes as function of steady-state membrane voltage, channel densities, patch area, temperature and so on. For both schemes, there is an increase in noise with membrane depolarization. This may affect the ability of the neuron to function as an integrator. We also calculate the power spectral densities and amplitude distributions of noise predicted by both kinetic schemes and evaluate how well quasi-active and passive linear approximations reproduce the simulated noise characteristics. Finally, we study how noise magnitudes and the quality of the linear approximations vary depending on parameters such as patch area, channel densities and temperature.

6.2 Methods

The successful elucidation of the ionic basis underlying neuronal excitability in the squid giant axon by Hodgkin and Huxley (Hodgkin & Huxley, 1952) led to the development of more sophisticated mathematical models which described the initiation and propagation of

action potentials by explicitly modeling the different ionic currents flowing across a neuronal membrane. In the original Hodgkin and Huxley model, membrane currents were expressed in terms of macroscopic deterministic conductances representing the selective permeabilities of the membrane to different ionic species. However, it is now known that the macroscopic currents arise as a result of the summation of stochastic microscopic currents flowing through a multitude of ion channels in the membrane.

Ion channels are protein macromolecules which switch randomly between discrete conformational states due to thermal agitation (Hille, 1992). In many cases, ion channel kinetics can be described in terms of the operation of a set of binary sub-units which can be open or closed. For instance, the conductance of an ion channel can be written as

$$g_i(V_m, t) = \gamma_i m^M h^H, \quad (6.1)$$

where γ_i denotes the open conductance of the channel and the variables m and h correspond to two different kinds of sub-units, *viz.*, activation and inactivation respectively. M and H represent the number of activation and inactivation sub-units respectively. In standard deterministic models of channel kinetics (like the classical Hodgkin-Huxley model), m and h are continuous variables which lie between 0 and 1 and obey first order kinetics,

$$\frac{dm}{dt} = \frac{m_\infty(V_m) - m}{\tau_m(V_m)}, \quad \frac{dh}{dt} = \frac{h_\infty(V_m) - h}{\tau_h(V_m)}, \quad (6.2)$$

where m_∞ (h_∞) is the steady-state value and τ_m (τ_h) is the time constant of activation (inactivation), which are functions of the transition rates between open and closed states of the subunits,

$$\begin{aligned} m_\infty(V_m) &= \frac{\alpha_m}{\alpha_m + \beta_m}, & \tau_m &= \frac{1}{\alpha_m(V_m) + \beta_m}, \\ h_\infty(V_m) &= \frac{\alpha_h}{\alpha_h + \beta_h}, & \tau_h &= \frac{1}{\alpha_h + \beta_h}, \end{aligned}$$

where α_m and β_m are the rates for the activation subunits and α_h and β_h are the rates for the inactivation subunits. For instance, for the rapidly inactivating HH Na⁺ channel,

$M = 3$, $H = 1$. For the non-inactivating K^+ channel, we will use the variable n to denote activation and N to indicate the number of activation gates; for the HH K^+ channel, $N = 4$.

This classical treatment represents the average behavior of large numbers of channels as continuous variables. Since ion channels behave probabilistically, stochastic models of ion channels finite-state Markov chains with state transition probabilities proportional to the kinetic rates between different conformational states (Clay & DeFelice, 1983; Strassberg & DeFelice, 1993). Although some recent studies have argued that ion channels have an infinite continuum of states and should be more appropriately abstracted using fractal models (Liebovitch & Toth, 1990; Liebovitch & Toth, 1991), we will use the Markov model description given the long history of its use. Thus, in finite-state Markov models of the HH K^+ and Na^+ channels, the state variables n , m and h denote the probabilities that the activation and inactivation gates are open and α_i and β_i denote the conditional transition probabilities between different states.

In the limit of a large number of channels, stochastic Markov models converge to their corresponding deterministic versions (Fox & Lu, 1994). However, for small channel numbers, the stochastic models can exhibit a wide variety of behaviors (spontaneous spiking, bursting, chaos, and so on) that are not observed in deterministic models (DeFelice & Isaac, 1992; White *et al.*, 1998). It has been shown that stochastic channel transitions can potentially explain the irregularity of spike timing observed in cortical neurons (Schneidman *et al.*, 1998). Furthermore, it was shown that the variability in spike timing depends on temporal properties of the input; this ability to alter the accuracy of their representation strategies depending on the nature of their inputs may enable neurons to act as “smart encoders” which adapt to the statistical structure of their ecological environment (Mainen & Sejnowski, 1995; Schneidman *et al.*, 1998).

The Markov models corresponding to the two kinetic schemes we study in this chapter are shown in **Fig. 6.1**. Salient differences between the MJHS and HH schemes are summarized in **Table 6.1**. In order to determine the magnitude and dynamics of membrane voltage fluctuations due to channel noise, we shall consider three different approaches. The first approach is simply to model each channel using a Markov kinetic scheme and to gener-

ate the transitions between conductance states in a Monte Carlo simulation. This approach accurately captures the effect of kinetic non-linearities, but is computationally very demanding. The other two approaches we consider are based on assuming that the magnitude of the voltage fluctuations about the steady-state value is small and that channel kinetics are approximately linear near this value; these assumptions permit closed-form solution of expressions for the noise fluctuations, thus reducing computational demands.

6.2.1 Monte-Carlo Simulations

Our Monte-Carlo simulations are similar to previous approaches (Skaugen & Walløe, 1979; Skaugen, 1980b; Skaugen, 1980a; Strassberg & DeFelice, 1993; Chow & White, 1996; Schneidman *et al.*, 1998) used to study the effects of channel noise on neuron spiking behaviors. The number of channels in each state of the kinetic model (**Fig. 6.1**) was tracked during the course of the simulation, which was performed iteratively using a fixed time step $\Delta t = 10 \mu\text{sec}$. During each step, the number of subunits making transitions between states i and j was determined by drawing a pseudo-random binomial deviate (bnldev subroutine (Press *et al.*, 1992) driven by the ran1 subroutine of the second edition) with N equal to the number of subunits in state i and p given by the conditional probability of the transition between i and j . The conditional probability p of making a transition was computed using the corresponding rate function, $\alpha(v)$ or $\beta(v)$, from the kinetic model under consideration, scaled from the base temperature for the model and channel to a standard temperature of 27°C using a factor $Q_{10}^{\Delta T/10}$, where $\Delta T = 27 - T_B$ for the appropriate channel model. The current flowing through the conducting states of the channels was used to charge the membrane capacitance, as shown in **Fig. 6.4**. The membrane voltage corresponding to equation G1 was integrated across the time step using the backward Euler method of the NEURON simulation program (Hines & Carnevale, 1997). For each set of parameters, 492 seconds of model time were simulated, divided into 60 blocks of 8.2 seconds each when computing power spectral densities (PSDs). Action potentials, which occurred less than once per second, were removed from the voltage traces prior to computing statistics or

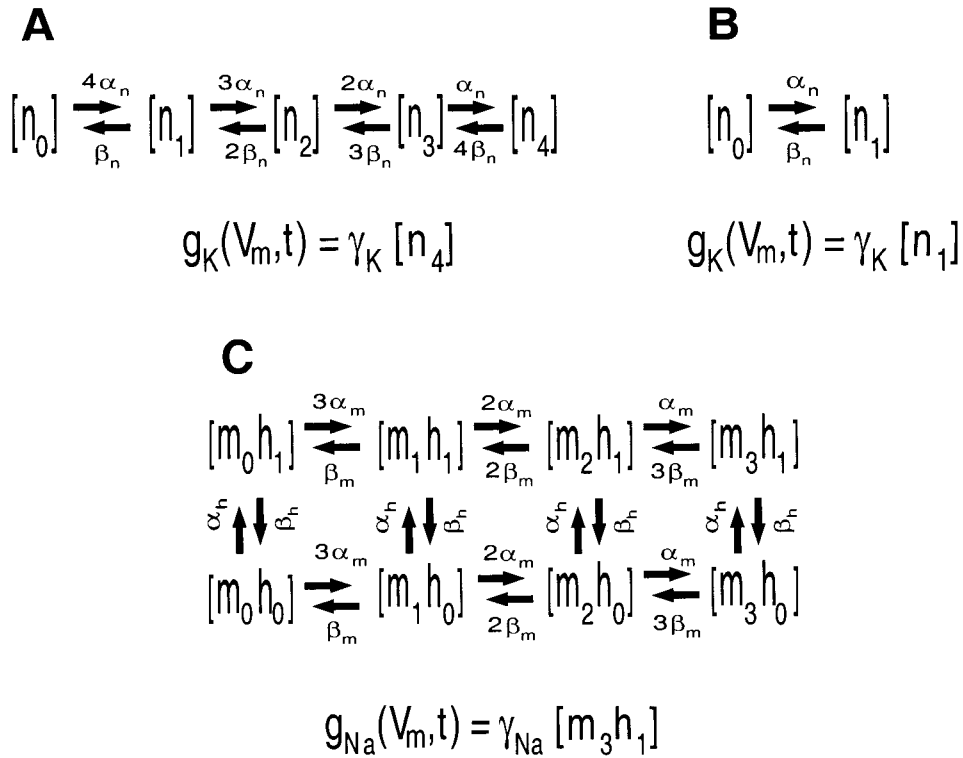


Figure 6.1: Finite State Markov Kinetic Schemes for Voltage-Gated Ion Channels.

A: Kinetic scheme for the voltage-gated Hodgkin-Huxley K^+ channel. $n_0 \dots n_3$ represent four closed states and n_4 is the open state of the channel. The K^+ conductance g_K is proportional to the number of open channels ($[n_4]$). γ_K is the single K^+ channel conductance. **B:** Kinetic scheme for the Mainen *et al.* K^+ channel. n_0 represents the closed state and n_1 the open state of the channel. The rates α_n and β_n are functions of the membrane voltage. **C:** Kinetic scheme for the HH and MJHS Na^+ channel. $m_0 h_1 \dots m_2 h_1$ represent the three closed states, $m_0 h_0 \dots m_3 h_0$ the four inactivated states and $m_3 h_1$ the open state of the channel. γ_{Na} denotes the open conductance of a single sodium channel. The rates α_m , β_m , α_h and β_h are functions of the membrane voltage.

PSDs. The standard deviation of voltage noise was computed for the samples at each time step of 492 seconds of simulated time. A portion of one simulation is shown in **Fig. 6.2**.

Due to random channel transitions, the membrane voltage fluctuates around the steady-state resting membrane voltage V_{rest} . By injecting constant currents of different magnitudes into the membrane patch, the steady-state voltage can be varied over a broad range. The range of possible steady-state voltages depends on the particular kinetic scheme. The current required to maintain the membrane at a steady-state voltage V_m^o can be determined from the steady-state i-v curve of the system, as shown in **Fig. 6.3**. Voltages for which the slope of the i-v curve is negative cannot be maintained as steady-states. By injecting an external current to offset the total membrane current, a fixed point in the negative slope region can be obtained, but since the fixed point is unstable, any perturbation, such as a stochastic ion channel opening or closing, causes the system to be driven to the closest stable fixed point. We measured subthreshold voltage noise only for stable holding voltages for which no spiking occurred.

6.2.2 Linearized Approximations

Assuming that the magnitude of the voltage fluctuations is small and that the membrane voltage fluctuates around its steady-state value, the kinetic equations can be linearized around their steady-state values (see Appendix G for details). In the simplest form of linearization, the patch is modeled as an RC circuit, as shown in **Fig. 6.4A**. The effect of the channel fluctuations is modeled as current noise I_n in parallel with the RC circuit. The power spectral density of I_n can be derived in terms of the channel kinetics (Stevens, 1972; DeFelice, 1981; Colquhoun & Hawkes, 1982). As in (Koch, 1984), we refer to this model as the passive linearized model.

If we include the voltage-dependence of the ionic conductances to first order, we get the equivalent circuit in **Fig. 6.4B**. r_i and l_i are small-signal phenomenological impedances which arise due to the dependence of the activation and inactivation probabilities on the membrane voltage and their first-order kinetics. As before, I_n models the effect of the channel fluctuations around the steady-state. **Fig. 6.4B** shows the equivalent circuit of the

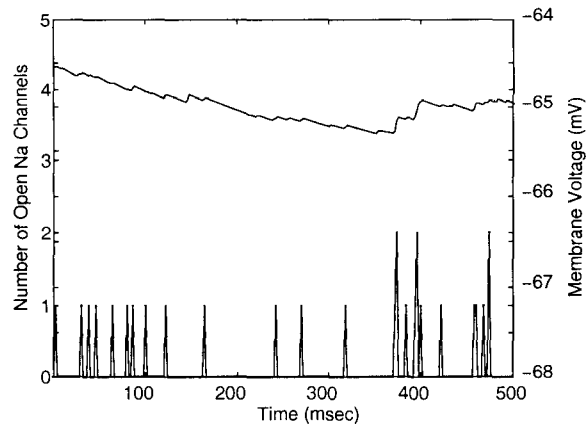


Figure 6.2: **Example of a Monte-Carlo Simulation.**

Monte-Carlo simulation of a $1000 \mu\text{m}^2$ membrane patch with stochastic Na^+ and deterministic K^+ channels with MJHS kinetics for the purpose of illustration only. Bottom record shows the number of open Na^+ channels as a function of time. Top trace shows the corresponding fluctuations of the membrane voltage. Holding current is injected to produce an average voltage of -65 mV .

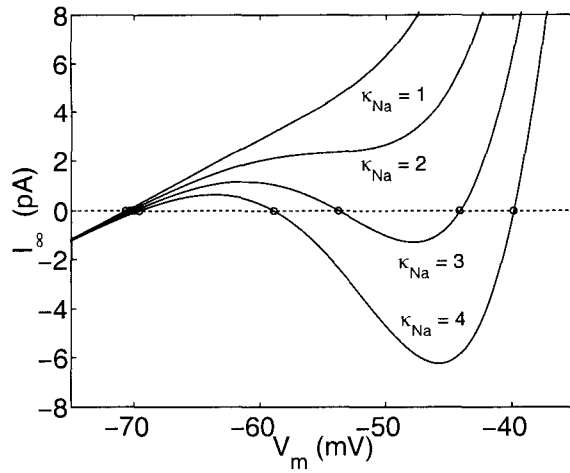


Figure 6.3: Steady-state i-v Curves for a Membrane Patch.

Steady-state i-V curves of a $1000 \mu\text{m}^2$ membrane patch for different multiples (κ_{Na}) of the nominal MJHS Na^+ channel densities. Circles indicate locations of fixed-points in the absence of current injection.

patch given by the parallel combination of a capacitance C , a (physical) conductance $G = g_K^o + g_{Na}^o + g_L$, three (phenomenological) series RL branches corresponding to K^+ activation, Na^+ activation and Na^+ inactivation. The current noise I_n is the same as before.

In order to verify the validity of these linearized approximations, we compare them to Monte-Carlo simulations of finite-state Markov kinetic schemes (**Fig. 6.1**) embedded in isopotential membrane patches. These simulations represent fully the non-linearities present in the kinetic scheme and allow us to compare the range of validity of the linearized, perturbative approximations for the two kinetic schemes. We believe that these approaches can be used generally to study kinetic schemes which can be described in terms of finite-state Markov models.

6.3 Results

Our goals in this research were to characterize and contrast the subthreshold noise predicted by two standard kinetic schemes for sodium and potassium ion channels and to then examine how accurately linearized quasi-active approximations to these schemes account for the noise. In the following sections we characterize the subthreshold noise by computing the variance, power spectral densities (PSDs), and distributions of voltage noise for the HH and MJHS kinetic schemes embedded in a $1000 \mu m^2$ patch of membrane. We also compute the change in noise magnitude predicted by these kinetic schemes when the patch area, channel densities and temperature are varied. For each of these characterizations, we determine how well linearized approximations predict the noise characteristics. In the last section, to illustrate the application of these approximations, we use the quasi-active linearized approximation of Na^+ and K^+ channel kinetics in a basic cylindrical model of a weakly-active dendrite to compute the efficacy of information transfer along the dendrite.

6.3.1 Magnitude of Subthreshold Noise

Fig. 6.2 shows the trans-membrane voltage and the number of open sodium channels during a stochastic simulation of ion channels in a patch of membrane. At -70 mV, only 1-2 Na^+ channels are open at any one time for the MJHS kinetic scheme. For the HH scheme

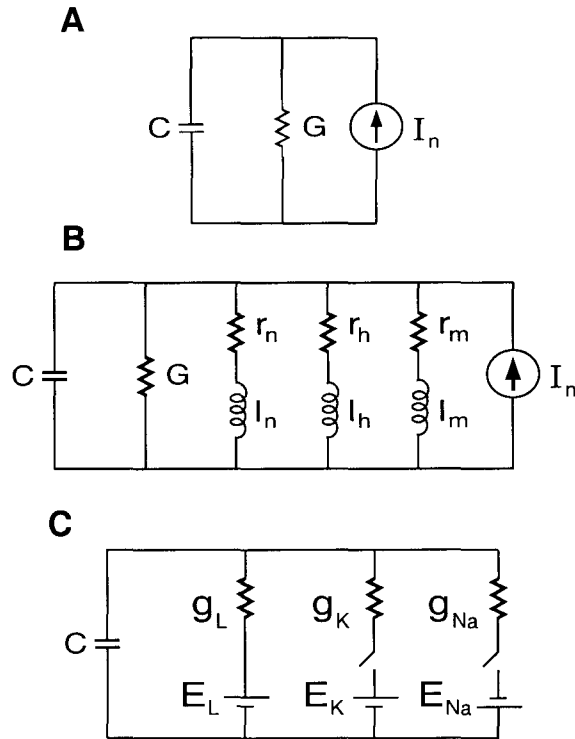


Figure 6.4: Models of a Membrane Patch Containing Stochastic Voltage-Gated Ion Channels.

A: Passive linearized model of the membrane patch containing stochastic voltage-gated ion channels (K^+ , Na^+). C denotes the transverse membrane patch capacitance. G is the sum of the steady-state conductances due to the active ion channels and the passive leak. The stochastic nature of the conductance fluctuations are modeled as a Gaussian current noise source I_n in parallel with the membrane. The power spectrum of I_n is computed from the Markov model of the channel kinetics.

B: Quasi-active linearized model which includes the small-signal phenomenological impedances due to voltage-dependence of the K^+ and Na^+ conductances. r_n , r_m and r_h denote the phenomenological resistances due to K^+ activation, Na^+ activation and inactivation respectively; l_n , l_m and l_h are the corresponding phenomenological inductances. I_n is a Gaussian current noise source as in A.

C: Stochastic model of the patch used for Monte-Carlo simulations. g_K and g_{Na} are stochastic ionic conductances with kinetics as in **Fig. 6.1**. E_L , E_K and E_{Na} denote the reversal potentials corresponding to the leak, K^+ and Na^+ conductances respectively.

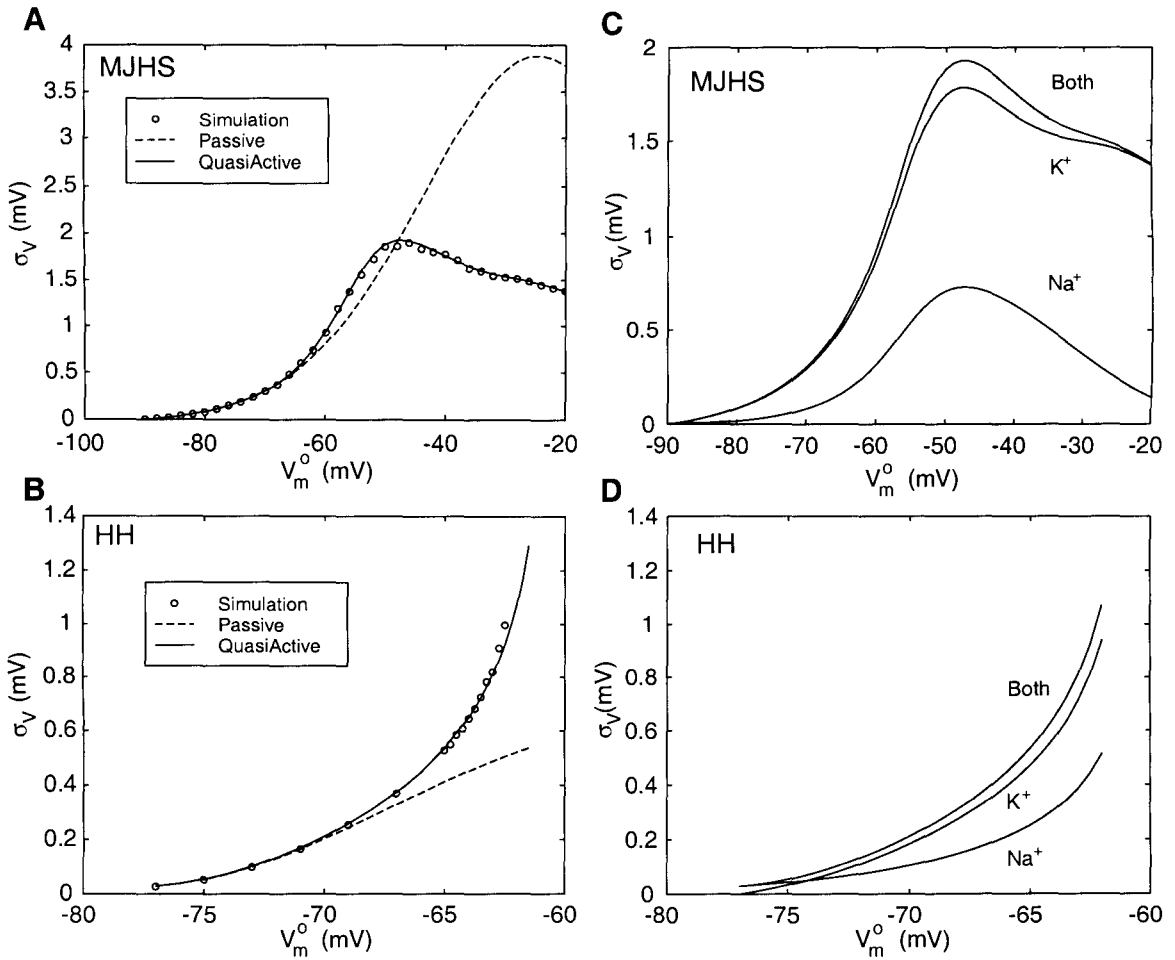


Figure 6.5: **Magnitude of Subthreshold Voltage Noise.**

A: Standard deviation, σ_V , of voltage fluctuations in a $1000 \mu m^2$ patch with MJHS kinetics as function of the steady-state voltage, V_m^o (current clamp mode). Circles: results of the Markov simulations; broken line: prediction of the passive linearized model; solid line: prediction of the quasi-active linearized model. **B:** σ_V of voltage noise for the HH kinetic scheme; note different voltage scale; symbols as in A. **C:** Individual contribution to σ_V from the K^+ and Na^+ noise sources for the MJHS kinetic scheme. **D:** As in C for the HH kinetic scheme.

at $V_{\text{rest}} = -65$ mV, 5 channels are open on average. **Fig. 6.5** shows the standard deviation of voltage noise predicted for the membrane patch using the HH and MJHS kinetic schemes. The HH scheme is strongly excitable and its threshold for firing an action potential is only 2.5 mV above the resting membrane potential (-65 mV); consequently, we only examine the subthreshold behavior below -62.5 mV. For both kinetic schemes, noise is nearly doubled as the trans-membrane voltage is depolarized from rest by 2.5 mV.

The underlying cause of this increase is the increasing probability that ion channels will spontaneously open. In the quasi-active linear model, this is reflected by a tuned LC circuit with a phenomenological inductance which is an increasing function of membrane voltage. **Fig. 6.5** shows individual ionic contributions to total voltage noise for the HH and MJHS kinetic schemes. These contributions were computed using a deterministic noise-free model of the channel not under consideration. The variances due to each channel add, so the standard deviation of the voltage noise with both noisy channels present is less than the sum of the standard deviations with each noisy channel separately. For both kinetic schemes, potassium channel noise is the dominant noise source.

For the MJHS kinetic scheme, noise continues to increase as the voltage is depolarized to -50 mV, for the reason given above. Above -50 mV, there is a decrease in voltage noise with further depolarization. This decrease is caused by the increasing membrane conductance, which reflects the large percentage of channels which are open in the steady-state. The inflection in the contribution of potassium channel noise between -40 and -30 mV is due to the rate of change of the sodium activation variable as a function of voltage; this change causes the membrane to act as tuned bandpass filter, which amplifies potassium channel noise.

For both kinetic schemes, comparison of the results from the Monte-Carlo simulations and quasi-active linearized approximations shows excellent agreement — to within 0.1 mV over all voltage ranges studied. In general, agreement with the quasi-active linear approximation will be good when noise fluctuations are small enough so that the linearization of the kinetic functions remains accurate. For example, for the K^+ channel, the linearization $n_{\infty}(V_m^o + \delta V_m) \approx n_{\infty}(V_m^o) + dn_{\infty}/dV_m \delta V_m$ is valid so long as $|\delta V_m| < 2$ mV. The results in

section 6.3.4 will show cases where this approximation fails to be as accurate. The passive linear approximation is much less accurate once the voltage fluctuations become larger than 0.5 mV.

6.3.2 Power Spectral Density of Subthreshold Noise

Fig. 6.6 shows the power spectral densities of voltage noise for the HH and MJHS kinetic schemes. The overall trends in the magnitude of the PSDs are reflected in the noise variances and were discussed above. The increasing value of the phenomenological inductance created by sodium channel activation shows itself in the PSDs for both kinetic schemes. For the MJHS scheme, the corner of the PSD for -40 mV is much sharper than the corners for -70 and -90 mV; this is caused by an LC circuit of phenomenological reactances which has a resonant frequency near 80 Hz. This tuned circuit of phenomenological reactances is even more evident in the PSD for the HH kinetic scheme. The PSD for -62.5 mV has a pronounced peak at 90 Hz, as measured by Mauro *et al.* (1970).

6.3.3 Amplitude Distribution of Subthreshold Noise

Fig. 6.7 shows the distributions of voltage noise for the HH kinetic scheme at two resting membrane potentials. At both voltages, the distribution of noise in a $1000 \mu m^2$ patch is Gaussian when the noise magnitude is 0.1 mV or larger. Similar results are obtained for the MJHS kinetic scheme. For more hyperpolarized voltages the noise magnitude is less than 0.1 mV, the shape of the distribution is less regular, and is difficult to interpret in light of the limited accuracy of numerical simulations; The magnitude is so small at this point, however, that the exact shape of the distribution will have little or no effect on neural information processing.

6.3.4 Dependence of Noise Magnitude on Patch Area

In this chapter, we have focused on comparing noise in two standard kinetic schemes which have been used in the literature. Each scheme is characterized by a number of kinetic parameters, such as voltages of half-activation and the power of the activation and inactivation

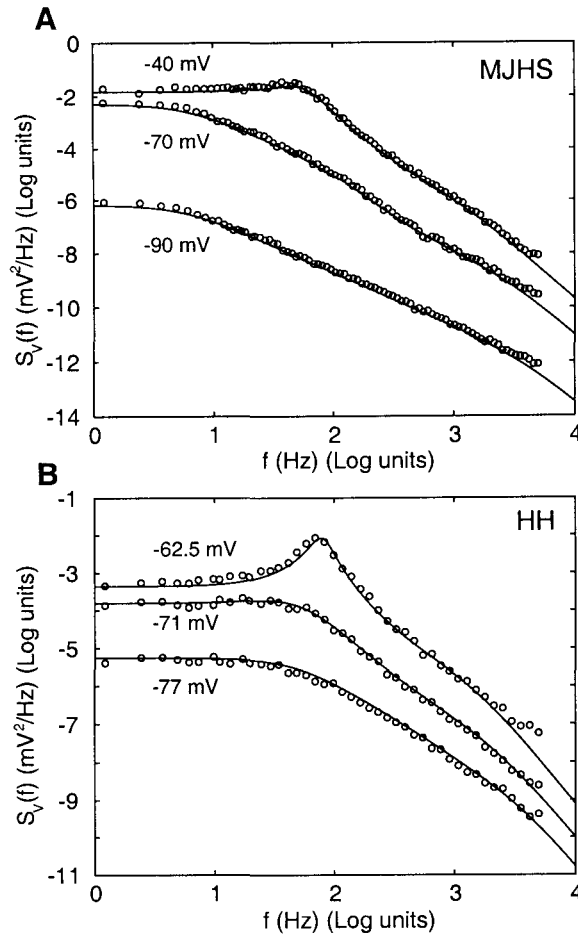


Figure 6.6: **Power Spectral Densities of Subthreshold Voltage Noise.**

A: Voltage power spectral densities for a $1000 \mu\text{m}^2$ patch with MJHS kinetics at different steady-state voltages. Circles indicate power spectral density estimates from simulations and the solid curves correspond to expressions for the quasi-active linearized model. The power spectral density is estimated by averaging ($n = 60$) the spectrograms (Hanning window, $f_c = 10 \text{ kHz}$) obtained from 8.2 second traces. **B:** Voltage PSDs for the HH kinetic scheme; symbols as in part A.

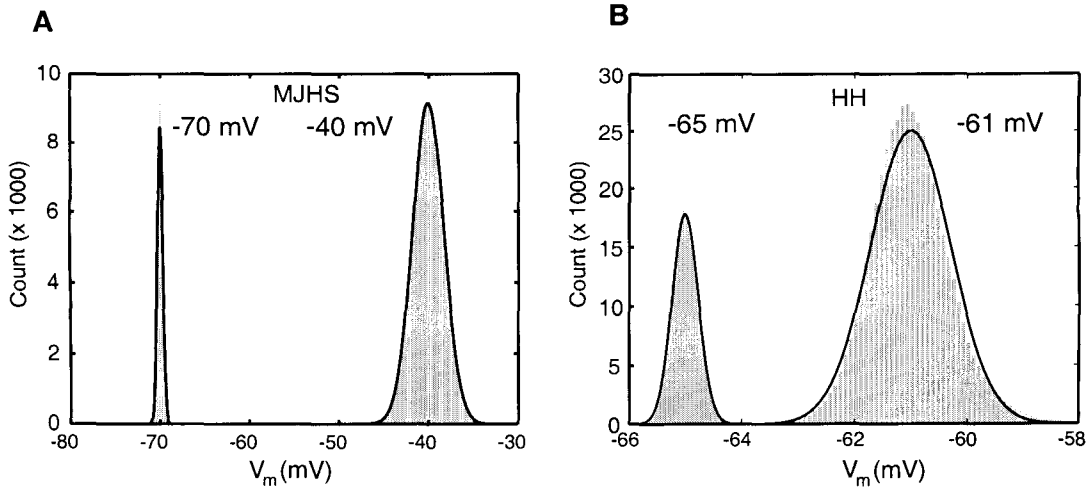


Figure 6.7: **Amplitude Distribution of Subthreshold Voltage Noise.**

A: Histograms of subthreshold voltage fluctuations due to channel noise in a $1000 \mu\text{m}^2$ membrane patch with MJHS kinetics for two different holding voltages ($V_m^o = -70 \text{ mV}$ and $V_m^o = -40 \text{ mV}$). Bars indicate results from simulations ($n = 49,1520$), solid curves show a normal distribution with the corresponding mean and standard deviation. **B:** Amplitude histograms for a $1000 \mu\text{m}^2$ patch with HH kinetics at $V_m^o = -65 \text{ mV}$ and -61 mV .

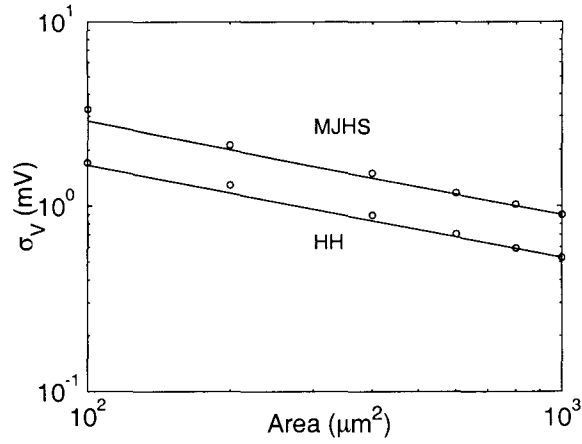


Figure 6.8: Dependence on Subthreshold Voltage Noise on Patch Area.

σ_V as a function of the patch area A for MJHS ($V_m^o = -60$ mV) and HH ($V_m^o = -65$ mV) kinetics. Circles indicate the results from the Monte-Carlo simulations, whereas the solid curve indicates the $1/\sqrt{A}$ behavior expected from the linearized, quasi-active model.

variables in the expressions for channel current; variation of these parameters changes the kinetic scheme from the standard model. Nonetheless, we wanted to determine how the results presented above vary with changes in several fundamental properties of the membrane patch, such as patch area and temperature.

Fig. 6.8 shows the membrane voltage noise for the MJHS kinetic scheme varies as a function of patch area. This figure shows that membrane noise decreases with increasing patch area, because the total membrane current represents the average behavior of a larger number of channels. In terms of linearized membrane patch models, the variance of the channel current noise increases linearly with the number of channels and the patch area, thus $\sigma_I^2 \propto A$. The impedance of the membrane patch, Z , is inversely proportional to area, $Z \propto A^{-1}$. Since $V = Z I$, $\sigma_V^2 = |Z|^2 \sigma_I^2 \propto A^{-1}$. Thus, as patch area decreases, the variance of the voltage noise becomes larger.

The quasi-active linearized approximation is accurate within 8% down to a patch area of $100 \mu\text{m}^2$, where the deviation between simulation and theory becomes substantial. For the reasons discussed in section 6.3.1, when noise fluctuations become larger than 2 mV, the quasi-active linearized approximation becomes less accurate.

6.3.5 Dependence of Noise Magnitude on Temperature

Fig. 6.9 shows the membrane voltage noise predicted by the MJHS and HH kinetic schemes as a function of temperature. Because the kinetic rate functions are scaled by the factor $Q_{10}^{\Delta T/10}$, increasing the temperature decreases the time constants for both ion channels and effectively speeds up ion channel transitions. Consequently, the corner frequency of the current noise PSD increases to a higher frequency. Since the membrane capacitance and leak resistance act as a low pass filter, less noise power is passed by this filter, resulting in lower membrane voltage noise. **Fig. 6.9** shows this decrease in noise magnitude as a function of temperature for both kinetic schemes.

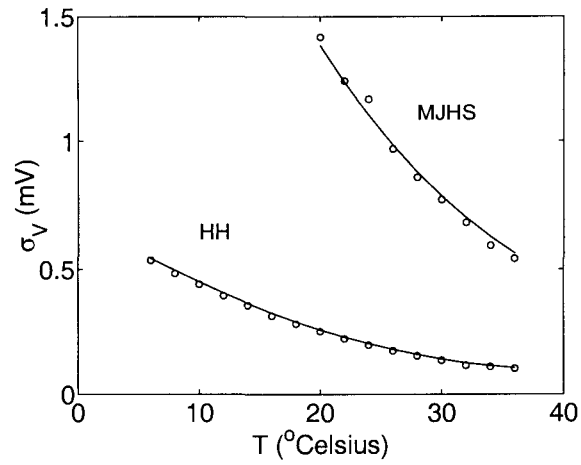


Figure 6.9: Dependence of Subthreshold Voltage Noise on Temperature.

σ_V as a function of temperature for MJHS ($V_m^o = -60$ mV) and HH ($V_m^o = -65$ mV) kinetics for a $1000 \mu\text{m}^2$ patch. Circles denote simulations and the solid curves represent the results of the quasi-active linearized model. Simulations for **Fig. 6.2** - **Fig. 6.8** were carried out at $T = 27$ °C.

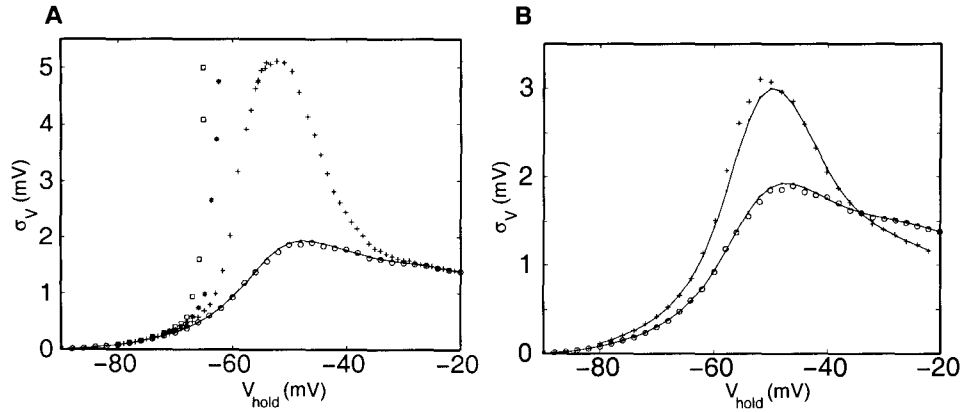


Figure 6.10: Dependence of Subthreshold Voltage Noise on Channel Densities.

Standard deviation of the voltage noise σ_V in a $1000 \mu\text{m}^2$ patch as a function of the steady-state membrane voltage V_m^o . Circles denote results of the Monte-Carlo simulations for the nominal MJHS parameter values. The solid curve corresponds to the theoretical expression obtained by linearizing the channel kinetics. **A:** Effect of increasing the sodium channel density by a factor (compared to the nominal value) of 2 (pluses), 3 (asterisks) and 4 (squares) on the magnitude of voltage noise. **B:** Effect of increasing both the sodium and potassium channel densities by a factor of two (pluses).

6.3.6 Dependence of Noise Magnitude on Channel Densities

Fig. 6.10 shows the voltage noise for a $1000 \mu\text{m}^2$ patch as a function of the holding voltage for different values of the channel densities. Noise increases as the membrane is depolarized from rest towards -50 mV and the rate of increase is higher for higher Na^+ densities. The range of V_m^o for subthreshold behavior extends up to -20 mV for nominal densities, but does not exceed -60 mV for higher Na^+ densities. For moderate levels of depolarization, an increase in the magnitude of the ionic current noise with voltage is the dominant factor which leads to an increase in voltage noise; for higher voltages phenomenological impedances are large and shunt away the current noise. Increasing Na^+ density increases voltage noise, whereas increasing K^+ density causes a decrease in noise magnitude (compare **Fig. 6.10A** and **Fig. 6.10B**). We linearized the closed-form expressions provide accurate estimates of the noise magnitudes when the noise is small (of the order 3 mV).

Increasing Na^+ channel density increases both the magnitude of the noise and its rate of increase with membrane voltage. On the other hand, increasing the rates of channel transitions by increasing temperature, leads to a decrease in noise. It has previously been shown that neural excitability increases with Na^+ channel density (Sabah & Leibovic, 1972) and decreases with temperature (Mauro *et al.*, 1970). Thus, our findings suggest that an increase in membrane excitability is inevitably accompanied by an increase in the magnitude of subthreshold voltage noise fluctuations. The magnitude and the rapid increase of voltage noise with depolarization suggests that channel fluctuations can contribute significantly to the variability in spike timing (Schneidman *et al.*, 1998) and the stochastic nature of ion channels may have a significant impact on information processing within individual neurons. It also potentially argues against the conventional role of a neuron as integrator of synaptic inputs (Shadlen & Newsome, 1998), as the slow depolarization associated with integration of small synaptic inputs would be accompanied by noise, making the membrane voltage a very unreliable indicator of the integrated inputs.

6.3.7 Application to Dendritic Cables

When the magnitudes of the noise and the phenomenological impedances are small, the non-linear kinetic schemes are well-modeled by their linearized approximations. These analytical approximations can be used to study noise in more sophisticated neuronal models incorporating realistic dendritic geometries, where Monte-Carlo simulations may be too computationally intensive to use. We found that the quasi-active approximation is valid for membrane geometries, besides a patch, by carrying out Monte-Carlo simulations for a finite linear cable and comparing them to the corresponding linearized approximations. The quasi-active approximation is valid over a larger steady-state voltage range in comparison to the passive approximation (data not shown). Previous work used the passive linearized approximation to compute how well the subthreshold electrotonic signal represented by the activation of a single synapse could be detected at a distance along a dendrite containing noise sources, such as a low density of K^+ and Na^+ channels as well as synapses activated by random background activity. We believe that the use of the quasi-active approximation in the context of this formalism will lead to better estimates of the efficacy of weakly-active dendritic structures at transmitting information. We are currently applying the quasi-active approximation to estimate noise in realistic dendritic morphologies.

6.4 Discussion

In the neuronal dendrite, soma, and axon hillock, the stochastic operation of individual ion channels represents a significant cellular source of noise. Previous work has shown that stochastic fluctuations of ion channels in a small patch of membrane can affect the accuracy and reliability of spike timing (Schneidman *et al.*, 1998). This random jitter in spike timing, however, is a result of underlying fluctuations in both the number of open channels and the membrane voltage when the cell is depolarized near threshold. The magnitude of these fluctuations is determined by the number of ion channels, their conductance states, and the rate of transitions between these states. In this chapter, we studied how the underlying ion channel kinetic model determines the subthreshold voltage fluctuations of an isopotential patch of membrane. For illustration, we compared two kinetic schemes in common use,

the canonical Hodgkin-Huxley (HH) scheme for the squid giant axon, and the Mainen *et al.* (MJHS) scheme for the dendrite of a neocortical pyramidal cell.

Our objective differs from that of Strassberg & DeFelice (Strassberg & DeFelice, 1993), who showed the convergence of the stochastic Markov model of the Hodgkin-Huxley kinetics and the deterministic macroscopic equations. A finite-state Markov model of a Hodgkin-Huxley like kinetic scheme can be represented by a master equation for a stochastic automaton, as reported by Fox & Lu (Fox & Lu, 1994; Fox, 1997). When the size of system is sufficiently large (which can be informally expressed as requiring large numbers of channels), Master equations can be approximated by continuous partial differential equations called Fokker-Planck equations. A Fokker-Planck equation can in turn be represented by a set of stochastic differential equations (Langevin equations), where the stochastic fluctuations are represented by additive Gaussian white-noise terms. The linearized approximations examined here can be viewed as specialized versions of these general approximations. Our objective was to determine how well the linearized approximations predict noise magnitudes for practical use with several kinetic schemes. This question can only be answered by empirical studies, such as those performed here (Fox & Lu, 1994; Fox, 1997). An additional advantage of the linearized approximations presented here is that they have electrical circuit analogs which can help develop an intuitive understanding of how changing the kinetic scheme changes noise.

For both the HH and MJHS kinetic schemes, subthreshold voltage noise caused by ion channel fluctuations increases rapidly as the membrane potential is depolarized 2-10 mV from rest. This is significant since noise of this magnitude could affect spike generation in two ways: noise may trigger spikes spontaneously if the cell is otherwise near threshold, or subthreshold noise may change the timing of spikes, even if insufficient to cause spikes independently. Both of these effects might prevent the neuron from accurately integrating its inputs; in this case, ion channel noise would interfere with the neuron acting as an integrator of balanced excitation and inhibition, which has been posited as a method of mean rate coding (Shadlen & Newsome, 1998). This case also implies that the spike output of the neuron more accurately represents volleys of simultaneous input which rapidly depolarize

the cell to threshold. A further examination of this issue requires the combination of the noise models described here with a model spiking mechanism; an effort presently underway in our laboratory.

In addition to these effects on spike timing, the effects of noise sources on computation and information processing inside individual neurons are of interest. In earlier chapters, we reported the effect of ion channel and synaptic noise on the accuracy of signal detection and estimation in a patch of membrane as well as in a simplified model of the dendrite. An important step will be to extend these analyses to neuron models with realistic geometries and channel densities. The simulation of the complete Markov kinetic schemes used here within each compartment of a large neuron model will be computationally intense (more than 36 hours on a 450 MHz Pentium II processor) and thus an important question is whether an equivalent linearized model of channel kinetics is accurate enough to predict the effects of these noise sources on information transmission and processing.

The results presented here demonstrate that subthreshold voltage fluctuations caused by stochastic sodium and potassium channels in the HH and MJHS kinetic schemes can be well approximated by their quasi-active linear equivalent circuits. The standard deviation of the noise fluctuations agrees within 8% in a voltage range starting from near the potassium reversal potential up to the threshold of neuronal firing in the HH scheme or to -20 mV in the MJHS scheme. Thus, over subthreshold voltage ranges, a quasi-active linearized approximation is quite accurate. The passive linearized approximation fits the data less well, particularly between -50 and -20 mV for the MJHS kinetics.

Why is the quasi-active linear approximation so accurate? As discussed in section 6.3.4, this accuracy arises because the membrane potential fluctuations due to stochastic ion channels are generally smaller than 2 mV. Over this small a voltage range, the curves representing channel activation and time constants can be accurately represented by lines. When this condition no longer obtains, for example, when the patch area is below $200 \mu\text{m}^2$, then the linear approximation becomes less accurate.

These approximations are accurate for computing subthreshold voltage noise, which is of interest in a variety of places within the nervous system, such as in non-spiking neurons

in the retina or in neuronal compartments which do not initiate spiking. A limitation of the applicability of these approximations is that they do not address spike timing and the initiation of action potentials. In order to study this issue, the linearized approximations must be combined with more accurate models of spike generation in other model compartments.

For the kinetic schemes examined here, the distribution of the voltage noise also simplifies in a fashion conducive to large scale modeling. As shown in section 6.3.3, the distribution of voltage noise is nearly Gaussian, particularly when the noise variance is high. This distribution allows the efficient computation of the effects of noise on information processing using closed form solutions for detection thresholds and reconstruction error (Chapter 4).

Overall, the quasi-active linear approximation to channel kinetics permits efficient evaluation of subthreshold voltage fluctuations for both the more excitable HH kinetic scheme, which at 27 °C initiates a spike only 2.5 mV above the resting potential, and the less excitable MJHS scheme, which does not initiate spikes at dendritic channel densities. This suggests that the quasi-active linearized approximation may be used to examine subthreshold noise in a variety of channel kinetic schemes and for quantitatively assessing the effects of biophysical noise sources on information transfer in realistic neuron models.

Given these results, the accuracy of linear approximations in representing subthreshold voltage fluctuations in real neurons will be determined by the accuracy of the underlying kinetics models in representing channel kinetics. The Hodgkin-Huxley kinetic scheme successfully explains the generation of the action potential, but fails to explain other aspects of neural excitability, such as spike frequency adaptation, bursting and so on. Both the HH and MJHS kinetic schemes do not model mechanisms, such as long term (longer than one second) changes in probability of channel transitions (Toib *et al.*, 1998; van den Berg & Rijnsburger, 1980; van den Berg *et al.*, 1975) and the interdependence of the activation and inactivation gates of the sodium channel. These effects could be incorporated into kinetic models using additional kinetic states; the effect on such modifications on channel noise can then be explored using the techniques applied in these studies.

Experimental measurement of noise in cortical pyramidal cells of the in-vitro cortical slice preparation is in rough agreement with the predictions of these models (see Chap-

ter 5). Dissection of the noise contribution of different ionic channel types, as well as more precise quantitative agreement between theory and experiment, is an ongoing effort in our laboratories. The data from in-vivo recordings of pyramidal cells in anesthetized cat suggest that synaptic noise may make a larger contribution to voltage noise than previously determined using in-vitro preparations (Pare *et al.*, 1997; Pare *et al.*, 1998; Destexhe & Pare, 1999). If synaptic noise is dominant, then further modeling will need to incorporate both synaptic and ionic channel noise into realistic neuronal cellular geometries in order to develop a quantitative understanding of the relative effects of these neuronal noise sources on information processing in cortical pyramidal cells.

Table 6.1: Comparison of Parameters for the Mainen *et al.* (MJHS) and Hodgkin-Huxley (HH) Kinetic Schemes.

		MJHS	HH
γ_K	Potassium channel conductance	20 pS	20 pS
γ_{Na}	Sodium channel conductance	20 pS	20 pS
η_K	Potassium channel density	1.5 channels/ μm^2	18 channels/ μm^2
η_{Na}	Sodium channel density	2 channels/ μm^2	60 channels/ μm^2
C_m	Specific membrane capacitance	0.75 $\mu\text{F}/\text{cm}^2$	1 $\mu\text{F}/\text{cm}^2$
E_K	Potassium reversal potential	-90 mV	-77 mV
E_{Na}	Sodium reversal potential	60 mV	55 mV
E_L	Leak reversal potential	-70 mV	-54 mV
g_L	Leak conductance	0.025 mS/ cm^2	0.3 mS/ cm^2
H	Na ⁺ inactivation subunits	1	1
M	Na ⁺ activation subunits	3	3
N	K ⁺ activation subunits	1	4
Q_{10K}	K ⁺ temperature scale factor	2.3	3
Q_{10Na}	Na ⁺ temperature scale factor	3	3
T_{BK}	K ⁺ base temperature	16 °C	6.3 °C
T_{BNa}	Na ⁺ base temperature	27 °C	6.3 °C
V_{rest}	Resting potential	-70.7 mV	-65 mV

Chapter 7 Variability and Coding Efficiency of Noisy Neural Spike Encoders

7.1 Introduction

In this chapter, we employ the signal estimation paradigm to assess the functional role of spike timing variability in neural coding by quantifying the ability of two types of neural spiking models (integrate & fire models and stochastic ion channel models) to encode information about random time-varying inputs. The goal is to reconstruct a random time-varying current injected into a spike encoding model from the corresponding spike train output. As before, the encoding efficacy is determined using optimal least mean square estimation. The coding fraction quantifies the fraction of variability in output spike train which conveys information about the input. Our findings suggest that spike timing variability can greatly reduce the ability of spike trains to encode rapid time-varying stimuli. Moreover, contrary to expectations based on earlier studies, we find that spiking models are more effective at encoding slowly varying stimuli than rapid ones.

7.2 Models of Spike Encoding

We consider two classes of mathematical spiking models which transform continuous, time-varying input signals into sequences of action potentials or spikes. The spike train output of a model in response to the injection of an input current $i(t)$ is denoted by $s(t)$. $s(t)$ is assumed to be a point process and is mathematically modeled as a sequence of delta functions at time instants $\{t_i\}$ when the model generates spikes in response to the current as

$$s(t) = \sum_i \delta(t - t_i).$$

The models we consider below are inherently noisy and generate irregular spike trains in response to repeated presentations of the same input and can be regarded as representations of irregular spiking behavior in real biological neurons. We use a specific signal processing task (signal estimation) to study the effects of spike timing variability on the encoding of time-varying input modulations in the context of these models.

7.2.1 Integrate-and-fire Models

Integrate-and-fire models (I&F) are simplified, phenomenological descriptions of spiking in biological neurons (Stein, 1967a; Stein, 1967b; Knight, 1971; Jack *et al.*, 1975; Tuckwell, 1988b). They retain two important aspects of neuronal firing, a subthreshold regime where the input to the neuron is passively integrated, and a voltage threshold which when exceeded leads to the generation of stereotypical spikes. The simplest member of this class is called the *perfect integrate-and-fire* model, which comprises of a single capacitance C followed by a fixed threshold V_{th} . Though physiologically inaccurate, this abstraction is often used because of its extreme simplicity and its analytical tractability to model biological spike trains. The membrane voltage of the perfect integrator in response to an input current $i(t)$ is given by

$$C \frac{dV_m}{dt} = i(t). \quad (7.1)$$

When the membrane voltage reaches V_{th} , a spike is generated and voltage is reset to zero. For the perfect integrator, the instants of successive spike occurrence t_i can be recursively obtained using the following equation:

$$\int_{t_i}^{t_{i+1}} dt i(t) = C V_{\text{th}}. \quad (7.2)$$

The average number of spikes generated per unit time by the model is called its *mean firing rate*. The dependence of the mean firing rate of a model (in response to constant current injection) on the magnitude of the injected current is called the f - I curve. The f - I curve for the perfect integrator is linear and is given by $\bar{\lambda} = I/(C V_{\text{th}})$, where $\bar{\lambda}$ denotes the

firing rate and I the constant current input. Biological neurons are characterized by an absolute refractory period following a spike occurrence during which a second spike cannot be generated. This fact can be incorporated in I&F models by maintaining the membrane potential at zero for a fixed duration t_{ref} immediately following a spike. The refractory period causes the f-I curve of the perfect I&F model to saturate at high firing rates

$$\bar{\lambda} = \frac{I}{C V_{\text{th}} + t_{\text{ref}} I}. \quad (7.3)$$

A more realistic spiking model of a biological neuron should account for the passive transmembrane resistance of nerve membranes and incorporate a leak resistance in addition to the capacitance in the subthreshold domain. This model is called the *leaky* integrate-and-fire model. Its membrane voltage in the subthreshold domain is given by

$$C \frac{dV_m}{dt} + \frac{V_m}{R} = i(t). \quad (7.4)$$

The f-I curve of a leaky I&F model with a refractory period t_{ref} is given by

$$\bar{\lambda} = \left[t_{\text{ref}} + \tau \log \left(\frac{I}{I - I_{\text{th}}} \right) \right]^{-1}, \quad \text{where } I_{\text{th}} = \frac{V_{\text{th}}}{R}, \quad \tau = RC. \quad (7.5)$$

Due to the leak conductance, there exists a threshold current for constant injected current magnitudes I_{th} , below which the model does not generate spikes.

Real neurons often show evidence of firing rate *adaptation*, which means that their firing rate decreases with time in response to constant, steady inputs. There are a lot of processes which can result in firing rate adaptation, the release of neurotransmitters and neuromodulators, presence of Ca^{2+} -dependent and other ion channels and so on. In order to account for the 50 to 100 millisecond time-course of adaptation, Wehmeier and colleagues (Wehmeier *et al.*, 1989) introduced a purely time-dependent shunting conductance g_{adapt} with a reversal potential equal to the resting potential (here assumed to be zero). Each spike increases g_{adapt} by a fixed amount G_{inc} . Between spikes, g_{adapt} decreases exponentially to zero with a time constant τ_{adapt} . This effectively models the effect of membrane calcium-dependent potassium conductance and reproduces the effect of an absolute and a relative

refractory period following spike initiation. We refer to this model as an *adapting integrate-and-fire* model. However, a refractory period t_{ref} is required in order to mimic the very short-term aspect of adaptation. In the subthreshold domain

$$C \frac{dV_m}{dt} + \frac{V_m(1 + R g_{\text{adapt}})}{R} = i(t), \quad (7.6)$$

$$\tau_{\text{adapt}} \frac{dg_{\text{adapt}}}{dt} + g_{\text{adapt}} = G_{\text{inc}} \sum_i \delta(t - t_i). \quad (7.7)$$

If V_m reaches V_{th} at time t_i , a spike is generated at t_i and $g_{\text{adapt}}(t_i)$ is increased by G_{inc} . The model is completely characterized by the parameters: V_{th} , C , R , t_{ref} , G_{inc} and τ_{adapt} . The f-I curve of the model is shown in **Fig. 7.1**.

The spiking models discussed so far are deterministic; repeated presentations of the same input stimulus give rise to identical spike trains. Biological neurons *in vivo*, however, show a substantial variability in the exact timing of action potentials to identical stimulus presentations (Softky & Koch, 1993; Holt *et al.*, 1996; Shadlen & Newsome, 1998). A simple modification to reproduce the random nature of biological spike trains is to regard the voltage threshold as a random variable drawn from some arbitrary probability distribution $p(V_{\text{th}})$ (Holden, 1976; Gestri *et al.*, 1980). We refer to this class of models as *integrate and fire models with random threshold*. In general, $p(V_{\text{th}})$ can be arbitrary but here we assume that it is given by a gamma distribution of order n ,

$$p_n(V_{\text{th}}) = c_n \left(\frac{V_{\text{th}}}{\bar{V}_{\text{th}}} \right)^{n-1} \exp \left(\frac{-nV_{\text{th}}}{\bar{V}_{\text{th}}} \right), \quad (7.8)$$

with

$$c_n = \frac{n^n}{(n-1)! \bar{V}_{\text{th}}},$$

where \bar{V}_{th} denotes the mean voltage threshold. n , the order of the distribution determines the variability of the spike trains in response to a constant current injection. For a perfect integrator, the interspike interval (denoted by T) is proportional to the voltage threshold. Thus, the resulting interspike intervals (ISIs) for the random threshold model are also

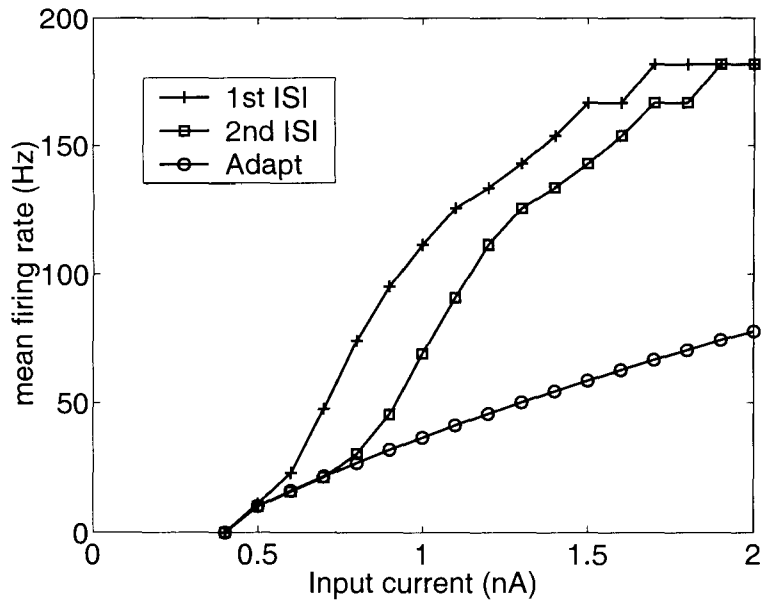


Figure 7.1: **f-I Curve of the Adapting I&F Model.**

The mean firing rate of the adapting integrate and fire model in response to constant current injection estimated using the 1st, 2nd and adapted ISIs. Adaptation linearizes the f-I curve. Model parameters adopted from (page 327, Koch, 1999): $\bar{V}_{th} = 16.4$ mV, $C = 0.207$ nF, $R = 38.3$ M Ω , $t_{ref} = 2.68$ msec, $G_{inc} = 20.4$ nS, $\tau_{adapt} = 52.3$ msec, $\Delta t = 0.5$ msec.

gamma distributed around their mean value μ_T

$$\mu_T = \frac{C\bar{V}_{th}}{I} + t_{ref}.$$

The standard deviation of the length of the ISIs is denoted by σ_T . A statistic used to measure the variability of the spike train is the coefficient of variation (CV) of the ISI distribution, defined as σ_T divided by the μ_T . For a non-adapting I&F model with random threshold the CV is given by

$$\frac{\sigma_T}{\mu_T} = \frac{1}{\sqrt{n}}. \quad (7.9)$$

Thus, one can obtain spike trains by of varying regularity by varying the parameter n . When $n = 1$ and the refractory period is zero, the model gives rise to Poisson spike trains. In the class of I&F models with gamma distributed threshold, the Poisson model gives rise to spike trains with highest variability. For constant current injection, $CV = 1$, in the case of the Poisson model. On the other hand, when $n \rightarrow \infty$, the model reduces to the perfect integrate-and-fire model discussed above. For constant current injection, all the ISIs of a perfect integrate-and-fire model are identical and so its $CV = 0$.

While CV cannot be evaluated in closed-form for the adapting I&F model, it decreases monotonically as n is increased. A schematic diagram of the adapting integrate and fire model with random threshold is shown in **Fig. 7.2A**.

Realistically speaking, the random voltage threshold model is not physiologically plausible since it is believed that the spiking mechanism in real neurons is very reliable (Calvin & Stevens, 1968; Mainen & Sejnowski, 1995). However, in the case of a perfect or non-leaky integrate-and-fire model, a random threshold can be shown to be equivalent to a random input current (Gestri *et al.*, 1980). Moreover, in most cases, the random threshold model is mathematically and computationally easier to deal with (Gabbiani & Koch, 1998). Thus, we shall use it as a phenomenological model to reproduce the variability commonly observed in neural spike trains.

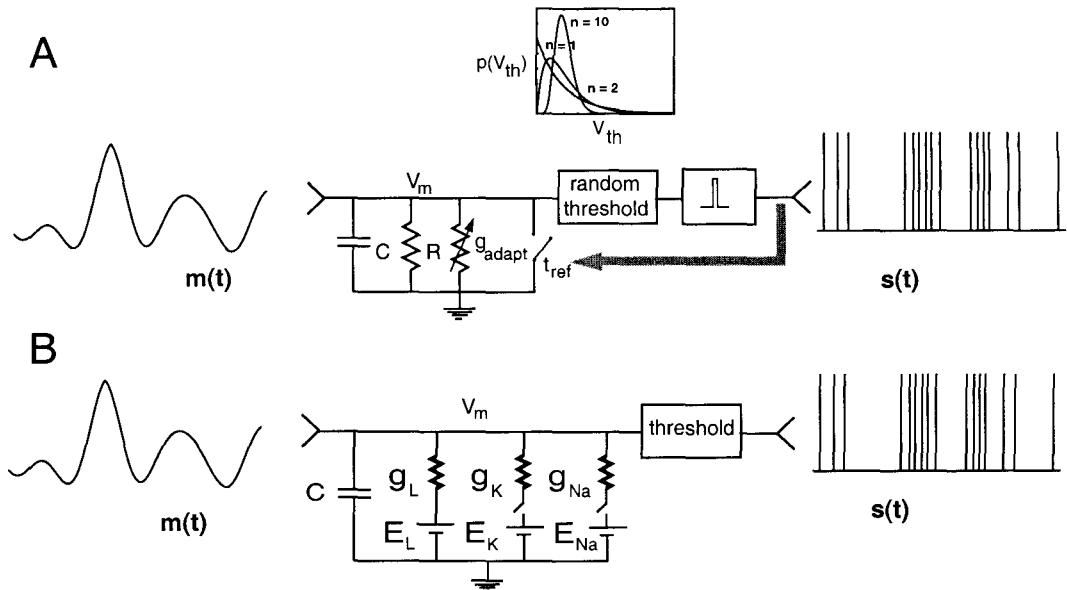


Figure 7.2: **Noisy Encoding Models of Spike Timing Variability.**

A: Schematic diagram of an adapting integrate and fire model with random threshold. The membrane is modeled as a parallel combination of a resistance R and a capacitance C . A time-varying current stimulus $m(t)$ is integrated by the membrane to generate the membrane voltage V_m . When V_m exceeds a threshold V_{th} a spike is generated and the integrator is reset for a duration equal to the refractory period t_{ref} . V_{th} is a random variable drawn from a probability distribution $p(V_m)$, which is modeled as an n th order gamma distribution. n determines the variability in spike timing (inset shows gamma distributions for $n = 1, 2$ and 10). Each spike increases the amplitude of the conductance g_{adapt} which corresponds to a calcium-dependent potassium conductance by an amount G_{inc} . g_{adapt} is responsible for firing rate adaptation and decays exponentially to zero between spikes with a time constant τ_{adapt} . **B:** A time-varying current input $m(t)$ is injected into a membrane patch containing stochastic voltage-gated ion channels which is capable of generating action potentials in response to adequately strong current inputs. When the membrane voltage exceeds an arbitrarily chosen reference value above resting potential (10 mV in this case), a spike is recorded in the output spike train $s(t)$. Parameters correspond to the kinetic model for regular spiking cortical neurons derived by Golomb & Amitai (1997)..

While a proper adjustment of model parameters allows I&F models to provide a fairly accurate description of the firing properties of some cortical neurons (Softky & Koch, 1993; Holt *et al.*, 1996; Shadlen & Newsome, 1998; Stevens & Zador, 1998b; Koch, 1999), it must be noted that many neurons cannot be modeled by integrate-and-fire models. Neuronal membranes contain several voltage- and ligand-gated ionic currents which are responsible for a variety of physiological properties which phenomenological models fail to capture.

7.2.2 Stochastic Ion Channel Models

In Chapter 6, we studied the influence of the stochastic nature of voltage-gated ion channels in excitable neuronal membranes on subthreshold membrane voltage fluctuations. Here we assess the influence of the stochastic nature of ion channels on the ability of the spiking mechanism to encode time-varying inputs. The ion-channel model we consider here is a stochastic variant of the single-compartment model of a regular-spiking cortical developed in (Golomb & Amitai, 1997). The original version contains Hodgkin-Huxley type ion channels and excitatory synapses. The original version consists of a fast sodium current, a persistent sodium current, a delayed-rectifier potassium current, an A-type potassium current (for adaptation), a slow potassium current, a passive leak current and excitatory synaptic (AMPA- and NMDA-type) currents. We are interested in the variability due to the stochastic nature of ion channels and so in the model here we assume that the synaptic currents are absent. In order to simulate stochastic Markov models of the ion channel kinetics, we performed Monte-Carlo simulations of single compartmental models of membrane patches of area A . As in the case of the I&F model, band-limited white noise current is injected into a patch of membrane containing stochastic voltage-gated ion channels and Monte-Carlo simulations are carried out to determine the response of the model to random suprathreshold stimuli (**Fig. 7.2B**). For a detailed description of the Monte-Carlo simulations, see (Schneidman *et al.*, 1998; Steinmetz *et al.*, 2000a).

When the length of the time step of the simulation is sufficiently small, the membrane voltage can be assumed to be constant over the duration of the step. Since they depend on the membrane voltage, the kinetic transition rates between different states and equiva-

lently the corresponding state transition probabilities¹ can be computed. Random numbers specifying the number of channels making transitions between any two states are drawn from multinomial distributions parametrized by the transition probabilities and used to determine the modified populations of channel in the different states. The membrane conductance due to an specific ion channel is determined by the tracking the number of members of the given channel type populating its open state. Knowing the conductances due to the different ion channels and the magnitude of the input current allows us to determine the total current entering the patch. This membrane current is integrated over the time step to compute the membrane voltage for the next time step. This procedure is applied iteratively to obtain the membrane voltage trajectory in response to the input current waveform. The voltage trajectory is transformed into a sequence of spikes by considering an instance of the membrane voltage crossing a threshold (here 10 mV with respect to resting potential) as a spike occurrence. This simple recipe to detect spikes works quite well for the model we consider here.

7.3 Optimal Linear Estimation

Let $m(t)$ be a zero-mean random time-varying input signal that we wish to encode using the output spike train $s(t)$ of a spiking neuron model. In general, the current $i(t)$ injected into the model can be expressed as a nonlinear function of $m(t)$ and can be expressed as

$$i(t) = f([k \star m](t)), \quad (7.10)$$

where \star denotes a convolution operation. $f(\cdot)$ is a static, memoryless nonlinearity which models nonlinear aspects of the neural processing (like rectification, saturation and so on) and $k(t)$ is a linear filter which models the temporal aspects of the neuron's input-output transformation. However, for the purposes of this paper, we assume that $i(t)$ has the form, $i(t) = I + m(t)$ where I is the constant component and $m(t)$ is the fluctuating component

¹The transition probabilities are computed by multiplying the corresponding rates by the length of the time step assuming the product is much smaller than one.

of the injected current. The following analysis can be easily extended to other nonlinear encoding schemes.

$s(t)$ is a point-process determined only by the sequence of spike times $\{t_i\}$. We assume that $m(t)$ and $s(t)$ are (real-valued) jointly weak-sense stationary (WSS) processes with finite variances, $\langle m^2(t) \rangle = \sigma_m^2 < \infty$, $\langle |s(t) - \bar{\lambda}|^2 \rangle < \infty$, where $\bar{\lambda} = \langle s(t) \rangle$ is the mean firing rate of the neuron.

Using the results of Appendix A, the coding fraction ξ and the lower bound on the information rate I_{LB} can be written as

$$\xi = \frac{1}{\sigma_m^2} \int_{-\infty}^{\infty} df \frac{[S_{sm}(f)]^2}{S_{ss}(f)}, \quad (7.11)$$

$$I[m(t); \hat{m}(t)] \geq I_{LB} = \frac{1}{2} \int_{-\infty}^{\infty} df \log_2 [SNR(f)] \quad (\text{in bits/sec}), \quad (7.12)$$

where $SNR(f)$ is the signal-to-noise ratio defined as

$$SNR(f) = \frac{S_{mm}(f)}{S_{\hat{m}\hat{m}}(f)}. \quad (7.13)$$

The information rate measures the amount of information about the input that can be reliably transmitted per second in the form of spike train. Quite clearly, I_{LB} depends on the rate at which spikes are generated, the higher the mean firing rate of the neuron, the higher is the maximum amount of information that can be transmitted per second. To eliminate this extrinsic dependence on mean firing rate we define a quantity, I_S , the mutual information per spike as $I_S = I_{LB}/\bar{\lambda}$. The coding fraction ξ and the information rates (I_{LB} , I_S) can be used to assess the ability of spike generation mechanisms to encode time-varying inputs in the specific context of signal estimation.

7.4 Results

We carried out simulations for the I&F model and the stochastic ion channel model and recorded the output spike times in response to the injection of pseudo-random, Gaussian, band-limited (flat power spectrum $S_{mm}(f)$ over bandwidth B_m) noise and computed the

coefficient of variation (CV) of the interspike interval distribution and the coding fraction for signal estimation task. CV measures the variability of the spike train in response to the input, whereas the coding fraction quantifies the fraction of the variability in the spike train which is functionally useful to accurately reconstruct the input modulations.

Fig. 7.3A shows the CV for the two models as a function of the mean firing rate $\bar{\lambda}$ of the spiking models for a input bandwidth of $B_m = 50$ Hz. For the I&F model the mean firing rate $\bar{\lambda}$ can be determined by the f-I curve, since $\bar{\lambda}$ depends only on the mean injected current I . For a membrane patch containing stochastic ion channels, in addition to the magnitude of the mean current I , $\bar{\lambda}$ depends on a variety of parameters such as the area of the patch A , the standard deviation of the input σ_m and bandwidth of the input B_m . For both models, I was varied while maintaining the contrast of the input, defined as $c = \sigma_m/I$, constant at $c = 1/3$. In both cases, CV increases monotonically with mean firing rate.

Fig. 7.3B shows the CV for the two models as a function of the bandwidth of the input B_m . For both models, I was adjusted so that the mean firing rate $\bar{\lambda}$ was approximately equal to 50 Hz. In both cases, CV decreases with increasing B_m which is in qualitative agreement with earlier experimental (Mainen & Sejnowski, 1995) and computational (Schneidman *et al.*, 1998) findings that demonstrated an inverse relationship between spike timing precision (using a measure different from CV) and the temporal bandwidth of the input. Within the class of I&F models, as expected, models with higher n which fire more regularly have lower CV values.

Next, we explored the dependence of coding efficiency on the mean firing rate and the input bandwidth. In **Fig. 7.3C** and **Fig. 7.3D**, the coding fraction ξ is plotted as a function of $\bar{\lambda}$ (for $B_m = 50$ Hz) and B_m ($\bar{\lambda} = 50$ Hz) respectively. For both spike encoding mechanisms, ξ increases with mean firing rate and decreases as with input bandwidth. This is contrary to intuition; an decrease in variability of spike timing with input bandwidth suggests an increase in encoding efficiency. However, we find that the noisy spike encoding models considered here encode slowly-varying stimuli more effectively than rapid ones. We believe that in the context of a signal estimation task, this is a generic property of all models

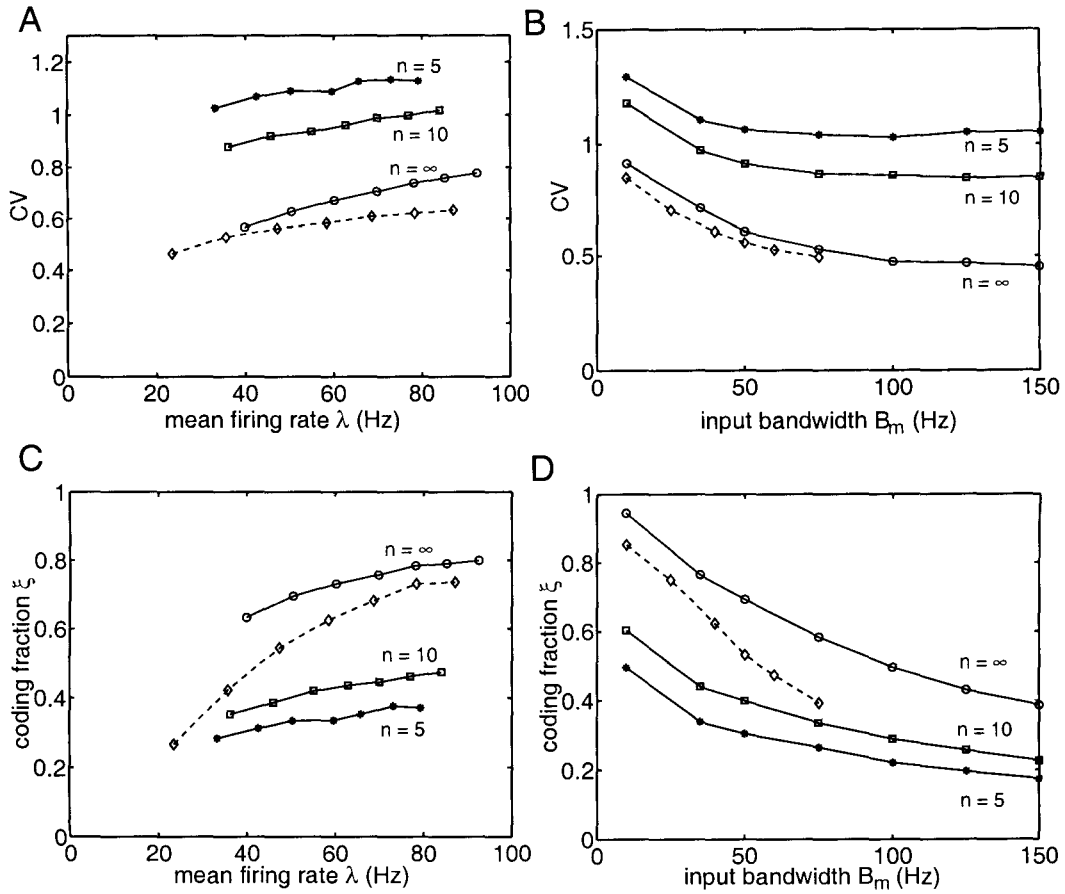


Figure 7.3: **Variability and Coding Performance of Spike Encoding Models.**

A: Coefficient of variability (CV) of the interspike interval distribution of the spike train generated by a spiking model as a function of the mean firing rate of the spike train $\bar{\lambda}$. The input to the model is a Gaussian, white, bandlimited (bandwidth $B_m = 50$ Hz) input, with mean I and standard deviation σ_m . The mean firing rate of the model is varied by changing the mean current I while maintaining the contrast of the input, defined as $c = \sigma_m/I$, constant ($c = 1/3$). The solid curves correspond to the adapting I&F model for different values of the order n of the gamma-distributed voltage threshold distribution. The dotted curve corresponds to a $1000 \mu\text{m}^2$ membrane patch containing stochastic ion channels derived from (Golomb & Amitai, 1997). **B:** CV as a function of input bandwidth B_m . $\bar{\lambda}$ for both the models was maintained at 50 Hz. Panels **C** and **D** show the dependence of the coding fraction ξ in the signal estimation task for the two types of spiking models on the mean firing rate $\bar{\lambda}$ (for $B_m = 50$ Hz) and the input bandwidth B_m (for $\bar{\lambda} = 50$ Hz) respectively. Model parameters for the adapting I&F model are derived from (Koch, 1999) and are summarized in the caption of **Fig. 7.2**. Parameters for the stochastic channel model are obtained from (Golomb & Amitai, 1997).

which encode continuous signals as firing rate modulations of sequences of discrete spike trains.

Next, we explored the dependence of the mutual information rates on the mean firing rate and input bandwidth. **Fig. 7.4A** and **Fig. 7.4B** respectively show that the lower bound of the mutual information rate I_{LB} increases with $\bar{\lambda}$ and B_m . This behavior can be better understood in light of the phenomenological expression: $I_{LB} = B_m \log_2(1 + \kappa \bar{\lambda}/B_m)$, where κ is a constant which depends on the details of the encoding scheme. The above expression is exact when the instantaneous firing rate of the model is a linear function of the input (as in the case of the perfect I&F model) and the input is a white bandlimited Gaussian signal with bandwidth B_m . From the expression one can deduce that for low firing rates I_{LB} increases linearly with $\bar{\lambda}$ but at higher rates I_{LB} becomes logarithmic with $\bar{\lambda}$. One can also conclude that I_{LB} increases with B_m for small bandwidths but quickly saturates at high bandwidths at the value $\kappa \bar{\lambda}/\ln 2$. This qualitatively agrees with **Fig. 7.4A** and **Fig. 7.4B**.

The dependence of the information rate per spike I_S on $\bar{\lambda}$ and B_m can be similarly explored. The expression for I_{LB} is sub-linear with respect of $\bar{\lambda}$ and thus, one can deduce that I_S should decrease monotonically with firing rate when the bandwidth B_m is held fixed. Infact, its maximum value, $I_S = \kappa$, occurs at $\bar{\lambda} = 0$. On the other hand when $\bar{\lambda}$ is held fixed, I_S should increase with B_m initially but saturate at high bandwidths at $\kappa/\ln 2$. Once again, **Fig. 7.4C** and **Fig. 7.4D** agree qualitatively with these predictions.

In order to further understand the role of variability in the context of signal estimation, we plot measures of coding efficiency (ξ and I_{LB}/B_m) versus the corresponding CV values for the two models as different parameters are varied. **Fig. 7.5A** and **Fig. 7.5B** show the dependence of coding performance on the variability of spike timing for the I&F model and, **Fig. 7.5C** and **Fig. 7.5D** show the corresponding behaviors for the stochastic ion channel model. For both models, estimation performance improves with variability when the mean firing rate and input bandwidth parameters are varied. This implies that the variability in the output spike train represents faithful encoding of the input modulations, and thus, greater variability leads to better signal estimation. On the other hand, when the order

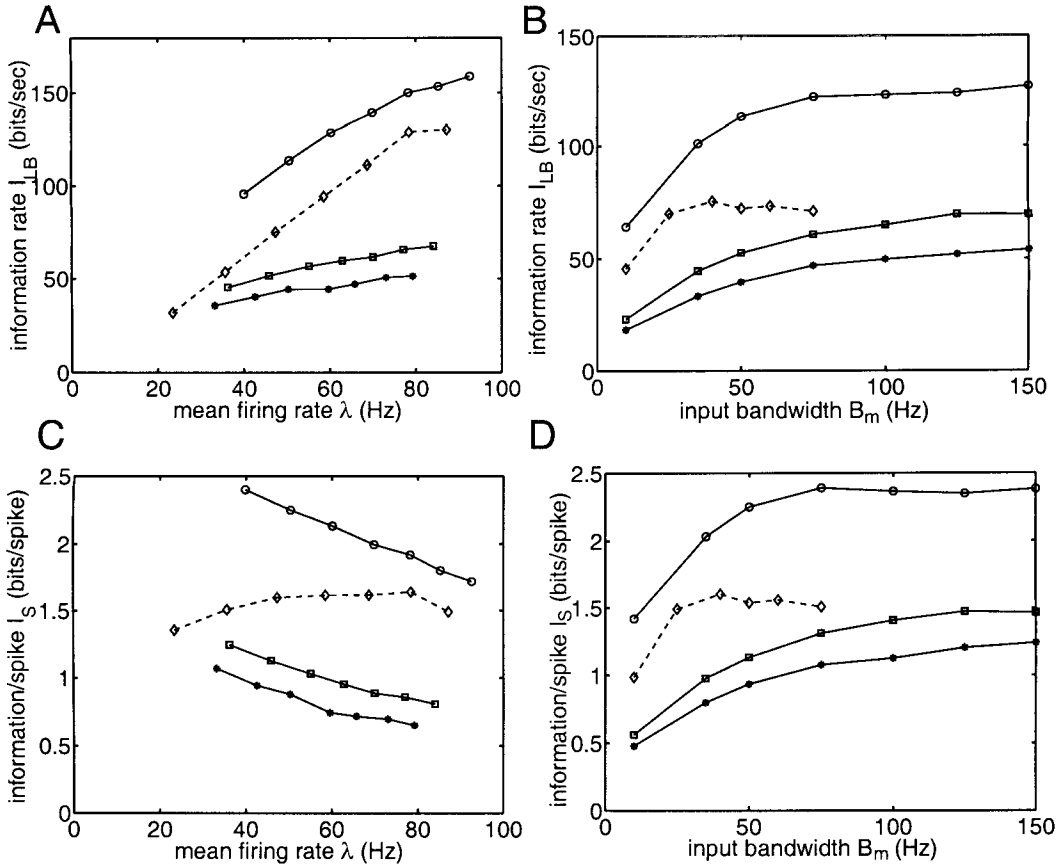


Figure 7.4: **Information Rates in Signal Estimation for Spiking Models.**

A: Lower bounds of the information rate I_{LB} for the two spiking model classes considered in this paper. The solid curves correspond to the adapting I&F model for different values of the order n of the gamma-distributed voltage threshold distribution. The dotted curve corresponds to a $1000 \mu\text{m}^2$ membrane patch containing stochastic ion channels derived from (Golomb & Amitai, 1997). As in **Fig. 7.3**, the input is a bandlimited Gaussian process with bandwidth $B_m = 50$ Hz. **B:** I_{LB} as a function of the input bandwidth B_m for $\bar{\lambda} = 50$ Hz. **C:** The mutual information transmitted per spike on average, $I_S = I_{LB}/\bar{\lambda}$, as a function of $\bar{\lambda}$ ($B_m = 50$ Hz). **D:** I_S as a function of input bandwidth B_m for $\bar{\lambda} = 50$ Hz. Model parameters summarized in the caption of **Fig. 7.2**.

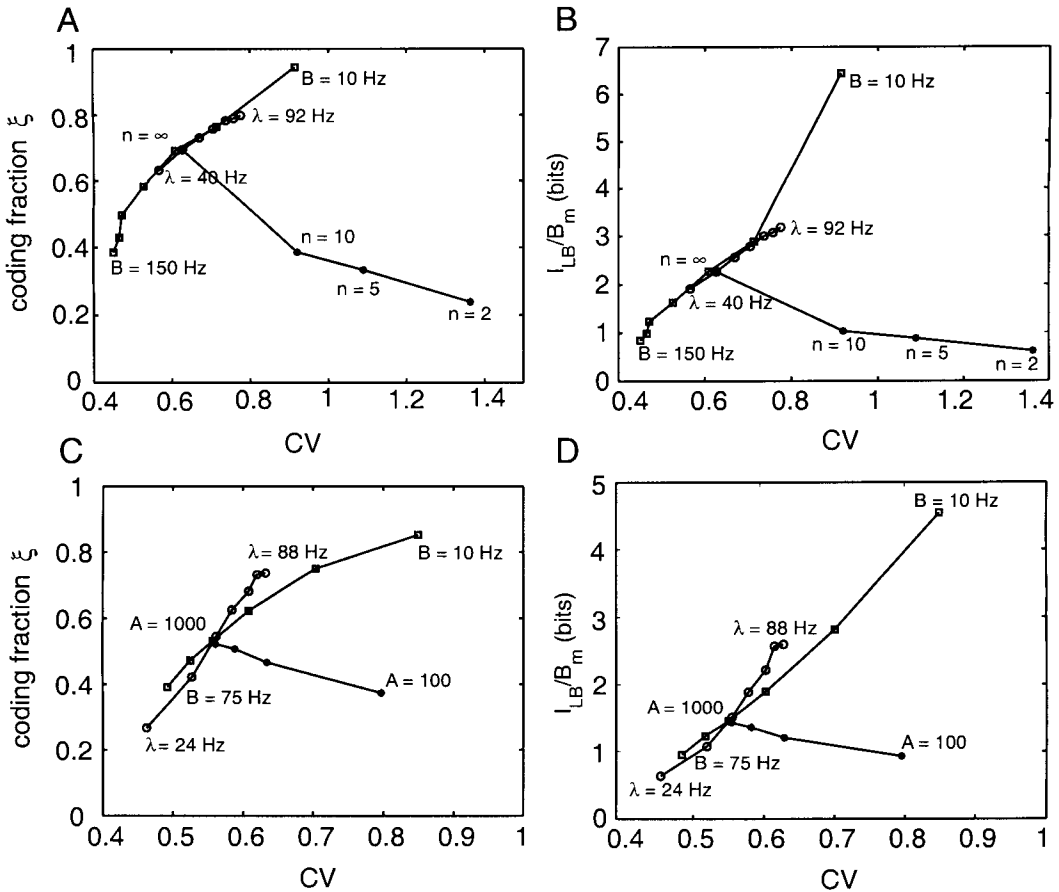


Figure 7.5: **Is it Signal or is it Noise?**

A: Parametric relationships between measures of coding efficiency and the variability of the spike train as different parameters were varied for the two spiking models. **A:** Coding fraction ξ and **B:** the mutual information transmitted per input time constant I_{LB}/B_m for the I&F model as a function of the CV of the spike train. Increase in estimation performance with CV when the mean firing rate $\bar{\lambda}$ and input bandwidth B_m were varied ($n = \infty$) suggests that the variability arises as a result of faithful encoding of the input and thus represents *signal*, whereas a decrease with CV when the order n of the threshold distribution was varied suggests that the variability impedes encoding and thus represents *noise*. **A:** Coding fraction ξ and **B:** the mutual information transmitted per input time constant I_{LB}/B_m for the stochastic ion channel model as a function of the CV of the spike train as the mean firing rate $\bar{\lambda}$ ($A = 1000 \mu\text{m}^2$, $B_m = 50$ Hz), input bandwidth B_m ($A = 1000 \mu\text{m}^2$, $\bar{\lambda} = 50$ Hz) and the area of the patch A ($B_m = 50$ Hz, $\bar{\lambda} = 50$ Hz) were varied.

of the gamma distribution for the I&F model or the area of the membrane patch for the stochastic ion channel model is varied, coding performance decreases with variability. This suggests that the variability is due to noise (randomness of the spiking threshold). Thus, we find that the role of variability on the coding efficiency of spiking models is ambivalent and the beneficial or detrimental consequences of the variability of spike timing depend on the specific nature of the signal processing task the neuron is expected to perform (signal estimation here) and the parameter that is varied.

Fig. 7.6A and **Fig. 7.6B** demonstrate that for the spiking models we have considered here, performance in the signal estimation task is determined by the ratio $\bar{\lambda}/B_m$ and not on the absolute values of $\bar{\lambda}$ and B_m . The quantity $\bar{\lambda}/B_m$ represents the number of spikes observed during the input time constant, a time interval over which the input is relatively constant. Thus, the larger the number of spikes available for the estimation task, the better the estimate of the neuron's instantaneous firing rate $\lambda(t)$ and consequently, the better the estimate of the instantaneous value of the input $m(t)$. Thus, estimation of the input is equivalent to estimating the instantaneous firing rate of model from the spike train. This is further explained in Appendix A. This suggests that the relevant variable which encodes the input modulations is the neuron's instantaneous firing rate arguing for the use of a mean rate code.

7.5 Discussion

In this chapter, we addressed the role of the variability of spike timing on the ability of spiking neuronal models to encode information about time-varying random signals. We considered two classes of models, the I&F models and Hodgkin-Huxley type stochastic ion channel models and computed the variability, coding fraction and information rate in response to injection of white bandlimited Gaussian inputs. For both types of encoding mechanisms, the coding fraction was higher for smaller input bandwidths. This suggests that noisy spike encoders encode slowly varying stimuli better than rapidly varying stimuli. This is in contrast to earlier results (Mainen & Sejnowski, 1995; Schneidman *et al.*, 1998)

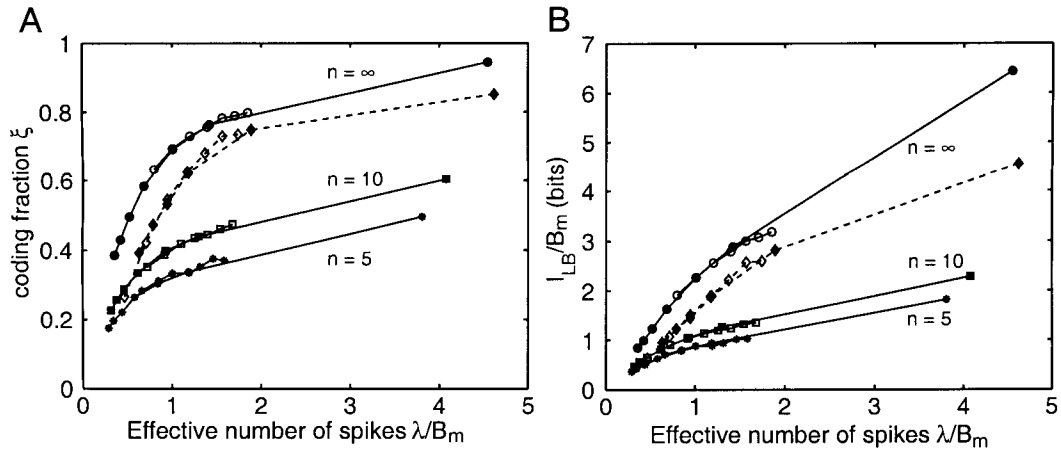


Figure 7.6: **Coding Efficiency as a Function of $\bar{\lambda}/B$.**

A: Coding fraction ξ and **B:** mutual information transmitted per input time constant, I_{LB}/B_m , for the two spiking models as a function of the mean number of spikes available per input time constant, $\bar{\lambda}/B_m$, for different combinations of B_m and $\bar{\lambda}$ (hollow symbols: B_m varied, empty symbols: $\bar{\lambda}$ varied). The solid curves correspond to the adapting I&F model (different symbols represent different values of the order, n , of the voltage threshold gamma distribution), whereas the dotted curve corresponds to a $1000 \mu\text{m}^2$ membrane patch containing stochastic ion channels (Golomb & Amitai, 1997). The contrast of the input, c , was maintained at $1/3$.

which used measures like spike timing reliability and precision and demonstrated that spike trains become less reliable and precise at lower input bandwidths.

The differences between these approaches reflect a fundamental difference in the proposed goals for computation within the nervous system. Measuring spike timing reliability and precision implicitly assumes that the exact times of individual spikes are meaningful and convey information. On the other hand, estimation of the coding fraction assumes that knowledge of the detailed time course of the input signal is the critical variable. In our opinion, this issue cannot be definitely resolved until the relevant neural codes are determined. In the absence of an unequivocal choice, we believe that the coding fraction represents a reasonable metric to assess the performance in signal estimation tasks. In cases where the signal estimation task has little relevance to the computational role of a neuron, for instance, when the neuron is involved in higher order feature extraction, other pertinent measures need to be employed.

Furthermore, our results suggests that the relationship between the observed variability of the spike trains and the performance in a given information-theoretic setting depends on the nature of the task. Thus, depending on the task, the variability might represent a very accurate encoding of the input modulations or may be an unavoidable consequence of noisy processes. We also found that mutual information rates for the signal estimation task depend greatly on the noise in the spike generating mechanism; noise in the form of variability of the spiking threshold can greatly reduce the ability of spiking systems to transmit information reliably.

While interpreting these results, two general limitations must be borne in mind. First, the coding fraction is computed using bandlimited white noise as the input. The actual neural code used by cortical pyramidal neurons, though presently unknown, possibly varies between different areas in the brain. Our input choice allows us to determine performance in encoding signals which have their power distributed over a range of frequencies. However, nervous systems have probably been inexorably optimized through evolution to process natural and ecologically relevant signals with specific statistical properties and white noise may not represent these signals accurately. Thus, the coding fraction for white noise stimuli

can only be interpreted as an indicator of average performance over a broad range of possible input signals. However, if knowledge of the statistical milieu in which a neuron processes information is available, the approach can be modified accordingly.

The second limitation which concerns the use of the estimation paradigm in general is that the coding fraction represents the performance of the optimal linear estimator; non-linear encoders may lead to far better performance. However, Bialek *et al.* (Rieke *et al.*, 1997) have shown that in most cases the difference in performance between linear and non-linear estimators is marginal. Thus, if the mean rate of neuronal firing or any function of it is the variable used to encode information, the coding fraction examined here is likely to be a good indicator of coding efficiency.

Our theoretical results can be tested experimentally by performing recordings similar to those of Mainen & Sejnowski (Mainen & Sejnowski, 1995). One would need to inject current into a neuron *in vitro* and analyze the coding fraction of the resulting spike train instead of measuring precision of the spike train. Preliminary experimental estimates of the coding fraction in cortical pyramidal cells for sinusoidally varying stimuli have been reported by Fellous *et al.* (1999).

Chapter 8 Conclusions

This thesis documents our efforts to develop a reductionist, bottom-up theory of neuronal communication which makes use of the knowledge of the underlying single-neuron biophysics to resolve information transmission between neurons. The approach we employ here is different from some of the other techniques used to decode the nature of the neural code which regard the neuron as a black-box. We are interested in deconstructing neuronal information transfer into its constituent biophysical components and assessing the role of each stage in this context, rather than arriving at an accurate estimate of neuronal capacity.

Our research program is driven by the hypothesis that noise fundamentally limits the precision, speed and accuracy of computation in the nervous system (Koch, 1999). Assessing the role of each biophysical stage in information transfer requires a characterization of the corresponding sources of variability that can cause loss of signal fidelity at different stages in the neuronal link. Some possible sources of biological noise in a single neuron include the probabilistic nature of the synaptic release mechanism and the variability in the amplitude of the postsynaptic response, the stochastic fluctuations of the ligand- and voltage-gated membrane channels, and the synaptic bombardment due to spontaneous background network activity.

In most of the previous approaches, noise analysis has been exploited as an investigative measurement technique. Decoding the neural code requires an understanding of the biophysical constraints which limit the temporal precision of neuronal spike trains. Our interest lies in understanding how the inherent sources of noise at the single-neuron level have bearing on the temporal precision with which neurons respond to sensory input or direct current injection. These questions have received renewed scrutiny in recent times. Previous investigations have used simulations of stochastic models of voltage-gated membrane ion channels to explore the possibility that the noise due to random channel fluctuations can explain the variability observed in neural spike trains (Strassberg & DeFelice, 1993; Fox &

Lu, 1994; Schneidman *et al.*, 1998). On the other hand, recent studies suggest that the unreliable and variable nature of synaptic transmission in cortical neurons can have a significant impact on the ability of neurons to transmit information (Dobrunz & Stevens, 1997; Zador, 1998). However, several experimental and computational studies propose that background synaptic activity may be the dominant noise source *in vivo* (Calvin & Stevens, 1967; Bell *et al.*, 1996; Reich *et al.*, 1997; Stevens & Zador, 1998a; Azouz & Gray, 1999; Destexhe & Pare, 1999). Thus, it is still unclear which of the above is the most significant source of biological noise.

We believe that this question can be readily addressed using information theoretical analysis. Information theory provides us with measures that can be used to study the relevance of the different membrane noise sources to biological signal processing. Application of these measures individually to the different biophysical components allows us to measure which noise source causes the greatest loss of information. To demonstrate the applicability of this hypothesis, we studied the effect of synaptic unreliability on the amount of information transmitted across synaptic connections in Chapter 2. We showed that single cortical synapses transmit information poorly in the signal estimation and signal detection tasks. However, a small amount of redundancy is sufficient to render synaptic transmission robust and reliable.

In Chapter 3, we characterized different sources of subthreshold noise (thermal noise, channel noise, spontaneous background noise) in neuronal membranes and investigated how these sources influence and, ultimately, limit the ability of one-dimensional cable structures to propagate information in Chapter 4. In Chapter 7, we studied the role of variability in spike timing of real neurons in conveying encoding time-varying input for two types of noisy spike encoders. We showed that depending on the nature of the task, variability might either represent faithful encoding of the input and lead to an improvement in performance or represent noise in the spike generation mechanism and lead to a substantial loss of performance.

The long term goal of our research program is to understand how the nervous system processes information using very noisy and unreliable components, such as individual neurons.

Our approach is reductionist: we use a combination of methods from three disciplines — information/signal detection theory, compartmental modeling, and membrane biophysics — to analyze the noise sources in component parts of the neuron, such as the synapse, dendrite, and soma, and to determine their impact on the ability of the neuron to transmit and process information. Ultimately, our goal is to answer questions like, “what is the channel capacity of an unreliable synapse onto a spine?”, “is the length of the apical dendrite of a neocortical pyramidal cell limited by considerations of signal-to-noise?”, “what influences the noise level in the dendritic tree of a real neuron endowed with voltage-dependent channels?”, “how accurately can the time course of an synaptic signal be reconstructed from the voltage at the spike initiation zone?” and so on.

The validity of our theoretical results needs to be assessed by comparison to experimental data obtained from a well-characterized neurobiological system. We currently are in the process of analyzing these noise sources using detailed biophysical models and studying the effect of the measured noise on the temporal precision of spike firing in anatomically and physiologically characterized neuronal models. This will allow us to estimate the information capacity of these neurons and explore the possible functional role of noise.

As we began this investigation in the search of a resolution of the neural coding conundrum, it is fitting that, in conclusion, we leave the reader with this point to ponder: “Is noise a bug or a feature?” That is to say, does neuronal noise simply impair the ability of neurons to detect weak signals and place a limit on the computational and communicational ability of the brain, or can noise also play a positive functional role (Koch, 1999)? In this thesis, we subscribe to the former world-view which obviously needs to be questioned in the face of several proposals which have been advanced to argue in favor of a computational role of noise, such as stochastic resonance (Berzukov & Vodyanoy, 1995; Levin & Miller, 1996) and exploitation of the stochastic nature of the firing threshold or of spike trains to implement multiplication (Srinivasan & Bernard, 1976; Suarez & Koch, 1989). Only time will tell which of these suppositions (or if both) prevails, but if history is any guide, it will be a long time before the matter is fully resolved.

Chapter 9 Appendix

A The Signal Estimation Problem

Consider the following problem of estimating a random signal in the presence of noise. Let $m(t)$ and $s(t)$ be (real-valued) jointly weak-sense stationary (WSS) processes with finite variances, $\langle m^2(t) \rangle = \sigma_m^2 < \infty$, $\langle |s(t) - \langle s(t) \rangle|^2 \rangle = \sigma_s^2 < \infty$. In these equations, $\langle \cdot \rangle$ denotes an ensemble average over the joint input and output distribution. Our goal is to recover the signal $m(t)$ from the noisy measurements $s(t)$ optimally. The criterion of optimality we adopt is the mean-square error (MSE) between $m(t)$ and an estimate of $m(t)$ obtained from $s(t)$, denoted by $\hat{m}(t)$. Thus, we choose $\hat{m}(t)$ such that the variance of the error between $m(t)$ and $\hat{m}(t)$ is minimized. For the sake of simplicity, we will restrict ourselves to linear estimates of the form

$$\hat{m}(t) = (g \star s)(t). \quad (\text{A1})$$

Since $\hat{m}(t)$ is completely specified by the filter $h(t)$, the objective is to derive the optimal filter which minimizes the MSE denoted by \mathcal{E} ,

$$\mathcal{E} = \langle [m(t) - \hat{m}(t)]^2 \rangle = \langle m^2(t) \rangle + \langle \hat{m}^2(t) \rangle - 2 \langle m(t)\hat{m}(t) \rangle. \quad (\text{A2})$$

Thus, estimation performance is quantified by \mathcal{E} ; the lower the value of \mathcal{E} , the better the performance.

This optimal linear estimation problem was first formulated and solved by Wiener (Wiener, 1949) and led to the development of statistical communication theory and information theory (Shannon, 1949; Cover & Thomas, 1991). Recently it was modified by Bialek and colleagues (Bialek *et al.*, 1991; Bialek & Rieke, 1992; Rieke *et al.*, 1997) and successfully applied to quantify information-processing in some peripheral biological systems (van Steveninck & Bialek, 1988; van Steveninck & Bialek, 1995; Rieke *et al.*, 1993;

Rieke *et al.*, 1995; Rieke *et al.*, 1997). Their approach is called the *reconstruction technique*, and has become an important tool in theoretical neuroscience (Theunissen & Miller, 1991; Wessel *et al.*, 1996; Gabbiani *et al.*, 1996; Gabbiani, 1996); for an extensive tutorial on the topic, see Gabbiani & Koch (1998).

Optimal linear estimators satisfy the *orthogonality principle* (Gabbiani, 1996) which can be expressed as

$$\langle [m(t_1) - \hat{m}(t_1)]s(t_2) \rangle = 0 \quad \forall t_1, t_2. \quad (\text{A3})$$

For additional properties on optimal linear estimators, refer to Papoulis (1991). If the constraint of causality is not imposed on the filter $h(t)$, the optimal filter can be obtained by substituting for $\hat{m}(t)$ from equation A1 in equation A3

$$R_{\text{sm}}(z) = (g \star R_{\text{ss}})(z), \quad (\text{A4})$$

where $R_{\text{sm}}(z) = \langle s(t)m(t+z) \rangle$ is the cross-correlation between $s(t)$ and $m(t)$ and $R_{\text{ss}}(z) = \langle s(t)s(t+z) \rangle$ is the auto-correlation of $s(t)$. Taking Fourier transforms on both sides of equation A4 gives us the transfer function $G(f)$ of the optimal filter in terms of the power spectrum of $s(t)$, denoted by $S_{\text{ss}}(f)$, and the cross-spectrum between $s(t)$ and $m(t)$, denoted by $S_{\text{sm}}(f)$,

$$G(f) = \frac{S_{\text{sm}}(f)}{S_{\text{ss}}(f)}, \quad (\text{A5})$$

where

$$G(f) = \mathcal{F}\{g(z)\}, \quad S_{\text{sm}}(f) = \mathcal{F}\{R_{\text{sm}}(z)\} \quad \text{and} \quad S_{\text{ss}}(f) = \mathcal{F}\{R_{\text{ss}}(z)\}. \quad (\text{A6})$$

$\mathcal{F}\{\cdot\}$ denotes the Fourier transform, which for a square integrable function $h(t)$ is defined as

$$H(f) = \mathcal{F}\{h(t)\} = \int_{-\infty}^{\infty} dz h(t) e^{-j2\pi ft}, \quad h(t) = \mathcal{F}^{-1}\{G(f)\} = \int_{-\infty}^{\infty} df H(f) e^{j2\pi ft}.$$

We define a *reconstruction* noise for the signal estimation problem as the difference between the stimulus and the optimal estimate $\hat{n}(t) = \hat{m}(t) - m(t)$. It is clear that $\mathcal{E} = \langle \hat{n}^2(t) \rangle$. The additive noise $\hat{n}(t)$ has zero mean and its auto-correlation is given by $R_{\hat{n}\hat{n}}(z) = R_{mm}(z) - (g \star R_{sm})(-z)$ (using equation A4). The power spectrum of the noise is given by

$$S_{\hat{n}\hat{n}}(f) = \mathcal{F}\{R_{\hat{n}\hat{n}}(z)\} = S_{mm}(f) - \frac{|S_{sm}(f)|^2}{S_{ss}(f)}, \quad (\text{A7})$$

where $S_{mm}(f)$ is the power spectral density of the input. Thus, the MSE can be expressed as

$$\mathcal{E} = \int_{\mathcal{S}} df S_{\hat{n}\hat{n}}(f) = \sigma_m^2 - \int_{\mathcal{S}} df \frac{|S_{sm}(f)|^2}{S_{ss}(f)}, \quad (\text{A8})$$

where the set $\mathcal{S} = \{f \mid S_{ss}(f) \neq 0\}$ is called the *support* of $S_{ss}(f)$. As in Gabbiani & Koch (1998), we define a normalized measure called the coding fraction,

$$\xi = 1 - \frac{\mathcal{E}}{\sigma_m^2}.$$

The coding fraction lies between 0 and 1, $0 \leq \xi \leq 1$, where $\xi = 0$ denotes chance performance and $\xi = 1$ denotes perfect reconstruction. Using equation A8, we can write

$$\xi = \frac{1}{\sigma_m^2} \int_{\mathcal{S}} df \frac{|S_{sm}(f)|^2}{S_{ss}(f)}. \quad (\text{A9})$$

Information theory (Shannon, 1949; Cover & Thomas, 1991) allows us to quantify the amount of statistical information one random quantity conveys about another, given their joint probability distribution. It also provides a model-independent measure of the similarity between random covarying quantities a and b , called the *mutual information* (denoted by $I(a; b)$) between a and b . For stochastic processes $m(t)$ and $s(t)$, the mutual information is measured in units of bits/sec and referred to as the *information rate*. In general, the information rate depends on the joint probability distribution of the two processes.

Our analysis so far has remained independent of the probability distributions of $m(t)$ and $s(t)$. Only a knowledge of the power spectra and cross-spectra of the two processes (second-order statistics) was needed to compute ξ . This is because we restricted ourselves to the class of linear estimators. In order to derive more sophisticated nonlinear estimators, which outperform linear estimators in general, one would need to make use of higher order (greater than second-order) statistical information about the processes. However, these nonlinear estimators are usually analytically intractable to derive and difficult to implement. Besides, it can be shown that if input and output processes are jointly Gaussian, the optimal linear estimator is also the most optimal estimator (over the class of all estimators). Since Gaussian processes are completely characterized by their second order moments (power spectra), the coding fraction and the information rate depend only on the joint spectral properties of $m(t)$ and $s(t)$.

The Gaussian assumption allows us to derive closed-form expressions for the information rate as well. In an experiment, the choice of the input usually lies with the experimenter, and so $m(t)$ can be assumed to be Gaussian by design. In cases for which the *Central Limit Theorem* (Papoulis, 1991) holds, the output can also be closely approximated by a Gaussian process and the information rate can be computed exactly. On the other hand, when the output does not behave like a Gaussian process, one can derive lower bounds on the information rate. According to the *data processing inequality* (Cover & Thomas, 1991), it can be shown that the mutual information between $m(t)$ and $s(t)$ is greater than the mutual information between $m(t)$ and $\hat{m}(t)$

$$I[m(t); s(t)] \geq I[m(t); \hat{m}(t)].$$

A lower bound for $I[(m(t); \hat{m}(t))]$ and thus for $I[m(t); s(t)]$ is given by (Gabbiani, 1996; Gabbiani & Koch, 1996)

$$I[m(t); s(t)] \geq I_{\text{LB}} = \frac{1}{2} \int_{\mathcal{S}} df \log_2 \left[\frac{S_{mm}(f)}{S_{\hat{m}\hat{m}}(f)} \right] \quad (\text{in bits/sec}). \quad (\text{A10})$$

The lower bound is reached when the reconstruction noise $\hat{n}(t)$ is Gaussian. Equation A10 differs from the expression for capacity of an additive Gaussian channel model, commonly used in information theory (Cover & Thomas, 1991), because unlike, in the case of the standard Gaussian channel, the reconstruction noise $\hat{n}(t)$ is not independent of the input $m(t)$.

B Estimation With Multiple Synapses

In the case of multiple synapses the postsynaptic membrane voltage is given by equation 2.20. We assume that the EPSP waveforms corresponding to the different synapses are identical, $h^l(t) = h(t)$, $\forall l$.

$$V(t) = \sum_{l=1}^{N_{\text{syn}}} \sum_i q_i^l W_i^l h(t - t_i) + n(t).$$

As before, the postsynaptic noise $n(t)$ is assumed to be independent of the input $m(t)$ and the presynaptic release processes. The cross-spectrum between the zero-mean membrane voltage $v(t)$ and $m(t)$ for N_{syn} synapses is a scaled version of the cross-spectrum for a single synapse equation 2.9,

$$S_{\text{vm}}(f) = N_{\text{syn}} p \bar{q} K(f) H(f) S_{\text{mm}}(f). \quad (\text{B1})$$

The autocorrelation function for the membrane voltage can be computed as follows:

$$\begin{aligned} R_{\text{vv}}(z) &= \langle V(t)V(t+z) \rangle \\ &= \left\langle \sum_{l=1}^{N_{\text{syn}}} \sum_{m=1}^{N_{\text{syn}}} \sum_i q_i^l q_j^m W_i^l W_j^m h(t - t_i) h(t + z - t_j) \right\rangle. \end{aligned} \quad (\text{B2})$$

The above expression can be simplified as a sum of the following four terms

$$\begin{aligned}
R_{\text{vv}}(z) &= \left\langle \sum_{l=1}^{N_{\text{syn}}} \sum_i (q_i^l)^2 (W_i^l)^2 h(t-t_i) h(t+z-t_i) \right\rangle \\
&+ \left\langle \sum_{l=1}^{N_{\text{syn}}} \sum_i \sum_{j, j \neq i} q_i^l q_j^l W_i^l W_j^l h(t-t_i) h(t+z-t_j) \right\rangle \\
&+ \left\langle \sum_{l=1}^{N_{\text{syn}}} \sum_{m=1, m \neq l}^{N_{\text{syn}}} \sum_i q_i^l q_i^m W_i^l W_i^m h(t-t_i) h(t+z-t_i) \right\rangle \\
&+ \left\langle \sum_{l=1}^{N_{\text{syn}}} \sum_{m=1, m \neq l}^{N_{\text{syn}}} \sum_i \sum_{j, j \neq i} q_i^l q_j^m W_i^l W_j^m h(t-t_i) h(t+z-t_j) \right\rangle. \tag{B3}
\end{aligned}$$

We assume that q_i^l and W_i^l are independent and identical random variables corresponding to conditionally independent synapses. Thus,

$$\left\langle q_i^l q_j^m \right\rangle = \bar{q}^2 + \sigma_q^2 \delta_{lm} \delta_{ij}, \quad \left\langle W_i^l W_j^m \right\rangle = p^2 + p(1-p) \delta_{lm} \delta_{ij}, \tag{B4}$$

where δ_{ij} denotes the Kronecker delta function. Using these expressions, $R_{\text{vv}}(z)$ can be simplified as

$$\begin{aligned}
R_{\text{vv}}(z) &= N_{\text{syn}} p (\bar{q}^2 + \sigma_q^2) \left\langle \sum_i h(t-t_i) h(t+z-t_i) \right\rangle \\
&+ N_{\text{syn}} p^2 \bar{q}^2 \left\langle \sum_i \sum_{j, j \neq i} h(t-t_i) h(t+z-t_j) \right\rangle \\
&+ N_{\text{syn}} (N_{\text{syn}} - 1) p^2 \bar{q}^2 \left\langle \sum_i h(t-t_i) h(t+z-t_i) \right\rangle \\
&+ N_{\text{syn}} (N_{\text{syn}} - 1) p^2 \bar{q}^2 \left\langle \sum_i \sum_{j, j \neq i} h(t-t_i) h(t+z-t_j) \right\rangle. \tag{B5}
\end{aligned}$$

Using the following expressions,

$$\left\langle \sum_i h(t-t_i) h(t+z-t_i) \right\rangle = \bar{\lambda} (h \star \hat{h})(z), \tag{B6}$$

$$\left\langle \sum_i \sum_{j, j \neq i} h(t-t_i) h(t+z-t_j) \right\rangle = (h \star \hat{h} \star k \star \hat{k})(z) \star R_{\text{mm}}(z), \tag{B7}$$

where $\hat{h}(t) = h(-t)$, the power spectrum of $v(t)$ can be obtained by taking the Fourier transform of $R_{vv}(z)$,

$$\begin{aligned} S_{vv}(f) &= N_{\text{syn}}^2 \bar{q}^2 p^2 |K(f)|^2 |H(f)|^2 S_{\text{mm}}(f) \\ &+ N_{\text{syn}} p \bar{\lambda} |H(f)|^2 [(\bar{q}^2 + \sigma_q^2) + (N_{\text{syn}} - 1) \bar{q}^2 p] + S_{\text{nn}}(f). \end{aligned} \quad (\text{B8})$$

Substituting for $S_{vm}(f)$ and $S_{vv}(f)$ in equation A9, the coding fraction ξ can be written as

$$\xi = \frac{1}{\sigma_m^2} \int_{\mathcal{S}} df \frac{[S_{\text{mm}}(f)]^2}{S_{\text{mm}}(f) + S_{\text{neff}}(f)}, \quad (\text{B9})$$

where

$$S_{\text{neff}}(f) = \frac{\bar{\lambda}}{|K(f)|^2} \left[\frac{(1 + CV_q^2)}{p N_{\text{syn}}} + \frac{N_{\text{syn}} - 1}{N_{\text{syn}}} \right] + \frac{S_{\text{nn}}(f)}{N_{\text{syn}}^2 p^2 \bar{q}^2 |H(f)|^2 |K(f)|^2}.$$

Assuming that the second term in the above expression is negligible, in comparison to the ideal case, the shot noise is multiplied by a factor

$$\kappa_N = \frac{1}{N_{\text{syn}}} \frac{1 + CV_q^2}{p} + \frac{N_{\text{syn}} - 1}{N_{\text{syn}}}. \quad (\text{B10})$$

Note that $\kappa_N \rightarrow 1$ in the limit of a large number of synapses, $N_{\text{syn}} \rightarrow \infty$.

C The Signal Detection Problem

In the signal estimation paradigm, both the signal and noise were continuous random processes. We now consider a different problem, that of detecting the presence of a known deterministic signal in noise. This scenario arises quite frequently in science and engineering (radar, communications, pattern recognition, psychophysics, *etc.*) and is commonly known as the *signal detection* problem. There exists a substantial amount of experimental literature on the so-called *lower envelope* principle which states that the performance of an animal on psychophysical threshold discrimination tasks is determined by single neurons (Parker & Newsome, 1998). The most dramatic illustration is from recordings of single peripheral fibers in the median nerve of conscious human volunteers (Vallbo & Johansson, 1976; Vallbo, 1995). Remarkably, the occurrence of a single action potential in the fiber

predicted the detection of the stimulus by the observer almost perfectly. This points to the functional utility for the system to be able to carry out a signal detection task of the type we study here.

The objective in signal detection is to decide which member from a discrete set of signals was generated by a source, on the basis of measurements (possibly noisy) of its output. We restrict ourselves to the binary case, where the set has two elements *viz.*, the *signal* (denoted by $m(t)$) and the *noise* (denoted by $n(t)$). We further assume that $m(t)$ is filtered by a known filter $h(t)$ and additively corrupted by $n(t)$, to give rise to the measured output (denoted by $s(t)$). Our goal is to decide whether the observations $s(t)$ (available over a period $0 \leq t \leq T$) are due to noise $n(t)$ (hypothesis H_0) or a filtered, noisy version of the signal $m(t)$ (hypothesis H_1). This can be formally expressed as the following:

$$\begin{aligned} \mathbf{H}_0 : s(t) &= n(t), & 0 \leq t \leq T & \quad \text{Noise} \\ \mathbf{H}_1 : s(t) &= (h \star m)(t) + n(t), & 0 \leq t \leq T & \quad \text{Signal + Noise} \end{aligned} \quad (\text{C1})$$

Thus, a signal detection task involves making a decision about the presence or absence of a known signal $m(t)$ buried in noise $n(t)$ on the basis of the observations $s(t)$. In psychophysics, such a procedure is known as a Yes/No task (Green & Swets, 1966). Within a neurobiological context, Newsome and his colleagues used a binary motion detection task to great effect (Newsome *et al.*, 1989; Britten *et al.*, 1992; Shadlen & Newsome, 1998) to study the extent to which individual cortical neurons explain the performance of the monkey.

Decision errors are of two kinds. A *false alarm* (F) error occurs when we decide in favor of the signal (H_1) when actually only noise was present (H_0), while a *miss* (M) error occurs when we decide in favor of the noise (H_0) when in fact the signal was present (H_1). The probabilities of these errors are denoted as

$$P_F = P[\text{Choose } H_1 \mid H_0 \text{ present}], \quad P_M = P[\text{Choose } H_0 \mid H_1 \text{ present}].$$

The probability of detection error P_e is given by

$$P_e = p_0 P_F + p_1 P_M, \quad (\text{C2})$$

where p_0 and $p_1 = 1 - p_0$ are the prior probabilities of H_0 and H_1 respectively. We define a likelihood ratio $\Lambda(s)$ as

$$\Lambda(s) = \frac{P[s | H_1]}{P[s | H_0]}, \quad (\text{C3})$$

where $P[s | H_1]$ and $P[s | H_0]$ denote the conditional probabilities of observing $s(t)$ under the hypotheses H_1 and H_0 respectively. Using Bayes' rule, $\Lambda(s)$ can be expanded as

$$\Lambda(s) = \frac{P[H_1 | s]}{P[H_0 | s]} \frac{P[H_0]}{P[H_1]}, \quad (\text{C4})$$

where $P[H_1 | s]$ and $P[H_0 | s]$ denote the posterior probabilities of the hypotheses conditioned on $s(t)$. The ratio $\mathcal{L}(s) = P[H_1 | s]/P[H_0 | s]$ is commonly referred to as the *posterior likelihood*, whereas $\mathcal{L}_0 = P[H_0]/P[H_1] = p_1/p_0$ is called the *prior likelihood*. All the information needed to disambiguate between the two hypotheses using $s(t)$ is contained in $\mathcal{L}(s)$. The decision rule which minimizes P_e is given by (Poor, 1994),

$$\begin{aligned} \text{Choose } H_1 & \text{ for } \{s(t) | \mathcal{L}(s) \geq 1\}, \\ \text{Choose } H_0 & \text{ for } \{s(t) | \mathcal{L}(s) < 1\}, \end{aligned} \quad (\text{C5})$$

which can be compactly written as

$$\mathcal{L}(s) \underset{H_0}{\overset{H_1}{\gtrless}} 1 \quad \Rightarrow \quad \Lambda(s) \underset{H_0}{\overset{H_1}{\gtrless}} \mathcal{L}_0^{-1}. \quad (\text{C6})$$

If the noise $n(t)$ is Gaussian, the above decision rule reduces to convolving $s(t)$ with a linear filter $g_d(t)$ and comparing the sampled value of the filter output at $t = T$ to a threshold. If the output exceeds the threshold, hypothesis H_1 is chosen, else H_0 is chosen. $g_d(t)$ is called a *matched filter* (Poor, 1994) and depends on the input signal $m(t)$, the filter

$g_d(t)$ and the auto-correlation of noise $n(t)$. For finite T , deriving the exact form of $g_d(t)$ involves solving an analytically intractable Fredholm integral equation (Helstrom, 1968) in general. However, in the limit $T \rightarrow \infty$ (which means we can delay our decision indefinitely), we can derive a simple closed-form expression for $g_d(t)$ in the frequency domain,

$$G_d(f) = \exp(-j 2\pi f T) \frac{H^*(f) M^*(f)}{S_n(f)}, \quad (\text{C7})$$

where $H(f) = \mathcal{F}\{h(t)\}$, $M(f) = \mathcal{F}\{m(t)\}$ and $S_n(f)$ is the noise power spectral density.

Let us denote the sampled value of the output of the matched filter at $t = T$ by the random variable r ,

$$r = (s \star g_d)(T) = \int_{-\infty}^{\infty} dt s(t) g_d(T - t). \quad (\text{C8})$$

Notice that r has the form of a correlation between the measurement $m(t)$ and the time-reversed matched filter $g_d(T - t)$. When the noise $n(t)$ is white ($S_n(f)$ has a flat spectrum), $g_d(t)$ is a shifted, time-reversed version of the filtered input signal $(h \star m)(t)$ and r is a correlation between $s(t)$ and $(h \star m)(t)$. We can rewrite the optimal decision rule in equation C6 in terms of r as

$$r \underset{H_0}{\overset{H_1}{\geq}} \Theta, \quad (\text{C9})$$

where Θ is the threshold chosen for optimal performance. Thus, the performance of the matched filter can be determined in terms of the statistical properties of the random variable r . Since $g_d(t)$ is a linear filter, r is a Gaussian random variable and its conditional means and variances (under H_0 and H_1) specify it completely,

$$\begin{aligned} \mu_0 &= \langle r \mid H_0 \rangle, & \sigma_0 &= \langle r^2 \mid H_0 \rangle - \mu_0^2, \\ \mu_1 &= \langle r \mid H_1 \rangle, & \sigma_1 &= \langle r^2 \mid H_1 \rangle - \mu_1^2. \end{aligned}$$

The error probabilities P_F and P_M can be computed as

$$P_F = \int_{\Theta}^{\infty} dr P[r \mid H_0] ; \quad P_M = \int_{-\infty}^{\Theta} dr P[r \mid H_1]. \quad (\text{C10})$$

The probability of error P_e ranges between $P_e = 0$, which implies perfect detection and $P_e = 0.5$ which implies chance performance (pure guessing).

D Detection With Multiple Synapses

It can be shown that the optimal decision rule for multiple synapses also involves comparing the correlation between the membrane voltage $V(t) = \sum_{l=1}^{N_{\text{syn}}} q^l W^l h(t) + n(t)$ and the EPSP shape $h(t)$ to a threshold Θ . The random variable r can be written as

$$r = q_N \sqrt{SNR} + \frac{\int dt h(t) n(t)}{\sqrt{S_{nn}(f) \int dt h^2(t)}}, \quad (\text{D1})$$

where $q_N = \sum_{l=1}^{N_{\text{syn}}} q^l W^l$. Since no spontaneous vesicle release occurs, $q_N \equiv 0$ in the absence of a presynaptic spike ($X = 0$). In this case, r is a zero-mean, unit variance Gaussian random variable with probability density,

$$\text{Prob}[r | X = 0] = \frac{1}{\sqrt{2\pi}} \exp\left(\frac{-r^2}{2}\right). \quad (\text{D2})$$

However, when a presynaptic action potential occurs ($X = 1$), q_N is a random variable which depends on the number of synapses at which vesicle release occurs and the postsynaptic magnitude subsequent to a release. The spike-conditioned density of r is given by

$$\text{Prob}[r | X = 1] = \frac{1}{\sqrt{2\pi}} \int_0^\infty dq_N P_N(q_N) \exp\left[\frac{-(r - q_N \sqrt{SNR})^2}{2}\right], \quad (\text{D3})$$

where $P_N(q_N)$ is the probability density of q_N . Since q_N is a sum of independent identical random variables, $P_N(q_N)$ can be obtained by convolving the probability density of the random variable $q_1 = qW$ with itself N_{syn} times. Thus,

$$P_N(q_N) = \underbrace{P_1(q_1) \star P_1(q_1) \cdots \star P_1(q_1)}_{N_{\text{syn}} \text{ times}}, \quad (\text{D4})$$

where

$$P_1(q_1) = (1 - p) \delta(q_1) + p P(q). \quad (\text{D5})$$

In the equation above $(1 - p) \delta(q_1)$ denotes the probability mass at $q_1 = 0$ corresponding to release failure and $P(q)$ is the postsynaptic EPSP amplitude distribution when a single release occurs. Thus, the error probabilities (P_F and P_M) can be written as

$$P_F = \text{Prob}[r \geq \Theta | X = 0] = \frac{1}{\sqrt{2\pi}} \int_{\Theta}^{\infty} dr \exp\left(\frac{-r^2}{2}\right), \quad (\text{D6})$$

$$\begin{aligned} P_M &= \text{Prob}[r < \Theta | X = 1] \\ &= \frac{1}{\sqrt{2\pi}} \int_{-\infty}^{\Theta} dr \int_0^{\infty} dq_N P_N(q_N) \exp\left[\frac{-(r - q_N \sqrt{SNR})^2}{2}\right]. \end{aligned} \quad (\text{D7})$$

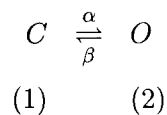
E Stochastic Analysis of Two-State Channels

The simplest and the most widely used model for single voltage-gated channels is the two-state model. Under this model, a channel is like a stochastic binary switch, that can either be in the open state that conducts current, or the closed state that does not. The random opening and closing of the channel modulates the current flowing through it and the statistics of channel fluctuations are reflected in the current fluctuations. At steady-state, the expected number of channels is constant and the average number of open channels contributes to the membrane resistance r_m . However, since the channels randomly flip between their open and closed states, the number of open channels is a random variable. For voltage-gated channels, the probabilities of channel transitions are functions of membrane voltage and thus in turn depend on the current flowing across the membrane. However, as we mentioned before, if the current flowing through the membrane is small, the voltage change due to channel openings is negligible and so the process of opening and closing of channels can be considered independent of the current flow.

This is a reasonable but important assumption. If the current flow through the channel is large, it would cause a significant change in membrane voltage which in turn would influence the channel kinetics. One can then no longer assume the channel statistics to

be stationary. This is exactly what happens when an action potential is initiated in an excitable membrane. During the course of an action potential, the channel statistics change with time and are thus non-stationary. Thus, our assumption holds when the membrane is close to its resting value, far from threshold. Alternatively, one can imagine a scenario in which the membrane is voltage-clamped to a certain value which ensures that the random current does not cause a change in channel kinetics.

The channel models we consider have a finite (two in this case) number of discrete states, as opposed to *fractal channel* models which assume an infinite continuum of states (Liebovitch & Todorov, 1996). Thus, the sequence of channel states in time can be regarded as a discrete-state continuous-time random process. Consider a single two-state channel which switches randomly between its closed (C) and open (O) state and can be described by the following kinetic scheme:



$\alpha\Delta t$ denotes the conditional probability of a channel transition from the closed state to the open state in a time interval Δt , and $\beta\Delta t$ denotes the probability of a corresponding transition from the open state to the closed state. For a finite-state process, the conditional probabilities (also called transition probabilities) can be represented as a square matrix function whose dimension equals the number of states (two, in our case). α and β have the dimensions of sec^{-1} and so they can be regarded as transition rates between the corresponding states. For a fixed voltage and given our assumptions, α , β are constants.¹ We assume that the channel transitions are memoryless, that is, the probability of a channel transition depends only on the present state of the channel and not on the history of the channel, *i.e.*, the channel's prior states. This is called the *Markov* property and so our memoryless assumption implies that the channel gating process is a Markov process. A Markov process is called *homogeneous* if the probability of a channel transition in an interval Δt depends

¹For voltage-gated channels, α and β are functions of V_m , but since we assume currents are small, V_m is close to its resting value and α and β can be considered to be constant.

only on the length of the interval and not its starting point. This implies that the transition matrix is a function of only one variable representing the length of the interval between transitions. Δt is chosen to be sufficiently small to ensure that there is a maximum of one transition in Δt . This can be expressed more formally as

$$\lim_{\Delta t \rightarrow 0} \frac{\text{Prob [2 or more transitions in } \Delta t \text{]}}{\Delta t} = 0. \quad (\text{E1})$$

Processes satisfying this property are called *ordinary* processes. The well-known Poisson point process is an example of an ordinary, homogeneous process.

Thus, we model channel transitions as an ordinary, homogeneous, discrete-state continuous-time Markov process which allows us to apply the theory of continuous-time Markov chains to derive the matrix differential equation, the *Chapman-Kolmogorov equation* (C-K)², for the state transition probabilities. Several excellent treatments of this exist in the literature (Colquhoun & Hawkes, 1982; Johnston & Wu, 1995).

For the two-state channel, let $\mathbf{x}(t)$ denote the state of the channel at time t . Let us numerically represent the closed state by 1 and the open state by 2. The matrix of transition probabilities between states is represented by $\Pi(t) = [\Pi_{ij}(t)]$ where $\Pi_{ij}(t) = \text{Prob}[\mathbf{x}(t) = j \mid \mathbf{x}(0) = i]$ is the probability that the channel is in state j at time t given that it was in state i at $t = 0$. Since $\mathbf{x}(t)$ is a homogeneous process, $\Pi_{ij}(t) = \text{Prob}[\mathbf{x}(t+z) = j \mid \mathbf{x}(z) = i]$ for any z . Similarly, let $\mathbf{P}(t) = [P_1(t) \ P_2(t)]$ denote the vector of state probabilities where $P_i(t) = \text{Prob}[\mathbf{x}(t) = i]$ is the probability that the channel is in state i at time t . Together, $\Pi(t)$ and $\mathbf{P}(t)$ completely specify $\mathbf{x}(t)$ since all the statistics of $\mathbf{x}(t)$ can be determined in terms of $\Pi(t)$ and $\mathbf{P}(t)$. For the two-state channel $\Pi(t)$ is a 2×2 matrix function. $\Pi(t)$ satisfies the C-K equation,

$$\frac{d\Pi(t)}{dt} = \Pi(t) \mathbf{Q}. \quad (\text{E2})$$

²Conventionally, Chapman-Kolmogorov equation refers to the equivalent integral form of the differential equations. In physics, the differential form is called the *Master equation*.

The initial condition for the above differential equation is $\Pi(0) = \mathbf{I}$, where $\mathbf{I} = [\delta_{ij}]$ is the unity matrix. $\mathbf{Q} = [q_{ij}]$ is called the *infinitesimal matrix* and is defined as

$$\mathbf{Q} = \lim_{\Delta t \rightarrow 0} \frac{\Pi(\Delta t) - \mathbf{I}}{\Delta t} = \Pi'(0). \quad (\text{E3})$$

It can be shown that as long as $\mathbf{x}(t)$ is an ordinary process, $\Pi'(0)$ is well defined and the above equality holds. The elements of \mathbf{Q} are called *transition probability rates* of $\mathbf{x}(t)$. Since $\Pi(t)$ is a matrix of conditional probabilities,

$$\sum_j \Pi_{ij}(t) = 1 \quad \forall t \Rightarrow \sum_j q_{ij} = 0. \quad (\text{E4})$$

A matrix for which the sum of columns adds up to 1 (Π above) is called a *Markov matrix*. For the two-state channel,

$$\mathbf{Q} = \begin{bmatrix} -\alpha & \alpha \\ \beta & -\beta \end{bmatrix}. \quad (\text{E5})$$

Since the columns of \mathbf{Q} add to zero, \mathbf{Q} is singular matrix. It can be shown that for an n state Markov process, \mathbf{Q} has $n - 1$ non-zero eigenvalues. Thus, in our case \mathbf{Q} has one non-zero eigenvalue. $\mathbf{P}(t)$ can be expressed in terms of $\Pi(t)$ and the initial state probability vector $\mathbf{P}(0)$ as

$$\mathbf{P}(t) = \mathbf{P}(0) \Pi(t). \quad (\text{E6})$$

A property of finite-state Markov processes is that, independent of the initial state, $\mathbf{P}(t)$ and $\Pi(t)$ tend to stationary solutions, \mathbf{P}^s and Π^s respectively, given by the equations,

$$\mathbf{P}^s \mathbf{Q} = 0, \quad \Pi^s \mathbf{Q} = 0. \quad (\text{E7})$$

One can easily see from the above equations that $P_1^s = \Pi_{11}^s = \frac{\beta}{\alpha + \beta}$ and $P_2^s = \Pi_{22}^s = \frac{\alpha}{\alpha + \beta}$ respectively. Thus, at steady-state, the state probabilities, P_i^s , and the transition probabilities, Π_{ii}^s , are equal irrespective of the initial state of the channel. The complete

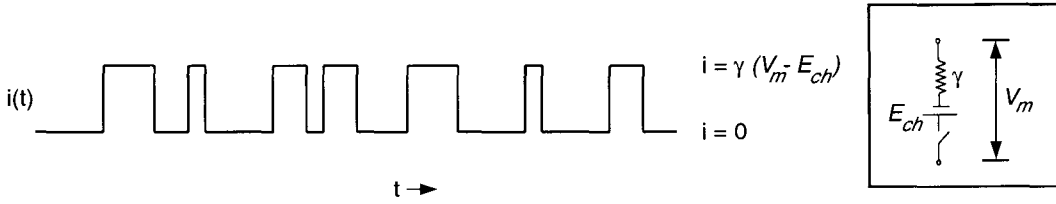


Figure 9.1: **Stochastic Fluctuations of a Two State Binary Channel.** Sample current record for a single two-state channel switching randomly between its open and closed state. The open state is characterized by a conductance γ and the closed state does not conduct. **Inset:** Equivalent electrical circuit of the channel.

solutions for $P_i(t)$ and $\Pi_{ii}(t)$ can be written as

$$P_1(t) = P_1^s - [P_1^s - P_1(0)]e^{-(\alpha+\beta)t}, \quad P_2(t) = P_2^s - [P_2^s - P_2(0)]e^{-(\alpha+\beta)t} \quad (\text{E8})$$

$$\Pi_{11}(t) = \Pi_{11}^s - [\Pi_{11}^s - 1]e^{-(\alpha+\beta)t}, \quad \Pi_{22}(t) = \Pi_{22}^s - [\Pi_{22}^s - 1]e^{-(\alpha+\beta)t}. \quad (\text{E9})$$

All the probabilities above follow an exponential time course with a time constant $\theta = 1/\alpha + \beta$, which is called the *relaxation* time constant. Let γ denote the conductance of a single channel in the open state (the closed state does not conduct current). $I(t)$, the current through the channel, fluctuates between 0 and $\gamma(V_m - E_{ch})$, as shown in **Fig. 9.1**, where E_{ch} is the reversal potential of the channel and V_m is the membrane potential. Since $I(t)$ is a binary process, its expected value $\langle I \rangle$ at equilibrium is equal to the product of $\gamma(V_m - E_{ch})$ and the steady-state open probability, P_2^s . Thus,

$$\langle I \rangle = P_2^s \gamma (V_m - E_{ch}) = \frac{\alpha}{\alpha + \beta} \gamma (V_m - E_{ch}). \quad (\text{E10})$$

Similarly,

$$\langle I^2 \rangle = P_2^s \gamma^2 (V_m - E_{ch})^2 = \frac{\alpha}{\alpha + \beta} \gamma^2 (V_m - E_{ch})^2. \quad (\text{E11})$$

Thus, the variance of the current fluctuations at equilibrium $\sigma_I^2 = \langle I^2 \rangle - \langle I \rangle^2$ is given by

$$\sigma_I^2 = \gamma^2 (V_m - E_{ch})^2 P_2^s (1 - P_2^s) = \gamma^2 (V_m - E_{ch})^2 \frac{\alpha\beta}{(\alpha + \beta)^2}. \quad (\text{E12})$$

The autocorrelation of $I(t)$, $R_I(z) = \langle I(t)I(t+z) \rangle$ is given by

$$R_I(z) = \gamma^2 (V_m - E_{\text{ch}})^2 \text{Prob}[\mathbf{x}(t) = 2; \mathbf{x}(t+z) = 2] \quad (\text{E13})$$

$$= \gamma^2 (V_m - E_{\text{ch}})^2 \text{Prob}[\mathbf{x}(t) = 2] \text{Prob}[\mathbf{x}(t+z) = 2 \mid \mathbf{x}(t) = 2] \quad (\text{E14})$$

$$= \gamma^2 (V_m - E_{\text{ch}})^2 P_2^s \Pi_{22}(z) \quad (\text{E15})$$

$$= \gamma^2 (V_m - E_{\text{ch}})^2 \frac{\alpha}{\alpha + \beta} \left[\frac{\alpha}{\alpha + \beta} + \frac{\beta}{\alpha + \beta} e^{-(\alpha + \beta)z} \right] \quad (\text{E16})$$

$$= \frac{\gamma^2 (V_m - E_{\text{ch}})^2 \alpha^2}{(\alpha + \beta)^2} + \frac{\gamma^2 (V_m - E_{\text{ch}})^2 \alpha \beta}{(\alpha + \beta)^2} e^{-(\alpha + \beta)z} \quad (\text{E17})$$

$$= \langle I \rangle^2 + \sigma_I^2 e^{-|z|/\theta}. \quad (\text{E18})$$

The auto-covariance function is defined as

$$C(z) = R(z) - \langle I \rangle^2 = \sigma_I^2 e^{-|z|/\theta} \quad (\text{E19})$$

and is shown in **Fig. 9.2A**. The power spectral density of the current fluctuations, $S_I(f)$, can be obtained by taking the Fourier transform of $C(z)$ according to the Wiener-Khinchine theorem,

$$S_I(f) = \mathcal{F}\{C(z)\} = \int_{-\infty}^{\infty} C(z) e^{-j2\pi f z} dz = 2 \int_0^{\infty} C(z) \cos(2\pi f z) dz. \quad (\text{E20})$$

Thus,

$$S_I(f) = \frac{2\alpha\beta}{\alpha + \beta} \frac{\gamma^2 (V_m - E_{\text{ch}})^2}{(\alpha + \beta)^2 + (2\pi f)^2} \quad (\text{E21})$$

$$= \frac{S_I(0)}{1 + (f/f_c)^2}, \quad (\text{E22})$$

where

$$S_I(0) = 2 \sigma_I^2 \theta \quad \text{and} \quad f_c = \frac{1}{2\pi\theta}. \quad (\text{E23})$$

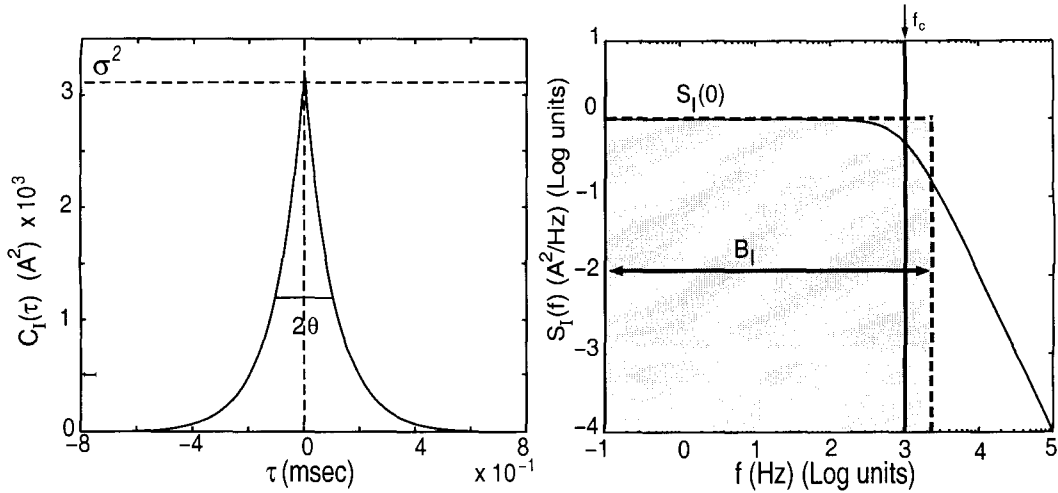


Figure 9.2: **Statistical Properties of Current Noise for a Binary Channel.** **A:** The noise covariance $C_I(z)$ (equation E19) is a double-sided exponential with a decay constant θ . **B:** The power spectral density $S_I(f)$ (equation E22) is a Lorentzian with a cut-off frequency $f_c = 1/2\pi\theta$. The bandwidth $B_I = \pi/2f_c$ corresponds to a frequency for which the area of the shaded rectangle equals $\sigma_I^2/2$ (since $S_I(f)$ is an even function). Parameters used: $f_c = 1000$ Hz, $S_I(0) = 1$ A²/Hz.

A power spectrum of the above form is called a *Lorentzian* spectrum. $S_I(f)$ can be expressed in terms of two parameters, its *amplitude*, $S_I(0)$ and its *cut-off* frequency, f_c , at which the magnitude of the power spectrum is half of its DC value ($\frac{1}{2}S(0)$). f_c can also be written in terms of the time constant θ as $f_c = \frac{1}{2\pi\theta}$. A commonly used definition of “bandwidth” of a random signal is the variance of the signal divided by twice the magnitude of its power spectrum at $f = 0$. This is illustrated in **Fig. 9.2B**. The shaded rectangle has one of its sides equal to $S_I(0)$ while the other side is equal to the bandwidth B_I so that its area is equal to half the variance of the signal (σ_I^2). Thus, for a Lorentzian spectrum of $I(t)$, $B_I = \frac{\sigma_I^2}{2S_I(0)} = \frac{\pi}{2}f_c$. In terms of the time constant θ , $B_I = 1/4\theta$.

Now consider a patch of neuronal membrane which contains N such binary channels. We assume that all the channels open and close independently of one another, that is, there are no cooperative effects between them. As before, we assume that the membrane voltage is maintained at V_m either artificially by clamping the patch or by assuming that the total current through the channels does not make V_m deviate significantly. Since the channels are identical, the statistics of every channel is the same as derived above. Because the N channels are in parallel, the total current through the patch (I) is the sum of the currents

through individual channels denoted by i_j ,

$$I = \sum_{j=1}^N i_j. \quad (\text{E24})$$

Thus,

$$\langle I \rangle = \sum_{j=1}^N \langle i_j \rangle = N P_2^s \gamma (V_m - E_{\text{ch}}). \quad (\text{E25})$$

Similarly

$$\langle I^2 \rangle = \sum_{j=1}^N \sum_{k=1}^N \langle i_j i_k \rangle. \quad (\text{E26})$$

Since the individual currents are independent of one another, $\langle i_j i_k \rangle = \langle i_j \rangle \langle i_k \rangle$,

$$\langle I^2 \rangle = N P_2^s \gamma^2 (V_m - E_{\text{ch}})^2 + N(N-1) (P_2^s \gamma (V_m - E_{\text{ch}}))^2. \quad (\text{E27})$$

Simplifying this expression yields

$$\sigma_I^2 = N \gamma^2 P_2^s (1 - P_2^s) (V_m - E_{\text{ch}})^2. \quad (\text{E28})$$

In other words, the variance of the current scales linearly, and not quadratically, with the number of channels N . Since the statistics of I are identical to i_j , $C_I(z)$ and $S_I(f)$ can be obtained by simply scaling their single channel counterparts. Usually, N is expressed as a product of the channel density (denoted by η) and the area of the membrane patch. We here, for convenience, express all quantities in terms of their corresponding specific units and multiply them by the patch dimensions when desired.

Most of the ion channels found in biological membranes, either voltage-gated or ligand-gated, have more than two states and do not resemble the binary switch model analyzed above. For instance, some channels have multiple open and closed states while others have additional blocked, inactivated or desensitized states. A host of kinetic models exist for a number of known channel types in both the voltage-gated and ligand-gated classes (Hille,

1992). Some of these models are quite complicated, containing tens of states and so their behavior can only be studied numerically. Several techniques have been developed to analyze these models and extract model parameters from experimental data (Johnston & Wu, 1995; Weiss, 1996a; Colquhoun & Hawkes, 1982).

Despite this complexity, the theoretical treatment of these multiple-state models is conceptually similar to that of the two-state model. Channel kinetics are characterized by the matrix \mathbf{Q} of transition probabilities and the power spectrum of the conductance fluctuations can be written as a sum of Lorentzian spectra with cut-off frequencies given by the non-zero eigenvalues of \mathbf{Q} (Johnston & Wu, 1995). We shall restrict ourselves to two such multi-state models, the voltage-gated K^+ and Na^+ channels underlying the classical Hodgkin-Huxley potassium and sodium currents.

F Derivation of Current Noise Spectra

For ion channels modeled as finite-state Markov chains (**Fig. 6.1**), it can be shown that under voltage-clamp at V_m^o , the autocovariance of the K^+ current noise in an isopotential membrane patch of area A can be derived as (DeFelice, 1981; Johnston & Wu, 1995)

$$C_{\text{IK}}(t) = A \eta_{\text{K}} \gamma_{\text{K}}^2 (V_m^o - E_{\text{K}})^2 n_{\infty}^N \left[n_{0|1}^N(t) - n_{\infty}^N \right], \quad (\text{F1})$$

where η_{K} denotes the K^+ channel density in the patch and γ_{K} denotes the open conductance of a single K^+ channel. $n_{0|1}(t)$ is the conditional probability for a potassium activation subunit to be in the open state at time t , given that it started in a closed state at $t = 0$ and is given by (Johnston & Wu, 1995)

$$n_{0|1}(t) = [n_{\infty} + (1 - n_{\infty})e^{-t/\tau_n}]. \quad (\text{F2})$$

On expanding equation F1 we obtain

$$C_{\text{IK}}(t) = A \eta_{\text{K}} \gamma_{\text{K}}^2 (V_m^o - E_{\text{K}})^2 n_{\infty}^N \times \sum_{i=1}^N \binom{N}{i} (1 - n_{\infty})^i n_{\infty}^{N-i} e^{-i|\tau|/\tau_n}. \quad (\text{F3})$$

By the Wiener-Khinchine theorem (Papoulis, 1991), the power spectral density of the K^+ current noise, $S_{IK}(f)$, is given by the Fourier transform of $C_{IK}(t)$,

$$S_{IK}(f) = A \eta_K \gamma_K^2 (V_m^o - E_K)^2 n_\infty^N \times \sum_{i=1}^N \binom{N}{i} (1 - n_\infty)^i n_\infty^{N-i} \frac{2 \tau_n / i}{1 + (2\pi f \tau_n / i)^2}. \quad (\text{F4})$$

Thus, the K^+ current noise spectrum can be expressed as a sum of N Lorentzian functions with cut-off frequencies $f_i = i/(2\pi\tau_n)$, $i = \{1, \dots, N\}$. When $n_\infty \ll 1$, $S_{IK}(f)$ is well approximated by a single Lorentzian with cut-off frequency $N/2\pi\tau_n$. Similarly, the auto-covariance of Na^+ current noise can be written as (DeFelice, 1981)

$$C_{INa}(t) = A \eta_{Na} \gamma_{Na}^2 (V_m^o - E_{Na})^2 \times m_\infty^M h_\infty^H \left[m_{0|1}^M(t) h_{0|1}^H(t) - m_\infty^M h_\infty^H \right] \quad (\text{F5})$$

where

$$m_{0|1}(t) = m_\infty + (1 - m_\infty) e^{-t/\tau_m}, \quad (\text{F6})$$

$$h_{0|1}(t) = h_\infty + (1 - h_\infty) e^{-t/\tau_h}. \quad (\text{F7})$$

For the HH and MJHS kinetic schemes ($M = 3$, $H = 1$), $S_{INa}(f)$ can be expressed as a sum of seven Lorentzians with cut-off frequencies corresponding to the time constants τ_m , τ_h , $2\tau_m$, $3\tau_m$, $\tau_m + \tau_h$, $2\tau_m + \tau_h$ and $3\tau_m + \tau_h$.

G Linearization of Active Membranes

Consider an isopotential membrane patch of area A containing voltage-gated K^+ and Na^+ channels as well as leak channels. The dynamics of the membrane potential are given by

$$-C \frac{dV_m}{dt} = I_K + I_{Na} + I_L + I_{inj}, \quad (\text{G1})$$

where C is the capacitance of the patch and I_K , I_{Na} and I_L are transmembrane currents given by

$$I_K = g_K (V_m - E_K), \quad (\text{G2})$$

$$I_{Na} = g_{Na} (V_m - E_{Na}), \quad (\text{G3})$$

$$I_L = g_L (V_m - E_L), \quad (\text{G4})$$

where g_i denotes the conductance and E_i denotes the reversal potential of the corresponding membrane current I_i . I_{inj} denotes the current injected into the patch with the convention that inward current is negative.

Quasi-active Linearization

The current through a given membrane conductance can be written in general as

$$I_i = g_i (V_m - E_i). \quad (\text{G5})$$

To first order, a deterministic deviation in I_i (denoted by δI_i) around the steady-state membrane voltage V_m^o can be expressed in terms of the corresponding deterministic deviations in V_m and g_i as

$$\delta I_i = g_i^o \delta V_m + \delta g_i (V_m^o - E_i) \quad (\text{G6})$$

where g_i^o denotes the steady-state conductance at V_m^o , $\delta I_i = I_i(V_m) - I(V_m^o)$, $\delta V_m = V_m - V_m^o$, and $\delta g_i = g_i(V_m) - g_i^o$. V_m^o can be obtained by solving for $dV_m/dt = 0$ (equation G1–equation G4),

$$V_m^o = \frac{g_K^o E_K + g_{Na}^o E_{Na} + g_L E_L - I_{inj}}{g_K^o + g_{Na}^o + g_L}. \quad (\text{G7})$$

The conductance of the leak channels is constant, thus, $\delta g_L = 0$. However, for the active K^+ and Na^+ ion channels, δg_K and δg_{Na} are functions of δV_m . It has been shown that to first order, the voltage and time dependence of active ion channels can be modeled by *phe-*

nomenological impedances (Mauro *et al.*, 1970; Koch, 1984). For the sake for completeness, we derive the phenomenological impedances corresponding to the K^+ and Na^+ conductances here.

Consider a first-order activation or inactivation variable (denoted generically by n)

$$\frac{d n}{d t} = \frac{n_{\infty} - n}{\tau_n}. \quad (G8)$$

Perturbing this equation to first-order yields

$$\frac{d(\delta n)}{d t} = -\frac{\delta n}{\tau_n} + \frac{\delta n_{\infty}}{\tau_n} - \frac{(n_{\infty} - n)}{\tau_n^2} \delta \tau_n. \quad (G9)$$

Since the deviations are assumed to take place around the steady state, the third term in the above expression is zero. Thus,

$$\frac{d(\delta n)}{d t} + \frac{\delta n}{\tau_n} = \frac{\delta n_{\infty}}{\tau_n}. \quad (G10)$$

Since n_{∞} is a function of V_m alone, $\delta n_{\infty} \approx (dn_{\infty}/dV_m) \delta V_m$, which gives,

$$\frac{d(\delta n)}{d t} + \frac{\delta n}{\tau_n} = \frac{n'_{\infty}}{\tau_n} \delta V_m, \quad (G11)$$

where $'$ denotes a derivative with respect to V_m evaluated at the steady-state voltage V_m^o .

The above equation can be rewritten as

$$\delta V_m = \frac{\tau_n}{n'_{\infty}} \frac{d(\delta n)}{d t} + \frac{\delta n}{n'_{\infty}}. \quad (G12)$$

Using Laplace transforms we can rewrite equation G12 as

$$\delta V_m(s) = \delta n(s) \left[\frac{\tau_n}{n'_{\infty}} s + \frac{1}{n'_{\infty}} \right], \quad (G13)$$

where $\delta V_m(s)$ and $\delta n(s)$ denote the Laplace transforms of δV_m and δn respectively. Thus, if δn is considered analogous to a current, equation G13 is identical to that of an electric circuit with a resistance r of magnitude $1/n'_{\infty}$ in series with an inductance $l = \tau_n/n'_{\infty}$. The

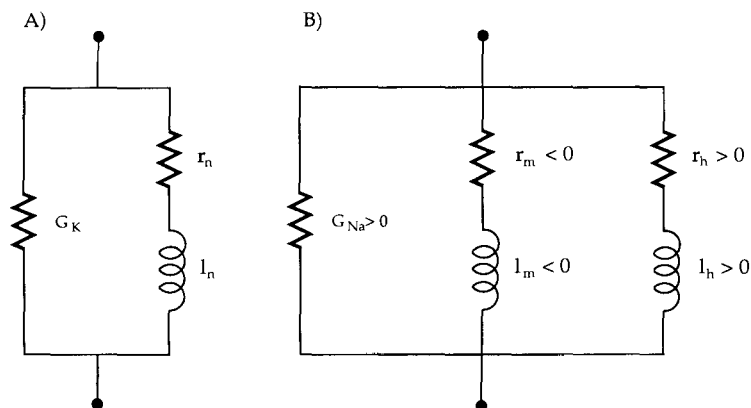


Figure 9.3: **Phenomenological Impedance of Active Voltage-Gated Conductances.**

A: Equivalent electric circuit corresponding to the delayed rectifier potassium current obtained by linearization around a fixed membrane potential. The circuit consists of a pure conductance, G_K , in parallel with a series, phenomenological RL branch with resistance r_n and inductance l_n . For $V > E_K$, all the three components are positive. **B:** Equivalent linearized electric circuit corresponding to the fast, inactivating Na^+ current potential. The circuit consists of a pure conductance, G_{Na} , in parallel with two series RL branches, one corresponding to activation (r_m, l_m) and the other to inactivation (r_h, l_h). For the physiological range of voltages $V < E_{\text{Na}}$, r_m and l_m are negative, whereas r_h and l_h are positive.

time constant of this series RL circuit is equal to $l/r = \tau_n$. Note that these quantities are evaluated at V_m^o . Since these impedances do not represent physically realistic components and are used, instead, to describe the voltage- and time-dependence of active ionic conductances, they are called phenomenological impedances (Sabah & Leibovic, 1969; Mauro *et al.*, 1970; Koch, 1984; Koch, 1999).

For the non-inactivating K^+ conductance,

$$g_K = A \eta_K \gamma_K n^N, \quad (\text{G14})$$

$\delta g_K = N \eta_K \gamma_K n_\infty^{N-1} \delta n$ and substituting for δn derived from equation G13 in equation G6 (after taking Laplace transforms on both sides) we obtain

$$\delta I_K(s) = \left[g_K^o + \frac{1}{r_n + s l_n} \right] \delta V_m(s), \quad (\text{G15})$$

where

$$g_K^o = A \eta_K \gamma_K n_\infty^N, \quad (\text{G16})$$

and the phenomenological impedances corresponding to K^+ activation (r_n, l_n) are given by

$$\begin{aligned} r_n &= \frac{1}{N A \eta_K n_\infty^{N-1} \gamma_K (V_m^o - E_K) n'_\infty}, \\ l_n &= \tau_n r_n. \end{aligned} \quad (\text{G17})$$

Notice that as $V_m^o \rightarrow E_K$, $r_n \rightarrow \infty$ and $l_n \rightarrow \infty$. Thus at its reversal potential, K^+ channel behaves as a pure conductance g_K^o . The equivalent electrical circuit corresponding to the K^+ channel is shown in **Fig. 9.3A**. Similarly, for the inactivating Na^+ current,

$$g_{Na} = A \eta_{Na} \gamma_{Na} m^M h^H, \quad (\text{G18})$$

δg_{Na} can be written as

$$\begin{aligned} \delta g_{Na} &= A \eta_{Na} \gamma_{Na} m^{M-1} h^{H-1} \times \\ &[H h \delta m + M m \delta h]. \end{aligned} \quad (\text{G19})$$

Substituting for δg_{Na} in equation G6, it can be observed that the equivalent electrical circuit for an inactivating conductance has two RL branches in parallel with a conductance g_{Na}^o . The expressions for the different components are given by the following expressions:

$$\begin{aligned} g_{Na}^o &= A \eta_{Na} \gamma_{Na} m_\infty^M h_\infty^H, \\ r_m &= \frac{1}{M A \eta_{Na} m_\infty^{M-1} h_\infty^H \gamma_{Na} (V_m^o - E_{Na}) m'_\infty}, \\ l_m &= \tau_m r_m, \\ r_h &= \frac{1}{H A \eta_{Na} m_\infty^M h_\infty^{H-1} \gamma_{Na} (V_m^o - E_{Na}) h'_\infty}, \\ l_h &= \tau_h r_h. \end{aligned} \quad (\text{G20})$$

Notice that for $V_m^o < E_{Na}$, $r_m < 0$, $l_m < 0$. Thus, for physiological values of the membrane voltage, the activation component corresponds to a negative resistance and a negative inductance. This is to be expected since the activation variable m is responsible for the positive-feedback characterizing the fast rising phase of an action potential. Since h is an inactivation variable which decreases as the membrane potential is increased, $h'_\infty < 0$ implying that for $V_m^o < E_{Na}$, $r_h > 0$, $l_h > 0$. The equivalent electric circuit corresponding to the Na^+ channel is shown in **Fig. 9.3B**.

Similarly, the equivalent impedance of the active membrane patch corresponding to equation G1 is given by parallel combination of capacitance C , a (physical) conductance $G = G_K + G_{Na} + g_L$, which is equal to the sum of resting channel conductances and two (phenomenological) series RL circuits arising due to the time-dependent nature of the ionic conductances. The complex admittance of the circuit is

$$Y(f) = G + j2\pi fC + \frac{1}{r_n + j2\pi fl_n} + \frac{1}{r_m + j2\pi fl_m} + \frac{1}{r_h + j2\pi fl_h} \quad (\text{G21})$$

where $G = g_K^o + g_{Na}^o + g_L$ denote the total steady-state patch conductance at the voltage V_m^o . The linearized equivalent circuit corresponding to the membrane is shown in **Fig. 9.4**.

So far we have considered the system to be deterministic; incorporating the voltage-dependence of the ionic conductances we derived the linearized equivalent circuit for the membrane patch. The effect of stochastic conductance fluctuations of the active ion channels can be modeled by including a noise current I_n

$$\begin{aligned} I_n &= I_K + I_{Na} \\ &= \tilde{g}_K(E_K - V_m^o) + \tilde{g}_{Na}(E_{Na} - V_m^o) \end{aligned} \quad (\text{G22})$$

in parallel with the admittance Y . \tilde{g}_K and \tilde{g}_{Na} denote the stochastic components of the conductance deviations around their respective steady-state values. The resulting voltage fluctuations are denoted by \tilde{V} . It is straightforward to derive the power spectral density of

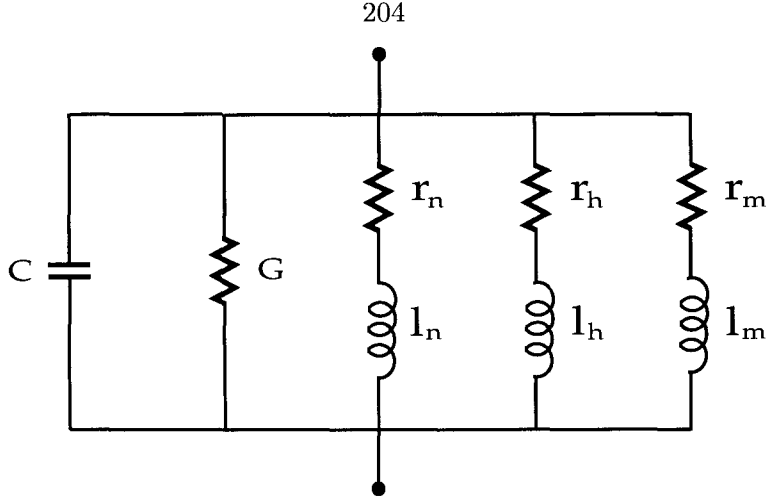


Figure 9.4: **Linearized Equivalent Electrical Circuit for the Membrane Patch.** Equivalent RLC circuit for a membrane patch containing K^+ and Na^+ conductances, voltage-independent synapses and passive leak channels. C denotes the transverse membrane capacitance and G the sum total of the resting conductances of the different sources. The small-signal phenomenological impedances due to K^+ and Na^+ conductances are given by the three series RL branches.

\tilde{V} (denoted by $S_V(f)$) for this linear system as in (Papoulis, 1991)

$$S_V(f) = \frac{S_{I_n}(f)}{|Y(f)|^2}. \quad (G23)$$

where $S_{I_n}(f)$ is the power spectrum of I_n . Since the noise sources are independent,

$$S_{I_n}(f) = S_{IK}(f) + S_{INa}(f). \quad (G24)$$

The variance of the voltage fluctuations σ_V^2 can be written as

$$\sigma_V^2 = \int_{-\infty}^{\infty} df \frac{S_{I_n}(f)}{|Y(f)|^2}. \quad (G25)$$

Using the expressions for the power spectral densities of the current noise due to channel fluctuations under voltage-clamp (S_{IK} and S_{INa}), derived in Appendix F the magnitude and spectral density of the resulting sub-threshold voltage noise can be computed.

Passive Linearization

For the passive linearized approximation (Koch, 1984), we neglect the voltage-dependent dynamics of the ionic conductances. This is equivalent to ignoring the second term on the right side of equation G6. Thus, the ionic conductances and the membrane voltage are expressed as

$$\begin{aligned} g_K &= g_K^o + \tilde{g}_K, \\ g_{Na} &= g_{Na}^o + \tilde{g}_{Na}, \\ V_m &= V_m^o + \tilde{V}. \end{aligned} \quad (\text{G26})$$

Let $\tilde{g} = \tilde{g}_K + \tilde{g}_{Na}$ denote the sum of the conductance fluctuations around steady-state. When $\tilde{g} \ll G$, equation G1 can be simplified as

$$\tau \frac{d\tilde{V}}{dt} + \tilde{V} = \frac{I_n}{G} \quad (\text{G27})$$

where $\tau = C/G$ is the passive membrane time constant. Refer to (Manwani & Koch, 1999a) for further details. Thus, under passive linearization, the patch is modeled as an RC circuit given by the parallel combination of the membrane capacitance C and a conductance G equal to the sum of the steady-state values of the ionic and leak conductances. As before, the effect of noise due to ionic channel conductance fluctuations can be modeled as a current noise source I_n in parallel with this RC circuit. The equivalent circuit corresponding to this approximation is shown in **Fig. 6.4A**. The complex admittance of this circuit is

$$Y(f) = G + j2\pi fC. \quad (\text{G28})$$

For passive linearization, $S_V(f)$ (equation G23) can be simplified as

$$S_V(f) = \frac{S_{I_n}(f)}{G^2 [1 + (2\pi f\tau)^2]}. \quad (\text{G29})$$

The variance of the voltage fluctuations σ_V^2 can be written as

$$\sigma_V^2 = \frac{1}{G^2} \int_{-\infty}^{\infty} df \frac{S_{In}(f)}{1 + (2\pi f\tau)^2}. \quad (\text{G30})$$

H Theoretical Analysis of Fast Multiplicative Conductance Fluctuations

In earlier chapters (Chapter 3 and Chapter 6), we derived expressions for the magnitude and power spectrum of the voltage noise due to stochastic conductance fluctuations (both ligand-gated and voltage-gated conductances) in neuronal membranes under simplifying assumptions, *viz.*, the small magnitude of voltage fluctuations allowing conductance fluctuations to be treated as current noise, and the linearization of membrane nonlinearities about the steady-state resting voltage. Here we carry out a theoretical analysis in the absence of these simplifying approximations. We will assume, however, that the dynamics of the conductance fluctuations are rapid compared to those governing the membrane voltage. We will refer to such conductances as *fast* conductances. While this assumption is valid for several biophysical processes (*e.g.*, the activation of voltage-gated ion channels like K^+ , Na^+ and Ca^{2+} , and ligand-gated conductances like AMPA-type glutamate, GABA-A and glycine), it does not include others (*e.g.*, inactivation of voltage-gated Na^+ channels).

Classification of Membrane Conductances

There exist a wide variety of mechanisms of ion-transport across nerve membranes which endow them with their electrical excitability. In a large number of cases, the membrane currents depend on the voltage difference across the membrane (Johnston & Wu, 1995; Weiss, 1996a; Weiss, 1996b),

$$i = f(V_m, t)$$

where i is the membrane current, V_m is the membrane voltage and the argument t indicates that, in general, the current i might also depend on time. Ion transport can be broadly classified into *passive* and *active* mechanisms. Ionic flux in the direction of its electrochemical

gradient is called passive. We shall restrict ourselves to passive membrane currents which include a diverse array of voltage-gated and ligand-gated ion channels. Examples of active currents and fluxes include the variety of ion-pumps and carrier mediated transport and exchange mechanisms in the neuronal membrane (Weiss, 1996a; Weiss, 1996b).

The physical constraint that the current corresponding to a particular ionic species be in the direction of its electrochemical gradient allows it to be expressed as (Hille, 1992)

$$i = g(V_m, t) (V_m - E), \quad (\text{H1})$$

where E is the membrane voltage for which $i = 0$ and is called the reversal potential. For currents due to the flow of a single ionic species, E coincides with the electrochemical Nernst potential corresponding to the ion. g is the voltage- and time-dependent also called the *chord* conductance. An alternative and equivalent definition of passive flux is that it involves only the dissipation of energy; no energy is generated. This implies that the product of the current and driving potential ($V_m - E$) for a passive mechanism is always non-negative, *i.e.*,

$$g(V_m, t) (V_m - E)^2 \geq 0 \Rightarrow g(V_m, t) \geq 0.$$

This implies that the chord conductance of a nonlinear passive conductor is positive, necessitating that its current-voltage curve (plotted with respect to $V_m - E$) lies in the first and third quadrants. Another type of membrane conductance is the *slope* conductance defined as the derivative of the current with respect to the membrane voltage

$$\frac{\partial i}{\partial V_m} = g(V_m, t) + (V_m - E) \frac{\partial g(V_m, t)}{\partial V_m}. \quad (\text{H2})$$

We classify membrane conductances into three types. The first class includes voltage-independent conductances for which $g(V_m, t)$ is independent of membrane voltage. We refer to them as *passive* conductances. Some examples of voltage-independent conductances include the leak conductance responsible to maintain the resting potential, ligand-gated conductances like AMPA and GABA, and so on. Conventionally, the term passive has often been used in the literature to refer to such voltage-independent conductances (Koch,

1984; Koch, 1999). Inasmuch as this usage is confusing and misleading given the discussion of passive flux mechanisms above, we adopt it here since we restrict our attention to passive flux mechanisms only.

The second class of conductances includes voltage- and time-dependent conductances for which the slope conductance is positive over the range of interest. The positivity of the slope conductance requires that $\partial g(V_m, t)/\partial V_m \geq -g(V_m, t)/(V_m - E)$. Such conductances are responsible for the recovery of the membrane voltage towards rest and will be referred to as *non-regenerative* conductances. The different types of voltage-gated K^+ conductances belong to this class.

The third class of conductances includes voltage-dependent conductances responsible for increased membrane excitability and action potential generation. The threshold behavior of nerve cells is due to the presence of regenerative conductances which have negative slope conductance over the physiologically relevant voltage range. We refer to them as *regenerative* conductances. Salient members of this class are voltage-gated ionic conductances like Na^+ and Ca^{2+} , and voltage-dependent synapses like NMDA and so on.

In general, membrane conductances are time-dependent and are not unique functions of the membrane voltage alone. Thus, for a given voltage, $g(V_m, t)$ denotes a family of conductances indexed by time t . However, we assume that the temporal dynamics of $g(V_m, t)$ are much faster than the rate of change of V_m and that the conductances quickly attain their steady-state values $g(V_m, \infty)$ corresponding to the relatively quasi-static voltage value. This is an alternative definition of fast conductances, which are uniquely determined by the magnitude of the membrane voltage alone. While there are some membrane processes like K^+ and Na^+ channel activation, AMPA and $GABA_A$ synapses which reach steady-state before the sub-threshold membrane voltage changes appreciably, the above approximation is not valid for slower processes like Na^+ channel inactivation, $GABA_B$ and NMDA-type synapses and so on. However, as long as there is a marked separation between the time scales at which the conductance and the membrane voltage change, one can regard the slower quantity to be constant relative to the other. This is the idea behind the principle of *adiabatic elimination* (also called the *slaving principle*) of variables (Gardiner, 1996).

Consider an isopotential patch of membrane characterized by a capacitance C and a leak conductance g_L in addition to a fast membrane conductance. The dynamics of the membrane voltage V_m of the patch are given by

$$-C \frac{dV_m}{dt} = I_m(V_m) \quad \text{where} \quad I_m(V_m) = g_L(V_m - E_L) + g(V_m)(V_m - E). \quad (\text{H3})$$

The steady-state relation between the membrane voltage and current, called the *i-V curve*, is given by $i = I_m(V_m)$ and can be determined by setting $dV_m/dt = 0$ in equation above. The i-V curves for membranes containing the three different types of conductances defined above are shown in **Fig. 9.5**. In all the three graphs, the origin is assumed to be at the resting potential of the membrane defined as the voltage V_{rest} for which $I_m(V_{\text{rest}}) = 0$. For passive conductances, the i-V curve is linear. For non-regenerative conductances, the i-V curve is nonlinear but intersects the voltage axis only once (at V_{rest}). Also because that slope conductance is always positive, it can be shown that the fixed point at V_{rest} is stable and the membrane eventually returns to V_{rest} . For regenerative conductances, the i-V curve can have multiple steady-states. The fixed point at V_{rest} is locally stable, whereas its adjacent fixed point is unstable because of the negative slope of the i-V curve in its neighborhood. This is a consequence of the negative slope conductance and can lead to spiking behavior in the membrane (Jack *et al.*, 1975).

The dynamical equation governing the membrane voltage (equation H3) is similar to the first order nonlinear differential equation

$$\frac{dx}{dt} = f(x)$$

which can be expressed as a gradient descent along a potential surface

$$\frac{dx}{dt} = -\frac{\partial U(x)}{\partial x} \quad \text{where} \quad U(x) = -\int^x dz f(z). \quad (\text{H4})$$

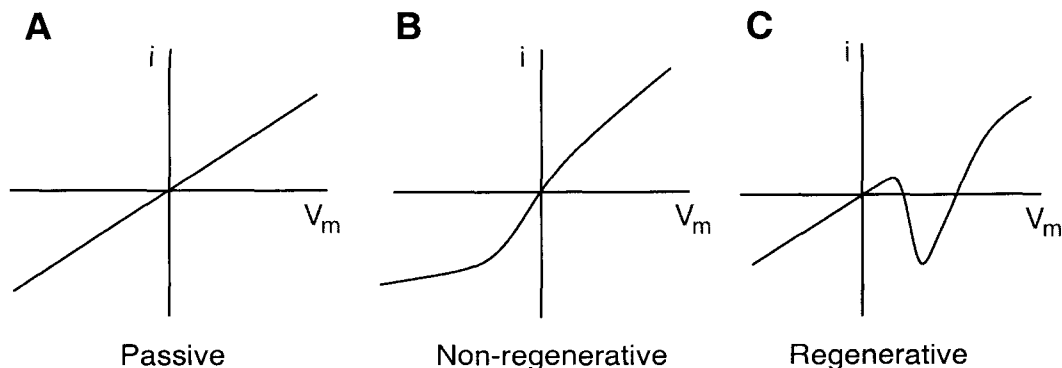


Figure 9.5: Classification of Membrane Conductances.

Current vs. voltage relationships in steady-state for an isopotential patch of membrane containing different types of membrane conductances. The origin of the voltage axis corresponds to the resting potential V_{rest} of the membrane. **A: Passive.** Passive conductances are independent of membrane-voltage and the i - V curve is linear. **B: Non-regenerative.** Non-regenerative conductances are responsible for the recovery of the membrane voltage to rest and are characterized by a positive slope conductance. The i - V curve has one fixed point and intersects the voltage axis only at the resting potential. **C: Regenerative.** Regenerative conductances are required for spiking behavior and are characterized by regions of negative slope conductance. The i - V curve has multiple fixed points.

Noise can be introduced in the deterministic state equation by adding a *Langevin* term which models the effect of random fluctuations

$$\frac{dx}{dt} = f(x) + \sigma \xi(t). \quad (\text{H5})$$

$\xi(t)$ is a Gaussian white noise process

$$\langle \xi(t) \xi(s) \rangle = \delta(t - s)$$

and σ is the magnitude of the Langevin term which can be determined from other physical considerations. For a constant σ , equation H5 represents an additive stochastic differential equation. The solution $x(t)$ of the above equation for a given initial condition x_0 has a stochastic trajectory and cannot be specified deterministically. However, one can talk about the conditional probability that $x(t)$ is at location x at time t given that it was at location y at an earlier time s defined as $p(x, t; y, s)$. Let $p(x, t)$ denote the marginal probability distribution $p(x, t) = \int dy p(x, t; y, s) p(y)$. $p(x, t; y, s)$ specifies the dynamical evolution of $p(x, t)$

and satisfies a deterministic partial differential equation called the *Fokker-Planck* equation. When a steady-state solution of $p(x, t)$ exists, it is defined as $p_s(x) = \lim_{t \rightarrow \infty} p(x, t)$. For equation H5 $p_s(x)$ is given by (Horsthemke & Lefever, 1984)

$$p_s(x) = N \exp \left[\frac{-2U(x)}{\sigma^2} \right] \quad (\text{H6})$$

where N is the constant of normalization which ensures that $\int dx p_s(x) = 1$. Thus, $p_s(x)$ is localized close to the fixed points of the energy surface $U(x)$ and has a maximum at the coordinate that corresponds to the minimum of the potential. The fixed point for the deepest potential well is globally speaking the most stable one and the other fixed points are called *metastable*. Thus, for additive noise, the number and position of the extrema of $p_s(x)$ and $U(x)$ coincide and fully characterize the steady-state behavior of the system.

Since the randomness in neuronal membranes occur in the form of conductance fluctuations, the additive noise approximation is not valid as the magnitude of the resulting current noise fluctuations are given by the product of the conductance fluctuations and the driving potential which is a function of the membrane voltage. Due to this coupling with voltage, conductance fluctuations represent a source of multiplicative noise. The steady-state behavior of systems driven by multiplicative noise can differ significantly from the deterministic fixed points of $U(x)$. It can be shown that multiplicative noise can lead to macroscopic behavior (*e.g.*, creation of fixed points or limit cycles) which is not present or can be predicted by the deterministic macroscopic equations. The theory of *noise-induced transitions* (Horsthemke & Lefever, 1984) addresses the behavior of such systems. This makes a point in favor of a potentially useful role of noise in biological systems. Stochastic resonance is a notable example of noise-induced behavior which can play a functionally advantageous role in biology (Berzukov & Vodyanoy, 1995; Levin & Miller, 1996). In the following, we derive the Fokker-Planck equations for multiplicative noise and use the results to study voltage noise due to conductance fluctuations.

Fokker-Planck Equations for Multiplicative Noise

Consider the following stochastic differential equation (SDE)

$$\frac{dv}{dt} = f(v) + \sigma g(v) \xi(t) \quad (\text{H7})$$

where $\xi(t)$ is a Gaussian white noise process with autocorrelation

$$\langle \xi(t) \xi(s) \rangle = \delta(t - s)$$

σ is a constant which determines the magnitude of the noise. Since the factor multiplying the noise term is a function of v itself, the noise is referred to be of *multiplicative* type, as opposed to the better known *additive* type when $g(v)$ is a constant.

In general, f and g can be functions of time but here we will assume that they are static, memoryless nonlinear functions of the dependent variable $v(t)$ alone. It can be shown that under mild conditions regarding the “smoothness” of functions f and g , the above equation implies that $v(t)$ is a Markov process with sample paths which are continuous everywhere (van Kampen, 1992; Gardiner, 1996). Markov processes defined by equation H7 are called *diffusion processes* and the functions $f(v)$ and $g(v)$ are called the *drift* and *diffusion* parameters of the process $v(t)$ respectively. The Wiener process and the Ornstein-Uhlenbeck process are special cases of diffusion processes (Gardiner, 1996). Because of the extreme irregularity of the white noise process, care has to be taken in interpreting the SDE defined in equation H7 since strictly speaking, the derivative of $v(t)$ is not defined in the ordinary sense. One way to get around this technical difficulty is to interpret $\xi(t)$ as a derivative in the generalized function sense of a Wiener process and bring the theory of generalized stochastic processes to bear on equation H7. Another way of looking at equation H7 and avoiding the framework of generalized stochastic process is to switch from its differential form

$$dv(t) = f(v(t)) dt + \sigma g(v(t)) dW(t), \quad (\text{H8})$$

to its equivalent integral form

$$v(t) = v_0 + \int_0^t ds f(v(s)) + \sigma \int_0^t ds g(v(s)) dW(s) \quad (\text{H9})$$

where $W(t)$ is a Wiener process. The first integral in equation H9 can be understood as an ordinary Riemann integral for each realization of $v(t)$ since the sample paths of $v(t)$ are as irregular as $W(t)$ and continuous everywhere. Thus, a formal definition of the SDE H8 depends on the interpretation of the second integral in equation H9. There are two reasonable interpretations of the second integral which lead to two different interpretations of equation H7 and consequently two distinct but equivalent calculi for stochastic differential equations. The nature of the interpretation depends on the value of v for which $g(v(s))$ is evaluated in the Riemann sum approximation

$$\int_0^t ds g(v(s)) dW(s) \approx \lim_{\Delta \rightarrow 0} \sum_i g(v_i) [W(t_{i+1}) - W(t_i)]$$

$$\text{where } \Delta = \max_i |t_{i+1} - t_i|, \quad v_i \in [v(t_i), v(t_{i+1})]$$

. In the formalism developed by Ito, v_i is chosen to be equal to the value at the beginning of the interval, $v_i = v(t_i)$, which implies that $g(v_i)$ is independent of $[W(t_{i+1}) - W(t_i)]$. The stochastic integral defined using this convention is called the Ito integral. Although the Ito interpretation leads to the cleanest formal treatment of the theory of stochastic differential equations involving diffusion processes, a new calculus has to be used to deal with such equations since the rules of ordinary calculus no longer apply.

On the other hand, in the formalism due to Stratonovich, v_i is chosen to be equal to the average of the two end-points, $v_i = [v(t_i) + v(t_{i+1})]/2$. The probability density of $v(t)$ satisfies the following Fokker-Planck (Risken, 1996) equation,

$$(I) \quad \frac{\partial p}{\partial t}(v, t) = -\frac{\partial}{\partial v} [f(v)p(v, t)] + \frac{\sigma^2}{2} \frac{\partial^2}{\partial v^2} [g^2(v)p(v, t)] \quad (\text{H10})$$

$$(S) \quad \frac{\partial p}{\partial t}(v, t) = -\frac{\partial}{\partial v} [f(v)p(v, t)] + \frac{\sigma^2}{2} \frac{\partial}{\partial v} \left\{ g(v) \frac{\partial}{\partial v} [g(v)p(v, t)] \right\}, \quad (\text{H11})$$

where (I) and (S) indicate whether equation H7 is interpreted as an Ito or a Stratonovich SDE. The steady-state (stationary) solution for the above partial differential equations with natural boundary conditions is given by (Sancho *et al.*, 1982; Horsthemke & Lefever, 1984)

$$p_s(v) = \frac{N}{g^\nu(v)} \exp \left[\frac{2}{\sigma^2} \int^v dw \frac{f(w)}{g^2(w)} \right] \quad (\text{H12})$$

where N is a normalization constant. The exponent $\nu = 1$ for the (S) form and $\nu = 2$ for the (I) form of the Fokker-Planck equation (Horsthemke & Lefever, 1984; van Kampen, 1992; Gardiner, 1996).

Passive Conductance Fluctuations

Using the results derived above, here we compute the magnitude of voltage noise due passive conductance fluctuations. Since ion channels have discrete conformational states, their conductances are quantized and, strictly speaking, conductance fluctuations should not be modeled as continuous stochastic processes. In fact the discrete random transitions of ion channels are best handled using *Master equations* (Frehland & Solleder, 1985; Frehland & Solleder, 1986; Solleder & Frehland, 1986; Fox & Lu, 1994; Fox, 1997). Master equations are almost impossible to solve in closed-form except in very simple cases (van Kampen, 1992). However, when the number of ion channels in question is large, it can be shown that the Master equations can be approximated by continuous Fokker-Planck equations which implies that the channel fluctuations can be approximated by continuous stochastic processes (van Kampen, 1992). We shall make this assumption here.

Consider the membrane voltage equation as before,

$$-C \frac{dV_m}{dt} = g_L (V_m E_L) + -g_a (V_m - E_a) - I_{inj} \quad (\text{H13})$$

where C is the capacitance of the patch, V_m is the membrane voltage, g_L and g_a are the leak and synaptic conductances and E_L and E_a are their respective reversal potentials. Note that both the conductance g_a and the membrane voltage V_m are stochastic quantities and

can be expressed as fluctuations around their deterministic steady-state values.

$$\tilde{g}_a = g_a - g_a^o, \quad \tilde{V} = V_m - V_m^o, \quad (\text{H14})$$

where g_a^o and V_m^o satisfy,

$$V_m^o = \frac{g_L E_L + g_a^o E_a + I_{\text{inj}}}{g_L + g_a^o}. \quad (\text{H15})$$

Rewriting equation H13 in terms of \tilde{g}_a and \tilde{V}

$$-C \frac{d\tilde{V}}{dt} = (g_L + g_a^o) \tilde{V} + \tilde{g}_a (\tilde{V} + V_m^o - E_a). \quad (\text{H16})$$

Let $G = g_L + g_a^o$ denote the total steady-state conductance and $\eta = \tilde{g}_a/G$ be the normalized conductance fluctuations. The above equation can be expressed as the following dimensionless equation

$$\frac{dv}{dT} = -v + (\epsilon - v) \eta(t), \quad (\text{H17})$$

where the dimensionless time is given by $T = t/\tau$. $\tau = C/G$ is the passive time constant of the membrane, $\epsilon = (E_a - V_m^o)/V_{\text{norm}}$ denotes the normalized reversal potential and $v = \tilde{V}/V_{\text{norm}}$ denotes the membrane voltage normalized with respect to some voltage V_{norm} . Equation H17 is a nonlinear stochastic differential equation since the magnitude of the stochastic term is the synaptic driving potential $(\epsilon - v)$, which is a function of the voltage v . Thus, the conductance fluctuations η represent a multiplicative source of noise. Notice that when the magnitude of the voltage fluctuations is small, $\epsilon - v \approx \epsilon$, and equation H17 reduces to a linear stochastic differential equation with additive noise which was used to obtain the results in Chapter 3. Since the fluctuations are assumed to be fast, we can assume that the correlation time scale of η_a is much smaller than τ . This means $\eta(t)$ can be approximated by a white noise process denoted by $\xi(t)$. Formally, we assume that $B_a \tau \gg 1$ where B_a is

the bandwidth of the conductance fluctuations \tilde{g}_a and replace equation H17 with

$$\frac{dv}{dT} = -v + \sigma(\epsilon - v)\xi(t) \quad (\text{H18})$$

where

$$\langle \xi(t)\xi(s) \rangle = \delta(t-s) \quad \text{and} \quad \sigma^2 = \frac{\sigma_a^2}{G^2} \frac{1}{2B_a}.$$

σ_a^2 is the variance of the conductance fluctuations \tilde{g}_a . Depending on whether the stochastic differential equation H18 is interpreted in the Ito sense or the Stratonovich sense, correspondingly, the probability density $v(t)$ satisfies the following Fokker-Planck equations (Risken, 1996),

$$(I) \quad \frac{\partial p(v, T)}{\partial T} = -\frac{\partial}{\partial v} [v p(v, T)] + \frac{\sigma^2}{2} \frac{\partial^2}{\partial v^2} [(\epsilon - v)^2 p(v, T)], \quad (\text{H19})$$

$$(S) \quad \frac{\partial p(v, T)}{\partial T} = -\frac{\partial}{\partial v} [v p(v, T)] + \frac{\sigma^2}{2} \frac{\partial}{\partial v} \left\{ (\epsilon - v) \frac{\partial}{\partial v} [(\epsilon - v) p(v, T)] \right\}. \quad (\text{H20})$$

For natural boundary conditions the steady-state solutions for equation H20 and equation H20 are given by (Sancho *et al.*, 1982; Horsthemke & Lefever, 1984)

$$p_s(v) = \frac{N}{(\epsilon - v)^\nu} \exp \left[\frac{2}{\sigma^2} \int^v dw \frac{-w}{(\epsilon - w)^2} \right] \quad (\text{H21})$$

where N is a normalization constant. The exponent $\nu = 1$ for the Stratonovich interpretation and $\nu = 2$ for the Ito interpretation (Horsthemke & Lefever, 1984; van Kampen, 1992; Gardiner, 1996). Equation H21 can be solved to obtain

$$p_s(v) = \frac{N}{(\epsilon - v)^{D+\nu}} \exp \left[-D \frac{\epsilon}{(\epsilon - v)} \right], \quad -\infty \leq v \leq \epsilon, \quad (\text{H22})$$

where $D = 2/\sigma^2$. The mean value of v is given by

$$\langle v \rangle_s = \int_{-\infty}^{\epsilon} dw w p_s(w) = \epsilon \left[1 - D \frac{\Gamma(D + \nu - 2)}{\Gamma(D + \nu - 1)} \right]$$

where

$$\Gamma(x) = \int_0^{\infty} dt t^{x-1} \exp(-t)$$

is the Gamma function which satisfies the recursive relation $\Gamma(x+1) = x\Gamma(x)$. Using the recursive relation, we can simplify the expression for the mean voltage as

$$\langle v \rangle_s = \epsilon \left(\frac{\nu - 2}{D + \nu - 2} \right). \quad (\text{H23})$$

Thus, $\langle v \rangle_s = 0$, in the Ito case whereas $\langle v \rangle_s = -\epsilon/(D-1)$ in the Stratonovich case. This discrepancy arises due to the fact, whereas in the Ito version $v(t)$ is a non-anticipatory function and depends only on the values of $\xi(s)$, $s < t$ which implies that $\langle v(t)\xi(t) \rangle = 0$; this does not hold in the Stratonovich case.

Similarly, in the Ito case (expression for the Stratonovich case is a little more involved but simple to compute exactly), the variance of v can be computed as

$$\sigma_v^2 = \langle v^2 \rangle_s = \langle v \rangle_s^2 = \frac{\epsilon^2}{D-1}. \quad (\text{H24})$$

When $D \gg 1$, it can be shown that the above expression yields a magnitude for the membrane voltage noise which coincides with the results derived in Chapter 3 which agrees without intuitive understanding that when the conductance fluctuations are small (D is large), the additive noise approximation is valid and the membrane voltage fluctuations approximately obey Gaussian statistics. **Fig. 9.6** shows the steady-state voltage distributions for three different values of D .

Non-regenerative Conductance Fluctuations

Here we consider the influence of voltage-dependent non-regenerative conductance fluctuations. Once again let

$$-C \frac{dV_m}{dt} = g_L (V_m - E_L) + g_b (V_m - E_b) \quad (\text{H25})$$

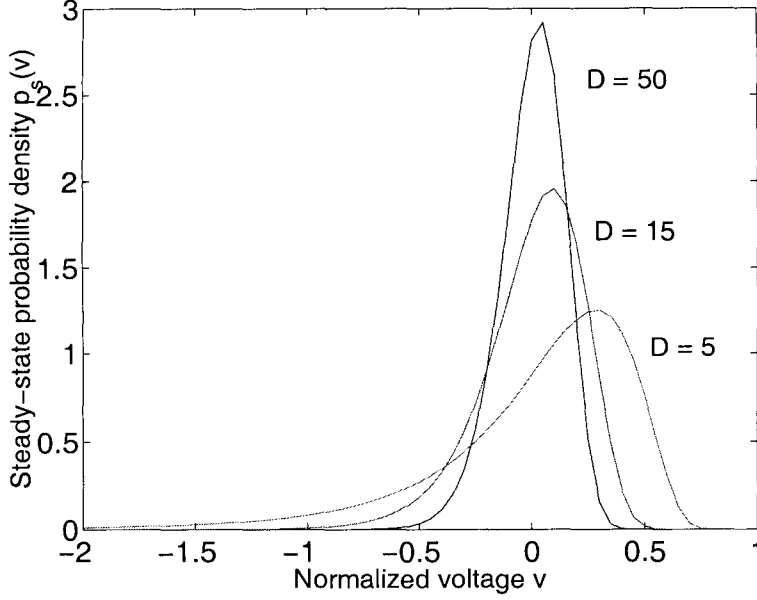


Figure 9.6: **Voltage Distribution for Passive Multiplicative Noise.**

Steady-state Ito distribution of voltage noise due to multiplicative, voltage-independent conductance fluctuations for three different noise magnitudes. Membrane noise is expressed in normalized units. As $D \rightarrow \infty$, $p_s(v)$ converges to a Gaussian. The normalized reversal potential of the conductance $\epsilon = 1$. The mean steady-state voltage for all the three curves is at the resting potential $v = 0$.

where g_b denotes a conductance of the non-regenerative type. For the sake of simplicity, we assume that the kinetics of the conductance $g_b = \bar{g}_b n$ can be expressed in terms of a single binary sub-unit n ($N = 1$ in Appendix G). \bar{g}_b is the maximal conductance of the sub-unit in the open state. n obeys first order dynamics

$$\frac{dn}{dt} = \frac{n_\infty(V_m) - n}{\tau_n(V_m)} + \sigma \xi(t). \quad (\text{H26})$$

where $n_\infty(V_m)$ and $\tau_n(V_m)$ are the voltage-dependent steady-state value and the time constant of n respectively. $\xi(t)$ is the Langevin term with magnitude σ . We assume that the dynamics of the conductance fluctuations are much faster compared to the dynamics of the membrane voltage. Formally, $\tau_n \ll 1$, which implies that $n(t) \approx n_\infty + \tau_n \sigma \xi(t)$. Substituting for $n(t)$ in equation H25,

$$-C \frac{dV_m}{dt} = g_L (V_m - E_L) + \bar{g}_b (V_m - E_b) n_\infty(V_m) + \bar{g}_b (V_m - E_b) \sigma \tau_n \xi(t), \quad (\text{H27})$$

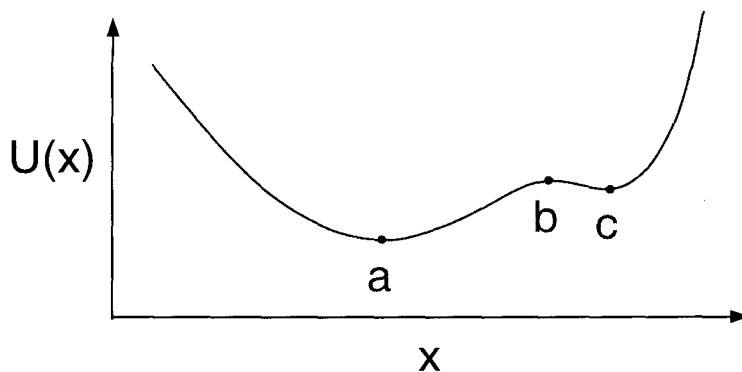


Figure 9.7: **Potential Surface for Regenerative Conductances.**

The potential surface $U(x)$ for regenerative conductances has multiple extrema since the $i - V$ curve has multiple zeros. Coordinates a and c are stable and metastable fixed points of $U(x)$, whereas b is an unstable fixed point. Conductance fluctuations may occasionally cause the membrane potential to jump from the vicinity of a to c crossing the barrier at b . In neuronal membranes, random sodium channel transitions represent a source of regenerative fluctuations and the barrier crossings can lead to the generation of spontaneous action potentials.

which can be expressed as

$$\frac{dV_m}{dt} = f(V_m) + g(V_m) \xi(t), \quad (\text{H28})$$

where

$$f(V_m) = -\frac{g_L(V_m - E_L) + \bar{g}_b(V_m - E_b)n_\infty(V_m)}{C}$$

$$g(V_m) = -\frac{\bar{g}_b(V_m - E_b)\sigma\tau_n}{C}.$$

The above equation is similar in form to equation H7 and substituting for the functions f and g , we can obtain the steady-state distribution and the corresponding mean and variance of the voltage noise. Because of the non-regenerative property, $f(V_m) = 0$ only at the resting potential V_{rest} .

Regenerative Conductance Fluctuations

The analysis of regenerative conductance fluctuations is complicated because of the multiplicity of the fixed points of $U(x)$ (see **Fig. 9.7**). In the two earlier cases the membrane

voltage fluctuations occurred in the vicinity of the resting potential. For regenerative noise, a unique steady-state voltage does not exist. Thus, while the membrane voltage hovers around one metastable location (say a), every once in a while the fluctuations can cause it to jump in the neighborhood of the other metastable location (c). The frequency of these jumps depends on the size of the barrier (at b) relative to the noise magnitude. The lower the size of the barrier, the more frequent the noise-induced barrier crossings. An instance of regenerative conductance fluctuations in neuronal membranes is the presence of sodium channel transitions. The corresponding barrier crossings can lead to the generation of spontaneous action potentials. Thus, the effect of regenerative conductance fluctuations is two-fold, subthreshold voltage fluctuations when the voltage is in the vicinity of the steady-state and occasional spontaneous spiking when the voltage makes a transition.

The derivation of the frequency of the spontaneous firing due to channel fluctuations had been carried out before (Chow & White, 1996). Instead of repeating the analysis here, we present the underlying principles behind the approach. A one-dimensional multiplicative stochastic differential equation type can be transformed into an additive equation by a change of variables such that the coefficient of the noise term becomes a constant. Subsequently, the expression for the mean escape rate for a particle to cross over a potential barrier due to thermal noise derived by Kramers (Kramers, 1940; van Kampen, 1992) can be used to derive the mean spontaneous firing rate. Kramers' analysis relies on the assumption that the system is *quasi-stationary* which requires that the magnitude of the noise (temperature) be small compared to the height of the barrier. For our case, the reciprocal of number of sodium channels plays the role of noise. Thus, the analysis is valid when the number of sodium channels is large. The analysis of subthreshold voltage noise can be carried out as in the case of the passive and non-regenerative conductances.

I Analysis of Nonlinear Poisson Encoding Schemes

We assume that statistics of spike train $s(t) = \sum_i \delta(t - t_i)$ are Poisson and the relationship between the stimulus $m(t)$ and instantaneous firing rate $\lambda(t)$ is nonlinear,

$$\lambda(t) = \langle s(t) \rangle_{s|m} = f[(k \star m)(t)]. \quad (\text{I1})$$

The accuracy of optimal linear decoding the stimulus using the spike train depends on the specific nature of the nonlinearity involved. A neuron which encodes specific features of its time-varying input rather than mirroring the input modulations in its firing rate will yield poor estimation results. Instances of such nonlinear feature extractions can be found in (Rieke *et al.*, 1995; Gabbiani *et al.*, 1996). In contrast, other nonlinearities like firing rate saturation and half-wave rectification do not significantly alter stimulus estimation performance (Wessel *et al.*, 1996). In fact, certain types of nonlinearities can even improve the encoding of time-varying stimuli in single spike trains under adequate conditions (Gabbiani & Koch, 1998). In the following, we carry out the analysis of optimal linearly decoding for a few nonlinear encoding nonlinearities.

For the Poisson process, it can be shown that the cross-correlation between the stimulus and the spike train and the autocorrelation of the spike train are given by

$$R_{ms}(z) = R_{m\lambda}(z), \quad R_{ss}(z) = R_{\lambda\lambda}(z) + \bar{\lambda} \delta(z)$$

where $\bar{\lambda} = \langle s(t) \rangle_{s,m}$ is the mean firing rate of the neuron. Here the refractory period is assumed to be zero, but see (Franklin & Bair, 1995). Since the optimal linear filter $g(t)$ depends only on the cross-correlation $R_{ms}(\tau)$ and the autocorrelation $R_{ss}(\tau)$, any random process $y(t)$ which has the same cross-correlation, $R_{my}(z) = R_{ms}(z)$, with the stimulus and the same autocorrelation function, $R_{yy}(z) = R_{ss}(z)$ as the spike train, $s(t)$, will lead to exactly the same estimation problem. This is true even if the statistics of $y(t)$ differ from that of the spike train $s(t)$. Thus, for the case of the Poisson spike train model, if instead

of the point process $s(t)$ the following continuous process is observed,

$$y(t) = f[(k \star m)(t)] + \bar{\lambda}^{1/2} w(t), \quad (\text{I2})$$

where $w(t)$ is Gaussian white noise with unit variance and $R_{ww}(z) = \delta(z)$, estimation of the stimulus $m(t)$ from the spike train is equivalent to estimation using the signal $\lambda(t) = f[(k \star m)(t)]$ corrupted by Gaussian white noise $w(t)$.

Using results from nonlinear system identification, we can derive closed-form expressions for the estimation performance for a variety of encoding nonlinearities. It is known that the cross-correlation between a Gaussian stimulus $m(t)$ and its output across a static nonlinearity (*e.g.*, $\lambda(t) = f[(k \star m)(t)]$) is given by

$$R_{m\lambda}(z) = \alpha (k \star R_{mm})(z), \quad \alpha = \frac{\langle x(f(x) - \bar{\lambda}) \rangle}{\sigma_x^2}, \quad (\text{I3})$$

where σ_x^2 is the variance of $x(t) = (k \star m)(t)$ and $R_{mm}(z)$ is the autocorrelation of the stimulus. This result is known as *Bussgang's theorem* (Bendat, 1990). Using the expressions derived in Appendix A, the coding fraction and the lower bound on the information rate are given by

$$\xi = \frac{\alpha^2}{\sigma_m^2} \int_{-\infty}^{\infty} df \frac{|K(f)|^2 S_{mm}^2(f)}{S_{\lambda\lambda}(f) + \bar{\lambda}}, \quad (\text{I4})$$

$$I_{\text{LB}} = \frac{1}{2} \int_{-\infty}^{\infty} df \log_2 \left[\frac{S_{mm}(f)}{S_{\hat{n}\hat{n}}(f)} \right] \quad (\text{bit sec}^{-1}) \quad (\text{I5})$$

where $K(f)$, $S_{mm}(f)$ and $S_{\lambda\lambda}(f)$ are the Fourier transforms of $k(t)$, $R_{mm}(t)$ and $R_{\lambda\lambda}(z)$ respectively and $S_{\hat{n}\hat{n}}(f)$ is the power spectral density of the reconstruction noise

$$S_{\hat{n}\hat{n}}(f) = S_{mm}(f) - \frac{\alpha^2 |K(f)|^2 S_{mm}^2(f)}{S_{\lambda\lambda}(f) + \bar{\lambda}}. \quad (\text{I6})$$

The above expressions require a knowledge of the input and noise spectra. In the absence of detailed spectral information about the processes and their cross-spectrum except their variances and the scalar cross-correlation value, the estimation problem reduces to the scalar

estimation problem

$$y = f(x) + \bar{\lambda}^{1/2} w$$

where x , y and w are scalar random variables. To distinguish between the two estimation problems, we denote the coding fraction and mutual information for the scalar estimation problem by ξ^s and I_{LB}^s which are given by

$$\xi^s = \frac{\alpha^2}{\sigma_m^2} \frac{\left[\int_{-\infty}^{\infty} df K(f) S_{mm}(f) \right]^2}{\int_{-\infty}^{\infty} df S_{\lambda\lambda}(f) + \bar{\lambda}}, \quad (I7)$$

$$I_{\text{LB}}^s = \frac{1}{2} \log_2 \left[\frac{\int_{-\infty}^{\infty} df S_{mm}(f)}{\int_{-\infty}^{\infty} df S_{\hat{n}\hat{n}}(f)} \right] \quad (\text{bit sample}^{-1}). \quad (I8)$$

Using Jensen's inequality (Cover & Thomas, 1991), one can show that $\xi \geq \xi^s$ and $I_{\text{LB}} \geq I_{\text{LB}}^s$. The equality holds if and only if the spectra $K(f)$, $S_{mm}(f)$ and $S_{\lambda\lambda}(f)$ are flat over the bandwidth of interest. The inequality can be intuitively understood as follows. In the absence of information about the cross-correlation between $m(t)$ and $\lambda(t)$ (except the scalar correlation $R_{m\lambda}(0)$) and the autocorrelation of $m(t)$ and $\lambda(t)$ (except $\sigma_m^2 = R_{mm}(0)$ and $\sigma_\lambda^2 = R_{\lambda\lambda}(0)$), the best that can be done is to estimate $m(t)$ from the instantaneous value of $y(t)$. Given the lack of statistical information about the signal and noise, it is reasonable to expect that $\xi \geq \xi^s$. When the processes are white, the temporal course of correlations provides no information in addition to the corresponding instantaneous correlations and the expressions in the two cases converge. Thus, ξ^s can be regarded as a simple lower bound on estimation performance. Below, we compare estimation performance for some nonlinear encoding schemes with the linear encoding model studied in Chapter 2. The results are graphed in **Fig. 9.8**.

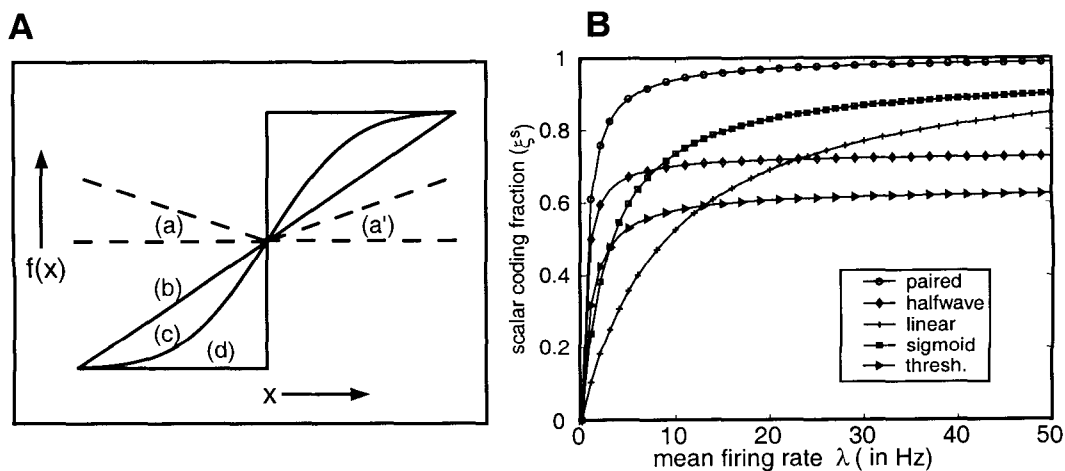


Figure 9.8: **Optimal Linear Estimation Performance for Nonlinear Encoding Schemes.** **A:** Examples of some nonlinearities which transform the input of a Poisson spiking neuron into its firing rate. The dotted lines represent a half-wave rectifying nonlinearity (a) and its complementary counterpart (a'). The straight line (b) corresponds to linear encoding, (c) corresponds to a saturating-type sigmoidal nonlinearity and (d) denotes a threshold function. **B:** Scalar coding fractions as a function of the mean firing rate of the neuron $\bar{\lambda}$ for the nonlinearities shown in A. Sigmoidal performance corresponds to $\rho = 0.5$.

Linear encoding

When the input-output transformation is linear, $\lambda(t) = f(x(t)) = \bar{\lambda} + x(t)$, the power spectral density and variance of the firing rate are given by

$$S_{\lambda\lambda}(f) = S_{xx}(f) = |K(f)|^2 S_{mm}(f),$$

$$\sigma_\lambda^2 = \sigma_x^2 = \int_{-\infty}^{\infty} df |K(f)|^2 S_{mm}(f).$$

Substituting for $f(x)$ in equation I3, $\alpha = 1$. We define the *contrast* of the firing rate as $c_\lambda = \sigma_\lambda/\bar{\lambda}$. For the firing rate to be positive $\lambda(t) \geq 0$, we need to restrict how large c_λ can be. Since the input $m(t)$ (thus $x(t)$) is Gaussian, there will be a finite probability that $\lambda(t) < 0$ which can be reduced by increasing the magnitude of the mean firing rate $\bar{\lambda}$ relative to the standard deviation of the firing rate fluctuations σ_λ . For linear encoding, we will require that $\bar{\lambda}$ be at least three times as large as σ_λ which ensures that the probability that $\lambda(t)$ is negative is negligible (less than 0.01). This implies that $c_\lambda \leq 1/3$. The coding fraction and the scalar coding fraction can be computed using equation I4 and equation I7

respectively.

$$\xi = \frac{1}{\sigma_m^2} \int_{-\infty}^{\infty} df \frac{|K(f)|^2 S_{mm}^2(f)}{|K(f)|^2 S_{mm}(f) + \bar{\lambda}}, \quad \xi^s = \frac{r^2 \sigma_x^2}{\sigma_m^2} \frac{\sigma_x^2}{\sigma_\lambda^2 + \bar{\lambda}}$$

where $r = (k \star R_{mm})(0)/\sigma_x^2$. In terms of the contrast and the mean firing rate, ξ^s can be expressed as

$$\xi^s = \frac{r^2 \sigma_x^2}{\sigma_m^2} \frac{\bar{\lambda}}{\bar{\lambda} + 1/c_\lambda^2}. \quad (\text{I9})$$

The minimum value and maximum values of ξ^s and ξ are zero (when $\bar{\lambda} \rightarrow 0$) and one (when $\bar{\lambda} \rightarrow \infty$) respectively. The coding fractions are monotonically decreasing functions of the mean firing rate which indicates that the estimation is *shot noise limited* which means that estimation noise arises because of an inability to estimate the firing rate perfectly, and the better the estimation of the firing rate the better is the performance at the estimation task.

Threshold encoding

The function $f(x)$ is a threshold *hard limiter* of the form

$$f(x) = \frac{\lambda_{\max}}{2} [1 + \text{sgn}(x)] \quad (\text{I10})$$

where $\text{sgn}(x)$ denotes the sign function. Thus, the firing rate is either 0 when $x(t) < 0$ or λ_{\max} when $x(t) > 0$. Although, biologically implausible, this scenario is a special case of the sigmoidal encoding discussed subsequently. Since x is a zero-mean Gaussian random variable with variance σ_x^2 , its probability density is given by

$$p(x) = \frac{1}{\sqrt{2\pi \sigma_x^2}} \exp\left(\frac{-x^2}{2\sigma_x^2}\right).$$

Thus,

$$\begin{aligned}\bar{\lambda} &= \langle f(x) \rangle = \frac{\lambda_{\max}}{2} \\ \langle x(f(x) - \bar{\lambda}) \rangle &= \frac{\lambda_{\max}}{2} \int_{-\infty}^{\infty} dx |x| p(x) = \frac{\lambda_{\max} \sigma_x}{\sqrt{2\pi}}, \\ \sigma_{\lambda}^2 &= \frac{\lambda_{\max}^2}{4} \int_{-\infty}^0 dx p(x) + \frac{\lambda_{\max}^2}{4} \int_0^{\infty} dx p(x) = \frac{\lambda_{\max}^2}{4}.\end{aligned}$$

Using Bussgang's theorem, the cross-correlation between $m(t)$ and $\lambda(t)$ can be computed

$$R_{m\lambda}(z) = \frac{\lambda_{\max}}{\sqrt{2\pi} \sigma_x} (k \star R_{mm})(z).$$

The auto-correlation of $\lambda(t)$ can be computed using *Price's theorem* (Bendat, 1990),

$$R_{\lambda\lambda}(z) = \frac{\lambda_{\max}^2}{2\pi} \sin^{-1} \left[\frac{R_{xx}(z)}{\sigma_x^2} \right].$$

The scalar coding fraction for the hard-limiter (denoted by ξ_{hl}^s) can be derived by substituting for the above quantities in equation I7,

$$\xi_{\text{hl}}^s = \frac{r^2 \sigma_x^2}{\sigma_m^2} \frac{2\bar{\lambda}}{\pi(\bar{\lambda} + 1)}. \quad (\text{I11})$$

For a given value of σ_x , the maximum value of $\xi_{\text{hl}}^s = 2r^2 \sigma_x^2 / \pi \sigma_m^2 \approx 0.64 r^2 \sigma_x^2 / \sigma_m^2$ occurs when $\bar{\lambda} \rightarrow \infty$.

Thus, using the output of a hard-limiting nonlinearity, a scalar optimal linear estimator can estimate the input within an error equal to 36% of the input variance. Since the hard-limiter is effectively a 1-bit quantizer (A-D converter), it is understandable that perfect estimation cannot occur even in the absence of noise (infinite firing rate). When only 1 bit of information about a Gaussian random variable is available, the minimum possible MSE that can be achieved by arbitrarily complicated encoding and decoding schemes can be computed using rate-distortion theory and is equal to 25% of the input variance which corresponds to an effectively coding fraction of 0.75 (Cover & Thomas, 1991). Thus, in the absence of noise, the simple encoding-decoding scheme of quantizing inputs into binary

values followed by optimal scalar estimation achieves a level of performance reasonably close to ideal. The performance can be further improved if the complete spectral information about the processes is used.

Sigmoidal encoding

The function $f(x)$ is a sigmoidal *smooth limiter* is of the form

$$f(x) = \frac{\lambda_{\max}}{2} \left[1 + \operatorname{Erf} \left(\frac{x}{\sqrt{2}\sigma_f} \right) \right]. \quad (\text{I12})$$

A simple calculation gives

$$\begin{aligned} \bar{\lambda} &= \frac{\lambda_{\max}}{2}, \\ \langle x(f(x) - \bar{\lambda}) \rangle &= \lambda_{\max} \int_0^{\infty} dx x \operatorname{Erf} \left(\frac{x}{\sqrt{2}\sigma_f} \right) = \frac{\lambda_{\max}}{\sqrt{2\pi}} \frac{\sigma_x^2}{\sqrt{\sigma_x^2 + \sigma_f^2}}, \\ \sigma_{\lambda}^2 &= \frac{\lambda_{\max}^2}{2} \int_0^{\infty} dx \left[\operatorname{Erf} \left(\frac{x}{\sqrt{2}\sigma_f} \right) \right]^2 = \frac{\lambda_{\max}^2}{2\pi} \sin^{-1} \left[\frac{\sigma_x^2}{\sigma_x^2 + \sigma_f^2} \right]. \end{aligned}$$

Similarly,

$$\begin{aligned} R_{m\lambda}(z) &= \frac{\lambda_{\max}}{\sqrt{2\pi}} \frac{(k \star R_{mm})(z)}{\sqrt{\sigma_x^2 + \sigma_f^2}}, \\ R_{\lambda\lambda}(z) &= \frac{\lambda_{\max}^2}{2\pi} \sin^{-1} \left[\frac{R_{xx}(z)}{\sigma_x^2 + \sigma_f^2} \right]. \end{aligned}$$

The scalar coding fraction for the smooth limiter (denoted by ξ_{sl}^s) is given by

$$\xi_{\text{sl}}^s = \frac{r^2 \sigma_x^2}{\sigma_m^2} \frac{\rho}{\sin^{-1} \rho} \frac{\bar{\lambda}}{\bar{\lambda} + \pi/(2 \sin^{-1} \rho)}, \quad (\text{I13})$$

where $\rho = 1/[1 + (\sigma_f/\sigma_x)^2]$, $0 \leq \rho \leq 1$. ρ determines the dynamic range of the sigmoidal nonlinearity, for $\rho = 1$, we recover the expressions for the hard limiter. For an arbitrary value of ρ , the maximum value of ξ_{sl}^s occurs when $\bar{\lambda} \rightarrow \infty$. On the other hand, we can also maximize ξ_{sl}^s with respect to ρ for a given value of $\bar{\lambda}$. The optimal value of scalar coding

fraction with respect to ρ is denoted by ξ_{sl}^{s*} and is given by

$$\xi_{\text{sl}}^{s*} = \cos \theta, \quad (\text{I14})$$

where θ satisfies the transcendental equation,

$$\tan \theta = \theta + \frac{\pi}{2\bar{\lambda}}.$$

Half-wave rectification

The function $f(x)$ is of the form

$$f(x) = \begin{cases} x, & x \geq 0, \\ 0, & x < 0. \end{cases} \quad (\text{I15})$$

For which the corresponding expressions are

$$\begin{aligned} \bar{\lambda} &= \frac{\sigma_x}{\sqrt{2\pi}}, \\ \langle x(f(x) - \bar{\lambda}) \rangle &= \int_0^{\infty} dx x^2 p(x) = \frac{\sigma_x^2}{2}, \\ \sigma_{\lambda}^2 &= \int_0^{\infty} dx x^2 p(x) - \bar{\lambda}^2 = \frac{\sigma_x^2(\pi - 1)}{2\pi}. \end{aligned}$$

Similarly,

$$\begin{aligned} R_{m\lambda}(z) &= \frac{(k \star R_{\text{mm}})(z)}{2}, \\ R_{\lambda\lambda}(z) &= \frac{\sigma_x^2}{4} \left[\frac{R_{\text{xx}}(z)}{\sigma_x^2} + \frac{2}{\pi} \left(\frac{R_{\text{xx}}(z)}{\sigma_x^2} \sin^{-1} \left(\frac{R_{\text{xx}}(z)}{\sigma_x^2} \right) + \frac{\sqrt{\sigma_x^2 - R_{\text{xx}}^2(z)}}{\sigma_x} - 1 \right) \right]. \end{aligned}$$

Thus, the scalar coding fraction for the half-wave rectifier denoted by ξ_{hw}^s is given by

$$\xi_{\text{hw}}^s = \frac{r^2 \sigma_x^2}{\sigma_m^2} \frac{\pi}{2(\pi - 1)} \frac{\bar{\lambda}}{\bar{\lambda} + 1/(\pi - 1)}. \quad (\text{I16})$$

The maximal value of ξ_{hw}^s is $\pi/2(\pi - 1) \approx 0.74 r^2 \sigma_x^2/\sigma_m^2$.

Paired rectification

Consider the problem of encoding by a pair of complementary half-wave rectifying neurons studied by Gabbiani (Gabbiani, 1996; Gabbiani & Koch, 1996). One neuron encodes positive stimulus modulations while the other encodes negative stimulus modulations in its firing rate. It can be shown that while the encoding at the level of the individual neurons is non-linear (half-wave rectification), an optimal decoding of the stimulus combining spike trains from both neurons leads to a linear estimation problem which performs better than the linear encoding example considered before. Since the detailed derivation of this result has been carried out quite lucidly in (Gabbiani, 1996; Gabbiani & Koch, 1996), we will not repeat it here, and make use of an intuitive and simple argument instead.

Let $\lambda_+(t)$ and $\lambda_-(t)$ denote the firing rates of the neurons encoding the positive and negative stimulus modulations $x(t) = (k \star m)(t)$ respectively,

$$\lambda_+(t) = f_+(x(t)) = \begin{cases} x(t), & x \geq 0, \\ 0, & x < 0. \end{cases} \quad \lambda_-(t) = f_-(x(t)) = \begin{cases} -x(t), & x \leq 0, \\ 0, & x > 0. \end{cases} \quad (\text{I17})$$

Let $s_+(t)$ and $s_-(t)$ denote the spike trains corresponding to the firing rates $\lambda_+(t)$ and $\lambda_-(t)$ respectively. The estimation problem is to reconstruct the input by a linear combination of the two spike trains where the optimal filters involved in the combination operate individually on the respective spike trains. The corresponding continuous versions of the estimation problem are

$$y_+(t) = \lambda_+(t) + \bar{\lambda}_+^{-1/2} w_+(t); \quad y_-(t) = \lambda_-(t) + \bar{\lambda}_-^{-1/2} w_-(t).$$

By symmetry, $\bar{\lambda}_+ = \bar{\lambda}_- = \sigma_x / \sqrt{2\pi}$. Since we have two neurons here, in order to compare with earlier encoding schemes, we define $\bar{\lambda}_+ = \bar{\lambda}/2$ where $\bar{\lambda}$ represents the mean firing rate of the two neurons taken together. The random processes $w_+(t)$ and $w_-(t)$ are statistically independent as spike generation in the two neurons are assumed to take place independently. Furthermore, by symmetry (although this can be proved rigorously by the application of the orthogonality principle as in Gabbiani (1996), it is obvious that the estimate $\hat{m}(t)$ should

have the form

$$\hat{m}(t) = (g \star [y_+(t) - y_-(t)])(t). \quad (\text{I18})$$

Since $y_+(t) - y_-(t)$ is identical to $x(t)$, we recover a variant of the linear encoding problem, the difference being that here $\bar{\lambda} = \sqrt{2/\pi} \sigma_x$ depends on the standard deviation of the filtered input $x(t)$. It can be shown that the coding fraction and the scalar coding fraction denoted by ξ_{pr}^s are given by

$$\xi = \frac{1}{\sigma_m^2} \int_{-\infty}^{\infty} df \frac{|K(f)|^2 S_{\text{mm}}^2(f)}{|K(f)|^2 S_{\text{mm}}(f) + \bar{\lambda}}, \quad \xi_{\text{pr}}^s = \frac{r^2 \sigma_x^2}{\sigma_m^2} \frac{\sigma_x^2}{\sigma_x^2 + \bar{\lambda}}.$$

Substituting for σ_x in terms of $\bar{\lambda}$, we get

$$\xi_{\text{pr}}^s = \frac{r^2 \sigma_x^2}{\sigma_m^2} \frac{\bar{\lambda}}{\bar{\lambda} + 2/\pi}. \quad (\text{I19})$$

Notice that the scalar coding fractions have the generic form

$$\xi^s = \xi_{\text{max}} \frac{\bar{\lambda}}{\bar{\lambda} + 1/c_\lambda^2}, \quad (\text{I20})$$

where ξ_{max} is the maximum value of the scalar coding fraction in the absence of noise (limit of infinite firing rates) and $c_\lambda = \sigma_1/\bar{\lambda}$ is the contrast of the firing rate which determines the rate of increase of ξ^s with λ . The higher the value of c_λ , the better the estimation performance. This argument holds for the coding fraction (derived using spectral information) as well though, in general, ξ can be significantly greater than ξ^s . The contrast for the paired rectification is $\sqrt{\pi/2} \approx 1.25$ which is much larger than the value (1/3) linear encoding was restricted to. This leads to a substantial increase in the estimation performance and explains the somewhat low information rates observed for synaptic transmission in Chapter 2.

References

- Abbott, L. F., Varela, J. A., Sen, K., & Nelson, S. B. 1997. Synaptic depression and cortical gain-control. *Science*, **275**, 220–224.
- Abeles, M. 1982. *Local Cortical Circuits: An Electrophysiological Study*. Springer-Verlag.
- Abeles, M. 1990. *Corticonics: Neural Circuits of the Cerebral Cortex*. Cambridge University Press: Cambridge, United Kingdom.
- Ackley, D. H., Hinton, G. E., & Sejnowski, T. J. 1985. A learning algorithm for Boltzman machines. *Cog. Sci.*, **9**, 147–169.
- Adrian, E. D. 1932. *The Mechanism of Nervous Action: Electrical Studies of the Neurone*. University of Pennsylvania Press: Philadelphia, Pennsylvania.
- Allen, C., & Stevens, C. F. 1994. An evaluation of causes for unreliability of synaptic transmission. *Proc. Natl. Acad. Sci. USA*, **91**, 10380–10383.
- Allman, J. 1990. Evolution of Neocortex. *In*: Jones, E. G., & Peters, A. (eds), *Cereb. Cortex*, vol. 8A, pp. 269–283. Plenum Press: New York, New York.
- Andreou, A. G., & Furth, P. M. 1998. An Information-theoretic framework for comparing the bit-energy of signal representation at the circuit level. *In*: Sinencio, E. S., & Andreou, A. G. (eds), *Low Voltage, Low Power Integrated Circuits and Systems*. IEEE Press.
- Azouz, R., & Gray, C. M. 1999. Cellular mechanisms contributing to response variability of cortical neurons *in vivo*. *J. Neurosci.*, **19**, 2209–2223.
- Bair, W., & Koch, C. 1996. Temporal precision of spike trains in extrastriate cortex of the behaving macaque monkey. *Neural Comput.*, **8**, 1185–1202.

- Barlow, H. B. 1972. Single units and sensation: a neuron doctrine for perceptual psychology? *Perception*, **1**, 371–394.
- Barlow, H. B., Kaushal, T. P., Hawken, M., & Parker, A. J. 1987. Human contrast discrimination and the threshold of cortical neurons. *J. Opt. Soc. Am. A*, **4**, 2366–2371.
- Bekkers, J. M., Richerson, G. B., & Stevens, C. F. 1990. Origin of variability in quantal size in cultured hippocampal neurons and hippocampal slices. *Proc. Natl. Acad. Sci. USA*, **87**(14), 5359–5362.
- Bekkers, J. M., & Stevens, C. F. 1994. The nature of quantal transmission at central excitatory synapses. *Adv. Second Messenger Phosphoprotein Res.*, **29**, 261–273.
- Bekkers, J. M., & Stevens, C. F. 1995. Quantal analysis of EPSCs recorded from small numbers of synapses in hippocampal cultures. *J. Neurophysiol.*, **73**, 1145–1156.
- Bekkers, J. M., & Stevens, C. F. 1996. Cable properties of cultured hippocampal neurons determined from sucrose-evoked miniature EPSCs. *J. Neurophysiol.*, **75**, 1250–1255.
- Bell, A. J., Mainen, Z. F., Tsodyks, M., & Sejnowski, T. J. 1996. What are the causes of cortical variability. *Preprint*.
- Bendat, J. D. 1990. *Nonlinear System Analysis and Identification from Random Data*. John Wiley: New York, New York.
- Bernander, O., Douglas, R., Martin, K.A.C., & Koch, C. 1991. Synaptic background activity influences spatiotemporal integration in single pyramidal cells. *Proc. Natl. Acad. Sci. USA*, **88**, 11569–11573.
- Bernander, O., Koch, C., & Douglas, R. J. 1994. Amplification and linearization of distal synaptic input to cortical pyramidal cells. *J. Neurophysiol.*, **72**, 2743–2753.
- Berzakov, S. M., & Vodyanoy, I. 1995. Noise-induced enhancement of signal transduction across voltage-dependent ion channels. *Nature*, **378**, 362–364.
- Bialek, W. 1987. Physical limits to sensation and perception. *Ann. Rev. Biophys. Biophys. Chem.*, **16**, 455–478.

- Bialek, W., & Rieke, F. 1992. Reliability and information-transmission in spiking neurons. *Trends Neurosci.*, **15**, 428–434.
- Bialek, W., Rieke, F., van Steveninck, R. R. D., & Warland, D. 1991. Reading a neural code. *Science*, **252**, 1854–1857.
- Britten, K. H., Shadlen, M. N., Newsome, W. T., & Movshon, A. 1992. The analysis of visual motion: a comparison of neuronal and psychophysical performance. *J. Neurosci.*, **12**, 4745–4765.
- Burnod, Y., & Korn, H. 1989. Consequences of stochastic release of neurotransmitters for network computation in the central nervous system. *Proc. Natl. Acad. Sci. USA*, **86**, 352–356.
- Calvin, W. H., & Stevens, C. F. 1967. Synaptic noise as a source of variability in the interval between action potentials. *Science*, **155**, 842–844.
- Calvin, W. H., & Stevens, C. F. 1968. Synaptic noise and other sources of randomness in motoneuron interspike intervals. *J. Neurophysiol.*, **31**, 574–587.
- Chow, C., & White, J. 1996. Spontaneous action potentials due to channel fluctuations. *Biophys. J.*, **71**, 3013–3021.
- Clay, J. R., & DeFelice, L. J. 1983. Relationship between membrane excitability and single channel open- close kinetics. *Biophys. J.*, **42**, 151–157.
- Clay, J. R., & Shlesinger, M. F. 1977. Unified theory of 1/f and conductance noise in nerve membrane. *J. Theor. Biol.*, **66**, 763–773.
- Colbert, C. M., & Johnston, D. 1996. Axonal action-potential initiation and Na⁺ channel densities in the soma and axon initial segment of subicular pyramidal neurons. *J. Neurosci.*, **16**, 6676–6686.
- Colquhoun, D., & Hawkes, A. G. 1982. On the stochastic properties of bursts of single ion channel openings and of clusters of bursts. *Phil. Trans. Roy. Soc. Lond. B*, **300**, 1–59.

- Cook, E. P., & Johnston, D. 1997. Active dendrites reduce location-dependent variability of synaptic input trains. *J. Neurophysiol.*, **78**, 2116–2128.
- Courant, R., & Hilbert, D. 1989. *Methods of Mathematical Physics: Volume I*. Wiley: New York, New York.
- Cover, T. M., & Thomas, J. A. 1991. *Elements of Information Theory*. Wiley: New York, New York.
- DeFelice, L. J. 1977. Fluctuation analysis in neurobiology. *Int. Rev. Neurobiol.*, **20**, 169–208.
- DeFelice, L. J. 1981. *Introduction to Membrane Noise*. Plenum Press: New York, New York.
- DeFelice, L. J., & Isaac, A. 1992. Chaotic states in a random world. *J. Stat. Phys.*, **70**, 339–352.
- Destexhe, A., Mainen, Z. F., & Sejnowski, T. J. 1994. Synthesis of models for excitable membranes, synaptic transmission and neuromodulation using a common kinetic formalism. *J. Comput. Neurosci.*, **1**, 195–230.
- Destexhe, A., & Pare, D. 1999. Impact of network activity on the integrative properties of neocortical pyramidal neurons in vivo. *J. Neurophysiol.*, **81**, 1531–1547.
- Dobrunz, L. E., Huang, E. P., & Stevens, C. F. 1997. Very short-term plasticity in hippocampal synapses. *Proc. Natl. Acad. Sci. USA*, **94**, 14843–14847.
- Dobrunz, L. E., & Stevens, C. F. 1997. Heterogeneity of release probability, facilitation, and depletion at central synapses. *Neuron*, **18**, 995–1008.
- Dobrunz, L. E., & Stevens, C. F. 1999. Response of hippocampal synapses to natural stimulation patterns. *Neuron*, **22**, 157–166.
- Edwards, F. A., Konnerth, A., & Sakmann, B. 1990. Quantal analysis of inhibitory synaptic transmission in the dentate gyrus of rat hippocampal slices: a patch-clamp study. *J. Physiol.*, **430**, 213–249.

- Eskandar, E. N., Richmond, B. J., & Optican, L. M. 1992. Role of inferior temporal neurons in visual memory: I. Temporal encoding of information about visual images, recalled images and behavioral context. *J. Neurophysiol.*, **68**, 1277–1295.
- J. M. Fellous, R. P. N. Rao, A. R. Houweling, & Sejnowski, T. J. 1999. Spike timing reliability in the prefrontal cortex depends on the frequency content of its synaptic inputs. *In: Soc. Neurosci. Abstr.*
- Fishman, H. M. 1975. Noise measurements in axon membranes. *Fed. Proc.*, **34**, 1330–1337.
- Fishman, H. M., Poussart, D. M., & Moore, L. E. 1975. Noise measurements in squid axon membrane. *J. Membr. Biol.*, **24**, 281–304.
- Fox, R. F. 1997. Stochastic versions of the Hodgkin-Huxley equations. *Biophys. J.*, **72**, 2068–2074.
- Fox, R. F., & Lu, Y. 1994. Emergent collective behavior in large numbers of globally coupled independently stochastic ion channels. *Phys. Rev. E*, **49**, 3421–3431.
- Franklin, J., & Bair, W. 1995. The effect of a refractory period on the power spectrum of neuronal discharge. *SIAM J. Appl. Math.*, **55**, 1074–1093.
- Frehland, E. 1982. *Stochastic Transport Processes in Discrete Biological Systems*. Springer-Verlag: Berlin.
- Frehland, E., & Faulhaber, K. H. 1980. Nonequilibrium ion transport through pores. The influence of barrier structures on current fluctuations, transient phenomena and admittance. *Biophys. Struct. Mech.*, **7**, 1–16.
- Frehland, E., & Solleder, P. 1985. Nonequilibrium voltage noise generated by ion transport through pores. *Eur. Biophys. J.*, **11**, 167–178.
- Frehland, E., & Solleder, P. 1986. Nonequilibrium voltage fluctuations in biological membranes. I. General framework of charge transport in discrete systems and related voltage noise. *Biophys. Chem.*, **25**, 135–145.

- Gabbiani, F. 1996. Coding of time-varying signals in spike trains of linear and half-wave rectifying neurons. *Network: Comput. Neural Syst.*, **7**, 61–85.
- Gabbiani, F., & Koch, C. 1996. Coding of time-varying signals in spike trains of integrate-and-fire neurons with random threshold. *Neural Comput.*, **8**, 44–66.
- Gabbiani, F., & Koch, C. 1998. Principles of spike train analysis. In: Koch, C., & Segev, I. (eds), *Methods in Neuronal Modeling: From Ions to Networks*, second edn. MIT Press: Cambridge, Massachusetts.
- Gabbiani, F., Metzner, W., Wessel, R., & Koch, C. 1996. From stimulus encoding to feature extraction in weakly electric fish. *Nature*, **384**, 564–567.
- Gardiner, C. W. 1996. *Handbook of Stochastic Methods: For Physics, Chemistry and the Natural Sciences*. Second edn. Springer Verlag: Berlin, Germany.
- Gestri, G., Mastebroek, H. A. K., & Zaagman, W. H. 1980. Stochastic constancy, variability and adaptation of spike generation: Performance of a giant neuron in the visual system of the fly. *Biol. Cybern.*, **38**, 31–40.
- Golomb, D., & Amitai, Y. 1997. Propagating neuronal discharges in neocortical slices: computational and experimental study. *J. Neurophysiol.*, **78**, 1199–1211.
- Green, D. M., & Swets, J. A. 1966. *Signal Detection Theory and Psychophysics*. Wiley: New York, New York.
- Helstrom, C. 1968. *Statistical Theory of Signal Detection*. Pergamon Press: Oxford, England.
- Hessler, N. A., Shirke, A. M., & Malinow, R. 1993. The probability of transmitter release at a mammalian central synapse. *Nature*, **366**, 569–572.
- Hille, B. 1992. *Ionic Channels of Excitable Membranes*. Sinauer Associates: Sunderland, Massachusetts.
- Hines, M. L., & Carnevale, N. T. 1997. The NEURON simulation environment. *Neural Comput.*, **9**, 1179–1209.

- Hodgkin, A. L., & Huxley, A. F. 1952. A quantitative description of membrane current and its application to conduction and excitation in nerve. *J. Physiol. (Lond.)*, **117**, 500–544.
- Hoffman, D. A., & Johnston, D. 1998. Downregulation of transient K⁺ channels in dendrites of hippocampal CA1 pyramidal neurons by activation of PKA and PKC. *J. Neurosci.*, **18**, 3521–3528.
- Hoffman, D. A., Magee, J. C., Colbert, C. M., & Johnston, D. 1997. K⁺ channel regulation of signal propagation in dendrites of hippocampal pyramidal neurons. *Nature*, **387**, 869–875.
- Holden, A. V. 1976. *Models of the Stochastic Activity of Neurones*. Springer Verlag: New York, New York.
- Holt, G. R., Softky, W. R., Koch, C., & Douglas, R. J. 1996. Comparison of discharge variability in vitro and in vivo in cat visual cortex neurons. *J. Neurophysiol.*, **75**, 1806–1814.
- Hopfield, J. J. 1995. Pattern recognition computation using action potential timing for stimulus representation. *Nature*, **376**, 33–36.
- Hopfield, J. J. 1999. Odor space and olfactory processing: Collective algorithms and neural implementation. *Proc. Natl. Acad. Sci. USA*, **96**, 12506–12511.
- Horikawa, Y. 1991. Noise effects on spike propagation in the stochastic Hodgkin-Huxley models. *Biol. Cybern.*, **66**, 19–25.
- Horikawa, Y. 1993a. Noise effects on spike propagation during the refractory period in the FitzHugh-Nagumo model. *J. Theor. Biol.*, **162**, 41–59.
- Horikawa, Y. 1993b. Simulation study on effects of channel noise on differential conduction at an axon branch. *Biophys. J.*, **65**, 680–686.
- Horsthemke, W., & Lefever, R. 1984. *Noise-Induced Transitions: Theory and Applications in Physics, Chemistry and Biology*. Springer Verlag: Berlin.

- Huguenard, J. R., Hamill, O. P., & Prince, D. A. 1989. Sodium channels in dendrites of rat cortical pyramidal neurons. *Proc. Natl. Acad. Sci. USA*, **86**, 2473–2477.
- Jack, J. J. B., Noble, D., & Tsien, R. 1975. *Electric Current Flow in Excitable Cells*. Oxford University Press: Oxford, England.
- Johnson, J. B. 1928. Thermal agitation of electricity in conductors. *Phys. Rev.*, **32**, 97–109.
- Johnston, D., & Wu, S. M. 1995. *Foundations of Cellular Neurophysiology*. MIT Press: Cambridge, Massachusetts.
- Johnston, D., Magee, J. C., Colbert, C. M., & Cristie, B. R. 1996. Active properties of neuronal dendrites. *Ann. Rev. Neurosci.*, **19**, 165–186.
- Katz, B. 1969. *The Release of Neural Transmitter Substances*. Liverpool University Press: Liverpool, United Kingdom.
- Knight, B. 1971. Dynamics of encoding in a population of neurons. *J. Gen. Physiol.*, **59**, 734–766.
- Koch, C. 1984. Cable theory in neurons with active, linearized membranes. *Biol. Cybern.*, **50**, 15–33.
- Koch, C. 1997. Computation and the single neuron. *Nature*, **385**, 207–210.
- Koch, C. 1999. *Biophysics of Computation: Information Processing in Single Neurons*. Oxford University Press, New York, New York.
- König, P., Engel, A. K., & Singer, W. 1996. Integrator or coincidence detector: the role of the cortical neuron revisited. *Trends Neurosci.*, **19**, 130–137.
- Korn, H., & Faber, D. S. 1991. Quantal analysis and synaptic efficacy in the CNS. *Trends Neurosci.*, **14**, 439–445.
- Korn, H., & Faber, D. S. 1993. Transmitter release mechanism: Relevance for neuronal network functions. *Pages 5–17 of*: Poggio, T., & Glaser, D. A. (eds), *Exploring Brain Functions: Models in Neuroscience*. John Wiley: Chichester, England.

- Korn, H., Faber, D. S., & Triller, A. 1986. Probabilistic determination of synaptic strength. *J. Neurophysiol.*, **55**, 402–421.
- Kramers, H. A. 1940. Brownian motion in a field of force and the diffusion model of chemical reactions. *Physica*, **7**, 284.
- Larkman, A. U., Stratford, K., & Jack, J. 1991. Quantal analysis of excitatory synaptic action and depression in hippocampal slices. *Nature*, **350**, 344–347.
- Larsson, H.P., Kleene, S.J., & Lecar, H. 1997. Noise analysis of ion channels in non-space-clamped cables: Estimates of channel parameters in olfactory cilia. *Biophys. J.*, **72**, 1193–1203.
- Laurent, G., & Sivaramakrishnan, A. 1992. Single local interneurons in the locust make central synapses with different properties of transmitter release on distinct postsynaptic neurons. *J. Neurosci.*, **12**, 2370–2380.
- Lecar, H., & Nossal, R. 1971a. Theory of threshold fluctuations in nerves. I. Relationships between electrical noise and fluctuations in axon firing. *Biophys. J.*, **11**, 1048–1067.
- Lecar, H., & Nossal, R. 1971b. Theory of threshold fluctuations in nerves. II. Analysis of various sources of membrane noise. *Biophys. J.*, **11**, 1068–1084.
- Lestienne, R., & Strehler, B. L. 1987. Time structure and stimulus dependence of precisely replicating patterns present in monkey cortical neuronal spike trains. *Brain Res.*, **437**, 214–238.
- Lettvin, J. P., Maturana, H. R., McCulloch, W. S., & Pitts, W. H. 1959. What the frog's eye tells the frog's brain. *Proc. Inst. Rad. Eng.*, **47**, 1940–1951.
- Levin, J. E., & Miller, J. P. 1996. Broadband neural encoding in the cricket cercal sensory system enhanced by stochastic resonance. *Nature*, **380**, 165–168.
- Liebovitch, L. S., & Todorov, A. T. 1996. Using fractals and nonlinear dynamics to determine the physical properties of ion channel proteins. *Crit. Rev. Neurobiol.*, **10**, 169–87.

- Liebovitch, L. S., & Toth, T. I. 1990. Using fractals to understand the opening and closing of ion channels. *Ann. Biomed. Eng.*, **18**, 177–194.
- Liebovitch, L. S., & Toth, T. I. 1991. A model of ion channel kinetics using deterministic chaotic rather than stochastic processes. *J. Theor. Biol.*, **148**, 243–267.
- Lisman, J. E. 1997. Bursts as a unit of neural information: making unreliable synapses reliable. *Trends Neurosci.*, **20**, 38–43.
- MacKay, D., & McCulloch, W. S. 1952. The limiting information capacity of a neuronal link. *Bull. Math. Biophys.*, **14**, 127–135.
- Magee, J., Hoffman, D., Colbert, C., & Johnston, D. 1998. Electrical and calcium signaling in dendrites of hippocampal pyramidal neurons. *Ann. Rev. Physiol.*, **60**, 327–346.
- Mainen, Z. F., Joerges, J., Huguenard, J. R., & Sejnowski, T. J. 1995. A model of spike initiation in neocortical pyramidal neurons. *Neuron*, **15**, 1427–1439.
- Mainen, Z. F., Malinow, R., & Svoboda, K. 1999. Synaptic calcium transients in single spines indicate that NMDA receptors are not saturated. *Nature*, **399**, 151–155.
- Mainen, Z. F., & Sejnowski, T. J. 1995. Reliability of spike timing in neocortical neurons. *Science*, **268**, 1503–1506.
- Mainen, Z. F., & Sejnowski, T. J. 1998. Modeling active dendritic processes in pyramidal neurons. In: Koch, C., & Segev, I. (eds), *Methods in Neuronal Modeling*, second edn. pp. 171-210. MIT Press: Cambridge, Massachusetts.
- Major, G., Larkman, A. U., Jonas, P., Sakmann, B., & Jack, J. J. 1994. Detailed passive cable models of whole-cell recorded CA3 pyramidal neurons in rat hippocampal slices. *J. Neurosci.*, **14**, 4613–46 38.
- Manwani, A., & Koch, C. 1998. Synaptic transmission: An information-theoretic perspective. In: Jordan, M., Kearns, M. S., & Solla, S. A. (eds), *Advances in Neural Information Processing Systems 10*. pp 201-207. MIT Press: Cambridge, Massachusetts.

- Manwani, A., & Koch, C. 1999a. Detecting and estimating signals in noisy cable structures: I. Neuronal noise sources. *Neural Comput.*, **11**, 1797–1829.
- Manwani, A., & Koch, C. 1999b. Detecting and estimating signals in noisy cable structures: II. Information-theoretic analysis. *Neural Comput.*, **11**, 1831–1873.
- Manwani, A., & Koch, C. 1999c. Signal detection in noisy weakly-active dendrites. *In: Kearns, M. S., Solla, S. A., & Cohn, D. A. (eds), Advances in Neural Information Processing Systems 11*. MIT Press: Cambridge, Massachusetts.
- Manwani, A., & Koch, C. 2000. Detecting and estimating signals over noisy and unreliable synapses: Information-theoretic analysis. *Neural Comput.* In press.
- Manwani, A., Segev, I., Yarom, Y., & Koch, C. 1998. Neuronal noise sources in membrane patches and linear cables: An analytical and experimental study. *In: Soc. Neurosci. Abstr.* #719.4, pp. 1813.
- Manwani, A., Steinmetz, P. N., & Koch, C. 2000a. Channel noise in excitable neuronal membranes. *Pages 143–149 of: Solla, S.A., Leen, T.K., & Müller, K.-R. (eds), Advances in Neural Information Processing Systems 12*. MIT Press: Cambridge, Massachusetts.
- Manwani, A., Steinmetz, P. N., & Koch, C. 2000b. The impact of spike timing irregularity on the efficiency of neural encoding models. *Network: Comput. Neural Syst.* Submitted.
- Markram, H., & Tsodyks, M. 1996. Redistribution of synaptic efficacy between neocortical pyramidal neurons. *Nature*, **382**, 807–810.
- Mason, A., Nicoll, A., & Stratford, K. 1991. Synaptic transmission between individual pyramidal neurons of the rat visual cortex *in vitro*. *J. Neurosci.*, **11**, 72–84.
- Mauro, A., Conti, F., Dodge, F., & Schor, R. 1970. Subthreshold behavior and phenomenological impedance of the squid giant axon. *J. Gen. Physiol.*, **55**, 497–523.
- Mauro, A., Freeman, A. R., Cooley, J. W., & Cass, A. 1972. Propagated subthreshold oscillatory response and classical electrotonic response of squid giant axon. *Biophysik*, **8**, 118–132.

- Moore, E. F., & Shannon, E. E. 1956. Reliable circuits using less reliable relays. *J. Franklin Inst.*, **262**, 191–208.
- Murthy, V. N., Sejnowski, T. J., & Stevens, C. F. 1997. Heterogeneous release properties of visualized individual hippocampal synapses. *Neuron*, **18**, 599–612.
- Neher, E., & Stevens, C. F. 1977. Conductance fluctuations and ionic pores in membranes. *Ann. Rev. Biophys. Bioeng.*, **6**, 345–381.
- Neumcke, B. 1978. 1/f noise in membranes. *Biophys. Struct. Mech.*, **4**, 179–199.
- Newsome, W. T., Britten, K. H., & Movshon, J. A. 1989. Neuronal correlates of a perceptual decision. *Nature*, **341**, 52–54.
- Nowak, L. G., Sanches-Vives, M. V., & McCormick, D. A. 1997. Influence of low and high frequency inputs on spike timing in visual cortical neurons. *Cereb. Cortex*, **7**, 487–501.
- Papoulis, A. 1991. *Probability, Random Variables, and Stochastic Processes*. McGraw-Hill: New York, New York.
- Pare, D. E., Label, E., & Lang, E. J. 1997. Differential impact of miniature synaptic potentials on the soma and dendrites of pyramidal neurons in vivo. *J. Neurophysiol.*, **78**, 1735–1739.
- Pare, D. E., Shink, E., Gaudreau, H., Destexhe, A., & Lang, E. J. 1998. Impact of spontaneous synaptic activity on the resting properties of cat neocortical pyramidal neurons in vivo. *J. Neurophysiol.*, **79**, 1450–1460.
- Parker, A. J., & Newsome, W. T. 1998. Sense and the single neuron: Probing the physiology of perception. *Ann. Rev. Neurosci.*, **21**, 227–277.
- Perkel, D. H., & Bullock, T. H. 1968. Neural coding. *Neurosci. Res. Prog. Sum.*, **3**, 405–527.
- Poor, H. V. 1994. *An Introduction to Signal Detection and Estimation*. Springer Verlag: New York, New York.

- Press, W. H., Teukolsky, S. A., Vetterling, W. T., & Flannery, B. P. 1992. *Numerical Recipes in C: The Art of Scientific Computing*. 2nd edn. Cambridge University Press.
- Rall, W. 1959. Branching dendritic trees and motoneuron membrane resistivity. *Exp. Neurol.*, **1**, 491–527.
- Rall, W. 1960. Membrane potential transients and membrane time constant of motoneurons. *Exp. Neurol.*, **2**, 503–532.
- Rall, W. 1967. Distinguishing theoretical synaptic potentials computed for different somadendritic distributions of synaptic input. *J. Neurophysiol.*, **30**, 1138–1168.
- Rall, W. 1969a. Distributions of potential in cylindrical coordinates and time constants for a membrane cylinder. *Biophys. J.*, **9**, 1509–1541.
- Rall, W. 1969b. Time constants and electrotonic length of membrane cylinders and neurons. *Biophys. J.*, **9**, 1483–1508.
- Rall, W. 1989. Cable theory for dendritic neurons. In: Koch, C., & Segev, I. (eds), *Methods in Neuronal Modeling: From Synapses to Networks*. pp. 9-62. MIT Press: Cambridge, Massachusetts.
- Rapp, M., Yarom, Y., & Segev, I. 1992. The impact of parallel fiber background activity on the cable properties of cerebellar Purkinje cells. *Neural Comput.*, **4**, 518–533.
- Redman, S. 1990. Quantal analysis of synaptic potentials in neurons of the central nervous system. *Physiol. Rev.*, **70**, 165–198.
- Reich, D. S., Victor, J. D., Knight, B. W., Ozaki, T., & Kaplan, E. 1997. Response variability and timing precision of neuronal spike trains in vivo. *J. Neurophysiol.*, **77**, 2836–2841.
- Richmond, B. J., & Optican, L. M. 1992. The structure and interpretation of neuronal codes in the visual system. *Pages 104–119 of: Wechsler, H. (ed), Neural Networks for Perception*. Academic Press.

- Rieke, F., Warland, D., & Bialek, W. 1993. Coding efficiency and information rates in sensory neurons. *Europhysics Lett.*, **22**, 151–156.
- Rieke, F., Bodnar, D. A., & Bialek, W. 1995. Naturalistic stimuli increase the rate and efficiency of information-transmission by primary auditory afferents. *Proc. Roy. Soc. Lond. B*, **262**, 259–265.
- Rieke, F., Warland, D., van Steveninck, R. D. R., & Bialek, W. 1997. *Spikes: Exploring the Neural Code*. MIT Press: Cambridge, Massachusetts.
- Risken, H. 1996. *The Fokker-Planck Equation: Methods of Solution and Applications*. Second edn. Springer Verlag: Berlin.
- Rosenfalck, P. 1969. Intra- and extracellular potential fields of active nerves and muscle fibers. *Acta Physiol. Scand. Suppl.*, **321**, 1–168.
- Rosenmund, C., Clements, J. D., & Westbrook, G. L. 1993. Non-uniform probability of glutamate release at a hippocampal synapse. *Science*, **262**, 754–757.
- Rubinstein, J. T. 1995. Threshold fluctuations in an N sodium channel model of the node of Ranvier. *Biophys. J.*, **68**, 779–785.
- Sabah, N. H., & Leibovic, K. N. 1969. Subthreshold oscillatory responses of the Hodgkin-Huxley cable model for the squid giant axon. *Biophys. J.*, **9**, 1206–1222.
- Sabah, N. H., & Leibovic, K. N. 1972. The effect of membrane parameters on the properties of the nerve impulse. *Biophys. J.*, **12**, 1132–1144.
- Sancho, J. M., Miguel, M. San, Katz, S. L., & Gunton, J. D. 1982. Analytical and numerical studies of multiplicative noise. *Phys. Rev. A*, **23**, 1589–1609.
- Schneidman, E., Freedman, B., & Segev, I. 1998. Ion-channel stochasticity may be critical in determining the reliability and precision of spike timing. *Neural Comput.*, **10**, 1679–1703.

- Schwindt, P., & Crill, W. 1995. Amplification of synaptic current by persistent sodium conductance in apical dendrite of neocortical neurons. *J. Neurophysiol.*, **74**, 2220–2224.
- Segev, I., & Burke, R. E. 1998. Compartmental Models of Complex Neurons. *In*: Koch, C., & Segev, I. (eds), *Methods in Neuronal Modeling: From Ions to Networks*, second edn. MIT Press, Cambridge, Massachusetts.
- Segev, I., Burke, R. E., & Hines, M. L. 1998. Compartmental models of complex neurons. *In*: Koch, C., & Segev, I. (eds), *Methods in Neuronal Modeling: From Ions to Networks*, second edn. MIT Press: Cambridge, Massachusetts.
- Shadlen, M. N., & Newsome, W. T. 1994. Noise, neural codes and cortical organization. *Curr. Opin. Neurobiol.*, **4**, 569–579.
- Shadlen, M. N., & Newsome, W. T. 1995. Is there a signal in the noise? *Curr. Opin. Neurobiol.*, **5**, 569–579.
- Shadlen, M. N., & Newsome, W. T. 1998. The variable discharge of cortical neurons: implications for connectivity, computation, and information coding. *J. Neurosci.*, **18**, 3870–3896.
- Shannon, C. E. 1949. *A Mathematical Theory of Communication*. University of Illinois Press: Urbana, Illinois.
- Skaugen, E. 1980a. Firing behavior in nerve cell models with a two-state pore system. *Acta Physiol. Scand.*, **109**, 337–392.
- Skaugen, E. 1980b. Firing behavior in stochastic nerve membrane models with different pore densities. *Acta Physiol. Scand.*, **108**, 49–60.
- Skaugen, E., & Walloe, L. 1979. Firing behavior in a stochastic nerve membrane model based upon the Hodgkin-Huxley equations. *Acta Physiol. Scand.*, **107**, 343–363.
- Smetters, D. K., & Zador, A. 1996. Synaptic transmission: noisy synapses and noisy neurons. *Curr. Biol.*, **6**, 1217–1218.

- Softky, W. R. 1995. Simple codes versus efficient codes. *Curr. Opin. Neurobiol.*, **5**, 239–247.
- Softky, W. R., & Koch, C. 1993. The highly irregular firing of cortical cells is inconsistent with temporal integration of random epsps. *J. Neurosci.*, **13**, 334–350.
- Solleder, P., & Frehland, E. 1986. Nonequilibrium voltage fluctuations in biological membranes. II. Voltage and current noise generated by ion carriers, channels and electrogenic pumps. *Biophys. Chem.*, **25**, 147–159.
- Sorra, K. E., & Harris, K. M. 1993. Occurrence and three-dimensional structure of multiple synapses between individual radiatum axons and their target pyramidal cells in hippocampal area CA1. *J. Neurosci.*, **13**, 3736–3748.
- Spruston, N., Jaffe, D. B., & Johnston, D. 1994. Dendritic attenuation of synaptic potentials and currents: the role of passive membrane properties. *Trends Neurosci.*, **17**, 161–166.
- Srinivasan, M. V., & Bernard, G. D. 1976. A proposed mechanism for multiplication of neural signals. *Biol. Cybern.*, **21**, 227–236.
- Stein, R. B. 1967a. The frequency of nerve action potentials generated by applied currents. *Proc. R. Soc. Lond. B*, **167**, 64–86.
- Stein, R. B. 1967b. Some models of neuronal variability. *Biophys. J.*, **7**, 37–68.
- Steinmetz, P. N., Manwani, A., London, M., Segev, I., & Koch, C. 2000a. Sub-threshold voltage noise due to channel fluctuations in active neuronal membranes. *J. Comput. Neurosci.* In press.
- Steinmetz, P. N., Manwani, A., & Koch, C. 2000b. Variability and coding efficiency of noisy neural spike encoders. *Biosystems*. Submitted.
- Stevens, C. F. 1972. Inferences about membrane properties from electrical noise measurements. *Biophys. J.*, **12**, 1028–1047.
- Stevens, C. F. 1993. Quantal release of neurotransmitter and long-term potentiation. *Neuron*, **10**, 55–64.

- Stevens, C. F. 1994. Cooperativity of unreliable neurons. *Curr. Biol.*, **4**, 268–269.
- Stevens, C. F., Tonegawa, S., & Wang, Y. 1994. The role of calcium-calmodulin kinase II in three forms of synaptic plasticity. *Curr. Biol.*, **4**, 687–693.
- Stevens, C. F., & Wang, Y. 1994. Changes in reliability of synaptic function as a mechanism for plasticity. *Nature*, **371**, 704–707.
- Stevens, C. F., & Wang, Y. 1995. Facilitation and depression at single central synapses. *Neuron*, **14**, 795–802.
- Stevens, C. F., & Zador, A. M. 1998a. Input synchrony and the irregular firing of cortical neurons. *Nat. Neurosci.*, **1**, 210–217.
- Stevens, C. F., & Zador, A. M. 1998b. Novel integrate-and-fire-like model of repetitive firing in cortical neurons. *In: Proceedings of the 5th Joint Symposium on Neural Computation, UCSD, La Jolla, CA.*
- Stopfer, M., Bhagavan, S., Smith, B. H., & Laurent, G. 1997. Impaired odor discrimination on desynchronization of odor-encoding neural assemblies. *Nature*, **390**, 70–74.
- Strassberg, A. F., & DeFelice, L. J. 1993. Limitations of the Hodgkin-Huxley formalism: effect of single channel kinetics on transmembrane voltage dynamics. *Neural Comput.*, **5**, 843–855.
- Stratford, K. J., Tarczy-Hornoch, K., Martin, K. A., Bannister, N. J., & Jack, J. J. 1996. Excitatory synaptic inputs to spiny stellate cells in cat visual cortex. *Nature*, **382**, 258–61.
- Strong, S. P., Koberle, R., van Steveninck, R. D. R., & Bialek, W. 1998. Entropy and information in neural spike trains. *Phys. Rev. Lett.*, **80**, 197–200.
- Stuart, G., & Sakmann, B. 1995. Amplification of epsps by axosomatic sodium channels in neocortical pyramidal neurons. *Neuron*, **15**, 1065–1076.
- Stuart, G., & Spruston, N. 1998. Determinants of voltage attenuation in neocortical pyramidal neuron dendrites. *J. Neurosci.*, **18**, 3501–3510.

- Stuart, G. J., & Sakmann, B. 1994. Active propagation of somatic action potentials into neocortical pyramidal cell dendrites. *Nature*, **367**, 69–72.
- Suarez, H., & Koch, C. 1989. Linking linear threshold units with quadratic models of motion perception. *Neural Comput.*, **1**, 318–320.
- Theunissen, F., & Miller, J. P. 1995. Temporal encoding in nervous systems: a rigorous definition. *J. Comput. Neurosci.*, **2**, 149–162.
- Theunissen, F. E., & Miller, J. P. 1991. Representation of sensory information in the cricket cercal sensory system II: Information theoretic calculation of system accuracy and optimal tuning-curve widths of four primary interneurons. *J. Neurophysiol.*, **66**, 1690–1703.
- Toib, A., Lyakhov, V., & Marom, S. 1998. Interaction between duration of activity and rate of recovery from slow inactivation in mammalian brain Na⁺ channels. *J. Neurosci.*, **15**, 1893–1903.
- Traynelis, S. F., & Jaramillo, F. 1998. Getting the most out of noise in the central nervous system. *Trends Neurosci.*, **21**, 137–145.
- Tsodyks, M. V., & Markram, H. 1997. The neural code between neocortical pyramidal neurons depends on neurotransmitter release probability. *Proc. Natl. Acad. Sci. USA*, **94**, 719–723.
- Tuckwell, H. C. 1988a. *Introduction to Theoretical Neurobiology I: Linear Cable Theory and Dendritic Structure*. Cambridge University Press: New York, New York.
- Tuckwell, H. C. 1988b. *Introduction to Theoretical Neurobiology II: Nonlinear and Stochastic Theories*. Cambridge University Press: New York, New York.
- Tuckwell, H. C., & Walsh, J. B. 1983. Random currents through nerve membranes. I. Uniform poisson or white noise current in one-dimensional cables. *Biol. Cybern.*, **49**, 99–110.

- Tuckwell, H. C., & Wan, F. Y. 1980. The response of a nerve cylinder to spatially distributed white noise inputs. *J. Theor. Biol.*, **87**, 275–295.
- Vallbo, A. B. 1995. Single-afferent neurons and somatic sensation in humans. *Pages 237–252 of: Gazzaniga, M. (ed), The Cognitive Neurosciences*. MIT Press, Cambridge, Massachusetts.
- Vallbo, A. B., & Johansson, R. S. 1976. Skin mechanoreceptors in the human hand: Neural and psychophysical thresholds. *In: Zotterman, Y. (ed), Sensory Functions of the Skin in Primates*. Pergamon: Oxford, United Kingdom.
- van den Berg, R. J., de Goede, J., & Verveen, A. A. 1975. Conductance fluctuations in Ranvier nodes. *Pflug. Arch.*, **360**, 17–23.
- van den Berg, R. J., & Rijnsburger, W. H. 1980. Membrane current and noise measurements in voltage-clamped node of Ranvier. *J. Membr. Biol.*, **57**, 213–221.
- van Kampen, N. G. 1992. *Stochastic Processes in Physics and Chemistry*. Second edn. North-Holland.
- van Steveninck, R. D., & Bialek, W. 1988. Real-time performance of a movement-sensitive neuron in the blowfly visual system - Coding and information-transfer in short spike sequences. *Proc. Roy. Soc. Lond. B*, **234**, 379–414.
- van Steveninck, R. D., & Bialek, W. 1995. Reliability and statistical efficiency of a Blowfly movement-sensitive neuron. *Phil. Trans. Roy. Soc. Lond. B*, **348**, 321–340.
- van Steveninck, R. R. D., Lewen, G. D., Strong, S. P., Koberle, R., & Bialek, W. 1997. Reproducibility and variability in neural spike trains. *Science*, **275**, 1805–1808.
- van Vreeswijk, C., & Sompolinsky, H. 1996. Chaos in neuronal networks with balanced excitatory and inhibitory activity. *Science*, **274**(5293), 1724–6.
- van Vreeswijk, C., & Sompolinsky, H. 1998. Chaotic balanced state in a model of cortical circuits. *Neural Comput.*, **10**, 1321–1371.

- Verveen, A. A., & DeFelice, L. J. 1974. Membrane noise. *Prog. Biophys. Mol. Biol.*, **28**, 189–265.
- Vogels, R., & Orban, G. A. 1990. How well do response changes of striate neurons signal differences in orientation—a study in the discriminating monkey. *J. Neurosci.*, **10**, 3543–3558.
- von Neumann, J. 1956. *The Computer and the Brain*. Yale University Press: New Haven, Connecticut.
- Wan, F. Y., & Tuckwell, H. C. 1979. The response of a spatially distributed neuron to white noise current injection. *Biol. Cybern.*, **33**, 39–55.
- Wanke, E., DeFelice, L. J., & Conti, F. 1974. Voltage noise, current noise and impedance in space clamped squid giant axon. *Pflug. Arch.*, **347**, 63–74.
- Wehmeier, U., Dong, D., Koch, C., & Essen, D. Van. 1989. Modeling the mammalian visual system. *Pages 335–360 of: C. Koch, C., & Segev, I. (eds), Methods in Neuronal Modeling*. MIT Press: Cambridge, Massachusetts.
- Weiss, T. F. 1996a. *Cellular Biophysics I: Transport*. MIT Press: Cambridge, Massachusetts.
- Weiss, T. F. 1996b. *Cellular Biophysics II: Electrical Properties*. MIT Press: Cambridge, Massachusetts.
- Werner, G., & Mountcastle, V. B. 1963. The variability of central neural activity in a sensory system and its implications for the central reflection of sensory events. *J. Neurophysiol.*, **26**, 958–977.
- Wessel, R., Koch, C., & Gabbiani, F. 1996. Coding of time-varying electric field amplitude modulations in a wave-type electric fish. *J. Neurophysiol.*, **75**, 2280–2293.
- White, J. A., Budde, T., & Kay, A. R. 1995. A bifurcation analysis of neuronal subthreshold oscillations. *Biophys. J.*, **69**, 1203–1217.

- White, J. A., Klink, R., Alonso, A., & Kay, A. R. 1998. Noise from voltage-gated ion channels may influence neuronal dynamics in the entorhinal cortex. *J. Neurophysiol.*, **80**, 262–269.
- White, J. A., Rubinstein, J. T., & Kay, A. R. 2000. Channel noise in neurons. *Trends Neurosci.*, **23**, 131–137.
- Wiener, N. 1949. *Extrapolation, Interpolation and Smoothing of Stationary Time Series*. MIT Press: Cambridge, Massachusetts.
- Yuste, R., & Tank, D. W. 1996. Dendritic integration in mammalian neurons, a century after Cajal. *Neuron*, **16**, 701–716.
- Zador, A. 1998. Impact of synaptic unreliability on the information transmitted by spiking neurons. *J. Neurophysiol.*, **79**, 1219–1229.
- Zador, A. M., Agmon-Snir, H., & Segev, I. 1995. The morphoelectrotonic transform: a graphical approach to dendritic function. *J. Neurosci.*, **15**, 1669–1682.
- Zador, A. M., & Dobrunz, L. E. 1997. Dynamic synapses in the cortex. *Neuron*, **19**, 1–4.
- Zohary, E., Hillman, P., & Hochstein, S. 1990. Time course of perceptual discrimination and single neuron reliability. *Biol. Cybern.*, **62**, 475–486.